Dysregulation of neuronal calcium signaling impairs axonal transport independent of tau in a model of Alzheimer's disease

by

Kathlyn Jeanne Gan

M.Sc., Simon Fraser University, 2009

Thesis Submitted in Partial Fulfillment of the
Requirements for the Degree of
Doctor of Philosophy

in the
Department of Molecular Biology and Biochemistry
Faculty of Science

SIMON FRASER UNIVERSITY

Fall 2014

Approval

Name: **Kathlyn Jeanne Gan**

Degree: **Doctor of Philosophy**

Title: ***Dysregulation of neuronal calcium signaling impairs axonal transport independent of tau in a model of Alzheimer's disease***

Examining Committee: **Chair:** Dr. Carl Lowenberger
Professor

Dr. Michael Silverman
Senior Supervisor
Associate Professor _____

Dr. Nancy Hawkins
Supervisor
Associate Professor _____

Dr. Lynne Quarmby
Supervisor
Professor and Chair _____

Dr. Michel Leroux
Internal Examiner
Professor
Molecular Biology and Biochemistry _____

Dr. Grace Stutzmann
External Examiner
Associate Professor
Chicago Medical School
Rosalind Franklin University by video conference, Chicago, IL

Date Defended/Approved: October 30, 2014

Partial Copyright License

Ethics Statement

The author, whose name appears on the title page of this work, has obtained, for the research described in this work, either:

a. human research ethics approval from the Simon Fraser University Office of Research Ethics,

or

b. advance approval of the animal care protocol from the University Animal Care Committee of Simon Fraser University;

or has conducted the research

c. as a co-investigator, collaborator or research assistant in a research project approved in advance,

or

d. as a member of a course approved in advance for minimal risk human research, by the Office of Research Ethics.

A copy of the approval letter has been filed at the Theses Office of the University Library at the time of submission of this thesis or project.

The original application for approval and letter of approval are filed with the relevant offices. Inquiries may be directed to those authorities.

Simon Fraser University Library
Burnaby, British Columbia, Canada

update Spring 2010

Abstract

Neurons rely on microtubule-based, fast axonal transport of proteins and organelles for development, communication and survival. FAT impairment precedes overt cellular toxicity in multiple neurodegenerative diseases, including Alzheimer's disease (AD). Intracellular Ca^{2+} dysregulation is also widely implicated in early AD pathogenesis; however, its role in transport impairment is unknown. Our lab was first to demonstrate that soluble amyloid-β oligomers (AβOs), proximal neurotoxins in AD, impair vesicular transport of axonal brain-derived neurotrophic factor (BDNF). Contrary to a central paradigm, I show that BDNF transport is blocked independent of the microtubule-associated protein, tau, microtubule destabilization, and acute cell death. Significantly, BDNF transport is impaired by non-excitotoxic activation of calcineurin (CaN), a Ca^{2+}-dependent phosphatase. Based on these findings, I investigated Ca^{2+}-dependent mechanisms that underlie the spatiotemporal progression of AβO-induced transport defects and dysregulate KIF1A, the primary kinesin motor required for BDNF transport. Because CaN and its effectors, protein phosphatase-1 (PP1) and glycogen synthase kinase 3β (GSK3β), are present in both dendrites and axons, I investigated if postsynaptic AβO binding impairs dendritic transport prior to FAT disruption. AβOs induce dendritic and axonal BDNF transport defects simultaneously; however, maximal dendritic transport defects are observed prior to maximal impairment of FAT. I correlated the spatiotemporal progression of transport defects with Ca^{2+} elevation and CaN activation in dendrites and subsequently in axons. Postsynaptic CaN activation converges on axonal Ca^{2+} dysregulation to impair FAT. Specifically, AβOs colocalize with axonal VGCCs, and blocking VGCCs prevents FAT defects. Finally, BDNF transport defects are prevented by dantrolene, a compound that reduces Ca^{2+}-induced-Ca^{2+} release through ryanodine receptors in axonal and dendritic ER membranes. Together, these mechanisms activate CaN-PP1-GSK3β signaling and lead to inhibitory phosphorylation of KIF1A at a highly conserved consensus site within its dimerization domain. Collectively, this thesis establishes novel roles for Ca^{2+} dysregulation in BDNF transport disruption and tau-independent toxicity during early AD pathogenesis.

Keywords: Alzheimer's disease; amyloid-β oligomers; axonal transport; intracellular Ca^{2+} dysregulation; KIF1A inhibition; tau-independent toxicity

To my parents, for their unequivocal understanding, encouragement, and love

Acknowledgements

I am grateful to my senior supervisor, Dr. Michael Silverman, who offered excellent training and guidance, and who provided me with many invaluable opportunities for scientific, intellectual, and personal growth throughout my graduate career. I thank the members of my supervisory committee, Dr. Lynne Quarmby and Dr. Nancy Hawkins, for their insightful perspectives and encouragement. I also thank L. Chen and E. Fan for their expert technical assistance, training, and friendship, and the SFU Animal Care staff for their essential assistance in my experiments. I acknowledge V. Muresan, C.D. Link, T. Tomiyama, P. Copenhaver, and G. Morfini for their critical reading of my manuscripts, and D. Poburko and C. Krieger for essential discussions.

My research was funded by a C.D. Nelson Memorial Graduate Entrance Scholarship from Simon Fraser University and a Postgraduate Scholarship from the Natural Sciences and Engineering Research Council of Canada (NSERC).

Table of Contents

List of Tables

List of Figures

List of Acronyms

AD	Alzheimer's disease
AMPAR	α-amino-3-hydroxyl-5-methyl-4-isoxazole-propionate receptor
APP	Amyloid precursor protein
AβO	Amyloid-β oligomer
BACE	β-site APP cleaving enzyme
BDNF	Brain-derived neurotrophic factor
Ca^{2+}	Calcium
CaM	Calmodulin
CaMKII	Ca^{2+}/calmodulin-dependent kinase II
CaN	Calcineurin
Cdk5	Cyclin-dependent kinase 5
CK2	Casein kinase 2
CRISPR	Clustered regulatory interspaced short palindromic repeat-based endonuclease
DCV	Dense core vesicle
ER	Endoplasmic reticulum
ERAD	Endoplasmic-reticulum-associated protein degradation
FAD	Familial Alzheimer's disease
FAT	Fast axonal transport
GSK3β	Glycogen synthase kinase 3β
hPSC	Human pluripotent stem cell
I2	Inhibitor of protein phosphatase-2
iN	Induced neuron
IP3R	Inositol triphosphate receptor
iPSC	Induced pluripotent stem cell
JNK	c-Jun N-terminal kinase
KHC	Kinesin heavy chain
KIF	Kinesin
KLC	Kinesin light chain
LTD	Long-term depression
LTP	Long-term potentiation

MAP	Microtubule-associated protein
MEMRI	Manganese-enhanced magnetic resonance imaging
mGluR	Metabotropic glutamate receptor
NFT	Neurofibrillary tangle
NMDAR	N-methyl-D-aspartate receptor
PP1	Protein phosphatase-1
PP2B	Protein phosphatase 2B (calcineurin)
PS/PSEN	Presenilin
RyR	Ryanodine receptor
SAD	Sporadic Alzheimer's disease
SERCA	Sarcoendoplasmic reticulum Ca^{2+} transport ATPase
TALEN	Tal effector nuclease
VGCC	Voltage-gated Ca^{2+} channel

Chapter 1. General Introduction

1.1. Microtubule-based transport in neuronal physiology

1.1.1. Neuronal structure and chemical neurotransmission

Thought, perception, memory, and behaviour are dependent upon the function of the nervous system. Polarized nerve cells, or neurons, comprise the nervous system and typically consist of a cell body with branched, tapered dendrites and a long, thin axon of even calibre. The cell body contains the nucleus, endoplasmic reticulum, and Golgi apparatus and thus serves as the principal site for protein synthesis and post-translational modification (Craig and Banker, 1994). Dendrites receive and decode electrical signals at small, dynamic protrusions, termed spines. The axon can transmit electrical signals over distances ranging from 0.1 mm to 2 m. These electrical signals, termed action potentials, are initiated at a specialized region near the origin of the axon called the initial segment. Action potentials propagate rapidly along the axon in a unidirectional manner, without failure or distortion, and are regenerated at regular intervals along the axon. Near its end, the axon divides into fine branches that contact other neurons at specialized zones of communication, known as synapses. Upon arrival of an action potential at the axon terminal and localized Ca^{2+} influx through voltage-sensitive channels, vesicular neurotransmitters and signaling peptides are released from the presynaptic membrane and diffuse across the synaptic cleft. Subsequently, they bind and activate receptors within the postsynaptic membrane of dendritic spines. These receptors cause ion channels to open by direct and indirect mechanisms, thereby changing the membrane conductance and electrical potential of the postsynaptic cell. Ionotropic receptors gate ion channels directly; upon neurotransmitter binding, the receptor undergoes a conformational change that opens the channel. In contrast, activation of metabotropic receptors stimulates the production of second messengers, which activate downstream protein kinases that indirectly modulate channel activity

(Kandel et al., 2013). Collectively, these actions can alter the excitability of neurons and the strength of the synaptic connections within neural circuits. This process is crucial for reinforcing neural pathways that underlie learning and memory (Bliss and Collingridge, 1993).

1.1.2. Axonal transport in development, communication, and survival

Microtubule-based intracellular transport is required by all eukaryotic cells for proper spatiotemporal delivery of proteins and organelles (Figure 1.1). Intracellular transport is particularly critical for neurons due to their extreme morphological dimensions, polarity, and need for efficient communication between the cell body and distal neurites. Cytosolic proteins and cytoskeletal proteins, such as neurofilament subunits and tubulin, are moved from the cell body by slow axonal transport, ranging from 0.2 to 2.5 mm per day. In contrast, large membranous organelles are moved to and from the axon terminals by fast axonal transport (FAT), which can exceed 400 mm per day. Because the axon is largely devoid of biosynthetic machinery, it relies on FAT to supply axon terminals with neurotrophic factors, lipids and mitochondria, and to prevent accumulation of toxic aggregates by clearing recycled or misfolded proteins (Hinckelmann et al., 2013; Millecamps and Julien, 2013). Bidirectional FAT is driven by kinesin and cytoplasmic dynein (called dynein hereafter) motor proteins that use ATP hydrolysis to transport cargoes anterogradely towards the synapse or retrogradely towards the cell body, respectively. Additionally, protein complexes, termed adaptors, are associated with molecular motors and regulate specific cargo interactions by integrating extracellular and intracellular signals (Fu and Holzbaur, 2014). During neuronal development, c-Jun N-terminal protein kinase-interacting protein (JIP1) links Rab10 GTPase to conventional kinesin-1. JIP1 thereby mediates anterograde transport of Rab10-positive vesicles that contain lipids and membrane proteins for axonal elongation and polarity (Deng et al., 2014). Furthermore, FAT delivers preassembled vesicles to prospective sites of presynaptic terminal formation. Fasciculation and elongation protein zeta-1(FEZ1) functions as a kinesin-1 adaptor for transport of syntaxin-1 and Munc18, two proteins required for neurotransmitter vesicle exocytosis at the presynaptic plasma membrane. Loading and unloading of these cargoes is

regulated by protein kinases (Chua et al., 2012). Finally, FAT is crucial for protecting axons from damage inflicted by reactive oxygen species generation and oxygen-glucose deprivation. Following both insults, expression of nicotinamide mononucleotide adenyltransferase rescues bidirectional transport of mitochondria and vesicles containing axonal membrane proteins (Fang et al., 2014). These studies illustrate essential roles of FAT in neuronal development, communication and survival.

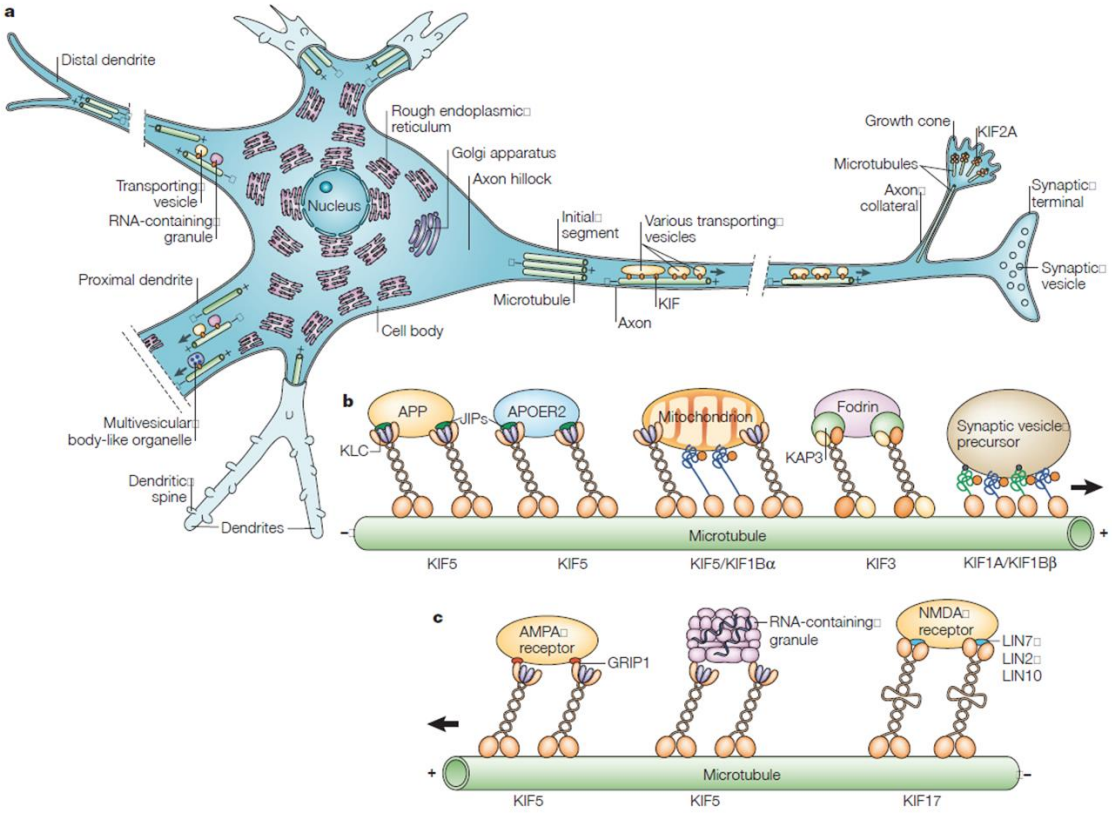

Figure 1.1 Axonal and dendritic transport

(A) A typical pyramidal neuron extends several branched dendrites and a single axon. (B) Kinesin motor proteins bind a variety of axonal cargoes, including APP, mitochondria, and synaptic vesicle precursors, and transport them anterogradely towards the synapse. (C) In dendrites, kinesins transport postsynaptic cargoes, such as NMDARs, AMPARs, and RNA-containing granules. Reproduced with permission from Hirokawa and Takemura, 2005.

1.1.3. Structures, functions, and regulation of conventional kinesin-1 (KIF5) and kinesin-3 (KIF1A)

The human and mouse genomes contain more than 40 kinesin genes, which are categorized into 14 subfamilies based on phylogenetically conserved similarities in their

motor domains and in other parts of the proteins (Miki et al., 2001; Lawrence et al., 2004; Hirokawa et al., 2010). Much of the current knowledge on structures, mechanochemical cycles, and regulation of kinesin motors is based on studies of conventional kinesin (kinesin-1, KIF5), the founding member of the kinesin superfamily (Figure 1.2). KIF5 is abundantly expressed in neurons, where it transports diverse membranous and non-membranous cargoes. Kinesin-1 is a heterotetramer that consists of two heavy chains (KHCs) and two light chains (KLCs) (Bloom et al., 1988). Mammals contain three KHC isoforms (KIF5A, B, and C) that form homo- or heterodimers. KIF5A and 5C are specific to the nervous system (Niclas et al., 1994; Kanai et al., 2000). Each KHC contains a globular head motor domain that binds to microtubules and hydrolyzes ATP, a neck linker, a stalk that is involved in dimerization, and a tail that inhibits the ATPase activity of the head and also binds to microtubules (Dietrich et al., 2008; Wong and Rice, 2010; Kaan et al., 2011). In mammals, four KLC isoforms (KLC 1-4) promote activation of kinesin-1 for cargo transport by simultaneously suppressing tail-head and tail-microtubule interactions (Gyoeva et al., 2004; Wong and Rice, 2010). In the absence of cargo, KLC1 maintains kinesin-1 in a soluble, autoinhibited state. Upon cargo binding to KLC1, autoinhibition is relieved, and the motor-cargo complex translocates along microtubules. KLCs are also critical for selective cargo binding. They consist of two major domains: a coiled-coil domain, which interacts with the stalk domain of KHC to form the tetramer (Diefenbach et al., 1998), and a series of 6 tandem repeats, termed tetratricopeptide repeats (TPRs), which mediate protein-protein interactions (Stenoien and Brady, 1997; Gindhart et al., 1998; Verhey et al., 2001; Pernigo et al., 2013). Downstream of the TPR domain is the C-terminal domain, which varies in both size and sequence. It is postulated that variation in the C-terminal sequences and 3'-untranslated regions is vital for targeting kinesin-1 to different cellular structures (McCart et al., 2003). Variant B preferentially binds to mitochondria (Khodjakov et al., 1998), whereas D and E associate with rough ER (Wozniak and Allan, 2006) and Golgi membranes (Gyoeva et al., 2000). To date, 19 variants of KLC1 have been identified in humans, with the calculated potential to produce 285,919 spliceforms (McCart et al., 2003). Expression levels, functions, and regulatory mechanisms of many neuronal KLC variants have yet to be discovered in healthy and disease states.

Other kinesins possess evolutionary adaptations in their cargo-binding and motor domains that generate diversity in cargo selection, motor processivity, regulation, subcellular localization, and physiological roles. Of particular relevance to this work, kinesin-3 family members are characterized by high sequence conservation within their motor domains, a forkhead-associated domain, and a C-terminal cargo-binding domain such as a pleckstrin homology, Phox homology, or liprin-binding domain (Shin et al., 2003; Miki et al., 2005) (Figure 1.2). *UNC-104*, the founding member of the kinesin-3 family, was identified in *C. elegans* and implicated in transport of synaptic vesicle precursors to the axon terminal (Hall and Hedgecock, 1991; Otsuka et al., 1991). KIF1A, the mammalian homologue of *UNC-104*, associates with membranous organelles containing synaptic vesicle proteins, such as synaptotagmin, synaptophysin, and Rab3A (Okada et al., 1995). KIF1A is also required for FAT of large dense core vesicles (DCVs) (Yonekawa et al., 1998; Barkus et al., 2008; Lo et al., 2011). Unlike synaptic vesicles, DCVs are formed and filled with secretory neuropeptides, including brain-derived neurotrophic factor (BDNF; see Section 1.6), in the cell body and must be transported over long distances to presynaptic and postsynaptic sites of release. KIF1A is well suited for DCV transport because it is highly processive, implying that it is fast and remains bound to microtubules for long durations, and, like KIF5A, exhibits varied mechanisms for binding to different cargoes (Klopfenstein and Vale, 2004; Hirokawa and Noda, 2008). The precise mechanism for KIF1A binding to DCVs is unknown.

In the absence of cargo, kinesin motors are kept inactive to prevent futile ATP hydrolysis and motility. Studies on mechanisms of KIF1A motor regulation have yielded conflicting results (Verhey et al., 2011). Some models contend that KIF1A is monomeric in the inactive state, and that activation results from concentration-driven dimerization prior to cargo binding or on the cargo surface (Klopfenstein et al., 2002; Tomishige et al., 2002). Other findings show that KIF1A is dimeric in the inactive state and is therefore not activated by cargo-induced dimerization (Hammond et al., 2009); rather, KIF1A motors are autoinhibited by two distinct mechanisms, and dimeric KIF1A motors are activated by cargo binding (Soppina et al., 2014). Furthermore, although both KIF1A monomers and dimers can diffuse along the microtubule surface, only dimeric motors undergo ATP-dependent, superprocessive motility. This property is intrinsic to the KIF1A motor domain, rendering it ideal for driving long-distance transport in neurons.

Intriguingly, KIF1A processivity is modulated by the p150 subunit of the dynactin complex (Culver-Hanlon et al., 2006; Berezuk and Schroer, 2007), which associates directly with dynein and participates in the coordination of bidirectional DCV transport (Kwinter et al., 2009). This may be accomplished by switching a particular motor "on" or "off" depending on the direction of travel, or by facilitating cargo binding of one motor protein class over the other (Welte, 2004). Irrespective of the mechanism, dynactin is postulated to serve as a platform for motor-cargo binding and coordination (Schroer, 2004). Notably, disrupting an interaction between dynactin and carboxypeptidase-E perturbs bidirectional transport of vesicular BDNF (Park et al., 2008). Recent work has shown that bidirectional transport, mediated by KIF1A and dynein/dynactin, is crucial for driving the continuous circulation of axonal DCVs in *Drosophila* motor neurons and relies on a switch in the driving motor at opposite ends of the circuit (Moughamian and Holzbaur, 2012; Wong et al., 2012). Ultimately, this mechanism yields an equal distribution of DCVs among synapses, despite sporadic and inefficient capture of vesicles at synaptic release sites, and ensures robust neurotransmission. Indeed, mutations in KIF1A perturb synaptic vesicle distribution and lead to neurodegeneration in mammalian neurons (Riviere et al., 2011; Klebe et al., 2012).

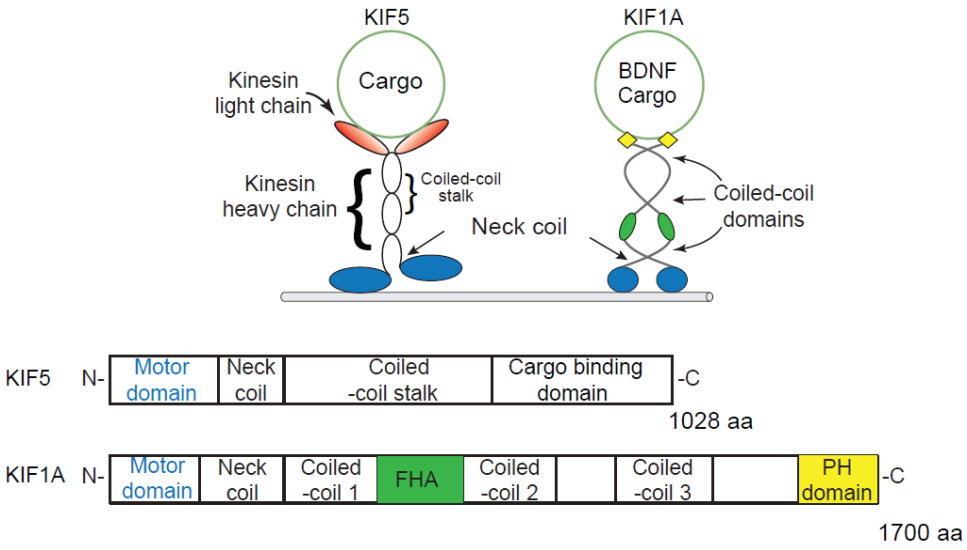

Figure 1.2 Structures of KIF5 and KIF1A

KIF5 is a heterotetramer that consists of two heavy chains (KHCs) and two light chains (KLCs). Each KHC contains a globular head motor domain, a neck linker, a stalk that is involved in dimerization, and a tail that inhibits the ATPase activity and binds microtubules. KLC isoforms promote activation of kinesin-1 for cargo transport. KIF1A contains a motor domain, a forkhead associated domain, and a cargo-binding domain such as a pleckstrin homology (PH) domain.

1.1.4. Structure, functions, and regulation of cytoplasmic dynein

Dynein performs a wide variety of basic cellular functions, such as transport of organelles, vesicles, proteins, and mRNA, maintenance of the Golgi apparatus, endosome recycling, and the positioning of the mitotic spindle (Yadav and Linstedt, 2011; Lipka et al., 2013; McNally, 2013). In neurons, it is required for migration, polarized trafficking into dendrites, and retrograde axonal transport (Vallee et al., 2009; Kapitein and Hoogenraad, 2011). The dynein molecule is a large (1.6 MDa) complex that contains two identical copies of heavy chains (HC), intermediate chains (IC), light intermediate chains (LIC), and light chains (LC8, LC7, TCTex). The HCs comprise the motor subunit, and together with six adjacent modules at the C-terminus, are responsible for ATP hydrolysis, microtubule binding, and generation of motile force (Cho and Vale, 2012). Five other subunits associate with the N-terminal region of the motor subunit to form a tail that binds to cargoes. Besides this core complex, other proteins regulate dynein function and localization (Kardon and Vale, 2009). Dynactin, purified as an activator of dynein, interacts with dynein ICs through its $p150_{Glued}$ subunit. $p150_{Glued}$ regulates dynein-cargo interactions, coordinates bidirectional transport, and facilitates dynein processivity by providing additional microtubule binding (Gill et al., 1991; Culver-Hanlon et al., 2006; Berezuk and Schroer, 2007). Recent studies contend that the dynein-dynactin complex is stabilized by the coiled-coil adaptor, Bicaudal 2 (BICD2), which significantly increases the speed and run length of the motor complex along microtubules and prevents futile ATP hydrolysis (McKenney et al., 2014; Schlager et al., 2014). Formation of this tripartite complex is postulated to improve coordination between the motor heads and/or increase the rigidity of the complex, which could increase processivity and enhance force production (Allan, 2014). Mutations in dynein HC, $p150_{Glued}$ and BICD2 are directly linked to neurodegenerative diseases such as Charcot-Marie-Tooth disease, amyotrophic lateral sclerosis, and congenital spinal muscular atrophy (Lipka et al., 2013). Moreover, expression of dynein IC is reduced in the frontal cortex of Alzheimer's disease patients (Morel et al., 2012). Due to the size and complexity of dynein, the existence of multiple isoforms for all subunits, and the lack of specific antibodies, mechanisms that regulate dynein-mediated transport, particularly of DCVs in healthy and disease states, are poorly understood relative to kinesin-based transport.

1.2. Transport defects in Alzheimer's disease

Due to their extreme morphological dimensions, polarity, and need for efficient communication between the cell body and distal neurites, neurons are particularly susceptible to FAT impairment. Substantial evidence implicates defective FAT in neurodegenerative diseases, and "transport-opathies" such as amyotrophic lateral sclerosis, Huntington's disease, and Alzheimer's disease (AD) have been reviewed extensively (Goldstein, 2012; Hinckelmann et al., 2013; Millecamps and Julien, 2013). Damage to axonal transport in these diseases typically involves disruption of motor-cargo binding or motor-microtubule interactions. Early neuropathology studies reported microtubule destabilization, synapse loss, and dystrophic neurites that exhibited morphological features of impaired transport (Terry, 1998). These changes were initially attributed to sporadic mutations or environmental insults that induced aggregation of toxic proteins and disrupted cellular metabolism and homeostasis (Goldstein, 2012; Hinckelmann et al., 2013). However, recent discoveries that genetic mutations in kinesins, dynein, adaptors, and microtubule-related proteins lead to neurodegeneration suggest a causal role for FAT in disease progression (Dumanchin et al., 1998; Lazarov et al., 2007; Farrer et al., 2009; Twelvetrees et al., 2010; Hinckelmann et al., 2013).

1.2.1. Amyloid-β generation and accumulation

Alzheimer's disease (AD) is the most prevalent cause of age-related dementia. Early-onset, familial AD (FAD) accounts for <5% of all cases, while late-onset, sporadic AD (SAD) comprises >95% and is not clearly linked to dominant or recessive mutations (Avramopoulos, 2009). Symptoms common to both forms of AD include deficits in spatial learning and memory, which are associated with degeneration in cognitive areas of the brain, such as the hippocampus and cortex. Two lesions represent hallmark diagnostic features of AD: extracellular amyloid-β (Aβ) plaques and intracellular neurofibrillary tangles (NFTs) comprised of aggregated tau protein. Aβ is generated when the amyloid precursor protein (APP) is misprocessed and undergoes a toxic gain of function (Figure 1.3). Full-length APP is a transmembrane protein that is translated at the ER, glycosylated and phosphorylated in the Golgi, and trafficked to the plasma membrane in post-Golgi carriers (Jiang et al., 2014). Proteolytic processing of APP

occurs by one of two pathways. In the prevalent non-amyloidogenic pathway, APP is first cleaved by α-secretase within the Aβ domain, thereby preventing Aβ production. The larger N-terminal fragment is secreted (sAPPα), whereas the smaller C-terminal fragment (C83) is further cleaved by γ-secretase and is readily degraded. During amyloidogenic processing, APP is first cleaved by β-secretase (β-site APP cleaving enzyme 1; BACE). The C-terminal product is subsequently cleaved by γ-secretase, a multi-subunit protein complex in which presenilin 1 (PS1) or PS2 is the catalytic subunit, producing Aβ (Citron et al., 1997; Zhang et al., 2013).

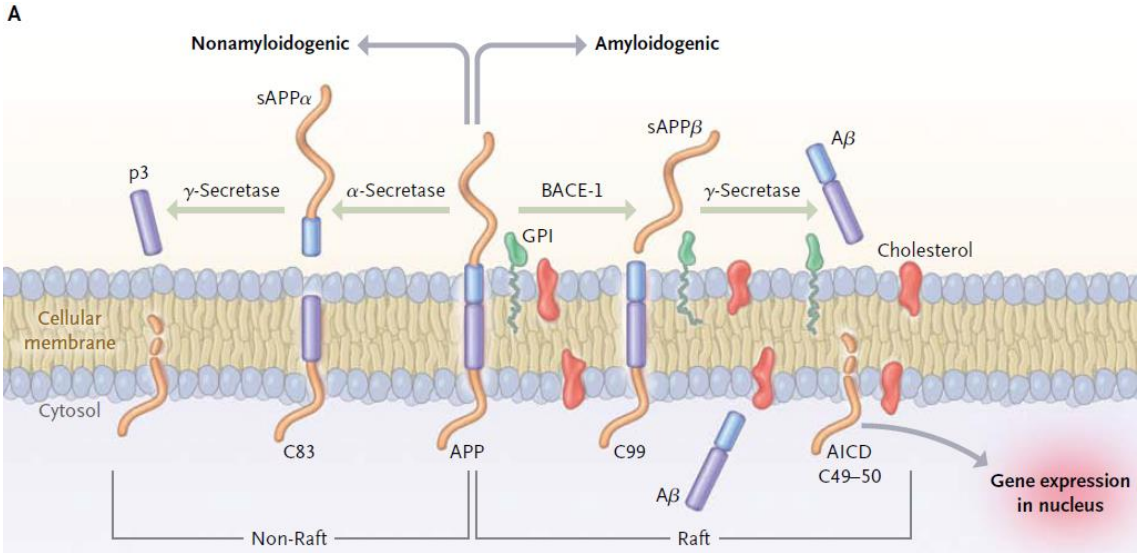

Figure 1.3 Proteolytic processing of the amyloid precursor protein (APP)

(Left) In non-amyloidogenic processing, cleavage by α-secretase releases a large amyloid precursor protein (sAPPα) ectodomain and an 83-residue C-terminal fragment. C83 is then digested by γ-secretase, liberating extracellular p3 and the amyloid intracellular domain (AICD). (Right) In amyloidogenic processing, cleavage by beta-site amyloid precursor protein–cleaving enzyme 1 (BACE-1) releases a shortened sAPPα. The retained C99 is also a γ-secretase substrate, generating Aβ and AICD. γ-Secretase cleavage occurs within the cell membrane, producing sAPPα and sAPPβ fragments. AICD is released into the cytoplasm after progressive ε-to-γ cleavages by γ-secretase. AICD is targeted to the nucleus, signaling transcription activation. Lipid rafts are tightly packed membrane micro-environments enriched in sphingomylelin, cholesterol, and glycophosphatidylinositol (GPI)–anchored proteins. Soluble Aβ is prone to aggregation. Reproduced with permission from Querforth and LaFerla, 2010. Copyright Massachusetts Medical Society.

Intracellular Aβ (iAβ) peptides are generated wherever APP and secretase complexes are present: localized to the ER, trans-Golgi network, endosomal, lysosomal, and mitochondria membranes, or *en route* to the plasma membrane (LaFerla et al., 2007) (Figure 1.4). At the ER membrane, iAβ activates apoptotic JNK signaling and

alters transcriptional profiles through the unfolded protein response, increasing levels of pro-apoptotic factors and BACE. Upon induction of ER stress, immature APP binds to the KDEL protein binding immunoglobin protein (BiP)/GRP78, which permits sorting into COPI vesicles for retrograde transport in post-ER compartments. In AD, APP is insufficiently cleared by BiP and endoplasmic-reticulum-associated protein degradation (ERAD), and its retention in early compartments of the secretory pathway increases Aβ generation by BACE cleavage (Kudo et al., 2006; Roussel et al., 2012; Li et al., 2013). Aberrant accumulation of iAβ in mitochondria leads to impairment of oxidative phosphorylation, increased ROS production, Ca^{2+} mishandling, and activation of apoptotic cascades (Pagani and Eckert, 2011). Although it is not precisely known how APP transport regulates Aβ generation, several reports explain the influence of vesicle formation and trafficking on protein processing and vesicle composition (Kuliawat and Arvan, 1994; Duncan et al., 2003; Handley et al., 2007; Dikeakos et al., 2009). The exact composition of APP-containing vesicles is contentious. One view asserts that APP and BACE are co-transported in the same vesicle (Kamal et al., 2001). In this model, APP binds directly to KLC1 and acts as a KHC motor adaptor (Kamal et al., 2000). Impaired transport could lead to premature proteolysis of APP and accumulation of Aβ in subcellular locations where it cannot be properly cleared. Conversely, other reports have failed to demonstrate a direct interaction between KLC1 and APP, and it is unclear whether APP-containing vesicles include secretases (Lazarov et al., 2005). Alternatively, APP vesicles may aberrantly fuse with BACE-containing endosomes (Das et al., 2013). In this model, fusion may be promoted by a JIP1-KLC association, which alters the directionality of APP transport and increases the probability of vesicle mislocalization (Fu and Holzbaur, 2013). Taken together, these studies support causative roles for iAβ and its transport in early AD pathogenesis.

Extracellular Aβ is generated by APP misprocessing at the plasma membrane. Cleavage by γ-secretase releases two major monomeric Aβ isoforms: $Aβ_{1-40}$ predominates and remains soluble; however, $Aβ_{1-42}$ is more prone to aggregation and is thus the major constituent of fibrils and plaques in AD patients (Querfurth and LaFerla, 2010). During AD progression, Aβ production shifts from $Aβ_{1-40}$ to $Aβ_{1-42}$. Although not fully characterized, this shift is driven by FAD mutations in APP, PS1, or PS2 (Citron et al., 1997; Zhang et al., 2013). Interestingly, $Aβ_{1-40}$ can impair fibril formation and prevent

neuronal death; thus, reduced production of this isoform may impede Aβ clearance (Zou et al., 2003; Yan and Wang, 2007; Jan et al., 2008). The normal function of Aβ is largely unclear. In picomolar amounts, it is neuroprotective and aids cellular mechanisms of learning and memory (Puzzo et al., 2008; Puzzo et al., 2011); however, in micromolar amounts, Aβ acquires many toxic properties. Although Aβ fibrils and plaques are ubiquitous in AD brain, they correlate poorly with the severity of dementia in transgenic mouse models and patients (Herrup, 2010).

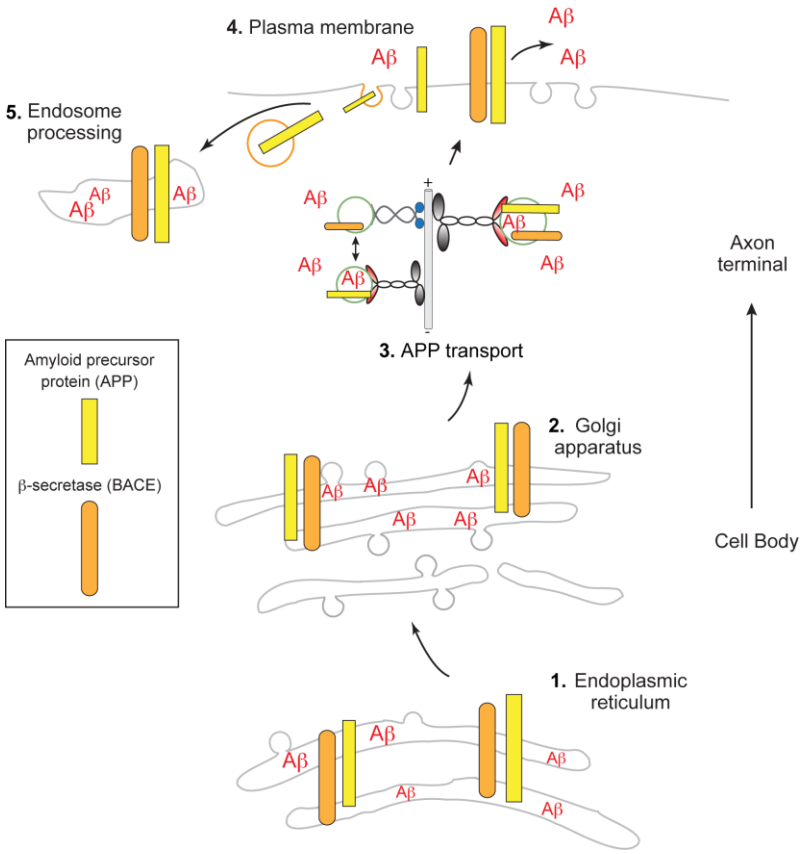

Figure 1.4 Generation of intracellular amyloid-β (Aβ)

Full-length APP is translated at the ER, glycosylated and phosphorylated in the Golgi, and trafficked to the plasma membrane in post-Golgi carriers. Intracellular Aβ peptides are generated wherever APP and secretase complexes are present: localized to the ER membrane (1), trans-Golgi network (2), or within Golgi-derived vesicles (3). The exact composition of APP-containing vesicles is contentious. (Right) APP and the amyloidogenic processing enzyme, β-secretase (BACE1), are packaged into the same Golgi-derived vesicle. (Left) Alternatively, APP and BACE1 may reside in different vesicle populations. Altered transport may lead to mislocalization and/or increased fusion of APP and BACE1 containing vesicles. Aβ generated at the plasma membrane may be released (4), and extracellular Aβ may be internalized and degraded through the endosome-lysosome pathway (5).

1.2.2. Failure of amyloid-β clearance in aging and sporadic AD

Neuronal aging greatly increases the risk of developing sporadic AD (SAD). Aging is associated with cumulative oxidative damage to proteins and membranes, translational errors leading to the synthesis of defective proteins, and various genetic and environmental insults to organelles and proteins (Roy et al., 2002; Sohal et al., 2002; Troen, 2003). In some age-related neurodegenerative diseases, including AD, gene mutations may generate misfolded or damaged forms of proteins and their metabolites, leading to increased proteolytic resistance and accumulation (Saido and Leissring, 2012). Inefficient elimination of these toxic cellular constituents compromises the ability of a neuron to withstand further insults and is postulated to cause SAD (Selkoe, 2001; Tanzi et al., 2004). Intracellular and extracellular mechanisms of proteolytic degradation enable greater Aβ clearance (8.3% per hour in humans) than production (7.6%), regulating Aβ steady-state levels and limiting its accumulation under physiological conditions (Bateman et al., 2006). In AD patients, Aβ clearance rate is significantly reduced, emphasizing its importance in disease progression (Mawuenyega et al., 2010).

The ubiquitin-proteosome and the autophagic-lysosomal systems are mainly responsible for the intracellular turnover of proteins and organelles. The former process involves selective degradation of proteins with short half-lives, which are marked for elimination by covalent ligation of ubiquitin (Ihara et al., 2012). Studies have shown that full-length APP is ubiquitinated under physiological conditions (Morel et al., 2013) and upon proteasome inhibition (Watanabe et al., 2012). It is hypothesized that ubiquitinated APP destined for proteosomal degradation is shunted away from sites where secretase complexes reside (Wang and Saunders, 2014). Given that ubiquitin-proteosome dysfunction is associated with aging and neurodegenerative diseases including SAD (Kourtis and Tavernarakis, 2011; Riederer et al., 2011), APP may be unable to evade amyloidogenic secretase cleavage. Indeed, reduced ubiquitination perturbs APP trafficking (Morel et al., 2013) and leads to Aβ accumulation within the Golgi apparatus (El Ayadi et al., 2012). The autophagic-lysosomal system is the sole pathway for degradation of organelles and large protein aggregates or inclusions. Aβ is generated during autophagic turnover of APP-containing organelles and is subsequently degraded

by lysosomes (Yu et al., 2005). Autophagosomes actively form within neuronal processes and synapses, but efficient clearance of these compartments requires their retrograde transport towards the cell body, where fusion with abundant lysosomes occurs. In aging and AD, maturation and retrograde transport of autophagosomes is impaired, promoting accumulation of autophagic vacuoles within large swellings along degenerating neurites (Nixon et al., 2005). Increased induction of autophagy and reduced clearance of autophagic vacuoles promotes Aβ accumulation (Nixon, 2007; Ihara et al., 2012) and may drive SAD pathogenesis.

Extracellular removal of Aβ can occur by clearance across the blood-brain barrier and degradation outside the central nervous system, phagocytosis by astrocytes and microglia, and by secreted or cell-surface proteases (Pacheco-Quinto et al., 2013). A large number of specific Aβ-degrading proteases have been identified, many of which are classified as zinc-metalloproteases or cysteine proteases and hydrolyze monomeric, oligomeric and fibrillar forms of Aβ. Neprilysin, the most extensively investigated and characterized Aβ-degrading protease, is a member of the M13 family of zinc metalloproteases and possesses an active site that faces the lumenal or extracellular side of membranes (Saido and Leissring, 2012). Thus, it is well suited for degradation of extracytoplasmic Aβ. Neprilysin is expressed exclusively in neurons, synthesized in the cell body, and delivered to presynaptic terminals by FAT, similar to transport of APP (Fukami et al., 2002); presumably, it degrades APP at synapses and nearby intracellular sites (Iwata et al., 2004). Levels of Aβ correlate inversely with the gene dosage and enzymatic activity of neprilysin. Inhibition of neprilysin significantly elevates endogenous Aβ in rat and mouse brain (Iwata et al., 2002; Dolev and Michaelson, 2004), and neprilysin overexpression reduces Aβ plaque deposition in APP-transgenic mice (Marr et al., 2003) and improves cognitive performance in some cases (Marr and Spencer, 2010). Furthermore, neprilysin mRNA and protein expression levels decline with age and AD progression (Reilly, 2001; Apelt et al., 2003), supporting the notion that impaired clearance of Aβ promotes its accumulation and contributes to sporadic AD.

1.2.3. Amyloid-β oligomers are the primary neurotoxins in AD

Substantial evidence suggests that the soluble, oligomeric form of Aβ (AβO) accumulates in AD brain prior to detectable formation of Aβ plaques and NFTs (Nishitsuji et al., 2009; Tomiyama et al., 2010) and is the most potent neurotoxin in AD (Ferreira and Klein, 2011). AβOs cluster at synapses, where they are thought to interact preferentially with postsynaptic membrane receptors at dendritic spines and modulate their activity (Cochran et al., 2013). Presynaptic AβO binding has not been investigated extensively, and specific axonal binding sites and protein interactions remain uncharacterized (Cataldi, 2013) (see Section 1.3). Glutamate receptors, which mediate dendritic Ca^{2+} elevation, appear to be centrally involved; inhibition or removal of surface AMPA (α-amino-3-hydroxyl-5-methyl-4-isoxazole-propionate) receptors reduces AβO binding to dendrites (Zhao et al., 2010), and metabotropic glutamate receptors (mGluR5) participate in AβO binding and clustering at synapses (Renner et al., 2010). Additionally, N-methyl-D-aspartate receptors (NMDARs) coimmunoprecipitate with AβOs from rat synaptosomal membranes (De Felice et al., 2007), and AβO binding is abolished in dendrites of NMDAR knock-down neurons (Jurgensen et al.; Decker et al., 2010b). Chronic AβO exposure leads to endocytic internalization of NMDARs and AMPARs (Snyder et al., 2005; Hsieh et al., 2006; Lacor et al., 2007). Collectively, these insults inhibit functional synaptic plasticity by impairing long-term potentiation and enhancing long-term depression (LTP and LTD respectively; see Section 1.4) (Shankar et al., 2008). This culminates in dendritic spine retraction, synapse deterioration or elimination, and cognitive deficits (Lacor et al., 2007; Shankar et al., 2008; Tomiyama et al., 2010). In addition to their deleterious effects at synapses, AβOs cause general neuronal dysfunction. Such impacts include Ca^{2+} dyshomeostasis (Berridge, 2010a; Chakroborty and Stutzmann, 2011) (see Section 1.3), proteasome inhibition and ER stress (Popugaeva and Bezprozvanny, 2013), oxidative stress and mitochondrial damage (Reddy, 2014), tau accumulation and hyperphosphorylation (Morris et al., 2011) (see Section 1.2.3), and impairment of FAT in cultured neurons and AD mouse models (Goldstein, 2012; Millecamps and Julien, 2013) (see Section 1.2.4). Thus, AβOs account for many major facets of AD pathology and provide a unifying mechanism for the initiation of AD pathogenesis.

1.2.4. Physiological and pathogenic roles of tau

Tau is one of several microtubule-associated proteins (MAPs) that promote microtubule assembly and stability in neurons. Tau plays diverse physiological roles in cytoskeletal organization and stabilization (Weingarten et al., 1975; Kempf et al., 1996), regulation of neurite outgrowth (Biernat and Mandelkow, 1999; Biernat et al., 2002), modulation of signaling cascades through scaffolding (Ittner et al., 2010), and adult neurogenesis (Zhao et al., 2008). It consists of four regions: an N-terminal projection region, a proline-rich domain, a microtubule-binding domain (MBD), and a C-terminal region (Mandelkow et al., 1996). In adult human brain, alternative splicing around the N-terminal region and MBD generates six main isoforms (Goedert et al., 1989). Physiological tau undergoes a complex array of post-translational modifications, including phosphorylation (Morris et al., 2011). A variety of kinases phosphorylate many serine and threonine residues on tau in both physiological and pathological conditions (Wang and Liu, 2008). Phosphorylation of tau within the MBD neutralizes its positive net charge (Jho et al., 2010), reducing its electrostatic interactions with tubulin, and alters its conformation (Fischer et al., 2009) to promote microtubule detachment.

More than 30 tau mutations have been reported in humans, and 17 have been detected in frontotemporal dementia associated with Parkinson's disease (Gomez-Isla et al., 1997). However, tau mutations associated with AD have yet to be discovered (Kim et al., 2014). In AD, tau is thought to mediate AβO toxicity and FAT disruption (Ittner and Gotz, 2011; Bloom, 2014). AβOs induce hyperphosphorylation of tau (p-tau), promoting its dissociation from microtubules and aggregation into neurofibrillary tangles (NFTs) (De Felice et al., 2008). AβOs also induce tau proteolysis by calpains and caspases, generating fragments that aggregate independently of hyperphosphorylation (Reifert et al., 2011). Despite the accumulation of p-tau in affected neurons, it is controversial whether tau is required for AβO toxicity. Tau $^{-/-}$ neurons are resistant to Aβ-induced death (King et al., 2006); by contrast, NFTs persist in viable neurons possessing intact microtubule networks until late-stage AD (Castellani et al., 2008). Recent studies suggest that p-tau inhibits FAT by interacting directly with motor-cargo complexes or initiating aberrant signaling cascades that alter FAT dynamics (LaPointe et al., 2009; Kanaan et al., 2011), and that tau reduction prevents AβO-induced defects in

mitochondria and neurotrophin receptor TrkA transport (Vossel et al., 2010). Conversely, axonal transport is not affected by deletion of normal mouse tau or by overexpression of wild type human tau with associated p-tau and aggregation (Yuan et al., 2008; Yuan et al., 2013). We previously reported that AβOs block FAT of dense core vesicles (DCV) and mitochondria in cultured neurons through an NMDAR-dependent mechanism that is mediated by a tau kinase, glycogen synthase kinase-3β (GSK3β) (Decker et al., 2010a). Notably, we did not observe concomitant microtubule destabilization, suggesting that the microtubule-binding capacity of tau did not affect transport of these cargoes.

Four independent lines of tau knockout ($tau^{-/-}$) mice have been established for analyzing tau pathology in AD. Most of them do not exhibit defects in learning, memory, and behavioural paradigms throughout their lives (Morris et al., 2011). Although other MAPs may partially compensate for tau loss in conventional $tau^{-/-}$ mice (Harada et al., 1994), Dawson et al. detected no changes in MAP1A, MAP1B, or MAP2 protein levels in their line of $tau^{-/-}$ mice (B6.129-*Mapt*^{tm1Hnd}/J) (Dawson et al., 2001). Electrophysiological recordings in hippocampal slices reveal that this line of $tau^{-/-}$ mice and wild type controls possess comparable NMDAR and AMPAR currents, synaptic transmission strength, and both short-term and long-term synaptic plasticity (Roberson et al., 2011; Shipton et al., 2011). These characteristics render B6.129-*Mapt*^{tm1Hnd}/J $tau^{-/-}$ mice suitable for evaluating the role of tau in AβO-induced transport disruption and are used in my studies.

1.2.5. Do FAT defects cause or arise from AD pathology?

In AD, it is controversial whether transport defects cause or arise from amyloid-β (Aβ)-induced mechanisms of cellular toxicity. Many studies indicate that pathological forms of APP, PS1, Aβ and tau can impair axonal transport during early and late stages of AD progression. Late transport defects arise from axonal dystrophy, microtubule dissolution, tau aggregation, and tau-induced kinase activation (Mandelkow et al., 2003; Stokin and Goldstein, 2006; LaPointe et al., 2009; Morfini et al., 2009; Kanaan et al., 2011). Early FAT defects occur prior to overt morphological decline and cell death (Goldstein, 2012). Vesicular trafficking of BDNF is impaired independent of tau, in the absence of cytoskeletal collapse and excitotoxic cell death (Ramser et al., 2013).

Neurons cultured from AD mice expressing mutations in APP or β- and γ-secretase complexes display FAT defects that precede amyloid plaque deposition and extensive NFT formation (Pigino et al., 2003; Lazarov et al., 2007; Stokin et al., 2008; Rodrigues et al., 2012). These findings are corroborated *in vivo* by manganese-enhanced magnetic resonance imaging of FAT (Minoshima and Cross, 2008; Gallagher et al., 2012). Furthermore, genetic reduction of kinesin-1 enhances formation of axonal swellings, increases Aβ production, and promotes its intracellular accumulation (Stokin et al., 2005). This critical finding implies that early FAT defects can induce Aβ toxicity. Recently, a novel, unbiased genetic screen identified KLC1 splice variant E (KLC1vE) as a modifier of Aβ accumulation in mice (Morihara et al., 2014). Expression levels of KLC1vE were significantly higher in AD patients than in unaffected individuals. These results also suggest that intracellular trafficking is causal in AD.

1.3. Ca^{2+} dysregulation in Alzheimer's disease

1.3.1. Physiological roles and mechanisms of Ca^{2+} signaling

Ca^{2+} is one of the most important second messengers in the nervous system, and its diverse signal transduction pathways mediate many fundamental cellular processes: membrane potential and excitability, neurotransmitter release, ATP production, memory formation and loss, cell proliferation, and cell death (Berridge, 2012; Kandel et al., 2013). Neurons use a variety of channels to regulate intracellular Ca^{2+} in a versatile, yet precise spatiotemporal manner. These channels are located either in the plasma membrane or on various organelles. Of relevance to this work, influx of extracellular Ca^{2+} is maintained by NMDARs, AMPARs, and voltage-gated Ca^{2+} channels. Ca^{2+} efflux from intracellular stores, such as the ER network, occurs through ryanodine receptors (RyRs) and inositol triphosphate receptors (IP3Rs) (Hamilton, 2005; Foskett et al., 2007). These channels are activated by Ca^{2+}, enabling them to excite each other and generate Ca^{2+} waves during the amplification and propagation of Ca^{2+} signals. Neurons express a large number of Ca^{2+} binding proteins that function as buffers, both in the cytoplasm (calbindin, calretinin, and parvalbumin) and within the ER lumen (calreticuin and calsequestrin) (Schwaller, 2009). The spatial and temporal

properties of Ca^{2+} signals are shaped by their rapid binding to these cytosolic buffers. The ER buffers enable accumulation of large amounts of Ca^{2+} necessary for rapid cell signaling. Mitochondria also act as cytosolic buffers by taking up excess Ca^{2+} through the mitochondrial Ca^{2+} uniporter (Baughman et al., 2011; De Stefani et al., 2011). Ca^{2+} uptake stimulates oxidative processes that produce ATP and can also generate reactive oxygen species (ROS), which contributes to the redox signaling pathway. In spite of these exquisite regulatory mechanisms, neurons are highly susceptible to drastic changes in Ca^{2+} concentration: insufficient Ca^{2+} impairs synaptic function, whereas excessive Ca^{2+} causes cell death (Berridge et al., 1998). Such fluctuations can be detrimental over the lifetime of a neuron (Khachaturian, 1989).

1.3.2. The Ca^{2+} hypothesis of Alzheimer's disease

The Ca^{2+} hypothesis of Alzheimer's disease, proposed by Khachaturian (1989) and further developed by Berridge (2010), states that sustained perturbations in intracellular Ca^{2+} homeostasis are a proximal cause of neurodegeneration in AD. Activation of the amyloidogenic pathway remodels neuronal Ca^{2+} signaling pathways responsible for cognition by enhancing the entry of extracellular Ca^{2+} and the release of internal Ca^{2+} (Figure 1.5). Indeed, resting Ca^{2+} levels in cortical neurons from 3xTg-AD mice are twice that found in non-Tg controls (Lopez et al., 2008), and early changes in cytosolic Ca^{2+} regulation are commonly observed in AD patients (Emilsson et al., 2006; Stutzmann et al., 2007; Bezprozvanny and Mattson, 2008). In apparent contradiction, resting Ca^{2+} levels in cortical neurons from Tg APP/PSEN1 mice are elevated only within a small fraction of dendritic spines located near amyloid-β deposits (Kuchibhotla et al., 2008; Chakroborty et al., 2012). This supports the notion that Aβ plaques do not contribute significantly to Ca^{2+}-induced neurotoxicity. Rather, sustained Ca^{2+} elevation may be induced by accumulation of diffusible extracellular and/or intracellular AβOs and excessive Ca^{2+} leakage through RyRs (see Sections 1.3.3 and 1.3.4). These processes may be exacerbated by normal aging. Ca^{2+} dysregulation underlies many diagnostic features, genetic mutations, and risk factors associated with AD (Chakroborty and Stutzmann, 2011; Berridge, 2013). Importantly, it often precedes detectable Aβ deposition and NFT formation and is thus implicated in early AD pathogenesis (Cheung et al., 2008; Chakroborty et al., 2009; Zhang et al., 2009; Chong et al., 2011).

1.3.3. AβOs facilitate Ca^{2+} influx through channels and pores in the plasma membrane

It is widely accepted that treatment of cultured neurons with AβOs triggers unregulated Ca^{2+} influx through the plasma membrane (Khachaturian, 1987; Demuro et al., 2005). This is largely mediated by direct or indirect interactions between AβOs and endogenous Ca^{2+} channels, including NMDARs and voltage-gated Ca^{2+} channels (VGCCs), or by insertion of AβOs into the plasma membrane to form non-selective, high conductance cation pores. NMDARs are highly permeable to Ca^{2+} (Garaschuk et al., 1996). AβOs impair neuronal function in cognitive regions of the brain, where NMDARs are the principal mediators of excitotoxicity and apoptosis during disease progression (Hardingham, 2009). Acute AβO exposure increases NMDAR-mediated Ca^{2+} influx (De Felice et al., 2007), leading to increased ROS production and aberrant calpain activation (Kelly and Ferreira, 2006). Chronic AβO exposure reduces NMDAR cell-surface expression, Ca^{2+} influx, and glutamatergic currents (Snyder et al., 2005; Shankar et al., 2008). These effects result in loss of spine density, reduced AMPAR currents, and impaired synaptic plasticity (Li et al., 2009; Ferreira and Klein, 2011). At presynaptic terminals, N and P/Q-type VGCCs mediate the release of neurotransmitters upon arrival of an action potential. Modulation of these channels is highly dependent on the nature of the AβO preparation, length of exposure, and model system employed (Ramsden et al., 2002). In cultured cerebellar granule cells and cortical neurons, AβOs markedly increase VGCC Ca^{2+} currents after 24 h of treatment. Blocking N-type currents with conotoxin GVIA prevents this increase, indicating AβO-mediated facilitation of Ca^{2+} entry. Inhibition of dendritic L-type currents does not reverse this facilitation (Price et al., 1998; MacManus et al., 2000). Conversely, a stable AβO globulomer preparation decreases the isolated P/Q-type Ca^{2+} current in cultured hippocampal neurons, but an increase observed upon expression of these channels in *Xenopus* oocytes (Mezler et al., 2012). Treatment with antagonists rectifies Ca^{2+} influx and protects against Aβ-induced toxicity.

AβOs can also incorporate into the plasma membrane and reorganize to form non-selective, high conductance cation pores (Arispe et al., 1993; Lin et al., 2001; Quist et al., 2005). Leakage of sodium, potassium, and Ca^{2+} ions through such pores could rapidly perturb cellular homeostasis. The existence of AβO pores is supported by

studies employing atomic force microscopy, electron microscopy, and theoretical modeling (Chakroborty and Stutzmann, 2014). High resolution transmission electron microscopy TEM revealed distribution of AβO pores in the plasma membrane of post-mortem brains of AD patients, but not in healthy patients (Inoue, 2008). Recent studies with mutant Aβ peptides enabled identification of key residues involved in cholesterol binding and pore formation; cholesterol promoted insertion of Aβs into the plasma membrane, induced formation of α-helical structures, and forced the peptide to adopt a tilted topology that favoured oligomerization. Pore formation is prevented by pharmacologically outcompeting cholesterol binding to Aβ (Di Scala et al., 2014).

1.3.4. AβOs promote Ca^{2+} leakage from the ER

ER Ca^{2+} signaling is compromised in AD and impairs synaptic plasticity (Fitzjohn and Collingridge, 2002; Bardo et al., 2006). Dysregulated Ca^{2+} efflux is mediated by mutant forms of presenilin and modulation of IP3R and RyR activity by AβOs. Mutations in the *PSEN1* and *PSEN2* genes that encode presenilin, a catalytic subunit of the γ-secretase complex, result in familial AD (FAD). These FAD mutations elevate γ-secretase activity, increasing Aβ production and independently perturbing intracellular Ca^{2+} signaling (Bezprozvanny, 2013; Wu et al., 2013). Wild type presenilin functions as an ER Ca^{2+} leak channel (Tu et al., 2006), which maintains ER Ca^{2+} homeostasis by constantly leaking Ca^{2+} into the cytosol and balancing SERCA pump activity. FAD mutations disrupt this leak function, leading to overfilling of the ER and exaggerated Ca^{2+} efflux in PS1/PS2 mutant fibroblasts (Tu et al., 2006; Nelson et al., 2007) and cultured hippocampal neurons from 3xTg-AD neurons (Zhang et al., 2010). Recently, an unbiased RNAi screen for Ca^{2+} homeostasis modulators identified an essential role for presenilins in mediating ER Ca^{2+} leakage (Bandara et al., 2013; Bezprozvanny, 2013), corroborating those findings. Furthermore, *PSEN1* mutations enhance IP3-mediated liberation of Ca^{2+} in cortical neurons (Stutzmann et al., 2004). AβOs injected into *Xenopus* oocytes induce local transients and global Ca^{2+} waves that are suppressed by IP3R antagonists; additionally, stimulation of IP3 production leads to excitotoxic Ca^{2+} liberation from the ER by intracellular AβOs (Demuro and Parker, 2013). ER Ca^{2+} leakage also occurs through RyRs, which are activated by cytosolic Ca^{2+} and amplified by regenerative Ca^{2+}-induced-Ca^{2+}-release (CICR) (Finch et al., 1991). NMDAR-

mediated Ca^{2+} influx drives aberrant RyR activation in dendrites of young AD mice (Goussakov et al., 2010), and enhanced CICR disrupts synaptic transmission, long-term plasticity, and memory performance (Adasme et al., 2011; Oules et al., 2012; Baker et al., 2013). Elevated expression of RyR and increased Ca^{2+} efflux are described in AD patients (Kelliher et al., 1999) and presymptomatic AD mice (Stutzmann et al., 2006; Chakroborty et al., 2009; Zhang et al., 2010). Presumably, these effects serve as a compensatory mechanism to stabilize pre-existing synaptic deficits and normalize the depressed synaptic network (Supnet and Bezprozvanny, 2010; Chakroborty and Stutzmann, 2014).

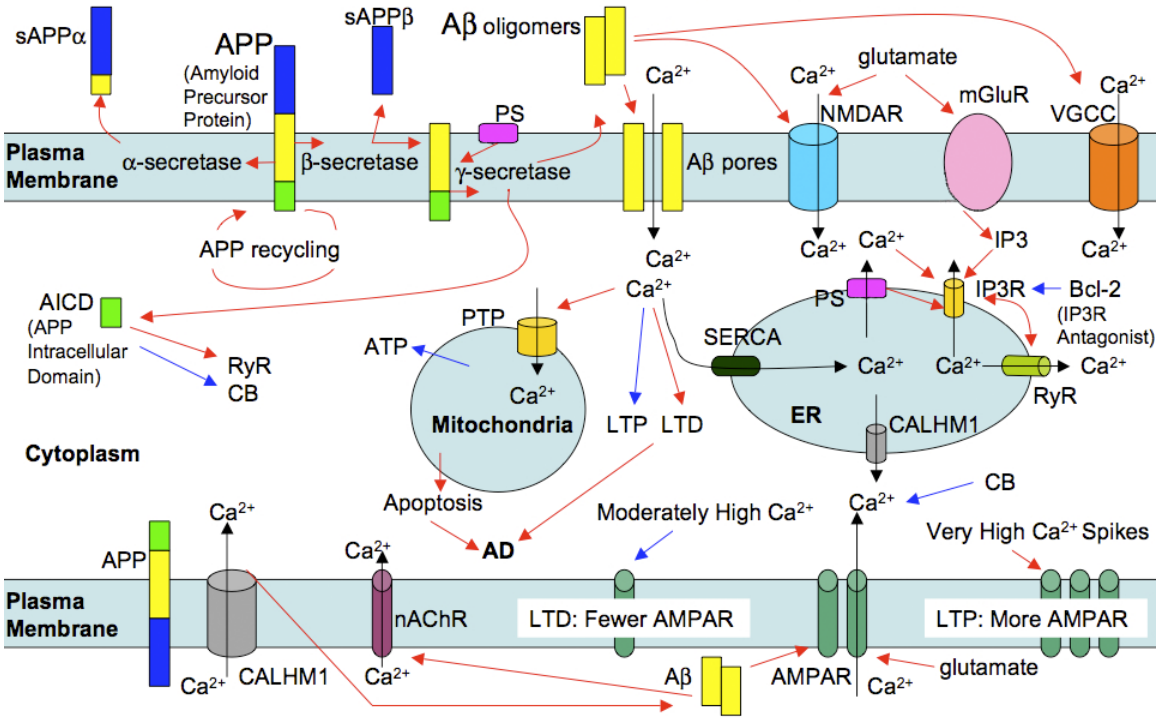

Figure 1.5 Ca^{2+} dysregulation in Alzheimer's disease

Activation of the amyloidogenic pathway remodels neuronal Ca^{2+} signaling pathways responsible for cognition by enhancing the entry of extracellular Ca^{2+} and the release of internal Ca^{2+}. AβOs facilitate Ca^{2+} influx through NMDARs, AMPARs, VGCCs, and cation pores in the plasma membrane. Ca^{2+}-induced-Ca^{2+} release promotes Ca^{2+} leakage from the ER through RyRs and IP3Rs. Mutations in the *PSEN1* and *PSEN2* genes that encode presenilin, a catalytic subunit of the γ-secretase complex, exaggerate Ca^{2+} efflux through these leak channels. These effects result in loss of spine density, reduced AMPAR currents, and impaired synaptic plasticity. Modified and reproduced with permission from Dr. Ghanim Ullah, University of South Florida.

1.3.5. A vicious cycle of Ca^{2+} dysregulation and Aβ generation drives cellular toxicity in AD

Many studies have demonstrated a bidirectional relationship between Ca^{2+} signaling and the amyloidogenic pathway (Green and LaFerla, 2008). As discussed previously, Aβ remodels neuronal Ca^{2+} signaling pathways by enhancing the entry of extracellular Ca^{2+} and the release of internal Ca^{2+}. On the other hand, age-associated changes in Ca^{2+} concentrations and dynamics can alter Aβ production in sporadic AD. *In vitro*, Ca^{2+} stimulates the formation of $Aβ_{1-40.}$ These peptides preferentially oligomerize, similar to mutant Aβ peptides associated with early-onset AD in the presence or absence of Ca^{2+} (Itkin et al., 2011). Elevated cytosolic Ca^{2+} increases Aβ generation (Querfurth and Selkoe, 1994) and induces transient phosphorylation of APP, which promotes further intracellular Aβ production (Pierrot et al., 2006). A vicious cycle of Ca^{2+} dysregulation and Aβ generation may impair synaptic morphology and function, trigger ER and mitochondrial stress responses, and activate calpain and caspase signaling cascades that culminate in excitotoxic cell death (Demuro et al., 2010). Ultimately, these events lead to extensive neurodegeneration and cognitive decline.

1.4. Calcineurin signaling in Alzheimer's disease

1.4.1. Structure and regulation of calcineurin

Calcineurin (CaN), also known as protein phosphatase 2B (PP2B) is a Ca^{2+}-dependent serine/threonine phosphatase that is highly expressed in the central nervous system. CaN is a heteromeric protein comprised of a catalytic subunit (CaNA) and a regulatory subunit (CaNB) (Klee et al., 1979). Among related phosphatases (PP1, PP2A), CaN is uniquely activated by cytosolic calmodulin (CaM) (Rusnak and Mertz, 2000). Ca^{2+} binding to CaNB induces a conformational change in CaNA, which exposes the CaM binding site (Yang and Klee, 2000). Ca^{2+}-CaM then activates CaN by displacing the autoinhibitory domain from the catalytic domain (Shen et al., 2008). CaN has a high affinity for Ca^{2+} and is activated by nanomolar concentrations (Cohen and Klee, 1988). CaN is non-competitively inhibited by the immunosuppressants cyclosporine A and FK506, when they are bound to their respective immunophilins,

cyclophilin A and FKBP12 (Liu et al., 1991). These compounds have enabled widespread investigation of CaN in healthy and diseases neurons.

1.4.2. Physiological roles of calcineurin in neurotransmission and synaptic plasticity

In neurons, CaN is present in the cell body and processes (Sola et al., 1999) and is particularly enriched in synaptic terminals (Kuno et al., 1992). Different binding partners restrict CaN to distinct subcellular compartments, such as nuclear factor of activated T-cells (NFAT) in the nucleus (Luo et al., 1996) and A-kinase anchor protein (AKAP) scaffolds in dendrites (Coghlan et al., 1995). Depending on local substrates, each subcellular pool of CaN regulates different processes, such as gene transcription, neurotransmission and synaptic plasticity (Groth et al., 2003). The latter two processes will be described here in detail. Presynaptic CaN regulates neurotransmission by dephosphorylating synapsin-1 to reduce exocytotic release of glutamate (Jovanovic et al., 2001). Phosphorylated synapsin-1 tethers neurotransmitter-containing vesicles to the cytoskeleton and enables movement of vesicles out of the reserve pool. At the postsynaptic membrane, CaN dephosphorylates NMDARs and impedes Ca^{2+} influx, effectively desensitizing these receptors to presynaptic stimuli (Lieberman and Mody, 1994). Importantly, CaN also regulates synaptic plasticity, the cellular basis for learning and memory. During LTP, high-frequency stimuli lead to a persistent increase in synaptic strength. After initial membrane depolarization and Ca^{2+} influx through NMDARs, Ca^{2+}-CaM activates downstream kinases (Ca^{2+}/calmodulin-dependent kinase II, CaMKII) and phosphatases (CaN) that regulate ion channel phosphorylation and insertion. CaM is more likely to activate CaN or CaMKII depending on the local Ca^{2+} concentration. Intense, confined transients result in preferential activation of CaMKII; however, as Ca^{2+} decreases, but before it returns to baseline, CaM is more likely to bind and activate CaN (Stefan et al., 2008). Of importance to this work, CaN directly inactivates inhibitor-1 by dephosphorylation at Thr-35. By this mechanism, CaN relieves inhibition of PP1 (Shenolikar and Nairn, 1991; Mulkey et al., 1994) and activates GSK3β to mediate LTD (Peineau et al., 2007), a decrease in synaptic efficacy that is essential for efficient memory storage. This system allows for bidirectional plasticity, where a shift in Ca^{2+} levels mediates a switch between synapse growth (positive) and synapse

pruning (negative). CaN mediates synapse pruning by a number of mechanisms, including NMDAR and AMPAR endocytosis, destabilization of actin in spines, and spine retraction (Baumgartel and Mansuy, 2012).

1.4.3. Pathogenic roles of calcineurin

Due to its compromised ability to regulate intracellular Ca^{2+} levels, the aging brain is susceptible to overactivation of CaN and aberrant downstream signaling. AβOs exacerbate CaN overactivation in models of AD, and *in vitro, ex vivo,* and *in vivo* studies illustrate how dephosphorylation of CaN substrates impacts ion channel activity, synaptic integrity, and cell death. In rat hippocampal slices, AβOs activate CaN and thereby counteract increases in AMPAR phosphorylation that occur upon LTP induction (Zhao et al., 2004; Dineley et al., 2010). In addition to impairing LTP, CaN overactivation in hippocampal slice cultures and in aged double transgenic AD mice (APP/PS1) facilitates LTD, reduces spine density, simplifies dendritic branching, and induces neuritic beading and dystrophies (Shankar et al., 2007; Wu et al., 2010). FK506 treatment prevents all those deleterious effects and strikingly restores associative learning and memory in adult APP mice (Dineley et al., 2007). Furthermore, CaN mediates Aβ-induced cellular toxicity. CaN dephosphorylates the Bcl-2-associated death promoter protein (pBAD), which enables it to dissociate from scaffolding proteins, translocate to the mitochondria, and form pro-apoptotic dimers with Bcl-X (Wang et al., 1999). This triggers cytochrome c release and initiates programmed cell death. In cortical neurons, these effects are attenuated by FK506 (Almeida et al., 2004). Although many reports implicate CaN in AβO-induced synapse failure and cell death, a role for CaN in AD-related transport impairment has not been investigated. As described previously, activated CaN relieves inhibition of PP1, which activates GSK3β. This suggests that CaN may instigate phosphorylation-dependent inhibition of motor-cargo interactions and/or motor protein activation.

1.5. Phosphorylation-dependent mechanisms of transport impairment

Several kinases impair motor protein activity and/or cargo binding in AD. JNK3, casein kinase 2 (CK2) and p38β inhibit retrograde FAT in isolated squid axoplasm; however, the molecular mechanisms by which these kinases inhibit dynein-based motility are undefined (Pigino et al., 2009; Morel et al., 2012; Kanaan et al., 2013). Kinesin-based transport is disrupted by GSK3β, JNK, CK2 and cyclin-dependent kinase 5 (Cdk5). First, GSK3β is implicated in many aspects of AD pathogenesis (Medina and Avila, 2014). As a negative regulator of axonal transport in *Drosophila*, GSK3β phosphorylates and reduces the number of motors that are bound to microtubules (Weaver et al., 2013). A second mechanism may involve disruption of motor protein-cargo binding. Phosphorylation of kinesin light chain-1 (KLC1) by PP1-GSK3β signaling dissociates KIF5 from vesicular cargoes in a squid axoplasm model of AD (Morfini et al., 2002). It is possible that activation of CaN leads to GSK3β-mediated impairment of axonal transport by similar mechanisms. Second, JNK plays several roles in regulating transport. JNK inhibitors prevent AβO-induced impairment of dense core vesicle and mitochondria trafficking in hippocampal neurons (Bomfim et al., 2012). The activated JNK pathway functions as a kinesin-cargo dissociation factor (Horiuchi et al., 2007). Additionally, mutations in the JNK-dependent phosphorylation site S421 in JIP1 alter both KHC activation *in vitro* and directionality of APP transport in neurons (Fu and Holzbaur, 2013). Third, CK2 activation disrupts transport in squid axoplasm (Pigino et al., 2009); however, it remains unclear whether CK2 is aberrantly activated or inhibited in AD (Perez et al., 2011). Finally, overactivated Cdk5 and hyperphosphorylation of neurofilaments perturbs their association with kinesin and impairs transport (Lee et al., 2011). Phosphorylation-dependent mechanisms of KIF1A dysregulation remain unknown.

1.6. BDNF transport defects mediated by KIF1A impairment may lead to neurodegeneration

BDNF, a neuropeptide transported in DCVs, is required for synaptic maturation and function, development of neuronal circuitry, learning, and memory. Impaired BDNF

transport compromises hippocampal synaptogenesis and learning enhancement, and reduced levels of BDNF correlate with AD progression (Diniz and Teixeira, 2011). Despite the importance of BDNF in neuronal physiology and disease (Lu et al., 2013; Scharfman and Chao, 2013), little is known about motors and associated regulatory mechanisms required for its axonal transport. A body of work, including our study, shows that KIF1A is the primary motor required for BDNF transport (Yonekawa et al., 1998; Barkus et al., 2008; Lo et al., 2011). Although KIF1A is implicated in neurodegenerative diseases (Riviere et al., 2011; Klebe et al., 2012), phosphorylation-dependent mechanisms that govern KIF1A-DCV interactions and KIF1A processivity are unclear, and their contribution to AD pathogenesis has not been investigated.

1.7. Hypothesis and specific objectives

I hypothesize that AβOs perturb BDNF transport through tau-independent Ca^{2+} signaling cascades that alter motor protein activity. The main objective of my thesis is to investigate novel Ca^{2+}-dependent mechanisms of KIF1A dysregulation in a cellular model of AD and determine how they can be prevented or reversed (Figure 1.6).

In Chapter 2, I determine if CaN mediates AβO-induced transport defects independent of tau. Through direct assessment of FAT at high temporal and spatial resolution in living neurons, I demonstrate that AβO-induced defects in axonal BDNF transport persist in the absence of tau, and cannot be attributed to microtubule destabilization or cell death. I combine multiple approaches, including live imaging, *in vitro* phosphatase assays, and immunoblotting, to demonstrate that inhibition of CaN by FK506 completely rescues BDNF transport defects, and that AβOs impair transport by overactivating CaN through non-excitotoxic Ca^{2+} signaling. Collectively, my work implicates CaN in FAT regulation and challenges a requirement for tau in AβO-induced transport disruption in primary neurons.

In Chapter 3, I identify dendritic and axonal mechanisms of Ca^{2+} elevation that regulate the spatiotemporal progression of BDNF transport defects. I show that tau-independent BDNF transport defects in dendrites and axons are induced concomitantly but exhibit different rates of decline: maximal dendritic transport defects precede

maximal impairment of FAT. Using cameleon FRET, proximal ligation assays, and immunohistochemistry, I correlate the spatiotemporal progression of transport defects with Ca^{2+} elevation and CaN activation in dendrites and subsequently in axons. Postsynaptic CaN activation converges on axonal Ca^{2+} dysregulation to impair FAT. The latter may be caused by axonal AβOs, which I observed in both primary neurons and transgenic AD mouse brain. Indeed, AβOs colocalize with axonal voltage-gated Ca^{2+} channels (VGCCs), and pretreatment with VGCC inhibitors prevents axonal, but not dendritic, defects. Finally, BDNF transport defects are reversed upon inhibition of RyRs present in dendritic and axonal ER. This work establishes a novel role for Ca^{2+} dysregulation in BDNF transport disruption and in tau-independent Aβ toxicity.

In Chapter 4, I identify phosphorylation-dependent mechanisms of KIF1A dysregulation. I demonstrate that AβOs impair KIF1A motility independent of tau. Furthermore, I used coimmunoprecipitation, immunoblotting, and tandem mass spectrometry to demonstrate that inhibition of GSK3β prevents KIF1A transport defects, and that aberrant phosphorylation at a conserved GSK3β consensus site within the dimerization domain of KIF1A reduces its motility. My findings implicate GSK3β in phosphorylation-dependent KIF1A dysregulation during early AD pathogenesis.

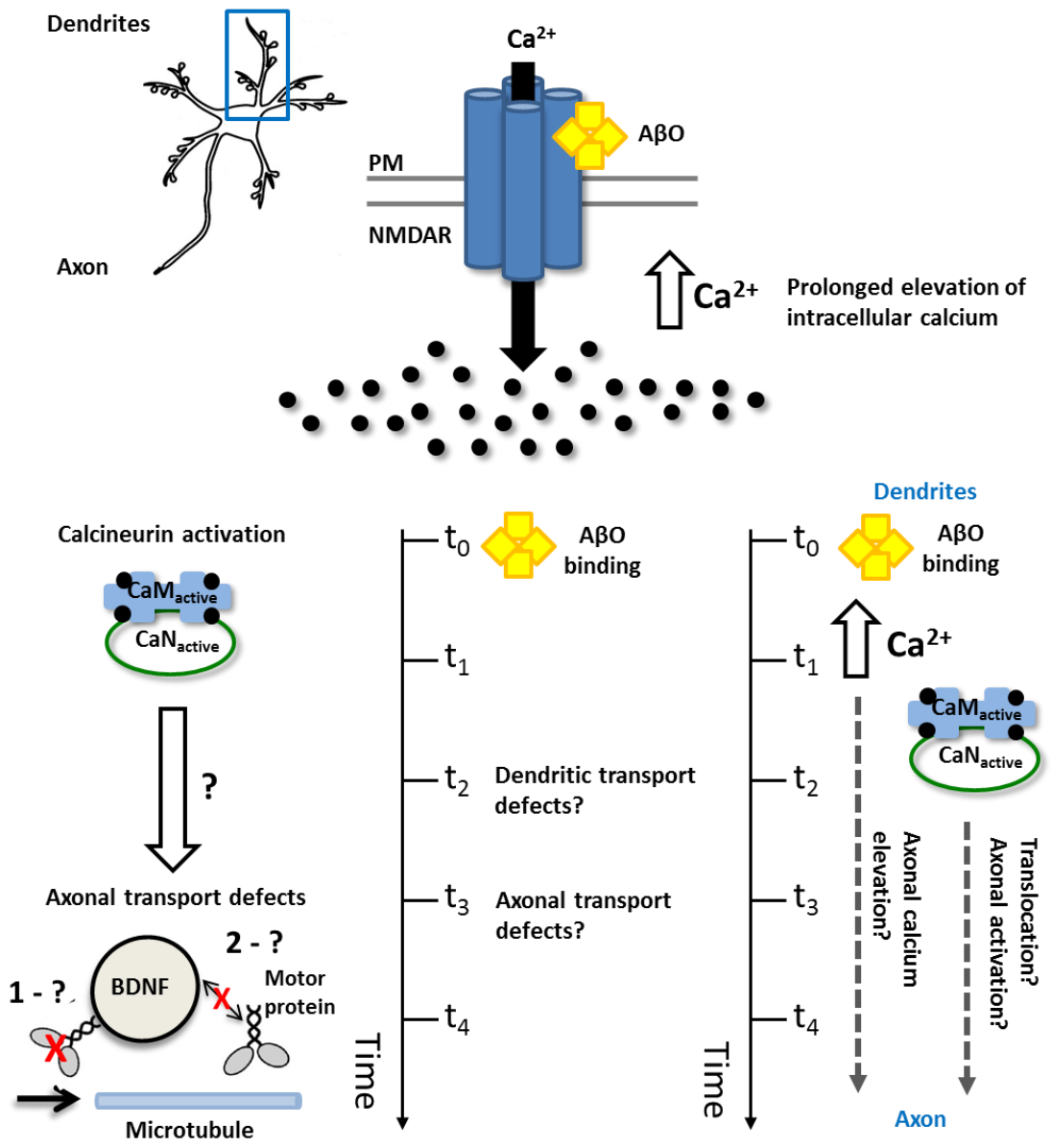

Figure 1.6 Dysregulation of neuronal Ca^{2+} signaling impairs axonal transport independent of tau in a model of Alzheimer's disease

I hypothesize that AβOs perturb BDNF transport through tau-independent Ca^{2+}-signaling cascades that alter motor protein activity. Because CaN, its effectors, and motor proteins associated with DCVs are present in both dendrites and axons, AβOs should induce dendritic, CaN-dependent defects that precede FAT disruption. The spatiotemporal progression of BDNF transport defects may be mediated by concomitant elevations in cytosolic Ca^{2+} and CaN activity.

Chapter 2. Aβ oligomers induce tau-independent disruption of BDNF axonal transport via calcineurin activation in cultured hippocampal neurons[1]

Elisa M. Ramser[1*], Kathlyn J. Gan[2*], Helena Decker[1, 3, 4, †], Emily Y. Fan[1], Matthew M. Suzuki[1], Sergio T. Ferreira[3], and Michael A. Silverman[1, 2, ‡]

[1] Department of Biological Sciences, Simon Fraser University, 8888 University Drive, Burnaby, British Columbia, V5A 1S6, Canada

[2] Department of Molecular Biology and Biochemistry, Simon Fraser University, 8888 University Drive, Burnaby, British Columbia, V5A 1S6, Canada

[3]Institute of Medical Biochemistry, [4] Morphological Sciences Program, Institute of Biomedical Sciences, Federal University of Rio de Janeiro, Rio de Janeiro, RJ 21944-590, Brazil

*** Co-first authors**

E.M.R., K.J.G., and E.Y.F. characterized transport defects in tau$^{-/-}$ neurons. E.M.R. detected tau fragmentation and activation of calpain and caspase-3, assessed tubulin polymerization and modifications by immunoblotting, and investigated the dose and time dependence of AβO-induced transport defects. K.J.G. assessed tubulin modifications by immunocytochemistry, designed and conducted CaN and GSK3β inhibition and transport rescue experiments, and measured CaN activation. E.Y.F. performed the PP1 inhibition and transport rescue experiments. H.D. quantified p-tau and analyzed its spatial distribution by immunocytochemistry. M.M.S. performed the ATP assays and assisted in data analysis of transport. E.M.R. analyzed her data and contributed to writing of the Introduction and Methods sections. K.J.G. analyzed data and wrote the majority of the paper. K.J.G., S.T.F., and M.A.S. interpreted data and revised the paper. M.A.S. conceived and supervised the study.

[1] The following chapter has been published in Molecular Biology of the Cell under the following reference: Ramser EM and Gan KJ et al. (2013) Amyloid-beta oligomers induce tau-independent disruption of BDNF axonal transport via calcineurin activation in cultured hippocampal neurons. MBoC 24:2494-2505.

2.1. Abstract

Disruption of fast axonal transport (FAT) is an early pathological event in Alzheimer's disease (AD). Soluble amyloid-β oligomers (AβOs), increasingly recognized as proximal neurotoxins in AD, impair organelle transport in cultured neurons and transgenic mouse models. AβOs also stimulate hyperphosphorylation of the axonal microtubule-associated protein, tau. However, the role of tau in FAT disruption remains controversial. Here, we show that AβOs reduce vesicular transport of brain-derived neurotrophic factor (BDNF) in hippocampal neurons from both wild type and tau knockout mice, indicating that tau is not required for transport disruption. FAT inhibition is not accompanied by microtubule destabilization or neuronal death. Significantly, inhibition of calcineurin (CaN), a Ca^{2+}-dependent phosphatase implicated in AD pathogenesis, rescues BDNF transport. Moreover, inhibition of protein phosphatase 1 (PP1) and glycogen synthase kinase 3β (GSK3β), downstream targets of CaN, prevents BDNF transport defects induced by AβOs. We further show that AβOs induce CaN activation through non-excitotoxic Ca^{2+} signaling. Results implicate CaN in FAT regulation and demonstrate that tau is not required for AβO-induced BDNF transport disruption.

2.2. Introduction

Fast axonal transport (FAT) is essential for neuronal function and survival. Disruption of FAT is an early pathological event in several neurodegenerative diseases, including amyotrophic lateral sclerosis, Parkinson's disease, and Alzheimer's disease (AD) (Muresan and Muresan, 2009). Amyloid-β oligomers (AβOs), increasingly considered proximal neurotoxins in AD, interact with glutamate receptors at the dendritic membrane, induce abnormal Ca^{2+} influx and oxidative stress, block long-term potentiation (LTP), and facilitate long-term depression, ultimately leading to synapse failure (Benilova et al., 2012). Importantly, AβOs impair FAT in cultured neurons and in AD mouse models (Muresan and Muresan, 2009). Although FAT disruption is implicated in AD pathogenesis, mechanisms underlying this process are poorly understood.

Tau, an axonal microtubule-associated protein, is thought to mediate AβO toxicity and FAT disruption. AβOs induce hyperphosphorylation of tau (p-tau), promoting its dissociation from microtubules and aggregation into neurofibrillary tangles (NFTs) (De Felice et al., 2008). AβOs also induce tau proteolysis by calpains and caspases, generating fragments that aggregate independently of hyperphosphorylation (Reifert et al., 2011). Despite the accumulation of p-tau in affected neurons, it is controversial whether tau is required for AβO toxicity. Tau $^{-/-}$ neurons are resistant to Aβ-induced death (King et al., 2006); by contrast, NFTs persist in viable neurons possessing intact microtubule networks until late-stage AD (Castellani et al., 2008). Recent studies suggest that p-tau inhibits FAT by interacting directly with motor-cargo complexes or initiating aberrant signaling cascades that alter FAT dynamics (LaPointe et al., 2009; Kanaan et al., 2011), and that tau reduction prevents AβO-induced defects in mitochondria and neurotrophin receptor TrkA transport (Vossel et al., 2010). Conversely, axonal transport is not affected by tau overexpression or suppression *in vivo* (Yuan et al., 2008). We previously reported that AβOs block FAT of dense core vesicles (DCV) and mitochondria in cultured neurons through an NMDA receptor (NMDAR)-dependent mechanism that is mediated by a tau kinase, GSK3β (Decker et al., 2010a). Notably, we did not observe concomitant microtubule destabilization, suggesting that the microtubule-binding capacity of tau did not affect transport of these cargoes.

Aberrant Ca^{2+} signaling is implicated in AD (Berridge, 2010b) and may contribute to FAT disruption. AβOs dysregulate Ca^{2+} influx through NMDARs, leading to cytosolic Ca^{2+} elevation and activation of the Ca^{2+}/calmodulin-dependent phosphatase, calcineurin (CaN). Although CaN mediates AβO-induced synapse failure (Reese and Taglialatela, 2011), a role for CaN in FAT regulation has not been investigated. Activated CaN relieves inhibition of protein phosphatase 1 (PP1), which activates GSK3β (Peineau et al., 2007), suggesting that CaN may be involved in FAT disruption.

Here, we show that AβOs impair transport of DCVs containing brain-derived neurotrophic factor (BDNF) in hippocampal neurons from both wild type (tau$^{+/+}$) and tau knockout (tau$^{-/-}$) mice, suggesting that tau is not required for transport disruption. FAT inhibition is not accompanied by microtubule destabilization or cell death. Significantly, AβOs impair BDNF transport by over-activating CaN through non-excitotoxic Ca^{2+}

signaling, and inhibition of CaN rescues transport defects. Furthermore, inhibition of protein phosphatase 1 (PP1) and glycogen synthase kinase 3β (GSK3β), downstream targets of CaN, prevents BDNF transport defects independent of tau. These findings implicate CaN in FAT regulation and challenge the requirement for tau in AβO-induced transport disruption.

2.3. Materials and Methods

2.3.1. Hippocampal cell culture and expression of transgenes

Primary hippocampal neuronal cultures from E16 wild type ($tau^{+/+}$) and tau knockout ($tau^{-/-}$) mice (The Jackson Laboratory) were prepared as described by Kaech and Banker (Kaech and Banker, 2006), and kept in Neurobasal/B27 (Invitrogen) or PNGM primary neuron growth media (Lonza). At 10-12 days *in vitro* (DIV), cells were co-transfected with pβ-actin-BDNF-mRFP and pmUBa-eBFP (received from Gary Banker, Oregon Health and Sciences University, Portland, OR) using Lipofectamine (Invitrogen). Cells expressed the plasmids for 24-36 hours before live imaging. Experiments assessing a role for GSK3β and PP1 utilized the following plasmids and were transfected as above: pcDNA3 HA-GSK3β S9A, pcDNA3 HA-GSK3β K85A (gifts from Jim Woodgett, Addgene plasmids 14754 and 14755), I-2/pCS2 (Addgene plasmid 16317). The absence of tau in $tau^{-/-}$ mice was confirmed by immunoblotting with the antibodies PHF-1 and tau-46 (Supplemental Figure 1). All experiments with animals were approved by and followed the guidelines set out by the Simon Fraser University Animal Care Committee: Protocol #943-B05.

2.3.2. AβO, FK506, and GSK3β Inhibitor VIII treatments

Soluble, full-length Aβ 1-42 peptides (AβOs; American Peptide) were prepared exactly according to the method of Lambert *et al*. (Lambert et al., 1998) and applied to cells at a final concentration of 500 nM for 18 hours, or 100 nM for up to 72 hours. Following AβO or vehicle exposure, cells were incubated with 1 μM FK506 (Sigma) or

equivalent volumes of vehicle (ethanol) for 1-3 hours prior to imaging of transport. 5 µM GSK3β inhibitor VIII (Calbiochem) was applied to cells prior to AβO exposure.

2.3.3. Live imaging and analysis of BDNF-mRFP transport

BDNF-mRFP transport was analyzed using a standard wide-field fluorescence microscope equipped with a cooled CCD camera and controlled by *MetaMorph* according to Kwinter *et al*. (Kwinter et al., 2009). All imaging, typically 100 frames, was recorded by the "stream acquisition module" in *MetaMorph*. Briefly, cells were sealed in a heated imaging chamber, and streaming recordings were acquired from double transfectants at an exposure time of 250 ms for 90s. This captured dozens of transport events per cell in 100-µm segments of the axon. Axons were initially identified based on morphology and confirmed retrospectively by immunostaining against MAP2, a dendritic cytoskeletal protein. Soluble BFP detection was necessary to determine the orientation of the cell body relative to the axon, and thus to distinguish between anterograde and retrograde transport events. Vesicle flux, velocity, and run lengths were obtained through tracing kymographs in *MetaMorph.* Vesicle flux was defined as the total distance traveled by vesicles standardized by the length and duration of each movie (in micron-minutes): $\frac{\sum_{i=1}^{n} d_i}{\ell \times t}$ where d are the individual DCV run lengths, ℓ is the length of axon imaged and t is the duration of the imaging session. A vesicle was defined as undergoing a directed run if it traveled a distance of ≥2 µm. This distance was determined as a safe estimate of the limit of diffusion based on the assumption that root-mean-squared displacement equals $\sqrt{2Dt}$, where D is the diffusion coefficient (D=0.01 $\mu m^2/s$ for DCVs) and t is the duration of the imaging period (t=50 s) (Abney et al., 1999). A run was defined as terminating if the vesicle was found to remain in the same position for at least 4 consecutive frames. "% flux" represents the flux in treated neurons normalized to controls (100%).

2.3.4. Immunocytochemistry

Neurons were fixed in 4% paraformaldehyde and blocked with 0.5% fish skin gelatin (Kwinter et al., 2009). To confirm AβO binding to dendrites, and to verify visually that AβOs remain oligomeric after 18 h in culture, cells were stained with an Aβ oligomer-specific antibody (NU-4, received from W. L. Klein, Northwestern University; 1:1000) or 6E10 (1:1000; Covance) and anti-MAP2 (1:2000; Millipore). To assess p-tau and tubulin modifications, neurons were stained with anti-p-tau PHF1 (1:300; received from P. Davies, Albert Einstein School of Medicine), anti-p-tau Ser262, Thr 231, Ser 396, Ser 404 (1:300; Sigma-Aldrich; received from D. Vocadlo, Simon Fraser University), anti-acetylated tubulin (1:2000; 6-11B-1, Sigma-Aldrich), anti-detyrosinated tubulin (1:2000; Millipore), or anti-tyrosinated tubulin (1:1000; TUB-1A2, Sigma-Aldrich). The presence of HA-GSK3β and myc-I-2 were confirmed retrospectively by antibody staining against the HA (1:100; Roche) or myc (1:500; Sigma) epitopes. Neurons were then incubated with compatible secondary antibodies conjugated to Cy3 (1:500; Jackson ImmunoResearch Laboratories), Alexa 488 (1:500, Invitrogen), Cy5 (1:500; Jackson ImmunoResearch Laboratories). To quantify tau phosphorylation and tubulin modifications, histograms were generated using *ImageJ* from the fluorescence intensity of each pixel across several images, and the average intensity and standard error of the mean were calculated. Appropriate thresholds were applied to eliminate background signal prior to histogram analysis, as described in De Felice *et al*. (De Felice et al., 2008). Phospo-tau axon gradient staining for each epitope, Ser 396 and Ser 404, was performed and quantified exactly according to Mandell and Banker (Mandell and Banker, 1996).

2.3.5. Immunoblotting

Neurons were treated with vehicle, AβOs and/or FK506 as described above. To induce caspase 3 activation, neurons were treated with 5 μM staurosporine (EMD Millipore). Neurons were lysed in RIPA buffer containing Complete Protease Inhibitor Cocktail (Roche) and Halt Phosphatase Inhibitor Cocktail (Thermo Scientific). Samples (5-10 μg) were resolved on 10-12% SDS-polyacrylamide gels and transferred to PVDF membranes. Membranes were incubated with the following primary antibodies overnight at 4°C: anti-p-tau PHF-1 (1:1000), anti-tau-5 and tau-46 (1:1000; received from C.

Krieger, Simon Fraser University), anti-acetylated tubulin (1:2000), anti-detyrosinated tubulin (1:1000), anti-tyrosinated tubulin (1:1000), anti-phospho-I1 Thr35 (Santa Cruz Biotechnologies; 1:500, pre-adsorbed on adult mouse whole brain homogenate), anti-CaN-A (1:1000; Enzo Life Sciences), anti-alpha II spectrin (1:1000; AA6, Millipore), anti-caspase-3 (1:1000; 8G10, New England Biolabs), and anti-tubulin (1:2000; DM1A, Millipore). Immunoreactive bands were visualized using enhanced chemiluminescent substrate (ECL) (Thermo Scientific) for detection of peroxidase activity from HRP-conjugated antibodies. Densitometric scanning and quantitative analysis were carried out using *ImageJ*.

2.3.6. Biochemical quantification of tubulin

Control and AβO-treated neurons were extracted with PHEM buffer (60 mM PIPES, pH 6.9, 25 mM HEPES, 10 mM EGTA, 2 mM $MgCl_2$, 10 µM Taxol, 0.2% Triton X-100, Protease and Phosphatase inhibitors), a microtubule stabilizing buffer, as described previously (Black et al., 1996). Equal protein amounts of Triton X-soluble and -insoluble fractions were analyzed by immunoblotting using anti-tubulin DM1A (1:2000; Sigma-Aldrich).

2.3.7. *In vitro* phosphatase activity assays

Neurons were treated with vehicle, AβOs and/or FK506 as described above. Total phosphatase activity, CaN activity, and the combined activity of PP1+PP2A were measured using a colorimetric assay based on RII substrate dephosphorylation (Calcineurin Cellular Activity Assay Kit, Calbiochem). Briefly, cells were scraped in lysis buffer, and protein extracts were collected by high-speed centrifugation and desalted using chromatography columns (GE Healthcare). To measure total phosphatase activity, lysates were incubated with RII according to manufacturer's instructions. To discriminate between CaN and PP1+PP2A activity, lysates were additionally incubated with 10 mM EGTA and 500 nM okadaic acid. RII was omitted from a parallel set of reactions to assess background phosphatase activity. Human recombinant calcineurin served as a positive control. Following incubation at 30 ^{o}C for 30 min, reactions were terminated with GREEN colour indicator and developed at room temperature for 30 min.

Absorbance was measured at 620 nm using a Spectramax M2 microplate reader (Molecular Devices), and nanomoles of phosphate released were determined from a standard curve. CaN activity was calculated by subtracting phosphatase activity in the presence of EGTA from total phosphatase activity. Similarly, PP1+PP2A activity was calculated by subtracting phosphatase activity in the presence of okadaic acid from total phosphatase activity.

2.3.8. ATP assay

ATP levels in control and AβO-treated neurons were assessed by luciferase-based detection of ATP, according to the manufacturer's protocol (CellTiter-Glo Luminescent Cell Viability Assay, Promega). Following vehicle and AβO exposures, neurons were washed briefly in PBS. Neurons were incubated in 200 µl of CellTiter-Glo luminescent reagent and 200 µl of PBS for 10 min at room temperature. Luminescence was measured using a microplate reader (Molecular Devices).

2.3.9. Statistical analyses

Statistical analyses were performed using *Microsoft Excel* or *GraphPad Prism*. Data are presented as mean ± SEM. Significant differences between treatments were analyzed by *t*-tests with equal or unequal variance at a 95% confidence interval. For live imaging experiments, a minimum of 15 cells from 3 independent cultures (n=3) were analyzed. For immunoblots, *in vitro* phosphatase assays, and ATP assays, neuronal lysates from at least 3 independent cultures were analyzed. To determine the strength of relationship between velocity and run length the Spearman's rank correlation coefficient was calculated. Spearman's correlation coefficient r between 0.3 and 0.5 indicates a moderate to low correlation between the two variables.

2.4. Results

2.4.1. AβO-induced disruption of axonal transport is not accompanied by tau hyperphosphorylation at microtubule binding sites, spatial redistribution, or fragmentation

AβOs induce tau hyperphosphorylation (p-tau) (De Felice et al., 2008), which may inhibit FAT by destabilizing microtubules. To determine whether p-tau correlates with transport disruption in cultured hippocampal neurons (Decker et al., 2010a), we assessed tau phosphorylation at Ser396 and Ser404, residues that are characteristically hyperphosphorylated in AD, and at Thr231 and Ser262, located in the microtubule binding domain of tau, by semi-quantitative immunocytochemistry and immunoblotting. In agreement with previous results for the AD-related epitope PHF-1 (Ser396/Ser404) (De Felice et al., 2008), we found a two-fold increase in p-tau at Ser396 and Ser404 after 4 h of exposure to 500 nM AβOs (Figure 2.1 A). It is noteworthy, however, that no perturbation of axonal transport was detected within this timeframe (Decker et al., 2010a). After 18 h of exposure to AβOs, when transport is markedly reduced (Decker et al., 2010a), a three to five-fold increase in p-tau (at the Ser396 and Ser404 residues) was observed (Figure 2.1 A), similar to PHF-1. Interestingly, however, p-tau at Thr231 and Ser262 showed no differences between AβO-treated and control neurons (Figure 2.1 A), suggesting that the association of tau with microtubules was unaffected. Total tau protein levels were also unchanged by AβO treatment (Figure 2.1 A). These results show that AβOs do not induce tau phosphorylation at residues associated with microtubule binding during the timeframe in which the transport defect is initiated.

To further assess axonal cytoskeletal integrity and its potential role in transport disruption induced by AβOs, we evaluated the proximo-distal gradient of p-tau, important for axonal development and function (Mandell and Banker, 1996). Excessive phosphorylation of tau and its subsequent detachment from microtubules may perturb this gradient and impair transport (Dixit et al., 2008). To determine the spatial distribution of axonal p-tau, we used an approach that extracts soluble tau while stabilizing tau associated with microtubules (Mandell and Banker, 1996). Semi-quantitative immunocytochemistry revealed no changes in the Ser396 or the Ser404 p-tau gradient after 18 h of AβO treatment, compared with control cells (Figure 2.1 B and Supplemental

Figure 1). These findings suggest that changes in tau solubility and association with the axonal cytoskeleton may not contribute significantly to transport impairment.

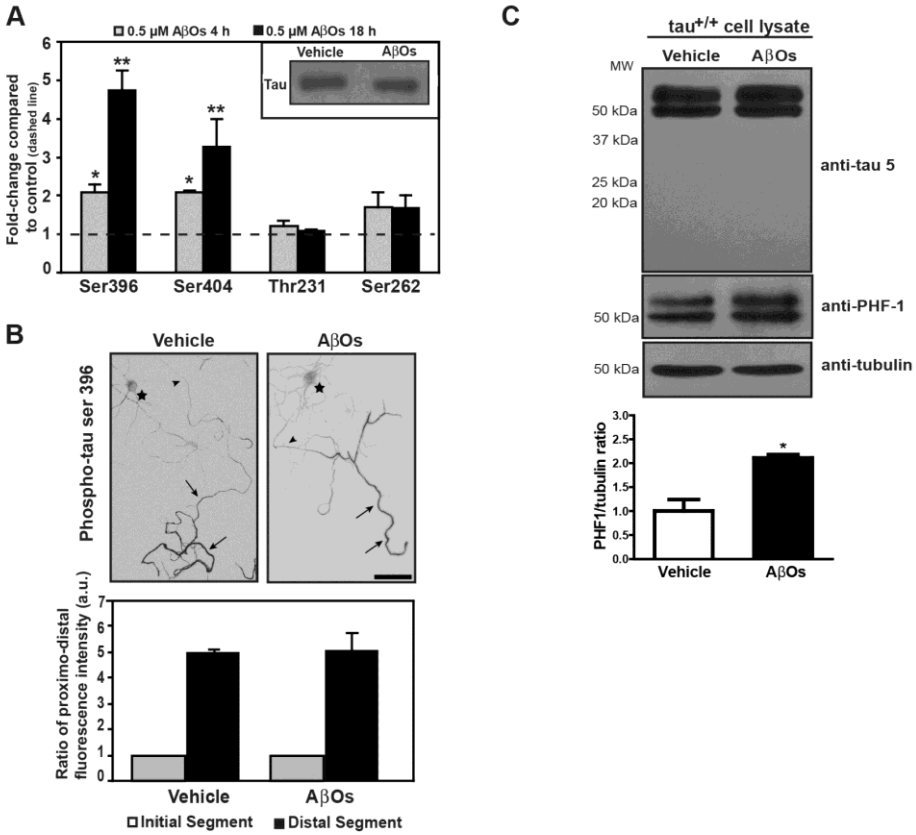

Figure 2.1 AβO-induced disruption of axonal transport is not accompanied by tau hyperphosphorylation at microtubule binding sites, spatial redistribution, or fragmentation.

(A) Quantification of tau hyperphosphorylation (p-tau) immunocytochemistry. After 4 and 18 h, AβOs increase p-tau at AD-related sites (Ser396 and Ser404), but do not elevate p-tau at residues located at the microtubule-binding domain of tau (Thr231and Ser262). Inset: AβOs do not change total tau levels. Graph shows mean ± SEM. A minimum of 24 cells from 3 independent cultures were analyzed per condition; *p < 0.05 and **p<0.005 relative to controls. The dashed line represents the control condition. (B) Representative images of p-tau immunocytochemistry (Ser396). AβOs do not disrupt the spatial gradient of axonal p-tau. A similar staining pattern was observed for Ser404 (Supplemental Figure 1). Star indicates cell body, arrowhead indicates proximal axon, and arrows indicate distal axon. Scale bar = 100 μm. Quantitation of phospho-tau immunofluorescence comparing the ratio of fluorescent signals between initial and distal portions of the axon. A minimum of 14 cells from 2 independent cultures were analyzed per condition a.u. = arbitrary units. (C) AβOs do not induce cleavage of full-length tau (50-70 kDa) and generation of a 17 kDa fragment after 18 h of treatment. Quantification of PHF p-tau in control and AβO-treated neuronal lysates. AβOs induce a two-fold increase in p-tau. Graph shows mean ± SEM from 3 independent cultures.

Independently of phosphorylation, AβOs induce tau fragmentation through activation of calpain and caspases, rendering tau prone to aggregation and potentially contributing to AβO toxicity (Reifert et al., 2011). To determine whether tau fragmentation contributes to AβO-induced transport impairment, we probed control and AβO-treated hippocampal cell lysates for PHF-1 p-tau and total tau. In agreement with immunocytochemistry data (Figure 2.1 A), we detected a two-fold increase in p-tau after 18 h of exposure to AβOs (Figure 2.1 C). However, we did not detect a reduction in full-length tau (50-70 kDa), nor appearance of a 17 kDa tau fragment (Reifert et al., 2011) (Figure 2.1 C). Moreover, calpain and caspase-3, known to induce tau fragmentation, are not activated under our experimental conditions (Supplemental Figure 3). Collectively, these results suggest that p-tau and tau fragmentation do not mediate AβO-induced BDNF transport disruption.

2.4.2. AβOs disrupt BDNF transport independent of tau

Recent studies suggest that tau impairs transport by promoting motor protein dissociation from microtubules (Seitz et al., 2002) or by disrupting motor protein-cargo interactions (Kanaan et al., 2011). To determine if tau is required for AβO-induced FAT disruption, $tau^{+/+}$ and $tau^{-/-}$ neurons expressing BDNF-mRFP, a DCV cargo, were imaged 18 h after exposure to 500 nM AβOs (Figure 2.2 A). Irreversible AβO binding to dendrites was confirmed retrospectively by immunocytochemistry (Figure 2.2 A and Supplemental Figure 4) using an oligomer-specific antibody (NU-4; (Lambert et al., 1998). Representative kymographs illustrate differences between BDNF transport in control (vehicle-treated) and AβO-treated neurons (Figure 2.2 B). Total axonal flux was similarly and markedly reduced by AβOs both in the presence and absence of tau (59% and 62% decrease, respectively; Figures 2.2 B,C and Table 2.1). AβOs also significantly decreased anterograde average velocity by approximately 12% in both $tau^{+/+}$ and $tau^{-/-}$ neurons, while a reduction in anterograde average run length was detected only in AβO-treated $tau^{+/+}$ neurons (18%) (Table 2.1). A correlation between average velocity and run length was not observed (Supplemental Figure 1). Results show that AβOs perturb BDNF transport similarly in $tau^{+/+}$ and $tau^{-/-}$ neurons and suggest that alternative mechanisms regulate transport in the absence of tau.

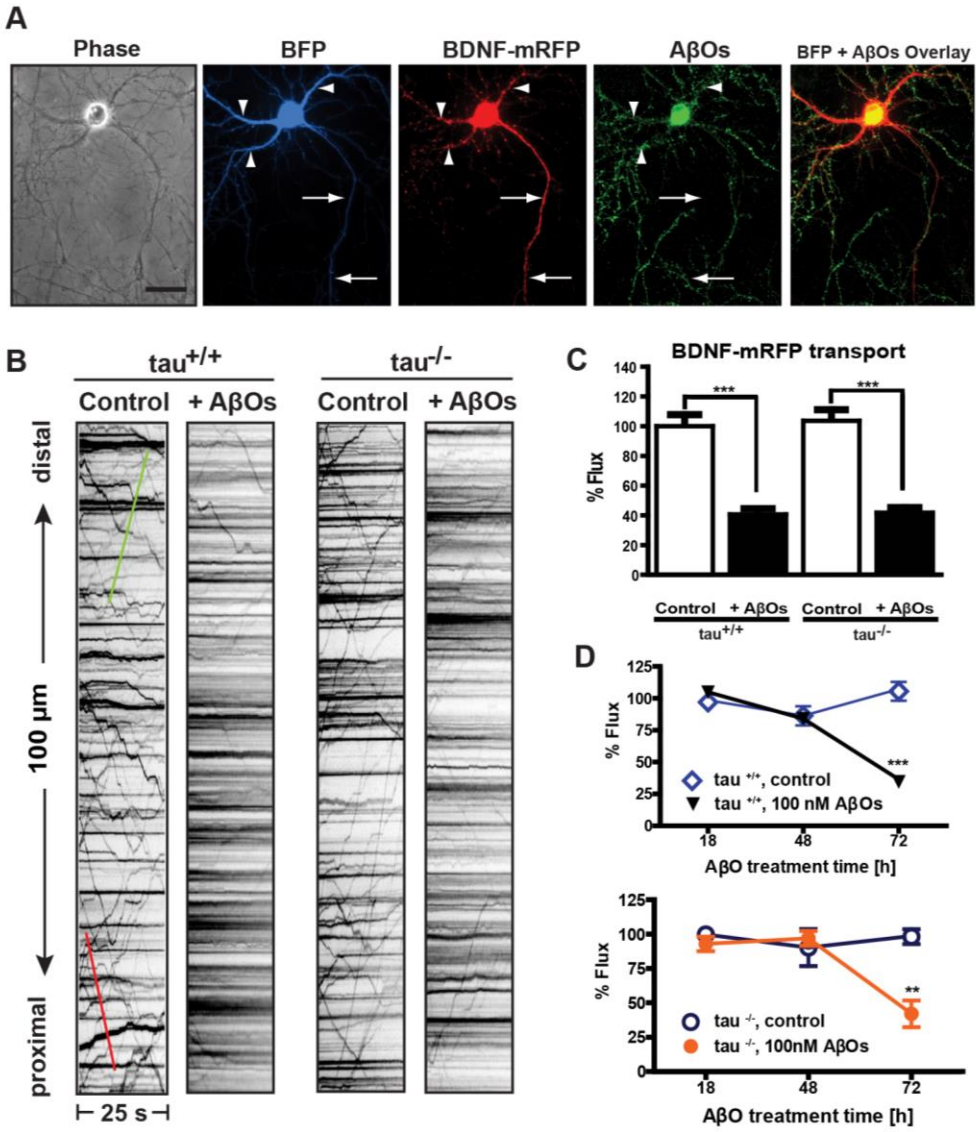

Figure 2.2 Tau is not required for AβO-induced disruption of BDNF transport.

(A) Expression of soluble BFP and BDNF-mRFP in an AβO-treated tau$^{-/-}$ neuron (from left to right). Overlay of BFP and AβO images shows binding of AβOs exclusively to dendrites. Immunocytochemistry shows that AβOs remain oligomeric after 18 h in culture. Arrows indicate axon; arrowheads indicate dendrites. Scale bar = 50 µm (B) Representative kymographs of BDNF transport in control and 500 nM AβO-exposed tau$^{+/+}$ and tau$^{-/-}$ neurons. Green trace indicates anterograde transport; red trace indicates retrograde transport. (C) Effects of 500 nM AβO treatment on BDNF flux. Flux is markedly reduced in both tau$^{+/+}$ and tau$^{-/-}$ neurons treated with AβOs. A minimum of 20 cells from 3 different cultures were analyzed per condition; ***$p < 0.001$ relative to controls. (D) BDNF transport disruption is dose and time dependent. 100 nM AβOs induce significant transport defects by 72 hrs. A minimum of 15 cells from 3 independent cultures were analyzed per condition. Statistical evaluation is presented in Tables 2.1 and 2.2.

2.4.3. AβO-induced disruption of BDNF transport is dose- and time-dependent

Next we investigated whether transport defects are induced by AβOs in a dose- and time-dependent manner. We treated tau$^{+/+}$ and tau$^{-/-}$ neurons with 100 nM AβOs and assessed BDNF transport after 18, 48 and 72 h. Bidirectional transport was markedly reduced in both tau$^{+/+}$ and tau$^{-/-}$ neurons after 72 h of AβO exposure (Figure 2.2 D). Additionally, we found significant reductions in average anterograde and retrograde run lengths in tau$^{+/+}$ and tau$^{-/-}$ neurons (~22% and 23% respectively), along with a significant decrease in average velocity in tau$^{-/-}$ neurons (~15%) (Table 2.2). These results differ from those obtained with 500 nM AβOs at 18 h (e.g., a decrease only in anterograde run length, Table 2.1) suggesting that the selective mechanisms for BDNF transport disruption depend on the conditions of AβO exposure.

2.4.4. BDNF transport defects occur independent of changes in microtubule stability and tubulin post-translational modifications

To verify that tau-independent transport defects do not result from microtubule destabilization, we assessed tubulin stability in control and AβO-treated tau$^{+/+}$ and tau$^{-/-}$ neurons by gently extracting soluble tubulin while stabilizing polymerized tubulin (Black et al., 1996). Immunoblots of these protein fractions revealed no change in the ratio of soluble to polymerized tubulin between control and AβO-treated tau$^{-/-}$ neurons, indicating that AβOs do not induce tubulin depolymerization in the absence of tau (Figure 2.3 A). Similar results were obtained for tau $^{+/+}$ neurons as reported in Decker *et al*. (Decker et al., 2010a). We next examined whether AβOs might alter post-translational tubulin modifications involved in microtubule stability (Henriques et al., 2010) and recruitment or control of motor proteins (Janke and Kneussel, 2010). We compared tubulin acetylation and detyrosination as indicators of microtubule stability. We also assessed levels of tyrosinated tubulin, an indicator of microtubule destabilization (Janke and Kneussel, 2010). AβOs did not alter levels of acetylation, detyrosination, and tyrosination in either control or AβO-treated tau$^{+/+}$ and tau$^{-/-}$ neurons (Figure 2.3 B). Additionally, we evaluated these tubulin modifications by semi-quantitative immunocytochemistry (Figure 2.3 C, D). No significant differences in acetylated tubulin immunofluorescence were observed

between control and AβO-treated tau$^{+/+}$ and tau$^{-/-}$ neurons (Figure 2.3 C, D). Similar results were obtained for detyrosinated and tyrosinated tubulin (Supplemental Figure 2). Together, these findings indicate that tau-independent transport defects do not result from microtubule destabilization and changes in tubulin modifications.

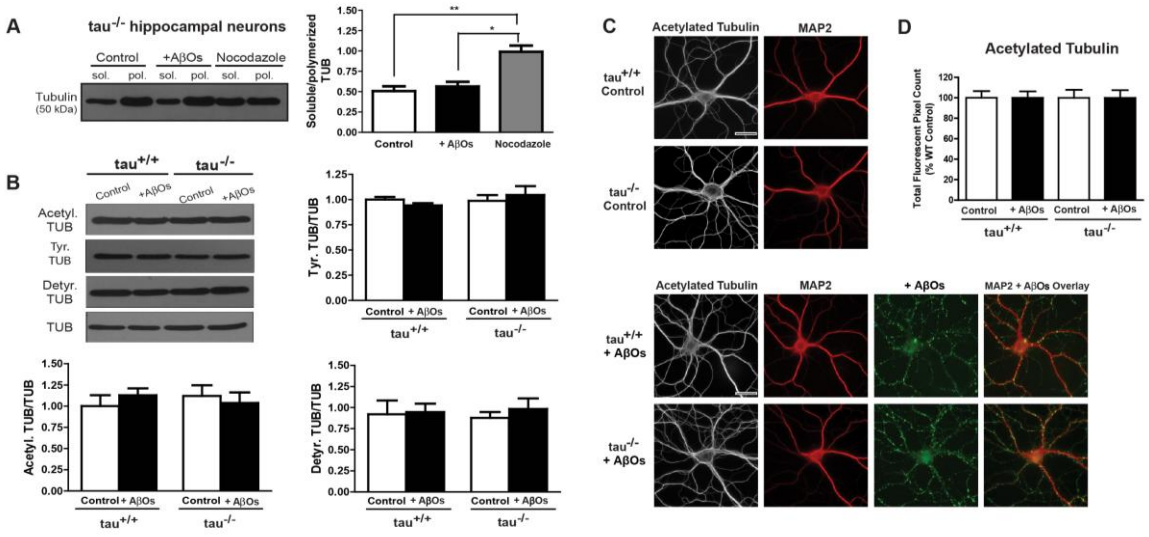

Figure 2.3 BDNF transport defects occur in the absence of changes in microtubule stability and tubulin post-translational modifications.

(A) Immunoblots of tubulin from tau$^{-/-}$ neurons extracted in PHEM buffer. No change in the ratio of soluble to polymerized tubulin between control and AβO-treated neurons was observed. Similar results were obtained for tau$^{+/+}$ neurons (data not shown). (B) Immunoblots of acetylated, tyrosinated, and detyrosinated tubulin. AβOs did not alter levels of these modifications in control and AβO-treated tau$^{+/+}$ and tau$^{-/-}$ neurons. Graphs show means ± SEM from 3 independent cultures. (C and D) Representative images and quantification of acetylated tubulin immunocytochemistry. AβO treatment does not induce significant changes in tubulin acetylation. Graphs show average total fluorescent pixel counts, normalized against the tau$^{+/+}$ control. Error bars represent SEM. A minimum of 20 cells from 3 independent cultures were analyzed per condition. Scale bar = 25 µm.

2.4.5. Calcineurin inhibition rescues AβO-induced transport defects

We have previously shown that AβOs reduce DCV transport through an NMDAR-dependent mechanism, which is mediated by GSK3β (Decker et al., 2010a). Dysregulated Ca^{2+} influx through NMDARs leads to elevation of resting intracellular Ca^{2+} (LaPointe et al., 2009; Demuro et al., 2010) and activation of the Ca^{2+}/calmodulin-dependent phosphatase, calcineurin (CaN) (Reese and Taglialatela, 2011). Activated

CaN relieves inhibition of protein phosphatase 1 (PP1), which in turn activates GSK3β (Peineau et al., 2007). Thus, we investigated whether CaN mediates AβO-induced transport disruption. We exposed tau$^{+/+}$ and tau$^{-/-}$ neurons to 500 nM AβOs for 18 h and subsequently treated them with 1 µM FK506, a highly specific, potent inhibitor of CaN (Schreiber and Crabtree, 1992). Remarkably, inhibition of CaN reversed AβO-induced transport defects in tau$^{+/+}$ and tau$^{-/-}$ neurons within 1 to 3 h of treatment (Figure 2.4). FK506 rescued both anterograde and retrograde flux (Figure 2.4 A-C). Average DCV velocity and run length were also restored to control levels (Table 2.1). These data support a key role for CaN in FAT disruption.

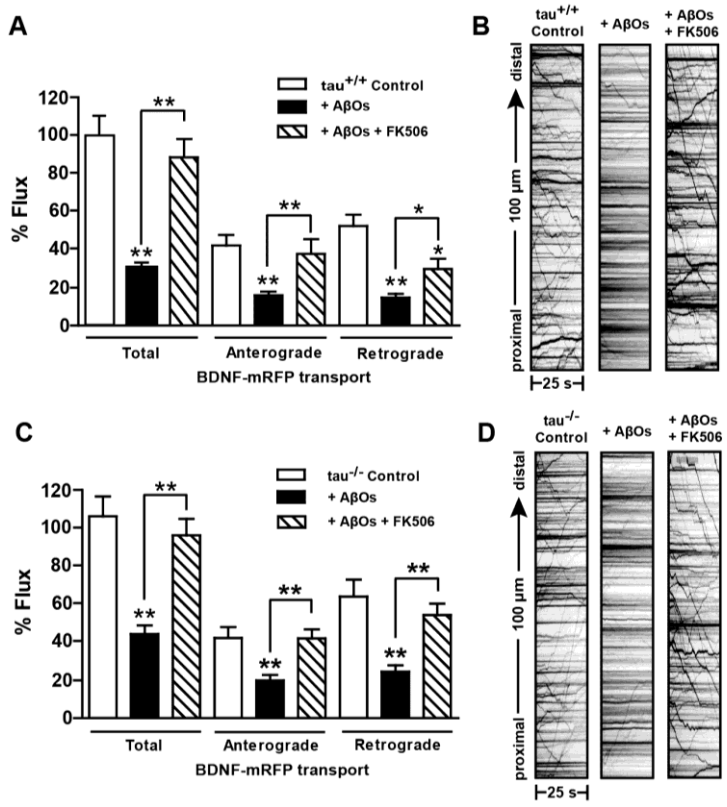

Figure 2.4 Inhibition of calcineurin by FK506 rescues AβO-induced transport defects independently of tau.

(A and B) Effects of AβOs and FK506 treatment on BDNF flux in tau $^{+/+}$ and tau$^{-/-}$ neurons. Flux is markedly reduced in cells treated with AβOs and is restored 1-3 h after treatment with 1 µM FK506. (C and D) Representative kymographs comparing BDNF transport in control and AβO-treated neurons. A minimum of 15 cells from 3 different cultures were analyzed per condition; *0.001<p<0.05, and **p<0.001 relative to controls. Scale bar = 25 µm. Complete statistical evaluation is presented in Table 2.1.

2.4.6. Calcineurin activity and protein phosphatase inhibitor-1 dephosphorylation are elevated by AβOs and normalized by FK506

To determine whether AβO-induced transport disruption involved changes in CaN activity, we employed an *in vitro* phosphatase assay based on colorimetric detection of RII substrate dephosphorylation. We treated $tau^{+/+}$ and $tau^{-/-}$ neurons with AβOs and FK506 and measured total phosphatase activity, CaN activity, and the combined activity of PP1/PP2A in their lysates (Figure 2.5 A, B). Total phosphatase activity was significantly elevated by AβOs (29%), significantly reduced by FK506 alone (55%), and restored to control levels in the presence of both agents (Figure 2.5 A, B). These effects were largely attributed to changes in CaN activity, which followed analogous trends (Figure 2.5 A, B). No significant differences in the combined activities of PP1/PP2A were detected by this method, attesting to RII substrate specificity for CaN. We confirmed these changes in CaN activity and assessed their potential impact on downstream PP1 activity by probing $tau^{+/+}$ and $tau^{-/-}$ neuronal lysates for phospho-inhibitor-1 (I-1) (Figure 2.5 C, D). CaN directly inactivates I-1 by dephosphorylation at Thr35; by this mechanism, CaN relieves inhibition of PP1 (Peineau et al., 2007). In both $tau^{+/+}$ and $tau^{-/-}$ neurons, I-1 phosphorylation was significantly reduced by AβOs (40%), significantly elevated by FK506 alone (100%), and restored to control levels in the presence of both agents (Figure 2.5 C, D). Collectively, these findings demonstrate that AβOs impair BDNF transport by activating CaN and suggest that PP1 is also involved in transport disruption.

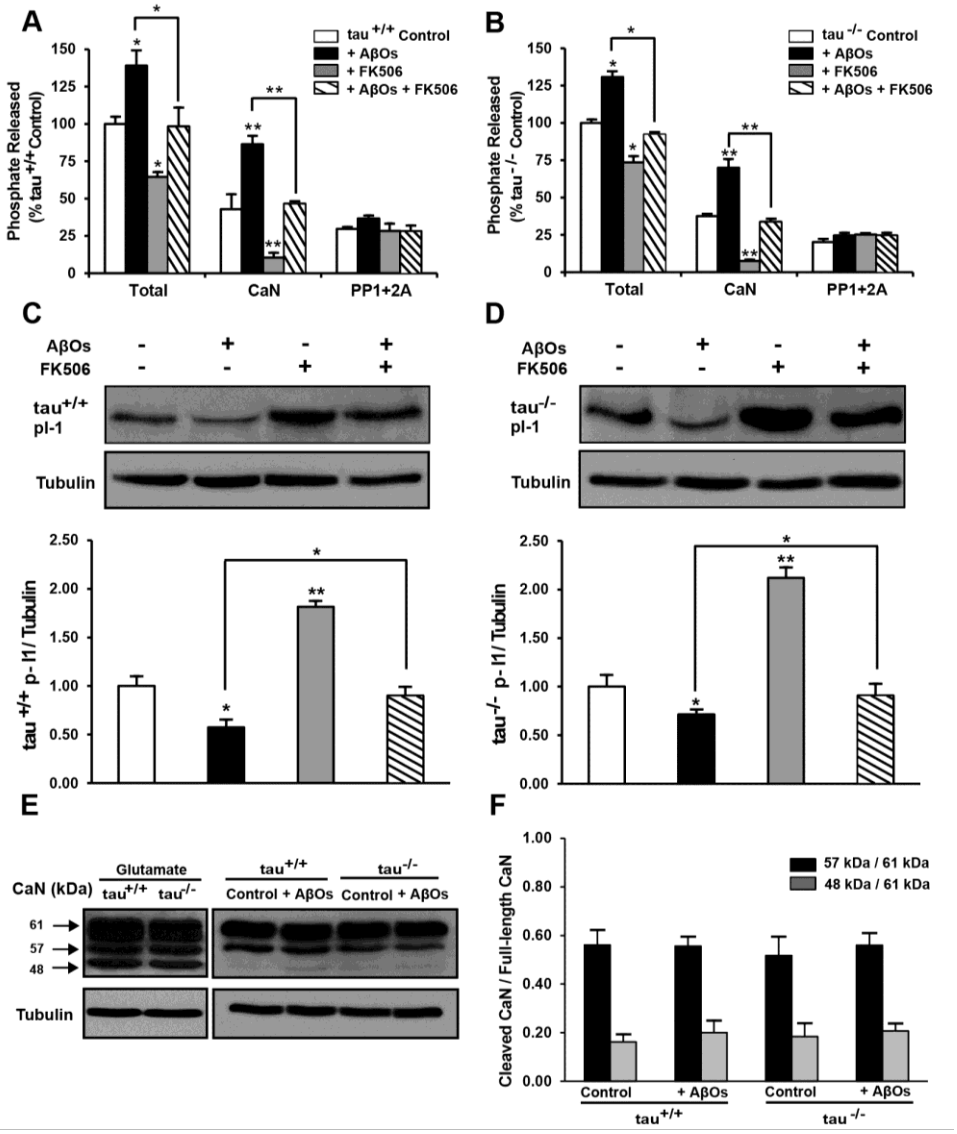

Figure 2.5 Calcineurin activity is elevated by AβOs and normalized by FK506.

(A and B) *In vitro* phosphatase assays on tau$^{+/+}$ and tau$^{-/-}$ primary neuronal lysates. Total phosphatase activity is significantly elevated by AβOs, significantly reduced by FK506 alone, and restored to control levels in the simultaneous presence of both agents. These effects are largely attributed to changes in CaN activity, which follows analogous trends. AβOs do not induce significant changes in the combined activity of PP1+PP2A. (C and D) Protein phosphatase inhibitor-1 (I-1) dephosphorylation in tau$^{+/+}$ and tau$^{-/-}$ neurons. Dephosphorylation of I-1 (29 kDa) is significantly elevated by AβOs, significantly reduced by FK506 alone, and normalized in the presence of both agents. Tubulin immunoblots indicate equal sample loading. (E and F) Calpain-dependent cleavage of calcineurin in tau$^{+/+}$ and tau$^{-/-}$ neurons. No significant differences in the ratios of truncated CaN (57 and 48 kDa) to full-length CaN (61 kDa) are detected between control and AβO-treated neurons. Tubulin immunoblots indicate equal sample loading. Graphs show mean ± SEM from 3 independent cultures; *p<0.05, and **p<0.001 relative to controls.

2.4.7. Inhibition of protein phosphatase-1 and glycogen synthase kinase 3β prevents AβO-induced transport defects

AβOs activate several phosphatases and kinases downstream of CaN, including protein phosphatase-1 (PP1) and glycogen synthase kinase 3β (GSK3β) (Krafft and Klein, 2010; Braithwaite et al., 2012). Activated CaN dephosphorylates inhibitor-1, which leads to activation of PP1 (Mulkey et al., 1994). PP1 activates GSK3β by dephosphorylation of Ser9 (Morfini et al., 2004; Lee et al., 2005; Szatmari et al., 2005; Peineau et al., 2007). This cascade is invoked during LTD induction (Peineau et al., 2008) and might also contribute to AβO-induced synaptotoxicity (Berridge, 2010b; Benilova et al., 2012). Moreover, PP1-GSK3β signaling has been shown to disrupt motor protein-cargo binding in squid axoplasm models of AD (Morfini et al., 2002; LaPointe et al., 2009; Kanaan et al., 2011). Thus, we investigated whether PP1 and GSK3β mediate AβO-induced transport defects in $tau^{+/+}$ and $tau^{-/-}$ neurons. First, we induced expression of I-2, an inhibitory subunit of PP1 (Zhang et al., 2003), for 24 h and subsequently treated neurons with 500 nM AβOs for 18 h (Figure 2.6 A). Inhibition of PP1 by this mechanism prevented reductions in bidirectional flux and restored average velocity and run length to control levels (Figure 2.6 B, C, Table 2.3). To determine whether GSK3β dysregulates transport, we pre-treated $tau^{+/+}$ and $tau^{-/-}$ neurons with a selective cell-permeant chemical inhibitor (Inhibitor VIII) or expressed a dominant-negative form of GSK3β (K85A) for 24 h prior to AβO treatment. Using both approaches, we found that AβO-induced BDNF transport defects were prevented in both $tau^{+/+}$ and $tau^{-/-}$ neurons (Figure 2.6 B, C, Table 2.4). Conversely, transfection with a constitutively-active form of GSK3β (S9A) (Stambolic and Woodgett, 1994) significantly inhibited transport in both $tau^{+/+}$ and $tau^{-/-}$ neurons, even in the absence of AβOs (Table 2.4). Collectively, these findings suggest that PP1-GSK3β signaling downstream of CaN mediates AβO-induced transport disruption.

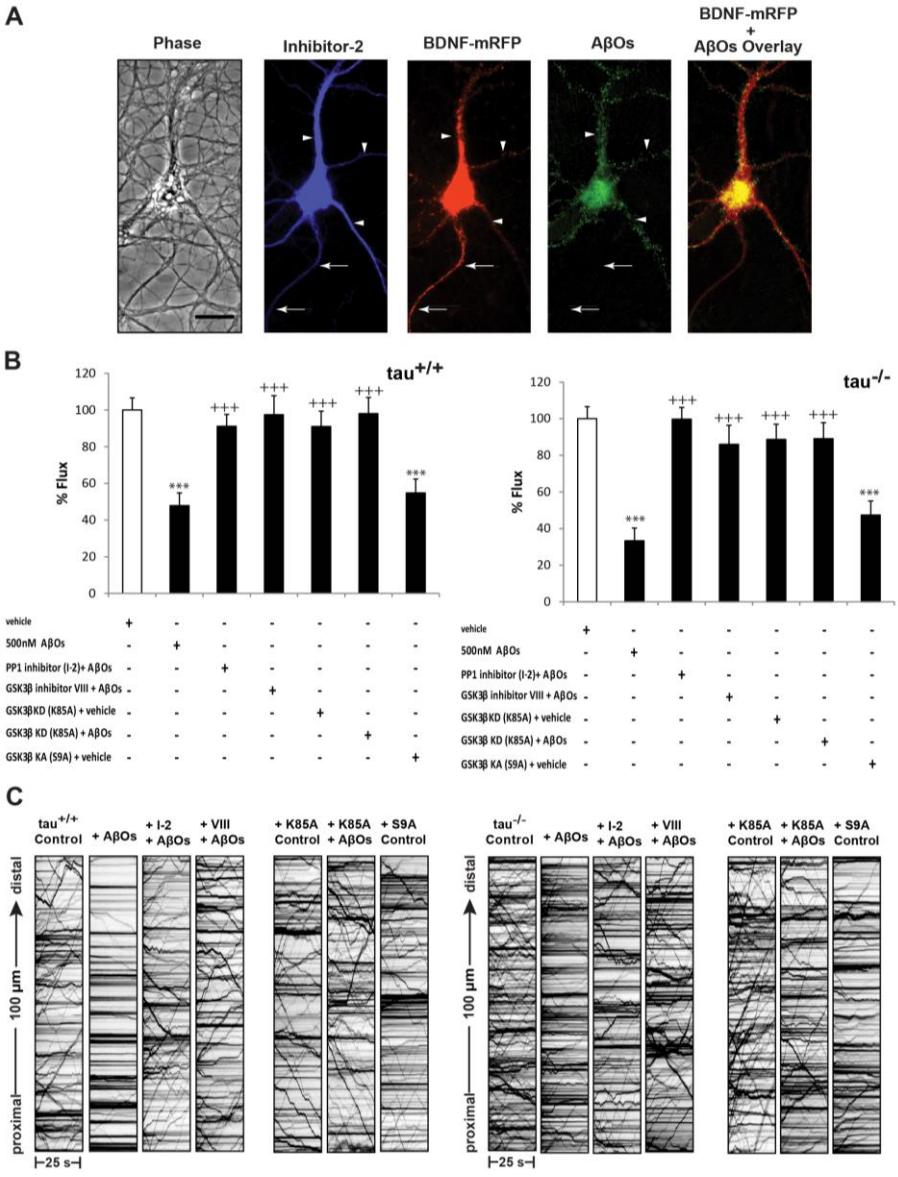

Figure 2.6 Inhibition of protein phosphatase-1 and glycogen synthase kinase 3β prevents AβO-induced transport defects.

(A) Expression of myc-tagged I-2 and BDNF-mRFP in an AβO-treated tau$^{-/-}$ neuron (from left to right). Overlay of BDNF-mRFP and AβO images shows binding of AβOs exclusively to dendrites. Retrospective immunocytochemistry was used to confirm I-2 expression and AβO binding. Arrows indicate axon; arrowheads indicate dendrites. Scale bar = 50 μm. (B) Effects of PP1 and GSK3β inhibition on BDNF flux in AβO-treated tau $^{+/+}$ and tau $^{-/-}$ neurons. Bidirectional flux is markedly reduced by AβOs, and transport defects are prevented by expression of I-2 for 24 h, pre-treatment with 5 μM Inhibitor VIII for 30 min, and expression of kinase-dead GSK3β (K85A) for 24 h. Flux is similarly impaired by expression of kinase-active GSK3β (S9A). (C) Representative kymographs comparing BDNF transport in control, AβO-treated, and inhibitor-treated tau $^{+/+}$ and tau $^{-/-}$ neurons. A minimum of 15 cells from 3 different cultures were analyzed per condition; ***p<0.001 relative to controls and $^{+++}$p<0.001 relative to AβO-treated cells. Complete statistical evaluation is presented in Tables 2.3 and 2.4.

2.4.8. AβO-induced activation of calcineurin and disruption of transport are not mediated by excitotoxic Ca^{2+} signaling

Finally, we investigated whether AβOs activate CaN through excitotoxic Ca^{2+} signaling by probing $tau^{+/+}$ and $tau^{-/-}$ neuronal lysates for truncated forms of CaN, generated by calpain-induced cleavage (Liu et al., 2005). In glutamate-induced excitotoxicity, activated calpain cleaves full-length CaN, producing constitutively active 57 and 48 kDa truncated forms (Figure 2.5 E). However, no differences in the ratios of truncated, active CaN to full-length CaN (61 kDa) were detected between control and AβO-treated lysates (Figure 2.5 E). We further measured levels of non-erythroid α-II spectrin (280 kDa), a well-defined physiological substrate of calpain, in AβO-exposed neurons. Immunoblots revealed that calpain-mediated cleavage of spectrin, which generates a characteristic 150 kDa fragment, was not increased by AβOs (Supplemental Figure 3). These results demonstrate that AβOs do not activate CaN through excitotoxic, calpain-mediated fragmentation.

During excitotoxicity, intracellular Ca^{2+} is sequestered into the mitochondrial matrix, decreasing the electrochemical gradient generated by the electron transport chain, thereby reducing ATP synthesis. The concurrent accumulation of intra-mitochondrial Ca^{2+} and reduced ATP synthesis is a primary cause of cell death. To rule out the possibility that transport disruption under our conditions resulted from these events, we measured ATP levels in control and AβO-treated $tau^{+/+}$ and $tau^{-/-}$ neurons using an *in vitro* luciferase-based ATP assay, and no changes in ATP levels were observed (Supplemental Figure 3). Furthermore, caspase-3, a key mediator of excitotoxic cell death, was not cleaved and activated (Supplemental Figure 3). Collectively, these results show that transport disruption does not result from excitotoxic CaN activation and cell death, suggesting that a mechanism downstream of CaN signaling triggers transport defects induced by AβOs.

2.5. Discussion

FAT disruption is an early pathological manifestation that leads to loss of synapse function and axonal degeneration in AD (De Vos et al., 2008). AβOs are central

to AD pathology and impair FAT. AβOs are known to induce tau hyperphosphorylation (De Felice et al., 2008), however, it is unclear whether tau is required for AβO mediated FAT disruption (Castellani et al., 2008). Here, through direct assessment of FAT at high temporal and spatial resolution in living neurons, we demonstrate that AβO-induced defects in axonal BDNF transport persist in the absence of tau, and cannot be attributed to microtubule destabilization or cell death. Our findings support the notion that tau is not essential for normal transport (Yuan et al., 2008; Vossel et al., 2010), and suggest that additional intracellular signaling mechanisms negatively regulate FAT in AβO-exposed neurons. We combined multiple approaches, including live imaging, *in vitro* phosphatase assays, and immunoblotting, to demonstrate that inhibition of CaN by FK506 completely rescues BDNF transport defects, and that AβOs impair transport by over-activating CaN through non-excitotoxic Ca^{2+} signaling. Collectively, our work implicates CaN in FAT regulation and challenges a requirement for tau in AβO-induced transport disruption in primary neurons.

Considerable evidence implicates tau in AβO toxicity, and a variety of proposed mechanisms explain how tau reduction might prevent or ameliorate it. Such mechanisms range from altered microtubule stability (Rapoport et al., 2002; King et al., 2006), elimination of a toxic tau fragment (Park and Ferreira, 2005), regulation of neuronal activity (Shipton et al., 2011), and changes in subcellular localization of the Src kinase, Fyn (Ittner et al., 2010). Intriguingly, we found that tau ablation does not prevent AβO-induced FAT defects (Figure 2). This suggests that the role of tau in AβO-induced toxicity depends on differences in model systems and relevant stages of AD progression examined, or to temporal differences in activation of distinct signaling mechanisms that lead to toxicity. For instance, tau reduction ameliorates cognitive deficits in human amyloid precursor protein (hAPP)-overexpressing mice. These mice exhibit extensive plaque formation, mimicking chronic Aβ accumulation during late-stage AD, when abnormal phosphorylation, distribution, and signaling properties of tau are prevalent and likely contribute significantly to LTP impairment and toxicity (Morris et al., 2011; Shipton et al., 2011). In contrast, we assessed FAT in neurons that were acutely exposed to AβOs. These conditions are likely more relevant to early-stage AD, when hyperphosphorylated and fragmented tau have not reached detrimental concentrations (Morris et al., 2011), and when evidence of transport defects exists in animal models

(Kim et al., 2011). We cannot rule out the possibility that p-tau ultimately accumulates and inhibits FAT by interacting directly with motor-cargo complexes or initiating aberrant signaling cascades that eventually alter FAT dynamics. Our findings imply that tau, although critical for AβO toxicity during late-stage AD, is probably not essential for initiating transport defects in early-stage AD.

AβOs instigate aberrant Ca^{2+} signaling prior to excessive tau hyperphosphorylation, NFT formation, cognitive decline, and other late-stage hallmarks of AD (Stutzmann, 2007). In cultured neurons and AD mouse models, AβOs persistently elevate resting cytosolic Ca^{2+} by allowing dysregulated Ca^{2+} influx through NMDARs and subsequent release of Ca^{2+} from internal stores (Lopez et al., 2008; Demuro et al., 2010). Inhibition of NMDARs prevents FAT defects (Decker et al., 2010a), rendering aberrant Ca^{2+} signaling a plausible mechanism for AβO-induced FAT disruption in the absence of tau. Our findings (e.g., Figures 2.4 and 2.5) corroborate numerous reports of detrimental CaN signaling during early AD pathogenesis (Supnet and Bezprozvanny, 2010). Within minutes of AβO treatment, a progression of Ca^{2+}/calmodulin-dependent CaN activation is observed, first in dendritic spines, and minutes to hours later in the cell body (Wu et al., 2012). Subsequent activation of downstream kinases, such as GSK3β, can lead to glutamate receptor internalization, spine retraction, LTP blockage, and LTD facilitation (Reese and Taglialatela, 2011). AβOs can further increase CaN signaling through non-apoptotic caspase-3 activation in dendritic spines (D'Amelio et al., 2011; Hyman, 2011). These observations are characteristic of early AD pathogenesis, as they occur in very young APP-overexpressing mice, prior to Aβ plaque deposition, NFT formation, and significant neuronal loss (de Calignon et al., 2009; de Calignon et al., 2010; D'Amelio et al., 2011). CaN activation is predominantly dependent on Ca^{2+}/calmodulin in our studies and similarly precedes apoptotic caspase-3 activation and cell death (Figures 2.1, 2.5, Supplemental Figure 3). Taken together, these results emphasize roles for Ca^{2+} dysregulation and CaN activation in AβO toxicity during early AD pathogenesis.

There are several mechanisms by which AβOs might disrupt axonal BDNF transport independently of tau. One mechanism could involve CaN-dependent inhibition of motor protein activity, mediated by GSK3β. GSK3β is implicated in many aspects of

AD pathogenesis (Hooper et al., 2008) and negatively regulates axonal transport of APP in *Drosophila* embryos (Weaver et al., 2013). Negative regulation of kinesin-1 (KIF5) and cytoplasmic dynein is accomplished by reducing the number of motors that are bound to microtubules. A second mechanism may comprise disruption of motor protein-cargo binding. Phosphorylation of kinesin light chain-1 (KLC1) by PP1-GSK3β signaling (Morfini et al., 2002) and casein kinase 2 (Pigino et al., 2009) dissociates KIF5 from vesicular cargoes in a squid axoplasm model of AD. Moreover, axonal trafficking of calsyntenin-1, a membrane protein that mediates the attachment of KIF5 to APP-containing vesicles, is impaired by phosphorylation of KLC1 (Vagnoni et al., 2011). Likewise, it is possible that CaN activation leads to GSK3β-mediated impairment of axonal BDNF transport by a similar mechanism(s).

Our results demonstrate that AβOs impair bidirectional BDNF transport, and that PP1 and GSK3β inhibition prevents reductions in anterograde and retrograde flux. It is possible that GSK3β largely governs anterograde transport; however, several recent studies have elucidated regulatory mechanisms that are coordinated through opposing motors, whereby disrupting one motor impairs bidirectional transport (Ally et al., 2009; Welte, 2009; Jolly and Gelfand, 2011). In Alzheimer's disease models, bidirectional transport of mitochondria (Rui et al., 2006; Vossel et al., 2010), amyloid precursor protein (Weaver et al., 2013), and organelles contained in squid axoplasm (Pigino et al., 2009) and primary hippocampal neurons (Hiruma et al., 2003) are similarly perturbed. Although this mechanism is commonly observed, subtler changes in axonal transport have been detected for different AβO treatments and cargoes (Tang et al., 2012).

Transport regulation is specific to the motor proteins and cargoes involved. Intriguingly, tau reduction prevents AβO-induced defects in axonal transport of mitochondria and TrkA (Vossel et al., 2010). The apparent difference between our current results and those of Vossel and co-workers (2010) may be attributed to different mechanisms of motor protein regulation. BDNF and other DCV cargoes are transported primarily by KIF1A (Park et al., 2008; Lo et al., 2011), whereas mitochondria and TrkA are transported primarily by KIF5. KIF5 interacts with the Ca^{2+}-sensitive mitochondrial protein, Miro, which inhibits KIF5 motility in a Ca^{2+}-dependent manner (Wang and Schwarz, 2009). This switch in KIF5 activity and subsequent inhibition of mitochondrial

transport are observed within minutes of intracellular Ca^{2+} elevation. Thus, imaging tau-deficient neurons at finer temporal resolution might have revealed a similar, temporary arrest in mitochondrial transport immediately following AβO application and coinciding with transient intracellular Ca^{2+} elevation (Vossel et al., 2010). It is possible that transport defects observed in wild type neurons within 1 h of AβO treatment may, indeed, be primarily attributed to tau. Moreover, micromolar concentrations of AβOs (as used in previous studies) may induce robust tau hyperphosphorylation, initiate its detachment from microtubules, and expose a phosphatase-activating domain within the N-terminus of tau that activates PP1-GSK3β signaling and impedes transport (Kanaan et al., 2011). By contrast, nanomolar concentrations of AβOs used here may permit observation of Ca^{2+}-mediated transport disruption, while the relative contribution of pathogenic tau is minimal. Typically, high Ca^{2+} is required for physiological cessation of transport (Schlager and Hoogenraad, 2009): specific Ca^{2+} dependent mechanisms that modulate KIF1A motility have yet to be characterized.

Based on our present findings and other current models of AD pathogenesis, we propose the following mechanism for AβO-induced disruption of axonal BDNF transport (Figure 2.7). AβOs elevate resting cytosolic Ca^{2+} by allowing dysregulated Ca^{2+} influx through NMDARs and Ca^{2+}-induced Ca^{2+} release from internal stores. Calmodulin binds free Ca^{2+} ions and subsequently activates CaN, dephosphorylating I-1 and relieving inhibition of PP1. Upon activation by PP1, GSK3β may disrupt BDNF transport by directly phosphorylating and inhibiting motor proteins and/or disrupting motor-DCV interactions, representing an early transport deficit in the progression of AD (Goldstein, 2012). These events occur prior to excessive tau hyperphosphorylation, NFT formation, and microtubule destabilization. Furthermore, transport defects are not secondarily influenced by cellular toxicity despite prolonged, irreversible AβO binding at low nanomolar concentrations. Notably, reduced levels of BDNF correlate with the progression of AD (Diniz and Teixeira, 2011), and this reduction could be related to transport and release of this neuropeptide. Finally, prevention or reversal of FAT defects and consequent axonal degeneration may help to ameliorate neuronal loss and cognitive decline in AD.

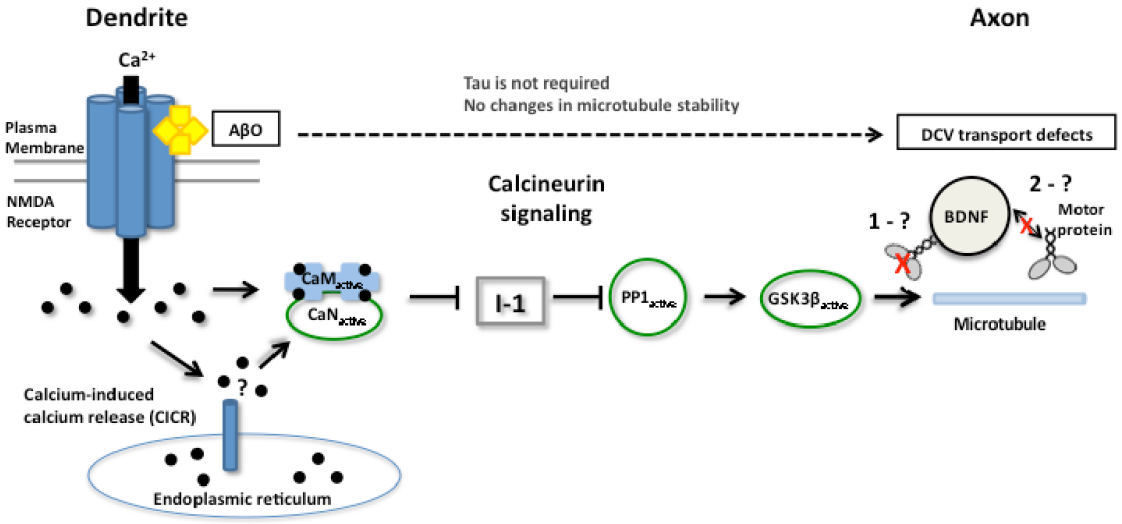

Figure 2.7 Proposed mechanism for fast axonal transport disruption in an Alzheimer's disease model.

At dendrites, AβOs aberrantly activate NMDARs and induce Ca^{2+} influx, elevating cytosolic Ca^{2+}. Activated calcineurin relieves inhibition of PP1, which activates GSK3β. GSK3β may inhibit motor protein activity (1), and/or disrupt motor-cargo interactions (2), and impede transport in the presence of AβOs.

2.6. Acknowledgements

This research was supported by grants from the National Science and Engineering Research Council of Canada (NSERC; 327100-06), the Canadian Foundation for Innovation (CFI; 12793), and the Canadian Institutes of Health Research (CIHR; 90396) to M.A.S. We thank L. Chen for her expert technical assistance, and C. D. Link and T. Tomiyama for their critical reading of this manuscript, and V. Gelfand for essential discussions. K.J.G. is funded by a C.D. Nelson Memorial Graduate Scholarship from Simon Fraser University and an NSERC Postgraduate Scholarship. H.D. thanks the Brazilian agency CAPES for fellowship support. S.T.F. is supported by grants from National Institute of Translational Neuroscience, Conselho Nacional de Desenvolvimento Científico e Tecnológico, and Fundação de Amparo à Pesquisa do Estado do Rio de Janeiro (Brazil). We also thank the Simon Fraser University Animal Care Services staff for their essential assistance in our experiments.

2.7. Supplemental Figures and Tables

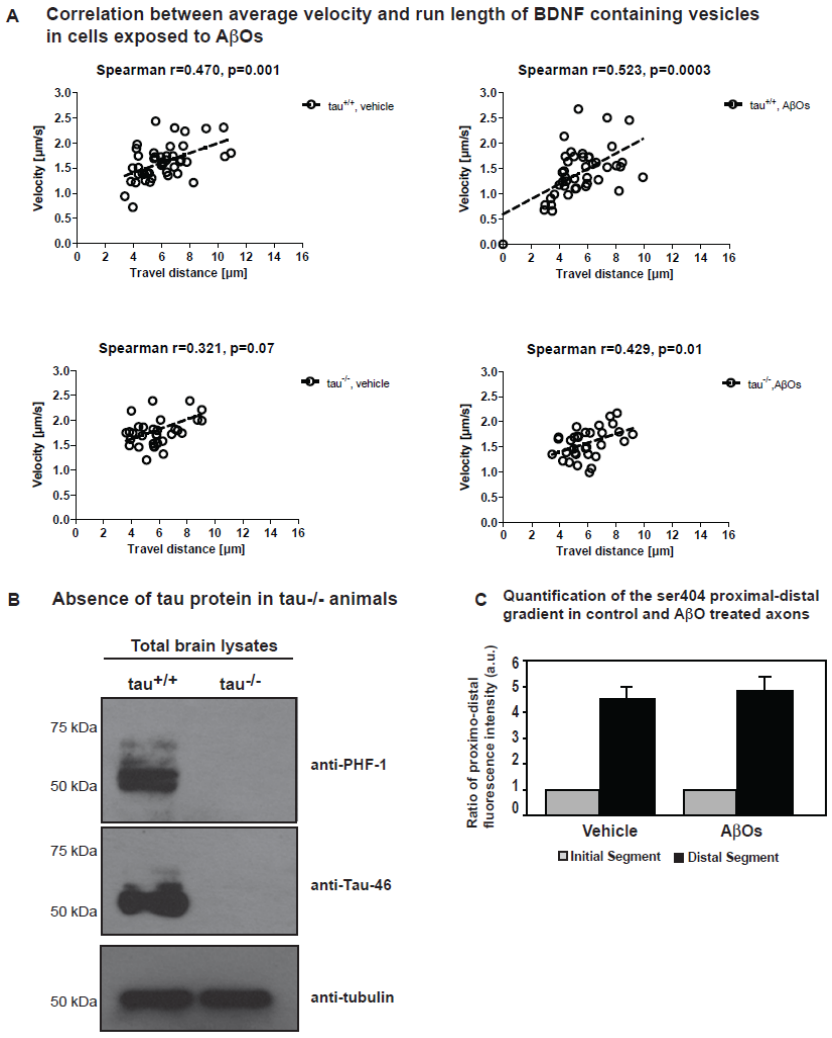

Figure 2.8 Supplemental Figure 1

(A) A weak correlation exists between average velocity and run length. There is only a weak correlation between velocity and run length of BDNF vesicles in vehicle- and AβO-treated tau$^{+/+}$ and tau$^{-/-}$ hippocampal neurons. Spearman rank correlation coefficients (r values) and p values are reported for each data set along with a trend line. The data distribution shown in (A) to (D) produced weak correlation coeffecients ranging from 0.32 to 0.52. (B) Absence of tau protein in mouse brains from tau$^{-/-}$ animals. Western blot analysis of tau in mouse brain lysates from tau$^{+/+}$ and tau$^{-/-}$ animals reveals the absence of tau protein in tau$^{-/-}$ animals. *Upper panel*: Phosphorylated tau was detected using an anti-PHF-1 antibody; *middle panel*: total tau protein level was detected using an anti-Tau-46 antibody. (C) Quantitation of phosphor tau ser404 immunofluorescence comparing the ratio of fluorescent signals between initial and distal portions of the axon. See Methods for details.

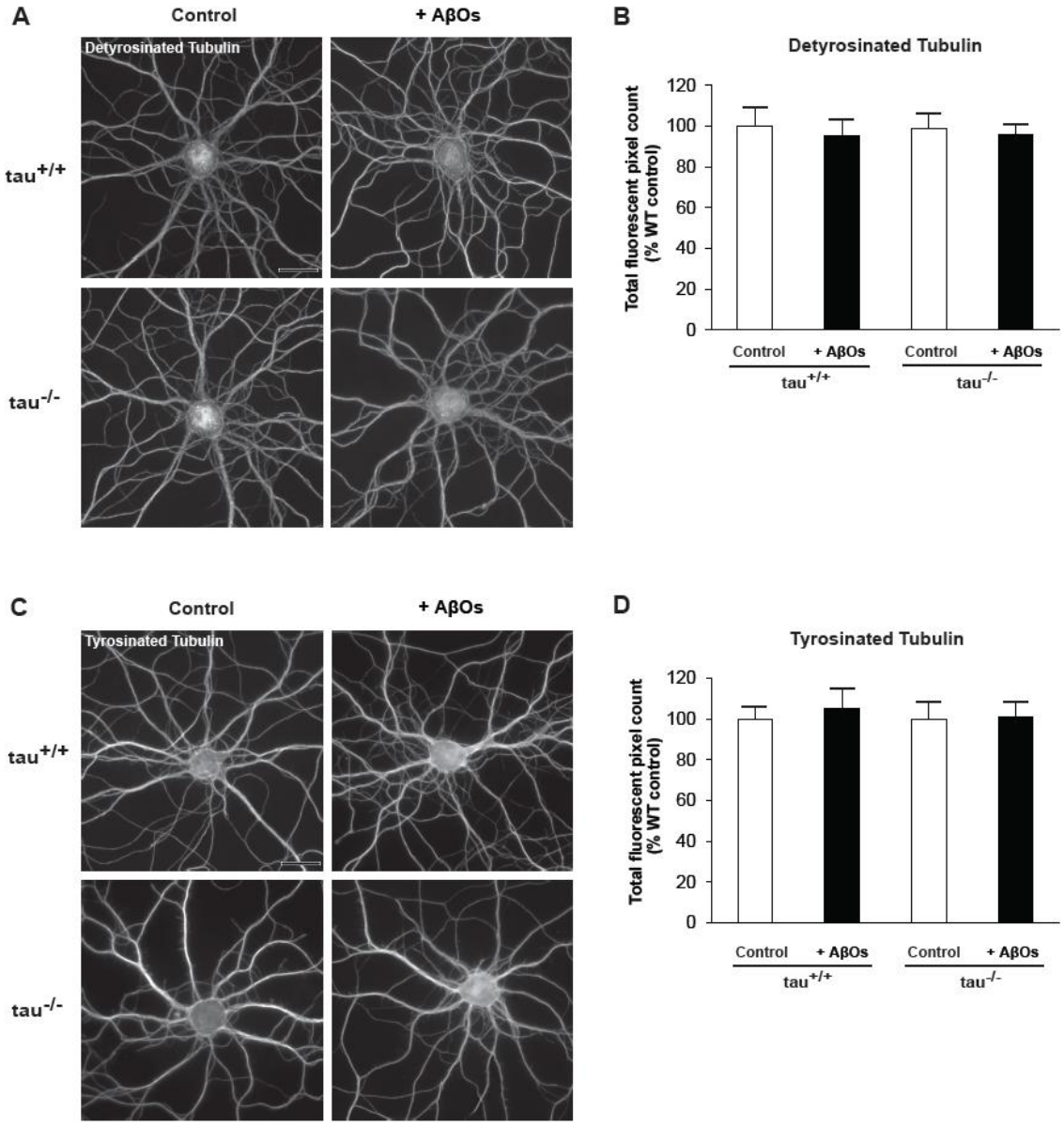

Figure 2.9 Supplemental Figure 2

Tubulin detyrosination and tyrosination are not altered by AβOs in tau$^{+/+}$ and tau$^{-/-}$ hippocampal neurons. Representative fluorescent micrographs of detyrosinated (A-B) and tyrosinated (C-D) tubulin immunocytochemistry in tau$^{+/+}$ and tau$^{-/-}$ neurons. Quantification reveals no difference in detyrosinated and tyrosinated tubulin appearance in control and AβO-treated tau$^{+/+}$ and tau$^{-/-}$ neurons. Scale = 25 μm.

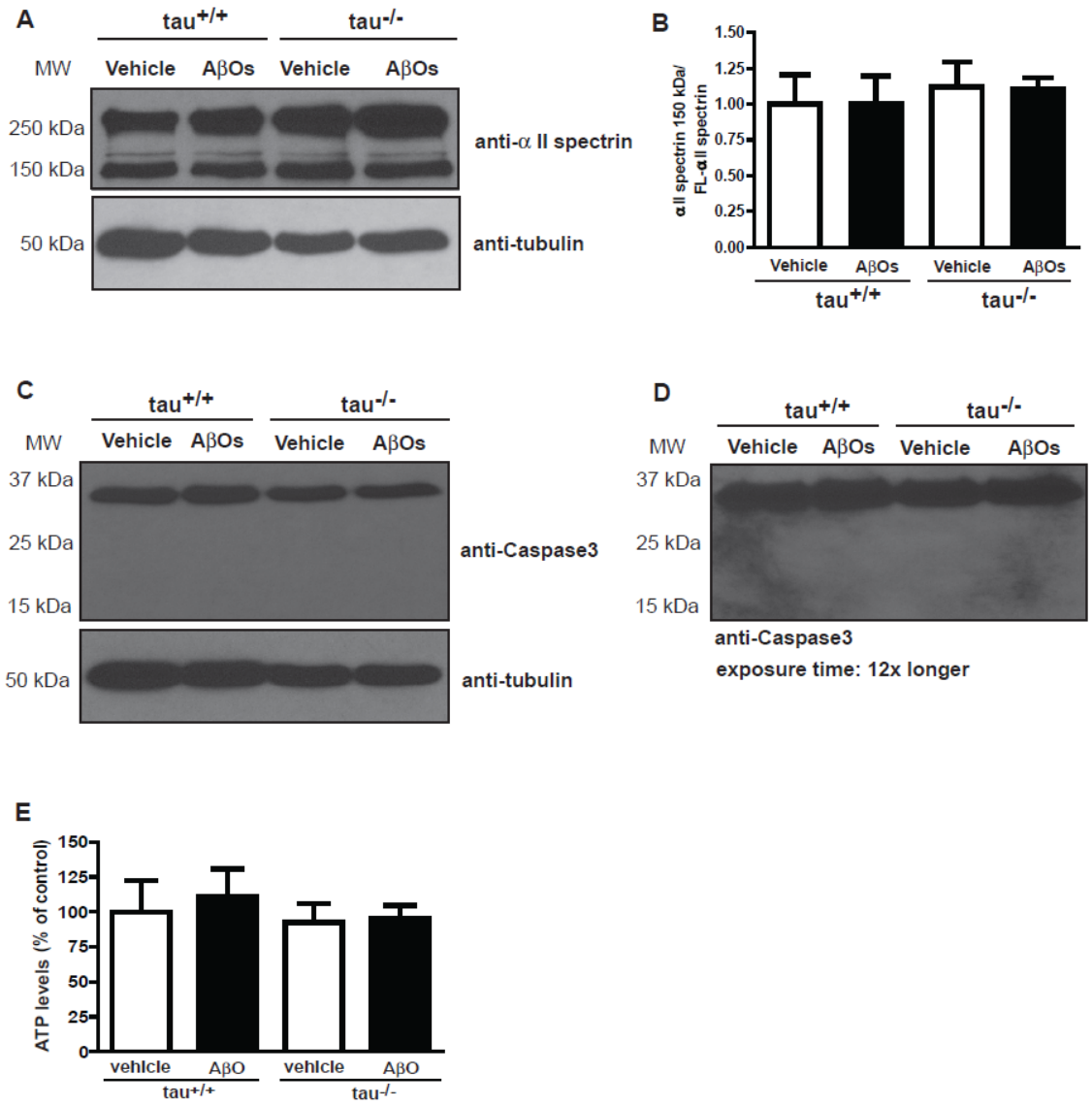

Figure 2.10 Supplemental Figure 3

Calpain and caspase 3 activities are not elevated in, nor are ATP levels affected in cultured neurons in the presence of 500 nM AβOs after 18 hours. (A) Calpain cleavage of α II spectrin in control and AβO-treated tau$^{+/+}$ and tau$^{-/-}$ cells was analyzed by western blotting with an anti-α II spectrin antibody. (B) Quantification of cleaved α II spectrin 150 kDa fragment reveals no difference in calpain activity in control and AβO-treated neurons. (C) Representative image of caspase 3 cleavage analyzed by western blotting using an anti-caspase 3 antibody. Caspase 3 cleavage product was not present in control and AβO-treated cell lysates. (D) Longer exposure time of the western blot image shown in c. (E) AβOs do not induce ATP reduction in tau$^{+/+}$ and tau$^{-/-}$ hippocampal neurons. Intracellular ATP levels were measured after 18 h of AβO exposure. Results are averages of triplicate samples from three independent assays cultures.

Table 2.1 Disruption of BDNF transport by 500 nM AβOs

Dense core vesicles

	Traffic values			%
	All events	Anterograde	Retrograde	All events
Flux (min^{-1})				
$tau^{+/+}$, vehicle 18 h	7.49±0.58	3.33±0.31	4.17±0.39	100.00±7.76
$tau^{+/+}$, AβOs 18 h	$3.04±0.30^{***}$	$1.53±0.18^{***}$	$1.51±0.20^{***}$	$40.63±4.06^{***}$
$tau^{+/+}$, FK506 + AβOs	$8.64±0.81^{+++}$	$3.86±0.73^{+++}$	$4.65±0.63^{+++}$	$115.34±10.74^{+++}$
$tau^{-/-}$, vehicle 18 h	7.76±0.55	3.99±0.41	3.77±0.36	103.64±7.39
$tau^{-/-}$, AβOs 18 h	$3.13±0.26^{***}$	$1.52±0.17^{***}$	$1.61±0.18^{***}$	$41.75±3.45^{***}$
$tau^{-/-}$, FK506 + AβOs	$8.95±0.91^{+++}$	$4.32±0.66^{+++}$	$5.11±0.81^{+++}$	$119.42±12.22^{+++}$
Velocity (µm/s)				
$tau^{+/+}$, vehicle 18 h	1.61±0.05	1.58±0.07	1.59±0.05	100.00±3.22
$tau^{+/+}$, AβOs 18 h	$1.42±0.08^{*}$	$1.39±0.10^{*}$	1.41±0.12	$87.75±4.95^{*}$
$tau^{+/+}$, FK506 + AβOs	1.62±0.08	1.55±0.12	1.58±0.06	100.65±4.88
$tau^{-/-}$, vehicle 18 h	$1.78±0.06^{\S}$	$1.80±0.08^{\S}$	$1.73±0.05^{\S}$	$110.10±3.94^{\S}$
$tau^{-/-}$, AβOs 18 h	$1.57±0.05^{**}$	$1.57±0.07^{*}$	$1.57±0.06^{*}$	$97.45±3.24^{**}$
$tau^{-/-}$, FK506 + AβOs	$1.78±0.15^{+++}$	$1.75±0.17^{++}$	$1.79±0.15^{++/\#}$	$110.25±9.35^{+++}$
Run length (µm)				
$tau^{+/+}$, vehicle 18 h	6.10±0.26	6.24±0.34	5.99±0.30	100.00±4.29
$tau^{+/+}$, AβOs 18 h	5.44±0.30	$5.11±0.34^{**}$	5.31±0.36	89.14±4.90
$tau^{+/+}$, FK506 + AβOs	$7.20±0.44^{++/\#}$	$7.41±0.76^{++}$	$6.80±0.37^{++}$	$117.97±7.28^{++/\#}$
$tau^{-/-}$, vehicle 18 h	6.07±0.26	6.47±0.40	5.73±0.28	99.36±4.29
$tau^{-/-}$, AβOs 18 h	5.92±0.25	6.17±0.42	5.83±0.32	96.92±4.17
$tau^{-/-}$, FK506 + AβOs	$7.66±0.61^{+++/\#\#}$	$7.60±0.69^{++/\#}$	$7.46±0.61^{++/\#\#}$	$125.42±9.93^{+++/\#\#}$

DCVs: $tau^{+/+}$: vehicle n=46 kymographs (46 cells, 2123 vesicles), AβOs n=40 kymographs (40 cells, 878 vesicles), FK506 + AβOs n=16 kymographs (16 cells, 730 vesicles); **$tau^{-/-}$**: vehicle n=38 kymographs (38 cells, 1825 vesicles), AβOs n=32 kymographs (32 cells, 669 vesicles), FK506 + AβOs n=15 kymographs (15 cells, 777 vesicles).

* $p<0.05$, when compared with vehicle (from each column)
** $p<0.01$, when compared with vehicle (from each column)
*** $p<0.0001$, when compared with vehicle (from each column)
$^{+}$ $p<0.05$, when compared FK506 + AβOs with AβOs (from each column)
$^{++}$ $p<0.01$, when compared FK506 + AβOs with AβOs (from each column)
$^{+++}$ $p<0.001$, when compared FK506 + AβOs with AβOs (from each column)
$^{\#}$ $p<0.05$, when compared FK506 + AβOs with vehicle (from each column)
$^{\#\#}$ $p<0.01$, when compared FK506 + AβOs with vehicle (from each column)
§ $p<0.05$, when compared $tau^{-/-}$ vehicle to $tau^{+/+}$ vehicle (from each column)

Table 2.2 Disruption of BDNF transport by 100 nM AβOs

Dense core vesicles				
	Traffic values			%
	All events	Anterograde	Retrograde	All events
Flux (min^{-1})				
$tau^{+/+}$, vehicle 18 h	6.14±0.77	3.24±0.45	2.89±0.43	100.00±12.47
$tau^{+/+}$, 100 nM AβOs 18 h	6.52±0.56	3.33±0.37	3.21±0.31	105.22±10.26
$tau^{-/-}$, vehicle 18 h	5.64±0.59	3.04±0.51	2.60±0.28	88.91±10.41
$tau^{-/-}$, 100 nM AβOs 18 h	5.26±0.48	3.09±0.42	2.17±0.25	81.64±8.20
$tau^{+/+}$, vehicle 48 h	6.90±0.72	3.73±0.55	3.17±0.30	100.00±10.51
$tau^{+/+}$, 100 nM AβOs 48 h	6.65±0.67	3.89±0.39	2.89±0.47	96.48±9.79
$tau^{-/-}$, vehicle 48 h	5.45±0.58	2.94±0.30	2.67±0.38	79.05±8.43
$tau^{-/-}$, 100 nM AβOs 48 h	6.63±1.03	3.13±0.54	3.50±0.55	96.17±14.91
$tau^{+/+}$, vehicle 72 h	5.50±0.46	3.02±0.35	2.51±0.25	100.04±8.40
$tau^{+/+}$, 100 nM AβOs 72 h	1,94±0.15***	0.92±0.10***	1.01±0.15***	35.17±2.66***
$tau^{-/-}$, vehicle 72 h	6.11±0.50	3.39±0.39	2.61±0.30	110.96±9.02
$tau^{-/-}$, 100 nM AβOs 72 h	2.55±0.44***	1.41±0.28***	1.14±0.20***	46.41±7.98***
Velocity (µm/s)				
$tau^{+/+}$, vehicle 18 h	1.67±0.05	1.62±0.10	1.50±0.09	100.00±3.17
$tau^{+/+}$, 100 nM AβOs 18 h	1.65±0.06	1.67±0.06	1.54±0.06	95.92±5.02
$tau^{-/-}$, vehicle 18 h	1.86±0.05	1.89±0.08	1.74±0.06	106.63±5.98
$tau^{-/-}$, 100 nM AβOs 18 h	1.87±0.06	2.01±0.07	1.67±0.05	108.36±5.12
$tau^{+/+}$, vehicle 48 h	1.86±0.04	1.83±0.06	1.79±0.05	100.00±2.29
$tau^{+/+}$, 100 nM AβOs 48 h	1.76±0.09	1.75±0.07	1.62±0.14	94.84±4.93
$tau^{-/-}$, vehicle 48 h	1.83±0.07	2.04±0.08	1.63±0.08	98.24±3.79
$tau^{-/-}$, 100 nM AβOs 48 h	1.88±0.05	2.02±0.08	1.77±0.06	102.93±2.77
$tau^{+/+}$, vehicle 72 h	1.86±0.08	1.97±0.09	1.75±0.09	100.00±4.38
$tau^{+/+}$, 100 nM AβOs 72 h	1.73±0.10	1.72±0.15	1.60±0.08	92.98±5.20
$tau^{-/-}$, vehicle 72 h	1.97±0.06	1.96±0.30	1.75±0.08	105.76±3.48
$tau^{-/-}$, 100 nM AβOs 72 h	1.68±0.07**/#	1.69±0.24	1.60±0.11	90.43±3.66**/#
Run length (µm)				
$tau^{+/+}$, vehicle 18 h	6.09±0.38	6.46±0.50	5.16±0.34	100.00±6.16
$tau^{+/+}$, 100 nM AβOs 18 h	6.07±0.23	5.99±0.31	5.50±0.25	95.55±5.39
$tau^{-/-}$, vehicle 18 h	5.88±0.25	6.14±0.37	5.74±0.37	92.85±6.01
$tau^{-/-}$, 100 nM AβOs 18 h	6.09±0.21	6.58±0.27	5.48±0.20	96.45±4.84
$tau^{+/+}$, vehicle 48 h	6.51±0.26	7.05±0.61	5.48±0.35	100.00±4.05
$tau^{+/+}$, 100 nM AβOs 48 h	6.39±0.39	6.71±0.43	5.21±0.53	98.21±6.01
$tau^{-/-}$, vehicle 48 h	5.82±0.24	6.16±0.36	5.23±0.20	89.37±3.68
$tau^{-/-}$, 100 nM AβOs 48 h	6.01±0.29	6.44±0.37	5.62±0.24	92.35±4.44
$tau^{+/+}$, vehicle 72 h	5.32±0.17	5.88±0.25	5.01±0.24	100.03±3.22
$tau^{+/+}$, 100 nM AβOs 72 h	4.15±0.21***	4.00±0.33***	3.73±0.24**/#	77.91±3.86***
$tau^{-/-}$, vehicle 72 h	5.81±0.26	6.16±0.30	5.24±0.26	109.18±4.84
$tau^{-/-}$, 100 nM AβOs 72 h	4.60±0.40*/#	4.77±0.50*/#	3.97±0.39*/#	86.37±7.59*/#

DCVs: 18 h : $tau^{+/+}$, vehicle n=24 kymographs (24 cells, 844 vesicles) / AβOs n=26 kymographs (26 cells, 973 vesicles); $tau^{-/-}$, vehicle n=22 kymographs (22 cells, 646 vesicles) / AβOs n=29 kymographs (29 cells, 733 vesicles); **48 h: :** $tau^{+/+}$, vehicle n=19 kymographs (19 cells, 637 vesicles) / AβOs n=15 kymographs (15 cells, 472 vesicles); $tau^{-/-}$, n=19 kymographs (19 cells, 506 vesicles) / AβOs n=16 kymographs (16 cells, 540 vesicles); **72 h: :** $tau^{+/+}$, vehicle n=25 kymographs (25 cells, 789 vesicles) / AβOs n=19 kymographs (19 cells, 276 vesicles); $tau^{-/-}$ vehicle n=25 kymographs (25 cells, 640 vesicles) / AβOs n=19 kymographs (19 cells, 479 vesicles).

* p<0.05, when compared with vehicle (from each column)
** p<0.01, when compared with vehicle (from each colum)
*** p<0.001, when compared with vehicle (from each column)
# these results differ from those obtained with 500 nM AβOs at 18 h

Table 2.3 Inhibition of PP1 prevents AβO-induced transport defects

	Dense core vesicles			
	Traffic values			%
	All events	Anterograde	Retrograde	All events (%)
Flux (min^{-1})				
$tau^{+/+}$ vehicle	8.30 ± 0.77	4.52 ± 0.52	3.78 ± 0.42	100.00 ± 9.28
$tau^{+/+}$ AβOs	3.19 ± 0.42***	1.57 ± 0.26***	1.62 ± 0.27***	38.43 ± 5.06***
$tau^{+/+}$ I-2 + AβOs	7.56 ± 0.53+++	4.19 ± 0.35+++	3.37 ± 0.40+++	91.08 ± 6.39+++
$tau^{-/-}$ vehicle	11.25 ± 0.79	6.32 ± 0.54	4.93 ± 0.46	100.00 ± 7.02
$tau^{-/-}$ AβOs	4.70 ± 0.55***	2.54 ± 0.34***	2.16 ± 0.35***	41.78 ± 4.89***
$tau^{-/-}$ I-2 + AβOs	10.57 ± 0.79+++	5.65 ± 0.56	4.93 ± 0.46+++	93.96 ± 7.02+++
Velocity (µm/s)				
$tau^{+/+}$ vehicle	1.47 ± 0.05	1.55 ± 0.06	1.37 ± 0.07	100.00 ± 3.40
$tau^{+/+}$ AβOs	1.34 ± 0.07	1.34 ± 0.10	1.29 ± 0.09	91.16 ± 4.76
$tau^{+/+}$ I-2 + AβOs	1.50 ± 0.04+	1.55 ± 0.06	1.43 ± 0.04	102.04 ± 2.72+
$tau^{-/-}$ vehicle	1.69 ± 0.06	1.76 ± 0.07	1.62 ± 0.07	100.00 ± 3.55
$tau^{-/-}$ AβOs	1.53 ± 0.06	1.54 ± 0.07*	1.45 ± 0.08	90.53 ± 3.55
$tau^{-/-}$ I-2 + AβOs	1.69 ± 0.05	1.73 ± 0.05+	1.66 ± 0.07	100.00 ± 2.96
Run length (µm)				
$tau^{+/+}$ vehicle	5.93 ± 0.24	6.36 ± 0.35	5.52 ± 0.31	100.00 ± 4.05
$tau^{+/+}$ AβOs	5.59 ± 0.38	5.78 ± 0.64	4.76 ± 0.43	94.27 ± 6.41
$tau^{+/+}$ I-2 + AβOs	5.69 ± 0.22	6.08 ± 0.29	5.37 ± 0.31	95.95 ± 3.71
$tau^{-/-}$ vehicle	6.09 ± 0.29	6.42 ± 0.51	5.77 ± 0.34	100.00 ± 4.76
$tau^{-/-}$ AβOs	5.69 ± 0.29	5.92 ± 0.43	4.99 ± 0.29	93.43 ± 4.76
$tau^{-/-}$ I-2 + AβOs	5.99 ± 0.29	6.39 ± 0.36	5.64 ± 0.41	98.36 ± 4.76

$tau^{+/+}$ vehicle: n=25 kymographs (25 cells, 1406 vesicles)
$tau^{+/+}$ AβO: n=18 kymographs (18 cells, 410 vesicles)
$tau^{+/+}$ I-2 + AβO: n=34 kymographs (34 cells, 1294 vesicles)
$tau^{-/-}$ vehicle: n=19 kymographs (19 cells, 1392 vesicles)
$tau^{-/-}$ AβO: n=27 kymographs (27 cells, 857 vesicles)
$tau^{-/-}$ I-2 + AβO: n=25 kymographs (25 cells, 1846 vesicles)

* p<0.05, when compared with vehicle
** p<0.01, when compared with vehicle
*** p<0.001, when compared with vehicle
+ p<0.05, when compared with AβOs
++ p<0.01, when compared with AβOs
+++ p<0.001, when compared with AβOs

Table 2.4 Inhibition of GSK3β prevents AβO induced transport defects

	Dense core vesicles			
		Traffic values		%
	All events	Anterograde	Retrograde	All events (%)
Flux (min $^{-1}$)				
tau $^{+/+}$ vehicle	14.76 ± 0.97	8.04 ±0.82	6.72 ± 0.48	100.00 ± 6.56
tau $^{+/+}$ AβOs	7.07 ± 1.02***	3.45 ± 0.77***	3.84 ± 0.35***	47.89 ± 6.92***
tau $^{+/+}$ VIII + AβOs	14.39 ± 1.53^{+++}	8.27 ± 1.39^{+++}	6.12 ± 0.54^{+++}	97.47 ± 10.37^{+++}
tau $^{+/+}$ K85A + vehicle	13.44 ± 1.23	7.38 ± 0.74	6.05 ±0.62	91.02 ± 8.32
tau $^{+/+}$ K85A + AβOs	14.48 ± 1.29^{+++}	7.81 ± 0.62^{+++}	6.67 ± 0.82^{+++}	98.10 ± 8.74^{+++}
tau $^{+/+}$ S9A + vehicle	8.09 ± 1.12***	4.75 ± 0.74***	3.33 ± 0.48***	54.79 ± 7.81***
tau $^{-/-}$ vehicle	18.33 ± 1.27	9.08 ± 0.93	8.37 ± 0.64	100.00 ± 6.77
tau $^{-/-}$ AβOs	6.11 ± 0.99***	3.41 ± 0.57***	2.70 ± 0.53***	33.35 ± 5.30***
tau $^{-/-}$ VIII + AβOs	15.77 ± 1.49^{+++}	9.34 ± 1.17^{+++}	6.43 ± 0.74^{+++}	86.06 ± 7.92^{+++}
tau $^{-/-}$ K85A + vehicle	16.26 ± 1.01	9.17 ± 0.77	7.09 ± 0.53^{+++}	88.70 ± 5.33
tau $^{-/-}$ K85A + AβOs	16.34 ± 0.81^{+++}	9.67 ± 0.54^{+++}	6.66 ± 0.52^{+++}	89.12 ± 4.28^{+++}
tau $^{-/-}$ S9A + vehicle	8.70 ± 1.22***	5.09 ± 0.73**	3.61 ± 0.67***	47.44 ± 6.46***
Velocity (µm/s)				
tau $^{+/+}$ vehicle	1.46 ± 0.06	1.56 ± 0.07	1.29 ± 0.06	100.00 ± 4.12
tau $^{+/+}$ AβOs	1.06 ± 0.07***	1.08 ± 0.08***	1.02 ± 0.07**	72.51 ± 4.85***
tau $^{+/+}$ VIII + AβOs	1.40 ± 0.05^{+++}	1.51 ± 0.06^{+++}	1.23 ± 0.05^{++}	95.85 ± 3.43^{+++}
tau $^{+/+}$ K85A + vehicle	1.54 ± 0.06	1.62 ± 0.08	1.52 ± 0.05	105.21 ± 4.35
tau $^{+/+}$ K85A + AβOs	1.54 ± 0.05^{+++}	1.58 ± 0.08^{+++}	1.50 ± 0.06^{+++}	105.28 ± 3.69^{+++}
tau $^{+/+}$ S9A + vehicle	1.07 ± 0.09**	1.09 ± 0.09**	0.90 ± 0.10**	73.28 ± 6.01**
tau $^{-/-}$ vehicle	1.41 ± 0.08	1.49 ± 0.09	1.32 ± 0.08	100.00 ± 5.76
tau $^{-/-}$ AβOs	0.95 ± 0.06***	0.99 ± 0.06**	0.93 ± 0.06***	67.58 ± 3.98***
tau $^{-/-}$ VIII + AβOs	1.41 ± 0.08^{+++}	1.45 ± 0.09^{++}	1.32 ± 0.08^{+++}	100.00 ± 5.81^{+++}
tau $^{-/-}$ K85A + vehicle	1.71 ± 0.06	1.75 ± 0.08	1.65 ± 0.06	120.81 ± 4.33
tau $^{-/-}$ K85A + AβOs	1.74 ± 0.07^{+++}	1.82 ± 0.08^{+++}	1.65 ± 0.08^{+++}	123.52 ± 4.85^{+++}
tau $^{-/-}$ S9A + vehicle	0.98 ± 0.08***	1.05 ± 0.09**	0.92 ± 0.12**	69.50 ± 5.93***
Run length (µm)				
tau $^{+/+}$ vehicle	9.67 ± 0.81	11.01 ± 0.99	7.47 ± 0.62	100.00 ± 8.37
tau $^{+/+}$ AβOs	5.32 ± 0.28***	5.61 ± 0.37***	4.72 ± 0.24**	54.98 ± 2.90***
tau $^{+/+}$ VIII + AβOs	8.96 ± 0.82^{+++}	10.56 ± 1.10^{+++}	6.62 ± 0.35^{++}	92.64 ± 8.48^{+++}
tau $^{+/+}$ K85A + vehicle	9.62 ± 0.58	10.24 ± 0.77	9.12 ± 0.51^{++}	99.56 ± 6.01
tau $^{+/+}$ K85A + AβOs	9.74 ± 0.61^{+++}	10.95 ± 0.79^{+++}	8.57 ± 0.52^{++}	100.80 ± 6.31^{+++}
tau $^{+/+}$ S9A + vehicle	8.94 ± 0.91	9.99 ± 1.24	7.80 ± 0.65	92.45 ± 9.46
tau $^{-/-}$ vehicle	6.72 ± 0.39	7.82 ± 0.59	5.48 ± 0.26	100.00 ± 5.75
tau $^{-/-}$ AβOs	4.99 ± 0.32**	5.45 ± 0.47**	4.37 ± 0.26**	74.40 ± 4.76**
tau $^{-/-}$ VIII + AβOs	7.06 ± 0.50^{+++}	7.82 ± 0.42^{++}	5.89 ± 0.60^{+}	105.11 ± 7.50^{+++}
tau $^{-/-}$ K85A + vehicle	8.28 ± 0.31	9.11 ± 0.53	7.38 ± 0.22	123.25 ± 4.68
tau $^{-/-}$ K85A + AβOs	8.58 ± 0.34^{+++}	9.75 ± 0.54^{+++}	7.97 ± 0.44^{+++}	127.64 ± 5.13^{+++}
tau $^{-/-}$ S9A + vehicle	6.03 ± 0.47	6.68 ± 0.6	4.41 ± 0.53	89.73 ± 6.96

tau$^{+/+}$ vehicle: n=18 kymographs (18 cells, 1261 vesicles)
tau$^{+/+}$ AβO: n=17 kymographs (17 cells, 1005 vesicles)
tau$^{+/+}$ VIII + AβO: n=15 kymographs (15 cells, 1097 vesicles)
tau$^{+/+}$ K85A + vehicle: n=17 kymographs (17 cells, 1162 vesicles)
tau$^{+/+}$ K85A + AβO: n=15 kymographs (15 cells, 1075 vesicles)
tau$^{+/+}$ S9A + vehicle: n=16 kymographs (16 cells, 682 vesicles)

tau$^{-/-}$ vehicle: n=15 kymographs (17 cells, 2167 vesicles)
tau$^{-/-}$ AβO: n=19 kymographs (19 cells, 933 vesicles)
tau$^{-/-}$ VIII + AβO: n=19 kymographs (16 cells, 1666 vesicles)
tau$^{-/-}$ K85A + vehicle: n=19 kymographs (17 cells, 1393 vesicles)
tau$^{-/-}$ K85A + AβO: n=19 kymographs (18 cells, 1432 vesicles)
tau$^{-/-}$ S9A + vehicle: n=19 kymographs (15 cells, 670 vesicles)

* p<0.05, when compared with vehicle
** p<0.01, when compared with vehicle
*** p<0.001, when compared with vehicle
+ p<0.05, when compared with AβOs
++ p<0.01, when compared with AβOs
+++ p<0.001, when compared with AβOs

Chapter 3. Dendritic and axonal mechanisms of Ca^{2+} elevation regulate the spatiotemporal progression of BDNF transport defects in amyloid-β oligomer-treated hippocampal neurons[2]

Kathlyn J. Gan[1] and Michael A. Silverman[1, 2]

[1] Department of Molecular Biology and Biochemistry, Simon Fraser University, 8888 University Drive, Burnaby, British Columbia, V5A 1S6, Canada

[2] Department of Biological Sciences, Simon Fraser University, 8888 University Drive, Burnaby, British Columbia, V5A 1S6, Canada

K.J.G. designed the study, performed all experiments, analyzed and interpreted data, and wrote the paper. M.A.S. designed and supervised the study, interpreted data, constructed figures, and assisted with writing the paper.

[2] The following chapter was submitted to The Journal of Neuroscience (JN-RM-3660-14) on September 2, 2014.

3.1. Abstract

Disruption of fast axonal transport (FAT) and intracellular Ca^{2+} dysregulation are early pathological events in Alzheimer's disease (AD). Soluble amyloid-β oligomers (AβOs), a causative agent of AD, impair vesicular transport of brain-derived neurotrophic factor (BDNF) by non-excitotoxic activation of calcineurin (CaN), a Ca^{2+}-dependent phosphatase implicated in AD. These transport defects occur independent of tau, microtubule destabilization, and acute cell death. Ca^{2+}-dependent mechanisms that regulate the onset, severity, and spatiotemporal progression of BDNF transport defects from dendritic and axonal AβO binding sites are unknown. Here, we show that tau-independent BDNF transport defects in dendrites and axons are induced simultaneously but exhibit different rates of decline: maximal impairment of dendritic transport precedes maximal impairment of FAT. The different rates of transport decline correlate with Ca^{2+} elevation and CaN activation first in dendrites and subsequently in axons. Although many axonal pathologies have been described in AD, studies have primarily focused only on the dendritic effects of AβOs despite compelling reports of presynaptic AβOs in AD models and patients. Indeed, we observed axonal AβOs in both primary neurons and transgenic AD mouse brain. AβOs colocalize with axonal voltage-gated Ca^{2+} channels (VGCCs), and pretreatment with VGCC inhibitors prevents axonal, but not dendritic, defects. Finally, BDNF transport defects are prevented by dantrolene, a clinical compound that blocks Ca^{2+}-induced- Ca^{2+}-release through ryanodine receptors in the endoplasmic reticulum membrane. This work establishes a novel role for Ca^{2+} dysregulation in BDNF transport disruption and in tau-independent Aβ toxicity during early AD pathogenesis.

3.2. Introduction

Impaired fast axonal transport (FAT) of organelles correlates with early stages of Alzheimer's disease (AD) progression and are observed prior to cell death (Adalbert and Coleman, 2012; Goldstein, 2012; Ye et al., 2012; Millecamps and Julien, 2013). AD mice expressing disease-associated mutations exhibit FAT defects that precede amyloid

plaque deposition and extensive neurofibrillary tangle formation (Kanaan et al., 2013). These data support a causal role for FAT disruption in AD. Although the mechanisms of dendritic transport are less well characterized, they are also critical for neuronal function and survival. Transport of glutamate receptors, endosomes, and BDNF is essential for spine growth, learning and memory (Park et al., 2006; Kennedy et al., 2010; Kennedy and Ehlers, 2011; Lu et al., 2013; Yoshii et al., 2013). Thus, transport dysregulation in both axons and dendrites has significant physiological consequences in diseased neurons.

According to the "Ca^{2+} hypothesis of AD", amyloid-β (Aβ) overproduction and toxicity are induced by aberrant Ca^{2+} signaling prior to accumulation of hyperphosphorylated tau (p-tau) and cognitive decline (Berridge, 2010a; Chakroborty and Stutzmann, 2011). Aβ oligomers (AβOs) increase Ca^{2+} influx through several membrane receptors, including NMDA and AMPA glutamate receptors and axonal voltage-gated Ca^{2+} channels (VGCCs; (Ferreira and Klein, 2011). This triggers a persistent elevation in resting cytosolic Ca^{2+}, which is primarily maintained by Ca^{2+}-induced- Ca^{2+} release (CICR) from the ER (Ferreira and Klein, 2011; Paula-Lima et al., 2011). Elevated cytosolic Ca^{2+} activates the Ca^{2+}/calmodulin-dependent phosphatase, calcineurin (CaN). Activated CaN relieves inhibition of protein phosphatase-1 (PP1), which in turn over-activates glycogen synthase kinase 3β (GSK3β) ultimately leading to synapse failure (Reese and Taglialatela, 2011).

In axons, GSK3β activation can induce hyperphosphorylation of tau and disrupt FAT by inhibiting motor protein activity and cargo binding (Morfini et al., 2002; Ferreira and Klein, 2011; Kanaan et al., 2013; Weaver et al., 2013). AβOs reduce vesicular transport of BDNF in primary neurons through an NMDAR-dependent mechanism, which is mediated by GSK3β (Decker et al., 2010a). Notably, we found that AβO-induced transport defects occur independent of tau, microtubule destabilization, and acute cell death (Ramser et al., 2013). We rescued FAT defects by inhibiting CaN, and we prevented them by inhibiting PP1 and GSK3β. Our findings implicated dysregulated Ca^{2+} signaling in BDNF transport disruption when the contribution of pathogenic tau is likely minimal.

The Ca^{2+}-dependent mechanisms that regulate the onset, severity, and spatiotemporal progression of BDNF transport defects from dendritic and axonal AβO binding sites are unknown. Particularly, it is unclear how the binding of AβOs to postsynaptic sites leads to FAT impairment. We show that defects in dendritic and axonal transport of BDNF are induced simultaneously but decline at different rates: maximal impairment of dendritic transport precedes maximal impairment of FAT. This correlates with Ca^{2+} elevation and CaN activation in dendrites and subsequently in axons. Postsynaptic CaN activation converges on axonal Ca^{2+} dysregulation to impair FAT. Specifically, AβOs colocalize with axonal VGCCs, and blocking VGCCs prevents FAT defects. Finally, BDNF transport defects are prevented by dantrolene, a compound that reduces CICR through ryanodine receptors in the ER membrane. This work establishes a novel role for Ca^{2+} dysregulation in BDNF transport disruption and tau-independent Aβ toxicity.

3.3. Materials and Methods

3.3.1. Hippocampal cell culture and expression of transgenes

Primary hippocampal neuronal cultures from E16 wild-type ($tau^{+/+}$) and tau-knockout ($tau^{-/-}$) mice (Jackson Laboratory, Bar Harbor, ME) were prepared as described by Kaech and Banker (Kaech and Banker, 2006) and kept in PNGM primary neuron growth media (Lonza, Basel, Switzerland). The glial feeder layer was derived from murine neural stem cells as described by (Miranda et al., 2012). At 10–12 d in vitro, cells were cotransfected with pβ-actin-BDNF-mRFP and pmUBa–enhanced blue fluorescent protein (BFP; from Gary Banker, Oregon Health and Sciences University, Portland, OR) using Lipofectamine (Invitrogen). Cells expressed the plasmids for 24–36 h before live imaging. The absence of tau in $tau^{-/-}$ mice was previously confirmed by immunoblotting with the antibodies PHF-1 and tau-46 (Supplemental Figure 1; (Ramser et al., 2013)). All experiments with animals were approved by and followed the guidelines of the Simon Fraser University Animal Care Committee, Protocol 943-B05.

3.3.2. AβO, FK506, VGCC inhibitor, and RyR inhibitor treatments

Soluble, full-length Aβ 1-42 peptides (AβOs; American Peptide) were prepared exactly according to the method of Lambert et al. (Lambert et al., 1998) and applied to cells at a final concentration of 500 nM for 18 hours. Following AβO or vehicle exposure, cells were incubated with 1 μM FK506 (Sigma) or equivalent volumes of vehicle (ethanol) for 1-3 hours prior to imaging of transport. For all VGCC inhibition experiments, cells were incubated with 100 μM Conotoxin GVIA (Alomone Labs, Jerusalem), 50 μM Agatoxin IVA (Alomone Labs), or 10 μM Nimodipine (Tocris Bioscience, Bristol, UK) for 30 min prior to AβO treatments. For all RyR inhibition experiments, cells were incubated with 0.5 μM dantrolene (Sigma-Aldrich, St. Louis, MO) for 1 h prior to AβO treatment.

3.3.3. Live imaging and analysis of BDNF-mRFP transport

BDNF-mRFP transport was analyzed using a standard wide-field fluorescence microscope equipped with a cooled charge-coupled device camera and controlled by MetaMorph (Molecular Devices, Sunnyvale, CA) as described previously (Kwinter and Silverman, 2009). All imaging—typically 100 frames—was recorded by the "stream acquisition module" in MetaMorph. Briefly, cells were sealed in a heated imaging chamber, and recordings were acquired from double transfectants at an exposure time of 250 ms for 90 s. This captured dozens of transport events per cell in 50-μm segments of the dendrite or 100-μm segments of the axon. Dendrites and axons were initially identified based on morphology and confirmed retrospectively by immunostaining against MAP2, a dendritic cytoskeletal protein. Soluble BFP detection was necessary to determine the orientation of the cell body relative to the axon and thus to distinguish between anterograde and retrograde transport events. Vesicle flux, velocity, and run lengths were obtained through tracing kymographs in MetaMorph. Vesicle flux was defined as the total distance traveled by vesicles standardized by the length and duration of each movie (in micron-minutes): $\frac{\sum_{i=1}^{n} d_i}{\ell \times t}$ where d are the individual DCV run lengths, ℓ is the length of axon imaged and t is the duration of the imaging session. A

vesicle was defined as undergoing a directed run if it traveled a distance of ≥2 μm. This distance was determined as a safe estimate of the limit of diffusion based on the assumption that root-mean-squared displacement equals $\sqrt{2Dt}$, where D is the diffusion coefficient (D=0.01 $\mu m^2/s$ for DCVs) and t is the duration of the imaging period (t=50 s; (Abney et al., 1999). A run was defined as terminating if the vesicle remained in the same position for at least four consecutive frames. Percentage flux represents the flux in treated neurons normalized to controls (100%).

3.3.4. Immunocytochemistry

Neurons were fixed in 4% paraformaldehyde and blocked with 0.5% fish-skin gelatin (Kwinter et al., 2009). To confirm AβO binding to dendrites and verify qualitatively that AβOs remained oligomeric after 18 h in culture, cells were stained with an Aβ oligomer–specific antibody (NU-4, 1:1000; from W. L. Klein, Northwestern University, Evanston, IL) or 6E10 (1:1000; Covance, Berkeley, CA) and anti-MAP2 (1:2000; Millipore, Billerica, MA). To assess axonal AβO binding and the presence of axonal ER, neurons were stained with anti-α-tubulin (1:1000, Sigma-Aldrich) or anti-reticulon 3 (1:1000; R458, from Riqiang Yan, Cleveland Clinic, Cleveland, OH) and anti-ryanodine receptor 2 (1:300; Alomone Labs), respectively. To determine AβO colocalization with VGCCs, AβO-treated cells were stained with anti-CaV 2.1, anti-CaV 2.2, and anti-CaV 2.3 (1:100, Alomone Labs). Neurons were subsequently incubated with compatible secondary antibodies conjugated to Cy3 (1:500; Jackson ImmunoResearch Laboratories, West Grove, PA), Alexa 488 (1:500, Invitrogen), or Cy5 (1:500; Jackson ImmunoResearch Laboratories). To semi-quantify AβO colocalization with VGCCs, linescans of overlapping signal intensity peaks were generated using Metamorph. Appropriate thresholds were applied to eliminate background signal before analysis.

3.3.5. FRET analysis of intracellular Ca^{2+}

AβO-induced changes in cytosolic Ca^{2+} were detected using a genetically-encoded Ca^{2+} sensor, termed cameleon (D3cpV, gift from T. Pozzan, U. of Padova). The cameleon is comprised of two Ca^{2+}-responsive elements, calmodulin and M13, which alter the efficiency of fluorescence resonance-energy transfer (FRET) between their

respective CFP donor and cpVenus acceptor fluorophores (Palmer and Tsien, 2006). Neurons were transfected with D3cpV and mounted in heated chambers for imaging as described in the previous section. Using a scanning confocal microscope equipped with Argon 457/514 nm lasers (Nikon A1R, SFU Imaging Centre), we acquired CFP, cpVenus, and FRET (CFP excitation, cpVenus emission) images of the soma, dendrites and axons. To assess crosstalk between the CFP and cpVenus channels, we expressed calmodulin-CFP and M13-cpVenus separately and measure donor and acceptor fluorescence through corresponding and opposing channels. Using Nikon Elements AR 3.2 software, we generated maximum intensity projections from each Z-stack, defined regions of interest (ROIs), and calculated background-corrected FRET ratios (FRET-$FRET_{background}$/CFP-$CFP_{background}$) within each ROI. Each experiment was performed on 12-15 cells from at least 3 independent cultures. Significance was determined using a Student's t-test.

3.3.6. *In situ* proximal ligation assay

Calcineurin activation in dendrites and axons was detected *in situ* using the Duolink proximity ligation assay (PLA; Sigma-Aldrich). Control and AβO-treated neurons were fixed and stained with monoclonal anti-calmodulin (1:200, EMD Millipore, Billerica, MA) and polyclonal anti-calcineurin A (1:100, Enzo Life Sciences, Farmingdale, NY) as described previously. Primary antibodies were detected with proximity probes, composed of secondary antibodies conjugated to oligonucleotides, which hybridized to form circular DNA strands when CaN and CaM were in close proximity. These strands served as templates for localized rolling-circle amplification and detection with fluorescently labelled oligonucleotides. PLA probe hybridization, ligation and amplification were performed in 40-µL open droplet reactions, exactly according to the manufacturer's protocol. PLA puncta were quantified in 100 µm-segments of primary dendrites and proximal axons using the "Count Nuclei" application in MetaMorph. Each experiment was performed on 15-20 cells from at least 2 independent cultures. Significance was determined using a Student's t-test.

3.3.7. Immunohistochemistry

Coronal brain sections from 3 month-old transgenic AD mice (APP_{Swe}/PS_{45}) and age-matched, wild type control animals were obtained from Weihong Song (University of British Columbia, Vancouver, Canada). To detect AβOs, sections were rinsed in PBST, blocked in 10% donkey serum and 0.1% bovine serum albumin for 1 h, and incubated with NU-4 primary antibody (1:1000) overnight at 4°C. After further washes in PBST, sections were incubated with a compatible secondary antibody conjugated to Cy3 (1:500, Jackson ImmunoResearch Laboratories) for 1.5 h at room temperature and counterstained with DAPI. Images were acquired on a Nikon A1R scanning confocal system equipped with multiple laser lines (Simon Fraser University Imaging Facility).

3.4. Results

3.4.1. AβOs induce dendritic, calcineurin-dependent transport defects that precede maximal impairment of FAT

We previously showed that AβOs impair axonal BDNF transport independent of tau by non-excitotoxic activation of calcineurin (CaN), a Ca^{2+}/calmodulin-dependent phosphatase implicated in AD (Ramser et al., 2013). It is unknown how the binding of AβOs to dendritic synaptic sites leads to FAT impairment. Because CaN, its effectors (PP1 and GSK3β), and KIF1A, the primary kinesin motor required for BDNF transport (Lo et al., 2011), are present in both dendrites and axons (Lee et al., 2003; Mansuy, 2003; Kanaan et al., 2013), we asked if AβOs induce dendritic, CaN-dependent transport defects that precede FAT disruption. Additionally, to determine if AβO-induced mislocalization of axonal tau to dendrites (Zempel et al.; Avila et al., 2004; Ittner and Gotz, 2011) impairs dendritic transport, $tau^{+/+}$ and $tau^{-/-}$ hippocampal neurons expressing BDNF-monomeric red fluorescent protein (mRFP) were imaged 4-26 h after exposure to 500 nM AβOs (Figure 3.1, Supplemental Figure 1). Irreversible AβO binding was confirmed retrospectively by immunocytochemistry (Figure 3.1 A) using an oligomer-specific antibody (NU-4) (Lambert et al., 2007). Representative kymographs illustrate differences between BDNF transport in control (vehicle-treated) and AβO-treated neurons (Figure 3.1 B, C). Total dendritic flux was similarly and markedly reduced in

AβO-treated cells, both in the presence and absence of tau (Figure 3.1 B, C and Table 3.1). Treatment with 1 μM FK506, a highly specific, potent inhibitor of CaN, rescued these defects (Schreiber and Crabtree, 1992). A complete list of transport statistics is provided in Table 1. To assess the spatiotemporal progression of transport defects, we measured and compared dendritic and axonal transport after 4-26 h of AβO treatment (Figure 3.1 C). BDNF transport defects were induced simultaneously in both compartments but exhibited different rates of decline: maximal impairment of dendritic transport defects were observed within 5 - 12 h of AβO treatment, prior to maximal impairment of FAT after 18 h of AβO exposure. As reported in our published work, we observed no concomitant reduction in cell viability nor structural alterations of the microtubule network (Decker et al., 2010a; Ramser et al., 2013). Thus, under our experimental conditions, BDNF transport defects arise prior to overt neurotoxicity and are likely an early and specific consequence of AβO treatment. Collectively, results show that AβO-induced dendritic transport defects precede FAT disruption and occur by a common tau-independent mechanism that is reversible upon CaN inhibition.

3.4.2. AβO-induced elevation of intracellular Ca^{2+} correlates with the spatiotemporal progression of BDNF transport defects

AβOs increase Ca^{2+} influx through several membrane receptors, including NMDARs, AMPARs, and voltage-gated Ca^{2+} channels (Ferreira et al., 2007). This triggers a persistent elevation in resting cytosolic Ca^{2+}, which activates downstream Ca^{2+}/calmodulin-dependent proteins, such as CaN (Berridge, 2010a; Reese and Taglialatela, 2011). Within minutes of AβO treatment, CaN activation is observed, first in dendritic spines, and minutes to hours later in the cell body (Wu et al., 2012). Because AβOs impair dendritic and axonal transport by a similar CaN-dependent mechanism, we asked if Ca^{2+} and active CaN are elevated first in dendrites and later in axons, reflecting the spatiotemporal progression of BDNF transport defects. To detect AβO-induced changes in neuronal cytosolic Ca^{2+}, we expressed a genetically-encoded Ca^{2+} sensor, termed cameleon (D3cpV), in neurons prior to treatment with either vehicle or 500 nM AβOs (Figure 3.2). In comparison to control neurons, a significant increase in FRET between the calmodulin-CFP donor and the M13-cpVenus acceptor was observed exclusively in the cell body and primary dendrites after 5 h of AβO treatment

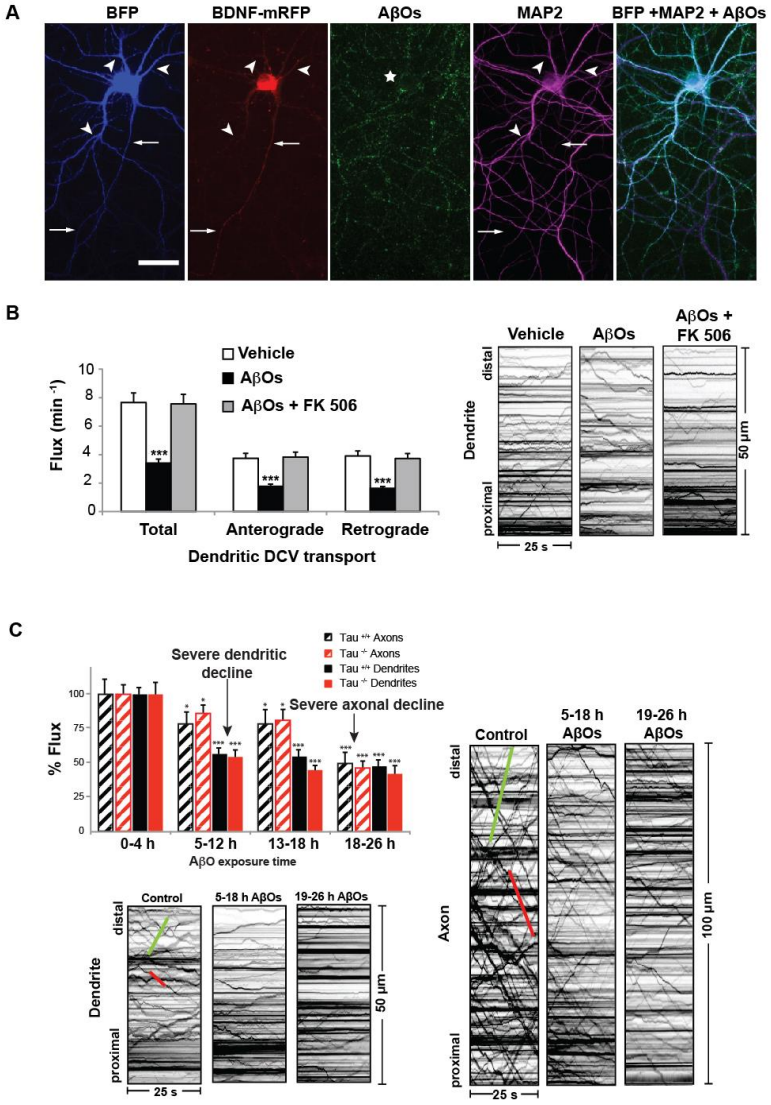

Figure 3.1 AβOs induce dendritic, calcineurin-dependent transport defects that precede maximal impairment of FAT.

(A) Expression of soluble blue fluorescent protein (BFP) and BDNF-mRFP in an AβO-treated tau$^{-/-}$ neuron (from left to right). Overlay of BFP and AβO images shows binding of AβOs to dendrites (MAP2-positive) and axons. Immunocytochemistry shows that AβOs remain oligomeric after 18 h in culture. Arrows indicate axons; arrowheads indicate dendrites. (B) Total dendritic flux was markedly reduced in AβO-treated tau$^{-/-}$ cells. Treatment with 1 µM FK506 rescued these defects. Representative kymographs illustrate differences between BDNF transport in control and treated neurons. (C) BDNF transport defects were induced simultaneously in both compartments but exhibited different rates of decline: significant dendritic transport defects were observed within 5-12 h of AβO treatment, prior to maximal impairment of FAT after 18 h of AβO exposure. Green trace indicates anterograde transport; red trace indicates retrograde transport. Graphs show means ± SEM. A minimum of 20 cells from 3 different cultures were analyzed per condition; ***$p < 0.001$ relative to controls. tau$^{+/+}$ transport data is presented in Supplemental Figure 1. Statistical evaluation is presented in Table 3.1. Scale bar = 25 µm.

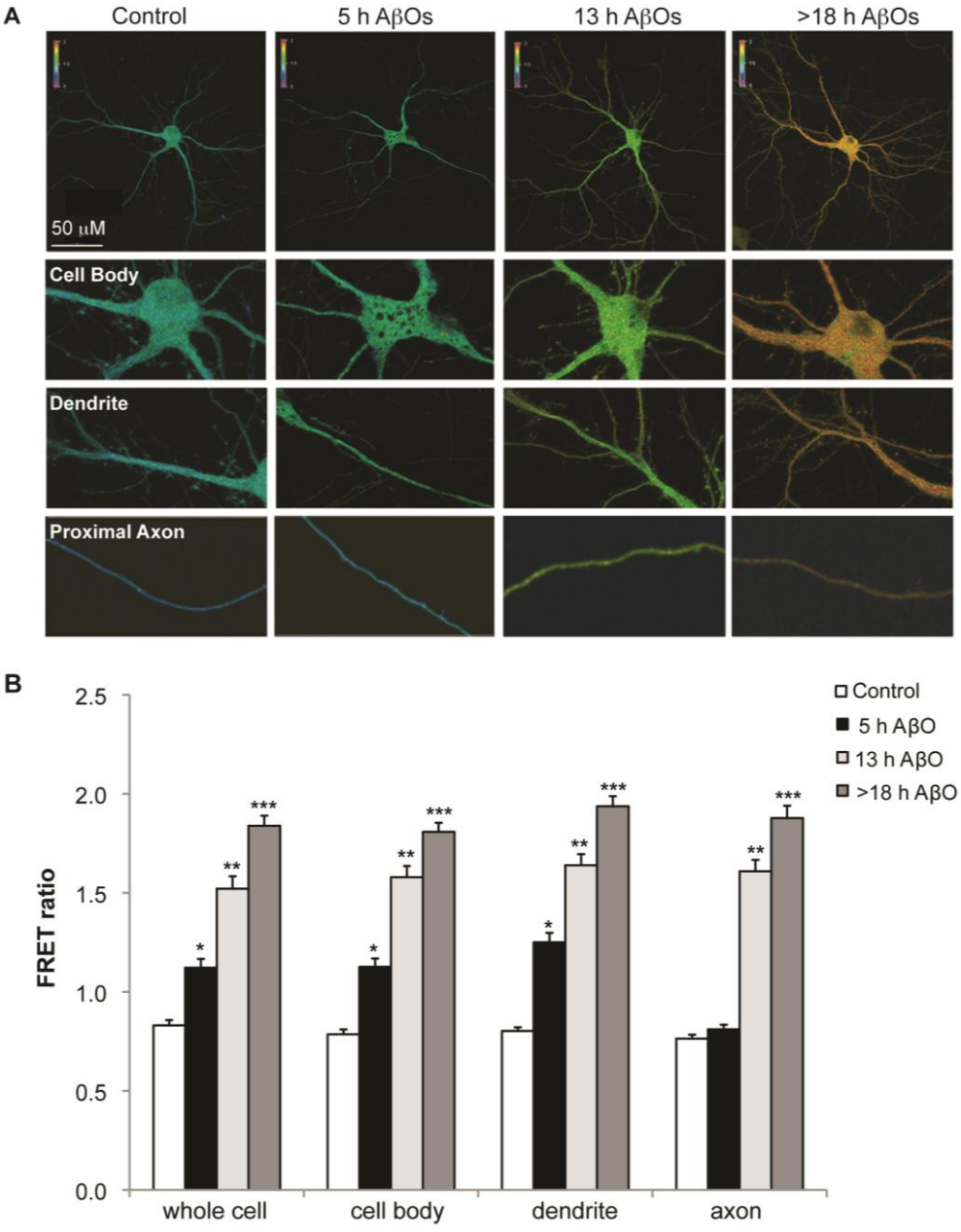

Figure 3.2 AβO-induced elevation of intracellular Ca^{2+} correlates with the spatiotemporal progression of BDNF transport defects.

(A, B) Representative images and quantification of cameleon FRET ratios in control and AβO-treated tau -/- neurons. In comparison to control neurons, a significant increase in FRET between the calmodulin-CFP donor and the M13-cpVenus acceptor was observed exclusively in the cell body and primary dendrites after 5 h of AβO treatment. After 13-18 h of AβO exposure, FRET ratios were also markedly increased in proximal axon segments within 300 μm of the cell body. Graphs show means ± SEM. A minimum of 15 cells from 3 independent cultures were analyzed per condition; *$p<0.05$, **$0.001<p<0.05$, and ***$p < 0.001$ relative to controls. Scale bar = 50 μm.

(Figure 3.2 A, B). After 13-18 h of AβO exposure, FRET ratios were also markedly increased in proximal axon segments within 300 µm of the cell body (Figure 3.2 A, B), indicated by the increased red shift of the thermoscale. Therefore, AβOs trigger an increase in cytosolic Ca^{2+} that is initially restricted to the somatodendritic domain and subsequently spreads through the axon. This coincides with the spatiotemporal progression of BDNF transport defects from dendrites to axons.

3.4.3. AβO-induced calcineurin activation coincides with the spatiotemporal progression of BDNF transport defects

Calmodulin (CaM) binds free Ca^{2+} ions and directly activates CaN (Reese and Taglialatela, 2011). Previously, we used in vitro phosphatase assays to detect elevation of CaN activity in cultured neurons treated with 500 nM AβOs for 18 h (Ramser et al., 2013). To determine the spatiotemporal progression of AβO-induced CaN activation, we performed in situ proximity ligation assays (PLA) (Soderberg et al., 2006) on control and AβO-treated neurons (Figure 3.3). First, CaM and CaN-specific primary antibodies for PLA analyses were validated by immunocytochemistry. As expected, CaM appeared soluble and ubiquitous, whereas CaN appeared punctate and localized predominantly to cell bodies and dendrites in control cells (Mansuy, 2003; Burgoyne, 2007; Wu et al., 2012) (Supplemental Figure 2). We visualized and quantified PLA puncta, indicative of CaN activation, in 100-µm segments of dendrites and axons after 4, 8, and 18 h of AβO exposure (Figure 3.3 B). In comparison to control cells, a significant increase in CaN activation was observed exclusively in the cell body and dendrites after 4 h of AβO treatment. After 18 h of AβO exposure, marked CaN activation was also detected in proximal axon segments (Figure 3.3 B). Results show that AβO-induced CaN activation is concomitant with cytosolic Ca^{2+} elevation in dendrites and axons and suggests that this response mediates the spatiotemporal progression of BDNF transport defects.

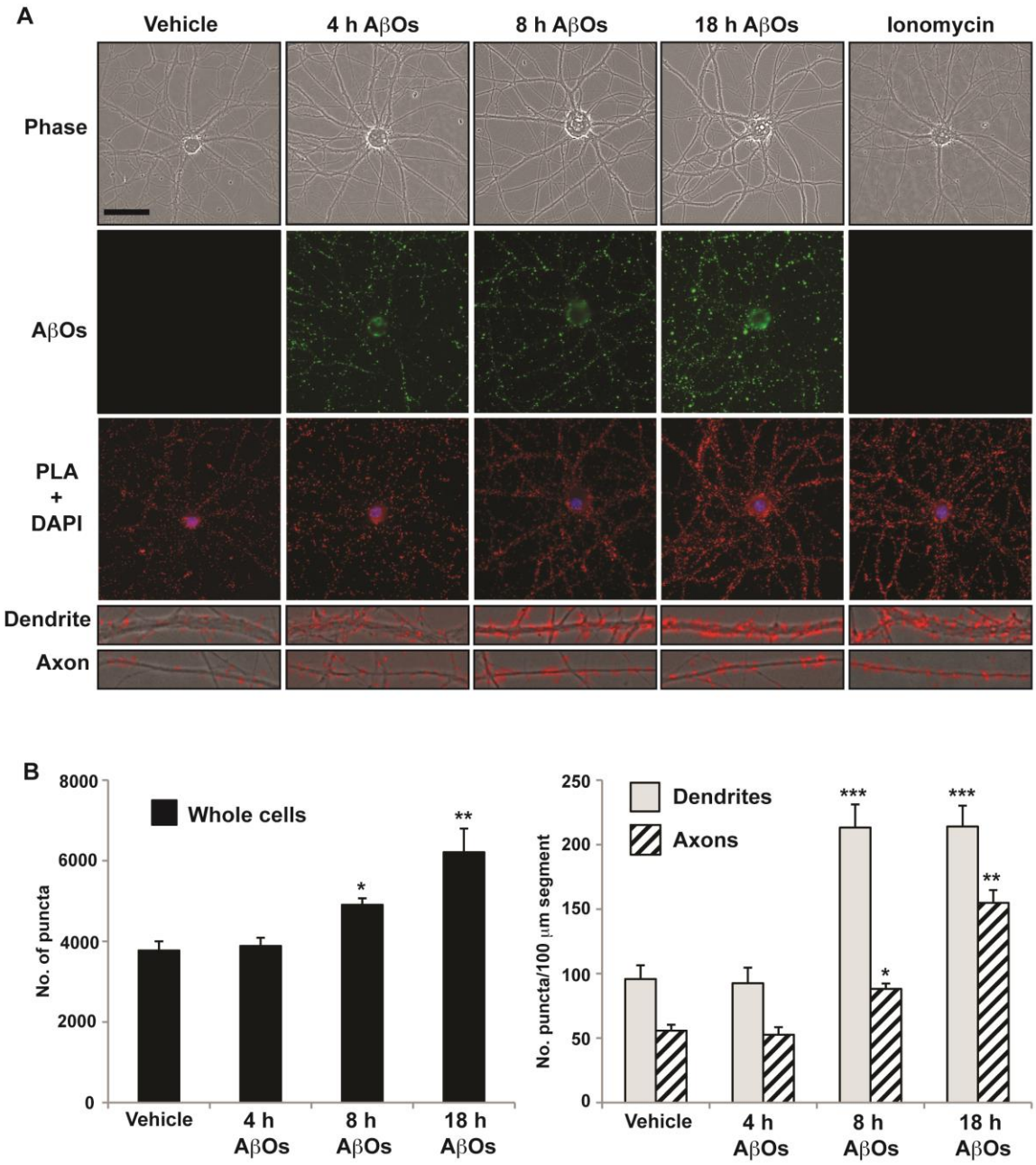

Figure 3.3 AβO-induced calcineurin activation coincides with the spatiotemporal progression of BDNF transport defects.

(A, B) Representative images and quantification of CaN-CaM puncta in control and AβO-treated tau -/- neurons. In comparison to control cells, a significant increase in CaN activation was observed by PLA exclusively in the cell body and dendrites after 5 h of AβO treatment. After 13-18 h of AβO exposure, marked CaN activation was also detected in proximal axon segments. Validation of CaN and CaM primary antibodies is shown in Supplemental Figure 4. Graphs show means ± SEM. A minimum of 15 cells from 3 independent cultures were analyzed per condition; *$p<0.05$, **$0.001<p<0.05$, and ***$p < 0.001$ relative to controls. Scale bar = 25 μm.

3.4.4. AβOs bind to axons and colocalize with presynaptic voltage-gated Ca^{2+} channels

Interestingly, although they decline at different rates, dendritic and axonal transport defects are induced simultaneously (Figure 3.1). This may be attributed to a novel, presynaptic mechanism of AβO-induced Ca^{2+} dysregulation that converges on postsynaptic mechanisms of CaN activation to impair FAT. Although AβOs are thought to bind exclusively to dendritic membrane proteins (Cochran et al., 2013), in vitro and in vivo evidence suggests that AβOs also modulate presynaptic voltage-gated Ca^{2+} channel (VGCC) activity (Cataldi, 2013). If Ca^{2+} elevation is restricted to the cell body and dendrites by extensive buffering mechanisms, axonal AβO binding may induce aberrant Ca^{2+} influx through VGCCs and contribute to FAT impairment. By immunocytochemistry with an Aβ oligomer-specific antibody (NU-4), we discovered that AβOs bind along the entire length of the axon in cultured neurons (Figure 3.4 A). To determine if axonal AβOs are also present in vivo, we performed immunohistochemistry on brain sections from double-transgenic AD mice (LaFerla 3X Tg). NU-4 staining revealed a punctate distribution of AβOs along dendrites and, strikingly, axons in the cortex (Figure 3.4 B). AβOs were not detected in age-matched wild type control mice (Figure 3.4 B). Based on reports that AβOs shift the steady-state activation of VGCCs towards more hyperpolarized values in HEK cells and increase Ca^{2+} influx in Xenopus oocytes (Mezler et al., 2012; Hermann et al., 2013), we asked if the P/Q and N-types, expressed abundantly in hippocampal neurons, constitute binding targets. Immunocytochemistry revealed a punctate distribution of both channel types in hippocampal neurons and a high degree of colocalization with AβOs (P/Q-type, 83.5%; N-type, 73.3%; Figure 3.4 C, Supplemental Figure 3). These results suggest that axonal AβOs associate directly or indirectly with presynaptic VGCCs and modulate their activity.

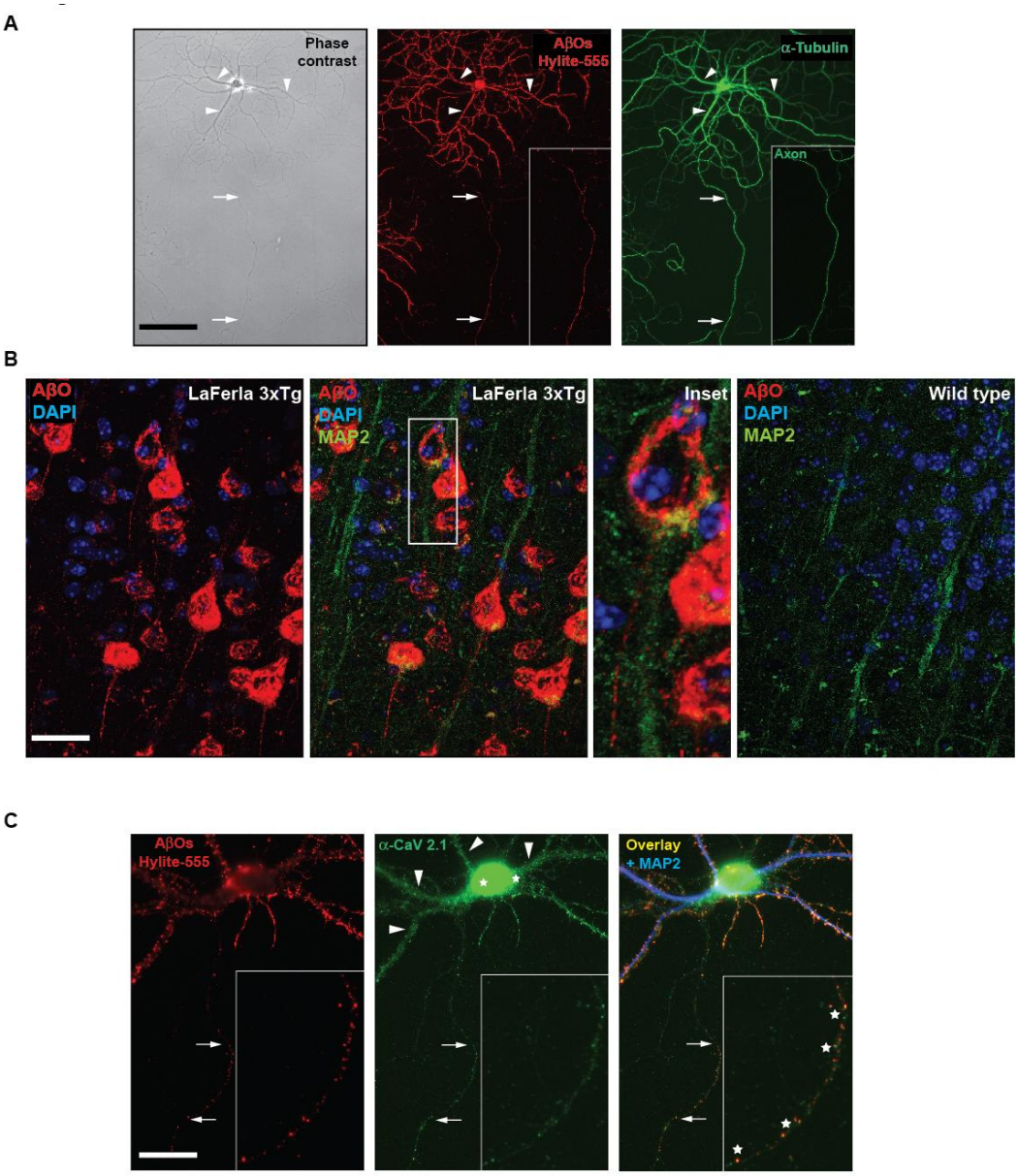

Figure 3.4 AβOs bind to axons and colocalize with presynaptic voltage-gated Ca^{2+} channels.

(A) Representative images of immunocytochemistry with an Aβ oligomer-specific antibody (NU-4) showed that AβOs bind along the entire length of the axon in cultured neurons. (B) Immunohistochemistry on coronal sections from transgenic AD mouse brain (LaFerla 3xTg) revealed a punctate distribution of AβOs along axons in the cortex. Axons were distinguished by the absence of MAP2 staining (inset). AβOs were not detected in age-matched wild type control mice. (C) Representative images of AβO and CaV 2.1 (P/Q-type VGCC) immunocytochemistry. 83.5% of axonal AβOs colocalize with P/Q-type VGCCs. A minimum of 15 cells from 3 independent cultures were analyzed. Scale bar = 100 μm

3.4.5. Inhibition of presynaptic voltage-gated Ca^{2+} channels prevents axonal, but not dendritic, BDNF transport defects

To determine if AβO-induced activation of presynaptic VGCCs impairs FAT, we incubated $tau^{+/+}$ and $tau^{-/-}$ neurons with 50 nM ω-agatoxin IVA (P/Q-type channel blocker) or 100 nM ω-conotoxin GVIA (N-type channel blocker) for 30 min. As a negative control, we exposed neurons similarly to 10 μM nimodipine, which inhibits postsynaptic L-type Ca^{2+} channels (spatial distribution of VGCCs reviewed in (Dolphin, 2012)). Subsequently, we treated $tau^{+/+}$ and $tau^{-/-}$ neurons with 500 nM AβOs for 18 h. Exposure to VGCC inhibitors did not prevent AβO binding (Figure 3.5 A). Remarkably, inhibition of P/Q and N-type VGCCs prevented axonal BDNF transport defects, independent of tau (Figure 3.5 B, Supplemental Table 2, Supplemental Figure 3). ω-agatoxin and ω-conotoxin maintained normal anterograde and retrograde flux in the presence of AβOs (Figure 3.5 B). Consistent with the low abundance of L-type Ca^{2+} channels in axons (Hell et al., 1993; Leitch et al., 2009), nimodipine pretreatment did not prevent AβO-induced transport defects (Figure 3.5 B). To confirm that Ca^{2+} influx mediates transport disruption, we chelated extracellular Ca^{2+} with 1.5 mM EGTA prior to AβO addition. Indeed, extracellular Ca^{2+} chelation precluded FAT disruption (Figure 3.5 B). By contrast, in dendrites, inhibition of P/Q and N-type VGCCs failed to prevent AβO-induced transport defects (Figure 3.5 C). No significant differences were observed in dendritic flux, velocity, and run length (Table 3.2). A complete list of transport statistics is provided in Table 3.2. This result suggests that Ca^{2+} influx through L-type channels may be negligible compared to NMDARs and other abundant postsynaptic channels and receptors, and thus does not regulate dendritic BDNF transport. Collectively, our findings indicate that AβO-induced Ca^{2+} influx through presynaptic P/Q and N-type VGCCs specifically blocks BDNF transport in axons.

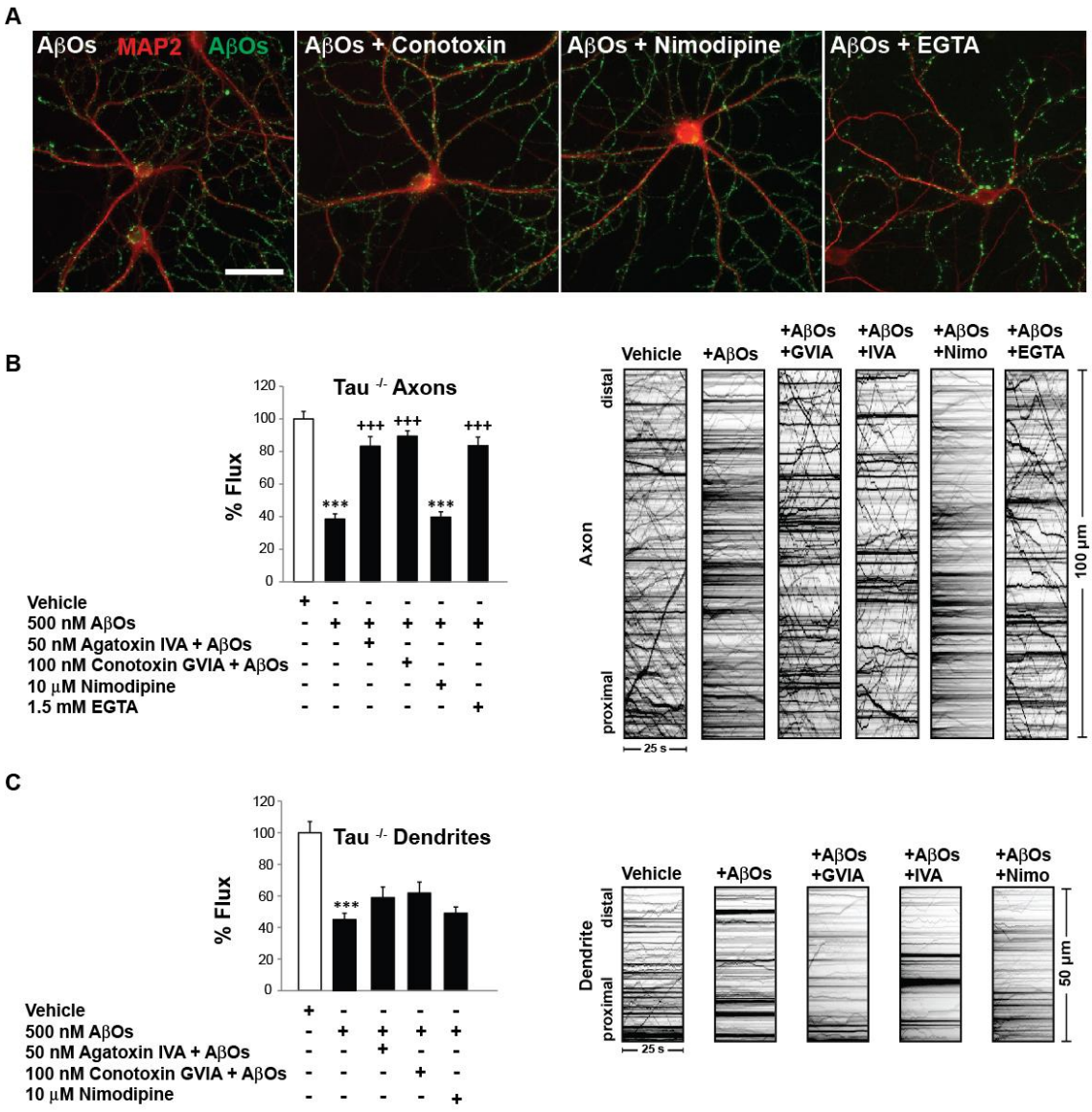

Figure 3.5 Inhibition of presynaptic voltage-gated Ca^{2+} channels prevents axonal, but not dendritic, BDNF transport defects.

(A) Representative images of MAP2 and AβO immunocytochemistry. Pre-treatment of $tau^{-/-}$ neurons with 50 μM ω-agatoxin IVA (P/Q-type channel blocker), 100 μM ω-conotoxin GVIA (N-type channel blocker), 10 μM nimodipine, or 1.5 mM EGTA did not prevent AβO binding. (B) Inhibition of P/Q and N-type VGCCs prevented axonal BDNF transport defects independent of tau. Consistent with the absence of L-type Ca^{2+} channels in axons, nimodipine pretreatment did not prevent AβO-induced transport defects. Extracellular Ca^{2+} chelation with EGTA precluded FAT disruption. (C) By contrast, in dendrites, inhibition of P/Q and N-type VGCCs failed to prevent AβO-induced transport defects. Pretreatment with Nimodipine or EGTA also did not prevent AβO-induced transport defects. Graphs show means ± SEM. A minimum of 15 cells from 3 different cultures were analyzed per condition; $^{***}p < 0.001$ relative to controls, and $^{+++}p < 0.001$ relative to AβO-treated cells. $tau^{+/+}$ transport data is presented in Supplemental Figure 2. Complete statistical evaluation is presented in Table 3.2. Scale bar = 25 μm.

3.4.6. Ryanodine receptor inhibition prevents axonal BDNF transport defects

Although there are many possible extracellular routes for AβO-induced Ca^{2+} influx, they may converge on Ca^{2+}-induced Ca^{2+} release (CICR) from the endoplasmic reticulum (ER). CICR is required for sustained Ca^{2+} elevation and signaling dysregulation in AD pathology (Demuro et al., 2010). Compounds that restore Ca^{2+} homeostasis can improve learning and memory in transgenic AD animal models (Oules et al., 2012). Traditionally, neuronal ER was thought to exist only in the cell body and dendrites; however, we and others have localized ER to axons of mammalian central nervous system neurons (Shimizu et al., 2008; Deng et al., 2014). We detected ER in the dendrites and axons of primary hippocampal neurons by staining for endogenous ryanodine receptors (RyRs) and reticulon-3 (Ret3), well-defined markers for the ER membrane (Figure 3.6 A, Supplemental Figure 5). Axons were distinguished by standard morphological criteria and by the absence of MAP2. To determine if CICR contributes to FAT impairment, we exposed $tau^{+/+}$ and $tau^{-/-}$ neurons to 0.5 μM dantrolene, a clinical compound that selectively blocks RyRs (MacLennan et al., 1990; Chakroborty et al., 2012). Subsequently, we treated neurons with 500 nM AβOs for 18 h. Remarkably, inhibition of RyRs prevented AβO-induced transport defects independent of tau (Figure 3.6 B, Supplemental Figure 4). Dantrolene treatment maintained normal anterograde and retrograde flux in the presence of AβOs (Figure 3.6 B, Supplemental Figure 4). A complete list of transport statistics is provided in Table 3.3. Taken together, our data demonstrate a central role for CICR in the disruption of FAT by ABOs and indicate that restoring Ca^{2+} homeostasis prevents these FAT defects.

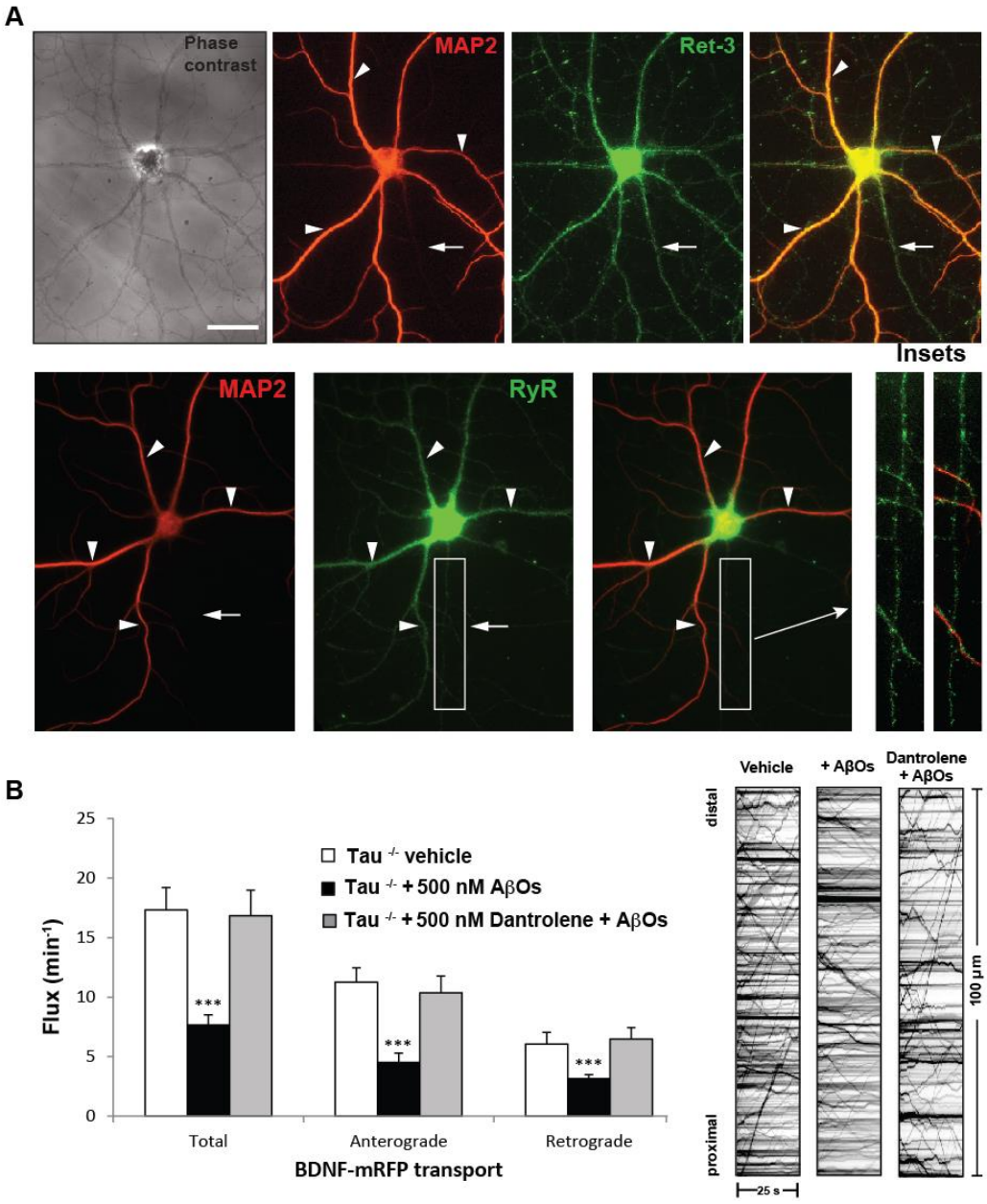

Figure 3.6 Ryanodine receptor inhibition prevents axonal BDNF transport defects.

(A) Representative images of Ret3 and RyR immunocytochemistry. ER was detected in the dendrites and axons of tau$^{-/-}$ neurons. Axons were distinguished by standard morphological criteria and by the absence of MAP2. (B) Inhibition of RyRs prevented AβO-induced transport defects independent of tau. Dantrolene treatment maintained normal anterograde and retrograde flux in the presence of AβOs. Graphs show means ± SEM. A minimum of 15 cells from 3 different cultures were analyzed per condition; ***$p < 0.001$ relative to controls. tau$^{+/+}$ transport data is presented in Supplemental Figure S3. Complete statistical evaluation is presented in Supplemental Table S3. Scale bar = 25 µm.

3.5. Discussion

Intracellular Ca^{2+} dysregulation and FAT disruption are early pathological manifestations that lead to loss of synapse function and axonal degeneration in AD (Berridge, 2013; Millecamps and Julien, 2013). AβOs are central to AD pathology and impair axonal organelle transport (Morfini et al., 2002; Decker et al., 2010a; Vossel et al., 2010; Wang et al., 2010; Tang et al., 2012; Ramser et al., 2013). Mechanisms that regulate the progression of FAT defects from dendritic and axonal sites of Ca^{2+} elevation are unknown. Here, through direct assessment of DCV trafficking at high spatial and temporal resolution in living neurons, we show that defects in dendritic and axonal transport of BDNF are induced simultaneously but decline at different rates: maximal impairment of dendritic transport precedes maximal impairment of FAT. We combined multiple approaches, including live imaging, cameleon FRET, proximal ligation assays, and immunohistochemistry, to correlate the spatiotemporal progression of transport defects with Ca^{2+} elevation and CaN activation in dendrites and subsequently in axons. Postsynaptic CaN activation converges on axonal Ca^{2+} dysregulation to impair FAT. Specifically, AβOs colocalize with axonal VGCCs, and blocking VGCCs prevents FAT defects. Finally, BDNF transport defects are prevented by dantrolene, a compound that reduces CICR through RyRs. Collectively, this work establishes a novel role for Ca^{2+} dysregulation in BDNF transport disruption and in tau-independent Aβ toxicity during early AD pathogenesis.

3.5.1. Dendritic BDNF transport defects may contribute to AβO-induced cellular toxicity

Although substantial evidence implicates axonal transport deficits in neurodegeneration, less is known about the roles and regulation of dendritic transport in normal and disease states. Selective transport establishes a polarized distribution of dendritic proteins (Silverman et al., 2001; Petersen et al., 2014). KIF1A coordinates dendrite branch morphogenesis and regulates the apposition of active zones and postsynaptic densities by controlling site-specific deposition of its cargo (Kern et al., 2013). In rat primary neurons, BDNF synthesized in the cell body is trafficked to proximal dendrites, where it promotes spine formation (Dean et al., 2009; Orefice et al.,

2013). When destined for postsynaptic release, BDNF increases dendritic branching and modulates synaptic function by autocrine and paracrine mechanisms (Kuczewski et al., 2009). Alternatively, dendritic BDNF might constitute a reserve pool for presynaptic BDNF, which could be rapidly recruited to or from axon terminals upon changes in synapse activity (Maeder et al., 2014). Collectively, these studies demonstrate critical roles for dendritic BDNF transport in postsynaptic development, function, and plasticity. Here, we show that AβOs impair bidirectional transport of BDNF in dendrites. Ultimately, this may compromise postsynaptic BDNF secretion, reduce synaptic efficacy, and lead to neurodegeneration in AD. Restoring BDNF transport increases its release and promotes neuronal survival (Borrell-Pages et al., 2006; Pineda et al., 2009). Furthermore, in frontotemporal lobar dementia, interaction between the risk factor TMEM106B and the microtubule-associated protein MAP6 regulates dendritic transport of lysosomes and dendritic branching (Schwenk et al., 2014). To our knowledge, we are first to implicate reduced dendritic transport of BDNF in AD pathogenesis.

3.5.2. Dendritic and axonal sources of Ca^{2+} elevation converge to disrupt BDNF transport

We demonstrate that dendritic and axonal BDNF transport defects are induced concomitantly but exhibit different rates of decline: significant dendritic transport defects precede maximal impairment of FAT. These findings suggest that dendritic and axonal sources of Ca^{2+} elevation converge to disrupt BDNF transport. AβOs are thought to interact preferentially with postsynaptic membrane receptors and modulate their activity (Cochran et al., 2013). Glutamate receptors, which mediate dendritic Ca^{2+} elevation, appear to be centrally involved (Ferreira and Klein, 2011); inhibition or removal of surface AMPARs reduces AβO binding to dendrites (Zhao et al., 2010), and metabotropic glutamate receptors (mGluR5) participate in AβO binding and clustering at synapses (Renner et al., 2010). Additionally, NMDARs coimmunoprecipitate with AβOs from rat synaptosomal membranes (De Felice et al., 2007), and AβO binding is abolished in dendrites of NMDAR knock-down neurons (Jurgensen et al.; Decker et al., 2010b). We previously showed that NMDARs mediate AβO-induced disruption of BDNF transport by activation of CaN-GSK3β signaling. Dendritic transport may decline more rapidly than FAT due to the abundance and density of postsynaptic glutamate receptors

at spines, and therefore greater proximity of the transport apparatus and its regulators to sites of Ca^{2+} influx and CICR from somatodendritic ER.

Interestingly, although they decline at different rates, dendritic and axonal transport defects are induced simultaneously. This may be attributed to a novel, presynaptic mechanism of AβO-induced Ca^{2+} dysregulation that converges on postsynaptic mechanisms of CaN activation to impair FAT. Presynaptic AβO binding has not been investigated extensively, and specific axonal binding sites and protein interactions remain uncharacterized. Here, we report that AβOs bind to axons in culture and transgenic AD mouse brain. Consistently, immunoelectron microscopy studies indicate that AβOs localize to axons and presynaptic terminals at higher density in AD mice and patients than in wild type mice or non-demented individuals (Kokubo et al., 2005a; Kokubo et al., 2005b). Furthermore, we show that AβOs colocalize with axonal VGCCs. Although other work has failed to demonstrate direct or indirect binding, AβOs markedly increase VGCC currents in cultured cortical and hippocampal neurons (Ramsden et al., 2002; Hermann et al., 2013). Treatment with antagonists rectifies Ca^{2+}influx (Bobich et al., 2004) and protects against Aβ-induced cellular toxicity (Anekonda and Quinn, 2011; Copenhaver et al., 2011). In the present study, inhibition of P/Q and N-type channels precludes axonal BDNF transport defects, further implicating VGCCs in AD progression.

Although there are many possible extracellular routes for AβO-induced Ca^{2+}influx, they may converge on CICR from the ER to disrupt transport. Indeed, we prevented axonal BDNF transport defects by inhibiting RyRs with dantrolene, attesting to ER involvement. In accordance with this finding, activity-dependent capture of DCVs at synaptic boutons requires CICR by presynaptic RyRs and activation of Ca^{2+}/calmodulin-dependent kinase II (CaMKII) (Wong et al., 2009). Additionally, overexpression of the ER transmembrane protein, reticulon-3 (RTN3), reduces anterograde transport of β-site amyloid precursor protein-cleaving enzyme 1 (BACE1) in cultured cells (Deng et al., 2014). Moreover, in young 3xTg-AD mice, a compensatory increase in RyR expression reduces the threshold for CICR, such that basal NMDAR activation elevates Ca^{2+} efflux from the ER in both dendrites and axons (Chakroborty et al., 2012). It is possible that AβO-induced Ca^{2+} release from axonal RyRs contributes to FAT disruption, notably in

the presence or absence of tau. Collectively, these results strongly support a role for Ca^{2+} dysregulation in presymptomatic neurodegeneration, which occurs prior to Aβ plaque deposition and excessive tau pathology (Stutzmann et al., 2007).

3.5.3. Ca^{2+}-dependent mechanisms of motor protein regulation

There are several Ca^{2+}-dependent mechanisms by which AβOs might disrupt BDNF transport. One mechanism could involve CaN-dependent inhibition of motor protein activity, mediated by GSK3β. GSK3β is implicated in many aspects of AD pathogenesis (Hooper et al., 2008) and negatively regulates axonal transport in squid axoplasm (Pigino et al., 2003), *Drosophila* neurons (Shaw and Chang, 2013), and mammals (DeFuria and Shea, 2007; Decker et al., 2010a; Tang et al., 2012; Cantuti Castelvetri et al., 2013; Ramser et al., 2013). Negative regulation of kinesin-1 (KIF5) and cytoplasmic dynein is accomplished by reducing the number of motors that are bound to microtubules (Dolma et al., 2014). A second mechanism might comprise disruption of motor protein-cargo binding. Dendritic trafficking of NMDAR-containing vesicles is perturbed upon phosphorylation of KIF17 by CaMKII, which attenuates the interaction between KIF17 and its cargo adaptor, Mint1 (Guillaud et al., 2008; Yin et al., 2011). Likewise, it is possible that activation of CaN-GSK3β signaling phosphorylates KIF1A and blocks BDNF transport. A third mechanism could require activation of a Ca^{2+}-sensing protein that directly inhibits motor motility. For example, the Ca^{2+}-sensitive mitochondrial protein, Miro, interacts with the motor domain of KIF5 to dissociate it from microtubules (Wang and Schwarz, 2009). Moreover, AβO treatment perturbs mitochondria transport in cultured neurons (Decker et al., 2010a; Vossel et al., 2010). KIF1A motility and BDNF transport might be impaired by an analogous mechanism.

Based on our present findings and other current models of AD pathogenesis, we propose the following mechanism for Ca^{2+}-dependent disruption of dendritic and axonal BDNF transport (Figure 3.7). AβOs bind to dendrites and axons, enhancing Ca^{2+} influx through dendritic glutamate receptors and axonal VGCCs. In turn, this induces CICR from postsynaptic and presynaptic ER to elevate resting cytosolic Ca^{2+}. Calmodulin binds free Ca^{2+} ions and subsequently activates CaN-GSK3β signaling in dendrites and axons. Upon activation, GSK3β may disrupt BDNF transport by directly phosphorylating

and inhibiting motor proteins and/or disrupting motor-DCV interactions. Finally, from a clinical perspective, our findings are significant because intracellular Ca^{2+} dysregulation and transport impairment precede excessive tau hyperphosphorylation, NFT formation, and microtubule destabilization (Stutzmann et al., 2007; Goldstein, 2012). Compounds targeted to these early disease mechanisms may be more effective at preventing or reversing cell death.

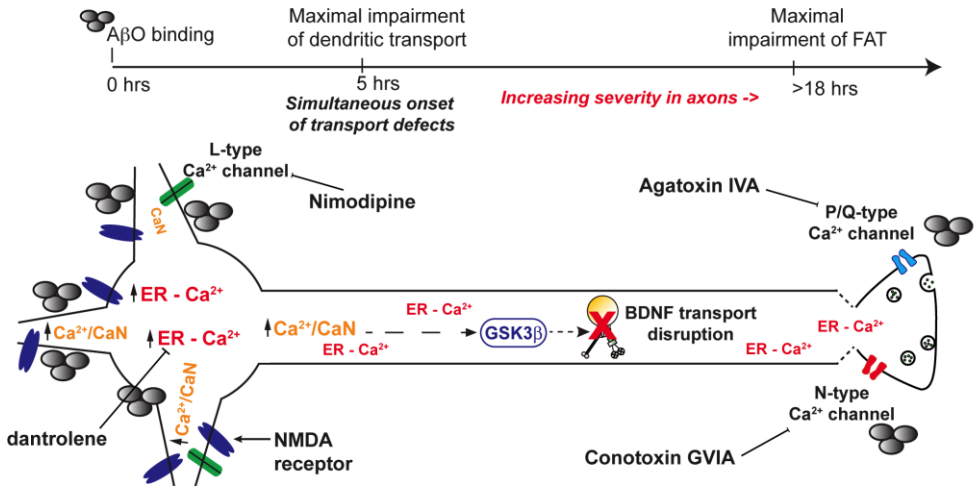

Figure 3.7 Proposed mechanism for Ca^{2+}-dependent disruption of dendritic and axonal BDNF transport.

AβOs bind to dendrites and axons, enhancing Ca^{2+} influx through dendritic glutamate receptors and axonal VGCCs. In turn, this induces CICR from postsynaptic and presynaptic ER to elevate resting cytosolic Ca^{2+}. Calmodulin binds free Ca^{2+} ions and subsequently activates CaN-GSK3β signaling in dendrites and axons. Upon activation, GSK3β may disrupt BDNF transport by directly phosphorylating and inhibiting motor proteins and/or disrupting motor-DCV interactions. Alternatively, a Ca^{2+}-sensing adaptor protein may directly impair motor protein motility.

3.6. Acknowledgements

This research was supported by grants from the National Science and Engineering Research Council of Canada (NSERC; 327100-06) and the Canadian Institutes of Health Research (CIHR; 90396) to M.A.S. We are grateful to L. Chen for her expert technical assistance and D. Poburko for essential discussions. We thank P. Copenhaver and G. Morfini for their critical reading of this manuscript, and C. Krieger for the Laferla 3xTg mice brains. K.J.G. is funded by a C.D. Nelson Memorial Graduate Scholarship from Simon Fraser University and an NSERC Postgraduate Scholarship.

3.7. Supplemental Figures and Tables

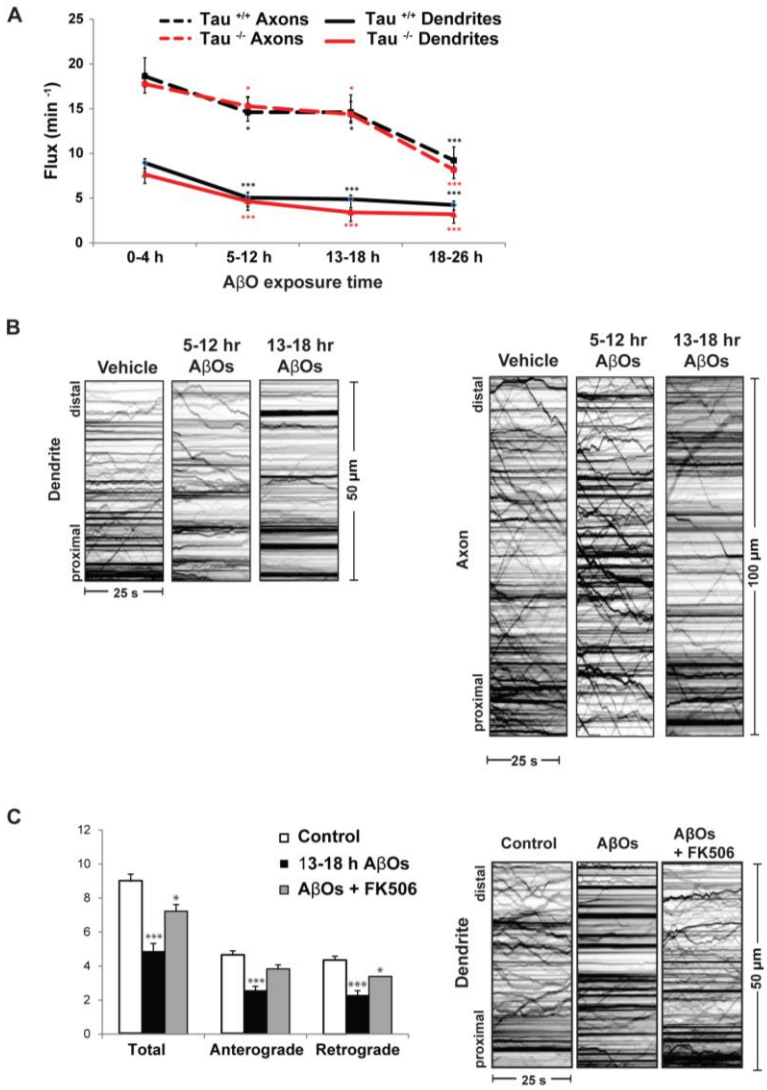

Figure 3.8 Supplemental Figure 1

AβOs induce dendritic, calcineurin-dependent transport defects that precede maximal impairment of FAT in tau$^{+/+}$ neurons. (A, B) BDNF transport defects were induced simultaneously in both compartments but exhibited different rates of decline: significant dendritic transport defects were observed within 5- 12 h of AβO treatment, prior to maximal impairment of FAT after 18 h of AβO exposure. (C) Total dendritic flux was markedly reduced in AβO-treated tau$^{+/+}$ cells. Treatment with 1 µM FK506 rescued these defects. Representative kymographs illustrate differences between BDNF transport in control and treated neurons. Graphs show means ± SEM. A minimum of 20 cells from 3 different cultures were analyzed per condition; ***p < 0.001 relative to controls. tau$^{-/-}$ transport data is presented in Figure 3.1. Complete statistical evaluation is presented in Table 3.1. Scale bar = 25 µm.

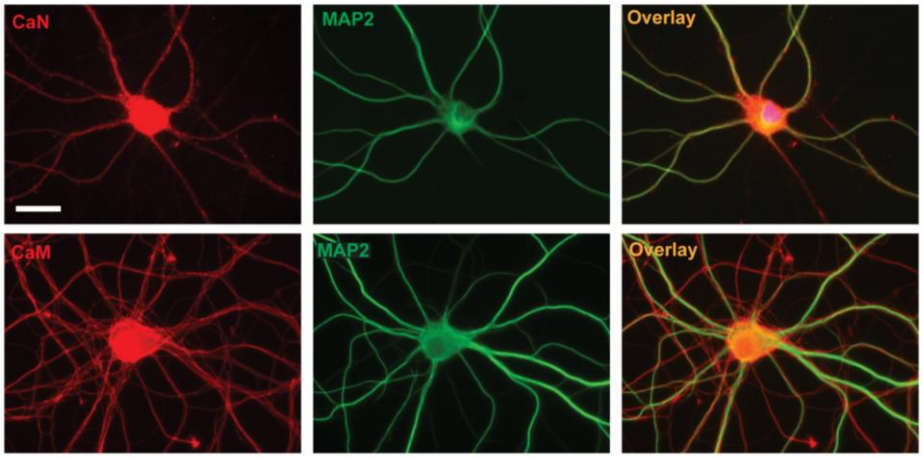

Figure 3.9 Supplemental Figure 2

Endogenous expression of calcineurin and calmodulin. CaN and CaM-specific primary antibodies for PLA analyses were validated by immunocytochemistry. As expected, CaM appeared soluble and ubiquitous, whereas CaN appeared punctate and localized predominantly to dendrites in control cells. Scale bar = 25 μm.

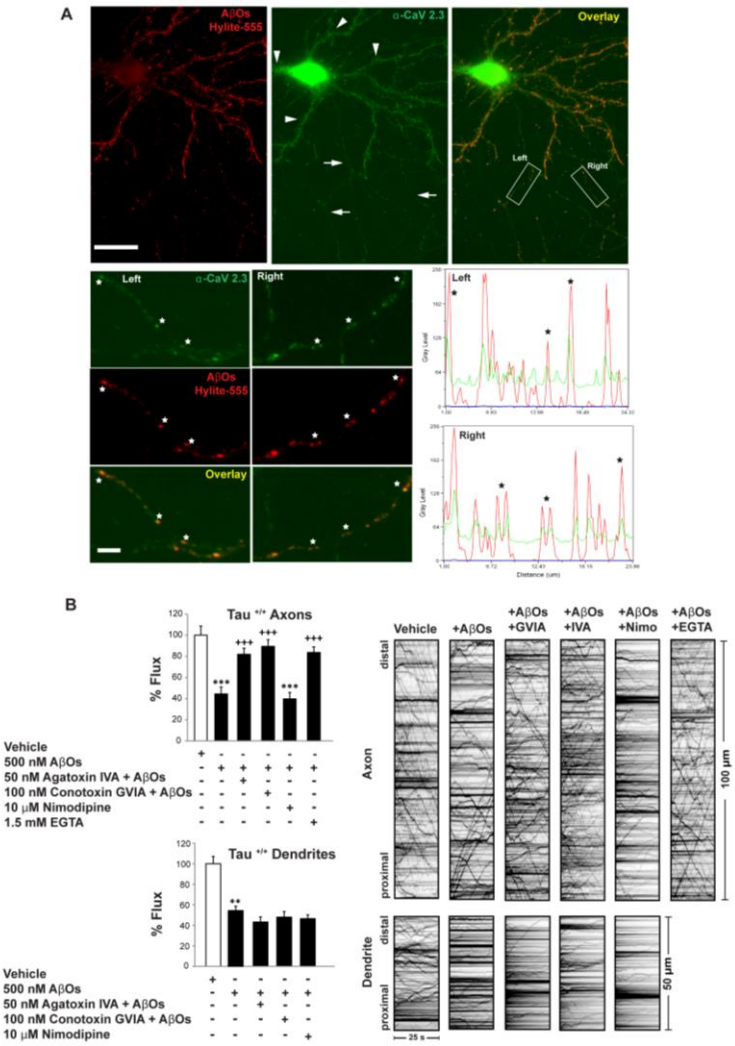

Figure 3.10 Supplemental Figure 3

Inhibition of presynaptic voltage-gated Ca^{2+} channels prevents axonal, but not dendritic, BDNF transport defects in $tau^{+/+}$ neurons. (A) Representative images of AβO and CaV 2.2 (N-type VGCC) experssion in hippocampal neurons, detected by immunocytochemistry. 73.3% of axonal AβOs colocalize with P/Q-type VGCCs. Overlapping red and green peaks on line scans of axonal regions indicate colocalization. (B) Inhibition of P/Q and N-type VGCCs prevented axonal BDNF transport defects in $tau^{+/+}$ neurons. Consistent with the absence of L-type Ca^{2+} channels in axons, nimodipine pretreatment did not prevent AβO-induced transport defects. Extracellular Ca^{2+} chelation with EGTA precluded FAT disruption. Conversely, in dendrites, inhibition of P/Q and N-type VGCCs failed to prevent AβO-induced transport defects. Nimodipine pretreatment also did not prevent AβO-induced transport defects. Graphs show means ± SEM. A minimum of 15 cells from 3 different cultures were analyzed per condition; $^{**}0.001<p<0.05$ and $^{***}p < 0.001$ relative to controls, and $+++p < 0.001$ relative to AβO-treated cells. $tau^{-/-}$ transport data is presented in Figure 2.5. Complete statistical evaluation is presented in Table 3.2. Scale bar = 25 μm.

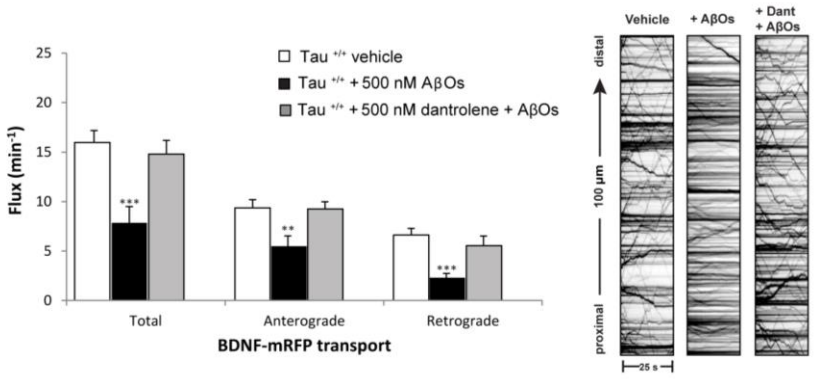

Figure 3.11 Supplemental Figure 4

Ryanodine receptor inhibition prevents axonal BDNF transport defects in tau$^{+/+}$ neurons. Inhibition of RyRs prevented AβO-induced transport defects independent of tau. Dantrolene treatment maintained normal anterograde and retrograde flux in the presence of AβOs. Graphs show means ± SEM. A minimum of 15 cells from 3 different cultures were analyzed per condition; ***p < 0.001 relative to controls. tau$^{-/-}$ transport data is presented in Figure 3.6. Complete statistical evaluation is presented in Table 3.3. Scale bar = 25 µm.

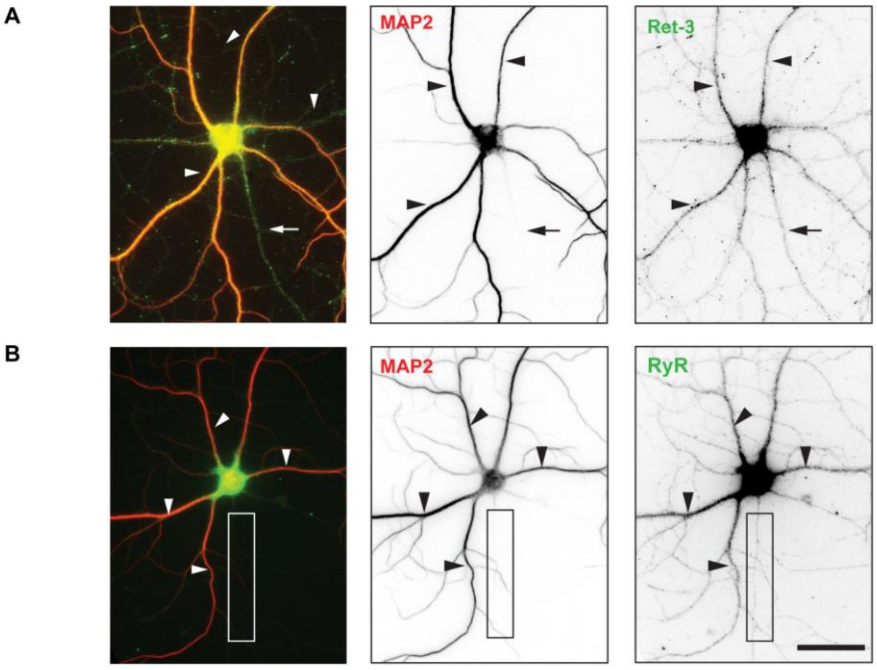

Figure 3.12 Supplemental Figure 5

Ryanodine receptor inhibition prevents axonal BDNF transport defects. (A) Representative black and white images of Ret3 and RyR immunocytochemistry from Figure 3.6. ER was detected in the dendrites and axons of tau$^{-/-}$ neurons. Axons were distinguished by standard morphological criteria and by the absence of MAP2. Arrows indicate axons; arrowheads indicate dendrites.

Table 3.1 Quantitative analysis of dendritic and axonal BDNF transport

	Dense Core Vesicles						%	
	All Events		Anterograde		Retrograde		All Events	
	Dendrites	Axons	Dendrites	Axons	Dendrites	Axons	Dendrites	Axons
Flux (min^{-1})								
tau $^{+/+}$ vehicle	8.96 ± 0.45	18.62 ± 2.06	4.61 ± 0.29	9.81 ± 1.42	4.35 ± 0.23	8.81 ± 0.95	100.00 ± 5.02	100.00 ± 11.06
tau $^{+/+}$ AβOs 13-18 h	4.89 ± 0.44***	14.61 ± 1.93*	2.58 ± 0.23***	7.36 ±1.49*	2.31 ± 0.25***	7.24 ± 0.75*	54.58 ± 4.91***	78.46 ± 10.37*
tau $^{+/+}$ AβOs + FK506	7.23 ± 0.39$^{***\#\#\#}$	--	3.84 ± 0.24***	--	3.39 ± 0.24$^{***\#\#}$	--	80.69 ± 4.35$^{***\#\#\#}$	--
tau $^{-/-}$ vehicle	7.66 ± 0.68	17.76 ± 1.25	3.75 ± 0.35	9.38 ± 0.82	3.91 ± 0.36	8.66 ± 0.67	85.49 ± 7.59	95.38 ± 6.71
tau $^{-/-}$ AβOs 13-18 h	3.41 ± 0.27***	14.38 ± 1.41	1.78 ± 0.15***	7.59 ± 0.87	1.64 ± 0.13***	6.79 ± 0.65	38.06 ± 3.01***	77.23 ± 7.57
tau $^{-/-}$ AβOs + FK506	7.56 ± 0.65$^{\#\#\#}$	--	3.84 ± 0.34$^{\#\#}$	--	3.72 ± 0.33$^{\#\#}$	--	84.38 ± 7.25$^{\#\#}$	--
Velocity (μm/s)								
tau $^{+/+}$ vehicle	1.43 ± 0.03	1.86 ± 0.12	1.44 ± 0.04	1.94 ± 0.12	1.42 ± 0.04	1.78 ± 0.13	100.00 ± 2.10	100.00 ± 6.45
tau $^{+/+}$ AβOs 13-18 h	1.34 ± 0.03*	1.85 ± 0.12	1.30 ± 0.04**	1.88 ± 0.14	1.37 ± 0.04	1.82 ± 0.13	93.71 ± 2.10*	99.46 ± 6.45
tau $^{+/+}$ AβOs + FK506	1.27 ± 0.04**	--	1.22 ± 0.05***	--	1.32 ± 0.04	--	88.81 ± 2.80**	--
tau $^{-/-}$ vehicle	1.31 ± 0.05*	2.03 ± 0.08	1.30 ± 0.06*	2.06 ± 0.09	1.33 ± 0.04	1.99 ± 0.08	91.61 ± 3.50*	109.14 ± 4.30
tau $^{-/-}$ AβOs 13-18 h	1.19 ± 0.03	2.10 ± 0.09	1.16 ± 0.04	2.13 ± 0.08	1.23 ± 0.04	2.07 ± 0.10	83.22 ± 2.10	112.90 ± 4.84
tau $^{-/-}$ AβOs + FK506	1.35 ± 0.04$^{\#\#}$	--	1.36 ± 0.04$^{\#\#}$	--	1.35 ± 0.04$^{\#}$	--	94.41 ± 2.80$^{\#\#}$	--
Run length (μm)								
tau $^{+/+}$ vehicle	4.53 ± 0.25	8.60 ± 1.14	4.44 ± 0.26	9.28 ± 1.32	4.68 ± 0.27	7.73 ± 0.88	100.00 ± 5.52	100.00 ± 13.26
tau $^{+/+}$ AβOs 13-18 h	4.56 ± 0.17	8.83 ± 0.82	4.54 ± 0.21	9.49 ± 1.25	4.64 ± 0.23	8.26 ± 0.95	100.66 ± 3.75	102.67 ± 9.29
tau $^{+/+}$ AβOs + FK506	5.06 ± 0.16$^{\#}$	--	5.01 ± 0.22	--	5.19 ± 0.17	--	111.70 ± 3.53$^{\#}$	--
tau $^{-/-}$ vehicle	5.11 ± 0.16	10.36 ± 0.46	4.92 ± 0.22	11.24 ± 0.55*	5.67 ± 0.16	9.80 ± 0.43**	112.80 ± 3.53	120.47 ± 4.44
tau $^{-/-}$ AβOs 13-18 h	4.75 ± 0.14	10.34 ± 0.09	4.77 ± 0.18	11.45 ± 0.08	4.79 ± 0.16	9.45 ± 0.64	104.86 ± 3.09	120.23 ± 0.87
tau $^{-/-}$ AβOs + FK506	5.48 ± 0.15$^{\#\#}$	--	5.50 ± 0.08$^{\#}$	--	5.54 ± 0.18$^{\#\#}$	--	120.97 ± 3.31$^{\#\#}$	--

tau$^{+/+}$ vehicle dendrites: n=18 kymographs (18 cells, 1187 vesicles); axons: n=15 kymographs (15 cells, 1753 vesicles)
tau$^{+/+}$ AβO dendrites: n=22 kymographs (22 cells, 710 vesicles); axons: n=16 kymographs (16 cells, 1383 vesicles)
tau$^{+/+}$ AβO + FK506 dendrites: n=22 kymographs (22 cells, 919 vesicles)
tau$^{-/-}$ vehicle dendrites: n=17 kymographs (17 cells, 739 vesicles); axons: n=15 kymographs (15 cells, 1423 vesicles)
tau$^{-/-}$ AβO dendrites: n=34 kymographs (34 cells, 737 vesicles); axons: n=18 kymographs (18 cells, 1276 vesicles)
tau$^{-/-}$ AβO + FK506 dendrites: n=21 kymographs (21 cells, 909 vesicles)

* p<0.05, when compared with vehicle
** p<0.01, when compared with vehicle
*** p<0.001, when compared with vehicle

# p<0.05, when compared with AβOs
p<0.01, when compared with AβOs
p<0.001, when compared with AβOs

Table 3.2 VGCC inhibition prevents AβO-induced transport defects

	Dense Core Vesicles						%	
	All Events		Anterograde		Retrograde		All Events	
	Dendrites	Axons	Dendrites	Axons	Dendrites	Axons	Dendrites	Axons
Flux (min^{-1})								
tau $^{+/+}$ vehicle	8.96 ± 0.45	16.79 ± 1.44	4.61 ± 0.29	9.99 ± 0.68	4.35 ± 0.23	6.80 ± 0.94	100.00 ± 5.02	100.00 ± 4.99
tau $^{+/+}$ AβOs	4.89 ± 0.44***	8.04 ± 0.98***	2.58 ± 0.23***	5.08 ±0.62***	2.31 ± 0.25***	2.96 ± 0.40***	54.58 ± 4.99***	47.84 ± 5.82***
tau $^{+/+}$ Aga + AβOs	3.94 ± 0.39***	14.91 ± 0.84^{+++}	2.29 ± 0.24***	8.62 ± 0.56^{+++}	1.68 ± 0.03***	6.28 ±0.48^{+++}	43.96 ± 3.88***	88.76 ± 4.99^{+++}
tau $^{+/+}$ Cono + AβOs	4.11 ± 0.33***	16.58 ± 0.83^{+++}	2.61 ± 0.27***	10.11 ± 0.49^{+++}	1.50 ± 0.21***	6.46 ± 0.61^{+++}	45.92 ± 3.76***	98.72 ± 5.00^{+++}
tau $^{+/+}$ Nimo + AβOs	3.83 ± 0.23***	7.96 ± 0.96***	2.06 ± 0.15***	4.95 ± 0.75***	1.76 ± 0.13***	3.00 ± 0.52***	42.76 ± 2.60***	47.39 ± 5.74***
tau $^{+/+}$ EGTA + AβOs	--	15.30 ± 0.97^{+++}	--	9.87 ± 0.61^{+++}	--	5.43 ± 0.57^{+++}	--	91.14 ± 5.82^{+++}
tau $^{-/-}$ vehicle	7.66 ± 0.68	17.47 ± 0.79	3.75 ± 0.35	9.39 ± 0.59	3.91 ± 0.36	8.07 ± 0.59	100.49 ± 7.12	100.00 ± 4.56
tau $^{-/-}$ AβOs	3.41 ± 0.27***	6.72 ± 0.55***	1.78 ± 0.15***	4.40 ± 0.39***	1.64 ± 0.13***	2.32 ± 0.26***	45.04 ± 4.03***	38.51 ± 3.19***
tau $^{-/-}$ Aga + AβOs	4.24 ± 0.48***	15.62 ± 0.59^{+++}	2.58 ± 0.33***	9.07 ± 0.62^{+++}	1.98 ± 0.07***	6.54 ± 0.45^{+++}	58.96 ± 6.80***	83.25 ± 5.90^{+++}
tau $^{-/-}$ Cono + AβOs	4.45 ± 0.50***	14.5 ± 1.03^{+++}	2.38 ± 0.29***	8.82 ± 0.55^{+++}	2.16 ± 0.21***	5.72 ± 0.58^{+++}	61.84 ± 6.99***	89.40 ± 3.35^{+++}
tau $^{-/-}$ Nimo + AβOs	3.53 ± 0.28***	6.94 ± 0.56***	1.79 ± 0.16***	4.76 ± 0.41***	1.74 ± 0.12***	2.17 ± 0.56***	49.12 ± 3.89***	39.73 ± 3.22***
tau $^{-/-}$ EGTA + AβOs	--	14.6 ± 0.92^{+++}	--	8.87 ± 0.60^{+++}	--	6.40 ± 0.54^{+++}	--	83.63 ± 5.27^{+++}
Velocity (μm/s)								
tau $^{+/+}$ vehicle	1.60 ± 0.03	1.60 ± 0.08	1.44 ± 0.04	1.72 ± 0.07	1.42 ± 0.04	1.43 ± 0.10	100.00 ± 2.10	100.00 ± 5.07
tau $^{+/+}$ AβOs	1.34 ± 0.03*	1.32 ± 0.05**	1.30 ± 0.04**	1.40 ± 0.06**	1.37 ± 0.08	1.21 ± 0.05**	93.71 ± 2.34	82.33 ± 3.35**
tau $^{+/+}$ Aga + AβOs	1.52 ± 0.02	1.62 ± 0.07^{++}	1.58 ± 0.03	1.67 ± 0.06^{++}	1.46 ± 0.06	1.39 ± 0.08^{++}	95.31 ± 3.10	101.11 ± 3.60^{++}
tau $^{+/+}$ Cono + AβOs	1.61 ± 0.07	1.74 ± 0.08^{++}	1.65 ± 0.05	1.92 ± 0.11^{++}	1.58 ± 0.03	1.58 ± 0.07^{++}	100.01 ± 2.80	108.71 ± 5.25^{++}
tau $^{+/+}$ Nimo + AβOs	1.22 ± 0.10	1.16 ± 0.08**	1.27 ± 0.07	1.24 ± 0.08**	1.17 ± 0.01	1.06 ± 0.08**	76.21 ± 2.15	72.74 ± 5.00 **
tau $^{+/+}$ EGTA + AβOs	--	1.65 ± 0.07^{++}	--	1.77 ± 0.08^{++}	--	1.50 ± 0.07^{++}	--	103.56 ± 4.91^{++}
tau $^{-/-}$ vehicle	1.31 ± 0.05	1.68 ± 0.06	1.30 ± 0.06	1.78 ± 0.07	1.33 ± 0.01	1.60 ± 0.08	100.00 ± 3.50	100.00 ± 3.85
tau $^{-/-}$ AβOs	1.19 ± 0.03	1.12 ± 0.04**	1.24 ± 0.04	1.20 ± 0.08**	1.17 ± 0.07	1.02 ± 0.05**	90.22 ± 2.10	66.68 ± 2.78**
tau $^{-/-}$ Aga + AβOs	1.48 ± 0.05	1.63 ± 0.05^{++}	1.50 ± 0.03	1.73 ± 0.02^{++}	1.46 ± 0.06	1.53 ± 0.07^{++}	102.41 ± 2.31	97.46 ± 3.23^{++}
tau $^{-/-}$ Cono + AβOs	1.34 ± 0.09	1.48 ± 0.05^{++}	1.36 ± 0.01	1.55 ± 0.07^{++}	1.32 ± 0.04	1.40 ± 0.07^{++}	102.96 ± 3.75	88.47 ± 3.22^{++}
tau $^{-/-}$ Nimo + AβOs	1.35 ± 0.08	1.21 ± 0.05**	1.36 ± 0.09	1.34 ± 0.06**	1.35 ± 0.03	1.05 ± 0.06**	94.41 ± 0.32	72.11 ± 3.53**
tau $^{-/-}$ EGTA + AβOs	--	1.58 ± 0.06^{++}	--	1.67 ± 0.06^{++}	--	1.49 ± 0.07^{++}	--	93.91 ± 3.78^{++}
Run length (μm)								
tau $^{+/+}$ vehicle	4.53 ± 0.25	15.54 ± 0.80	4.44 ± 0.26	18.63 ± 1.38	4.68 ± 0.27	12.19 ± 1.04	100.00 ± 5.52	100.00 ± 5.17
tau $^{+/+}$ AβOs	4.56 ± 0.17	10.19 ± 0.39**	4.54 ± 0.21	12.42 ± 0.63**	4.64 ± 0.23	7.61 ± 0.16**	100.66 ± 3.75	65.59 ± 2.55**
tau $^{+/+}$ Aga + AβOs	5.23 ± 0.16	12.18 ± 0.51	5.21 ± 0.27	14.91 ± 0.87	5.24 ± 0.17	9.49 ± 0.41	115.45± 3.53	78.36 ± 3.31
tau $^{+/+}$ Cono + AβOs	5.17 ± 0.20	13.60 ± 0.83	5.22 ± 0.29	17.45 ± 0.48	5.15 ± 0.18	10.66 ± 0.61	114.70 ± 4.62	87.49 ± 5.40
tau $^{+/+}$ Nimo + AβOs	5.06 ± 0.14	11.09 ± 0.90	5.10 ± 0.19	12.50 ± 1.11	5.02 ± 0.24	9.04 ± 1.01	111.69± 4.58	71.38 ± 5.78
tau $^{+/+}$ EGTA + AβOs	4.27 ± 0.10	15.87 ± 0.55^{++}	4.34 ± 0.30	19.29 ± 0.77^{++}	4.20 ± 0.19	11.29 ± 0.45^{++}	94.26 ± 3.72	102.11 ± 3.54^{++}
tau $^{-/-}$ vehicle	5.11 ± 0.16	13.75 ± 0.56	5.17 ± 0.28	17.19 ± 1.03	5.08 ± 0.26	13.75 ± 0.56	100.00 ± 3.59	100.00 ± 4.07
tau $^{-/-}$ AβOs	4.75 ± 0.14	11.31 ± 0.52	4.77 ± 0.31	13.95 ± 0.86	4.72 ± 0.13	8.31 ± 0.36	92.95 ± 3.09	82.30 ± 3.83
tau $^{-/-}$ Aga + AβOs	5.48 ± 0.15	14.09 ± 0.53	5.50 ± 0.26	17.2 ± 0.91	5.45 ± 0.31	11.06 ± 0.45	107.25 ± 3.31	102.39 ± 3.82
tau $^{-/-}$ Cono + AβOs	4.99 ± 0.12	13.89 ± 0.42	5.50 ± 0.29	16.94 ± 0.71	4.73 ± 0.28	10.87 ± 0.43	97.67 ± 2.99	101.03 ± 3.73
tau $^{-/-}$ Nimo + AβOs	5.23 ± 0.18	13.00 ± 0.74	5.30 ± 0.21	15.98 ± 0.93	5.17 ± 0.25	9.42 ± 0.90	102.34 ± 3.13	94.52 ± 5.37
tau $^{-/-}$ EGTA + AβOs	--	13.99 ± 0.51	--	17.78 ± 0.87	--	11.11 ± 0.53	--	101.75 ± 3.73

tau$^{+/+}$ vehicle dendrites: n=18 kymographs (18 cells, 1187 vesicles); axons: n=15 kymographs (15 cells, 886 vesicles)
tau$^{+/+}$ AβO dendrites: n=22 kymographs (22 cells, 710 vesicles); axons: n=16 kymographs (16 cells, 544 vesicles)
tau$^{+/+}$ Agatoxin + AβO dendrites: n=15 kymographs (15 cells, 510 vesicles); axons: n=18 kymographs (18 cells, 1037 vesicles)
tau$^{+/+}$ Conotoxin + AβO dendrites: n=15 kymographs (15 cells, 550 vesicles); axons: n=17 kymographs (17 cells, 893 vesicles)
tau$^{+/+}$ Nimodipine + AβO dendrites: n=15 kymographs (15 cells, 268 vesicles); axons: n=15 kymographs (15 cells, 538 vesicles)
tau$^{+/+}$ EGTA + AβO axons: n=15 kymographs (15 cells, 695 vesicles)

tau$^{-/-}$ vehicle dendrites: n=17 kymographs (17 cells, 718 vesicles); axons: n=15 kymographs (15 cells, 943 vesicles)
tau$^{-/-}$ AβO dendrites: n=28 kymographs (28 cells, 589 vesicles); axons: n=18 kymographs (18 cells, 534 vesicles)
tau$^{-/-}$ Agatoxin + AβO dendrites: n=15 kymographs (15 cells, 536 vesicles); axons: n=16 kymographs (16 cells, 728 vesicles)
tau$^{-/-}$ Conotoxin + AβO dendrites: n=15 kymographs (15 cells, 475 vesicles); axons: n=16 kymographs (16 cells, 723 vesicles)
tau$^{-/-}$ Nimodipine + AβO dendrites: n=15 kymographs (15 cells, 503 vesicles); axons: n=16 kymographs (16 cells, 402 vesicles)
tau$^{-/-}$ EGTA + AβO axons: n=16 kymographs (16 cells, 711 vesicles)

* p<0.05, when compared with vehicle
**p<0.01, when compared with vehicle
*** p<0.001, when compared with vehicle

+ p<0.05, when compared with AβOs
++ p<0.01, when compared with AβOs
+++ p<0.001, when compared with AβOs

Table 3.3 RyR inhibition prevents AβO-induced transport defects

	Dense core vesicles			
	Traffic values			%
	All events	Anterograde	Retrograde	All events (%)
Flux (min^{-1})				
tau$^{+/+}$ vehicle	15.97 ± 1.20	9.37 ± 0.82	6.61 ± 0.69	100.00 ± 6.56
tau$^{+/+}$ AβOs	7.85 ± 1.64***	5.52 ± 1.18***	2.33 ± 0.59***	47.89 ± 6.92***
tau$^{+/+}$ dantrolene + AβOs	14.79 ± 1.39^{+++}	9.25 ± 0.72^{+++}	5.54 ± 0.97^{+++}	97.47 ± 10.37^{+++}
tau$^{-/-}$ vehicle	17.32 ± 1.89	11.25 ± 1.19	6.06 ± 0.99	100.00 ± 6.77
tau$^{-/-}$ AβOs	7.68 ± 0.83***	4.52 ± 0.75***	3.15 ± 0.35***	33.35 ± 5.30***
tau$^{-/-}$ dantrolene + AβOs	16.83 ± 2.14^{+++}	10.35 ± 1.42^{+++}	6.48 ± 0.96^{+++}	96.06 ± 7.92^{+++}
Velocity (µm/s)				
tau$^{+/+}$ vehicle	1.39 ± 0.05	1.51± 0.06	1.28 ± 0.04	100.00 ± 4.12
tau$^{+/+}$ AβOs	1.17 ± 0.05*	1.44 ± 0.07*	1.05 ± 0.04**	72.51 ± 4.85*
tau$^{+/+}$ dantrolene + AβOs	1.37 ± 0.08^{+}	1.49 ± 0.09^{+}	1.26 ± 0.09^{++}	95.85 ± 3.43^{+}
tau$^{-/-}$ vehicle	1.50 ± 0.12	1.65 ± 0.11	1.33 ± 0.10	100.00 ± 5.76
tau$^{-/-}$ AβOs	1.09 ± 0.11***	1.14 ± 0.12**	1.01 ± 0.13***	67.58 ± 3.98***
tau$^{-/-}$ dantrolene + AβOs	1.44 ± 0.09^{+++}	1.53 ± 0.09^{++}	1.32 ± 0.10^{+++}	97.32 ± 5.81^{+++}
Run length (µm)				
tau$^{+/+}$ vehicle	9.29 ± 0.48	11.12 ± 0.32	7.14 ± 0.34	100.00 ± 8.37
tau$^{+/+}$ AβOs	9.63 ± 0.94	11.41 ± 1.15	6.41 ± 0.46	103.98 ± 2.90
tau$^{+/+}$ dantrolene + AβOs	9.42 ± 0.94	10.62 ± 0.83	6.69 ± 0.90	101.64 ± 8.48
tau$^{-/-}$ vehicle	12.34 ± 0.72	15.39 ± 0.83	8.89 ± 0.73	100.00 ± 5.75
tau$^{-/-}$ AβOs	8.36 ± 0.78**	8.52 ± 1.05**	7.96 ± 1.43**	74.40 ± 4.76**
tau$^{-/-}$ dantrolene + AβOs	10.22 ± 0.79^{++}	12.08 ± 0.92^{++}	8.19 ± 0.85^{+}	83.67 ± 7.50^{++}

tau$^{+/+}$ vehicle: n=15 kymographs (15 cells, 1261 vesicles)
tau$^{+/+}$ AβO: n=15 kymographs (15cells, 1005 vesicles)
tau$^{+/+}$ dantrolene + AβO: n=15 kymographs (15 cells, 1097 vesicles)
tau$^{-/-}$ vehicle: n=15 kymographs (17 cells, 2167 vesicles)
tau$^{-/-}$ AβO: n=15 kymographs (19 cells, 933 vesicles)
tau$^{-/-}$ dantrolene + AβO: n=15kymographs (16 cells, 1666 vesicles)

* p<0.05, when compared with vehicle
** p<0.01, when compared with vehicle
*** p<0.001, when compared with vehicle
+ p<0.05, when compared with AβOs
++ p<0.01, when compared with AβOs
+++ p<0.001, when compared with AβOs

Chapter 4. Glycogen synthase kinase-3β impairs KIF1A motility independent of tau in amyloid-β oligomer-treated hippocampal neurons

Kathlyn J. Gan[1], Elisa M. Ramser[2], Aumbreen Akram[1], and Michael A. Silverman[1, 2]

[1] Department of Molecular Biology and Biochemistry, Simon Fraser University, 8888 University Drive, Burnaby, British Columbia, V5A 1S6, Canada

[2] Department of Biological Sciences, Simon Fraser University, 8888 University Drive, Burnaby, British Columbia, V5A 1S6, Canada

K.J.G. designed the study, performed all live imaging experiments, analysed and interpreted her data, and wrote this chapter. E.M.R. and K.J.G. coimmunoprecipitated KIF1A and GSK3β. E.M.R. isolated KIF1A for tandem mass spectrometry analysis, performed by the University of Victoria Genome BC Proteomics Centre. A.A. reproduced the KIF1A-S402A and S402E live imaging results to initiate her M.Sc. research project (data not shown here). M.A.S. designed and supervised the study, interpreted data, constructed figures, and assisted with writing this chapter.

4.1. Abstract

Fast axonal transport (FAT) impairment is an early pathological event that precedes overt cellular toxicity in multiple neurodegenerative diseases, including Alzheimer's disease (AD). We previously demonstrated that AβOs impair vesicular transport of brain-derived neurotrophic factor (BDNF) in primary hippocampal neurons. Contrary to a central paradigm, we recently discovered that BDNF transport defects are induced independent of the microtubule-associated protein, tau, microtubule destabilization, and acute cell death. We prevented these defects by inhibiting glycogen synthase kinase 3β (GSK3β), a downstream kinase that regulates motor-cargo interactions. KIF1A, the primary kinesin motor required for BDNF transport, is implicated in neurodegeneration; however, precise phosphorylation-dependent mechanisms that regulate KIF1A are unclear, and their contribution to AD pathogenesis has not been investigated. In this study, we measured axonal KIF1A motility by live cell imaging of KIF1A-GFP in wild type ($tau^{+/+}$) and tau knockout ($tau^{-/-}$) hippocampal neurons. Treatment with 500 nM AβOs reduced bidirectional flux of KIF1A-GFP similarly in $tau^{+/+}$ and $tau^{-/-}$ neurons, indicating that tau is not required for KIF1A transport disruption. Notably, pretreatment with 5 μM Inhibitor VIII, a selective, cell-permeant chemical blocker of GSK3β, prevented KIF1A transport defects. We confirmed that KIF1A and GSK3β interact by coimmunoprecipitation in primary neurons. Subsequently, we performed tandem mass spectrometry on KIF1A isolated from 14-month old AD transgenic mouse brain (Tg2576) and compared KIF1A phosphorylation to an age-matched, wild type control. We detected phosphorylation in the dimerization domain of KIF1A at Ser 402, which conforms to a GSK3β consensus site and is likely to regulate KIF1A activation. Furthermore, an unphosphorylatable form of KIF1A, generated by a Ser-to-Ala point mutation at Ser 402, prevents transport defects in AβO-treated $tau^{+/+}$ and $tau^{-/-}$ neurons. This work will identify GSK3β-dependent mechanisms of KIF1A dysregulation that impair BDNF transport and discover how they can be prevented or reversed in early AD pathogenesis.

4.2. Introduction

The kinesin superfamily proteins are microtubule-based, plus-end directed motors that actively transport mitochondria, lysosomes, neuropeptide vesicles, synaptic vesicle precursors, protein complexes, and messenger RNAs (Hirokawa and Takemura, 2005). By transporting such diverse axonal and dendritic cargoes, kinesins play critical roles in neuronal morphogenesis, function, and survival (Hirokawa et al., 2010). Intriguingly, reports have shown that several kinesins are implicated in learning and memory, including KIF5 (Puthanveettil et al., 2008), KIF17 (Yin et al., 2011), and KIF1A (Kondo et al., 2012). KIF1A, the mammalian homologue of *UNC-104*, consists of a motor domain, a forkhead-associated domain for phosphopeptide recognition, and a C-terminal cargo-binding domain such as a pleckstrin homology (PH) domain. KIF1A associates with membranous organelles containing synaptic vesicle proteins, such as synaptotagmin, synaptophysin, and Rab3A (Okada et al., 1995). A body of work, including our study, shows that KIF1A is also required for fast axonal transport (FAT) of large dense core vesicles (DCVs) (Lo et al., 2011; Yonekawa et al., 1998; Barkus et al., 2008). Unlike synaptic vesicles, DCVs are formed and filled with secretory neuropeptides, including brain-derived neurotrophic factor (BDNF), in the cell body and must be transported over long distances to presynaptic and postsynaptic sites of release. KIF1A is well suited for BDNF transport because it is highly processive, implying that it is fast and remains bound to microtubules for long durations (Hirokawa et al., 2008; (Verhey et al., 2011).

BDNF is required for synaptic maturation and function, development of neuronal circuitry, learning, and memory (Rothman and Mattson, 2012; Lu et al., 2013; Scharfman and Chao, 2013). Reduced levels of BDNF correlate with Alzheimer's disease (AD) progression (Scharfman and Chao, 2013), and impaired transport of BDNF compromises hippocampal synaptogenesis and learning enhancement (Kondo et al., 2012). Mutations in KIF1A, the primary anterograde motor for BDNF transport, are implicated in neurodegenerative diseases such as hereditary sensory and autonomic neuropathy type 2 and autosomal recessive spastic paraplegia (Riviere et al., 2011; Klebe et al. 2012). Despite the importance of BDNF and its transport in neuronal physiology and disease, mechanisms that regulate KIF1A-DCV interactions and KIF1A

processivity are unclear, and their contribution to AD pathogenesis has not been investigated. Previously, we demonstrated that amyloid-β oligomers (AβOs), the primary neurotoxin in AD, impair axonal BDNF transport in primary hippocampal neurons (Decker et al., 2010a). Contrary to a central paradigm, we discovered that BDNF transport defects are induced independent of the microtubule-associated protein, tau, microtubule destabilization, and acute cell death (Ramser et al., 2013). We prevented these defects by inhibiting glycogen synthase kinase 3β (GSK3β), a downstream kinase that is implicated in many aspects of AD pathogenesis (Medina and Avila, 2014) and regulates kinesin-1 (KIF5) interactions with cargo and microtubules (Morfini et al., 2002; Weaver et al., 2013). Precise phosphorylation-dependent mechanisms that dysregulate KIF1A in AD are unknown.

Here, we show by live cell imaging that AβOs impair KIF1A motility in wild type ($tau^{+/+}$) and tau knockout ($tau^{-/-}$) hippocampal neurons, indicating that the microtubule-binding (Morris et al., 2011) and signaling properties (Kanaan et al., 2011) of tau are not required for KIF1A transport disruption. Notably, KIF1A and GSK3β interact, and inhibition of GSK3β prevents KIF1A transport defects. By tandem mass spectrometry on KIF1A isolated from 14-month old AD transgenic mouse brain (Tg2576), we detected significant phosphorylation in the dimerization domain of KIF1A at Ser 402, which conforms to a GSK3β consensus site and is likely to regulate KIF1A activation. Furthermore, an unphosphorylatable form of KIF1A, generated by a Ser-to-Ala point mutation at Ser 402, prevents transport defects in AβO-treated $tau^{+/+}$ and $tau^{-/-}$ neurons. This work implicates GSK3β in KIF1A dysregulation during early AD pathogenesis.

4.3. Materials and Methods

4.3.1. Hippocampal cell culture and expression of transgenes

Primary hippocampal neuronal cultures from E16 wild-type ($tau^{+/+}$) and tau-knockout ($tau^{-/-}$) mice (Jackson Laboratory, Bar Harbor, ME) were prepared as described by Kaech and Banker (Kaech and Banker, 2006) and kept in PNGM primary neuron growth media (Lonza, Basel, Switzerland). The glial feeder layer was derived from murine neural stem cells as described by (Miranda et al., 2012). At 10–12 d in

vitro, cells were cotransfected using Lipofectamine 2000 (Invitrogen) with plasmids encoding soluble blue fluorescent protein (pmUβA-eBFP) and KIF1A-GFP (GW1-KIF1A-eGFP; Lee et al., 2003). Cells expressed constructs for 36 h before imaging. Point mutations of the KIF1A phosphorylation site S402 (S402A and S402E) were generated using the QuickChange II mutagenesis kit (Agilent). Plasmid identity was confirmed by sequencing.

4.3.2. AβO and GSK3β inhibitor VIII treatments

Soluble, full-length Aβ 1-42 peptides (American Peptide) were prepared exactly according to the method of Lambert et al., 2007 and applied to cells at a final concentration of 500 nM for 18 h. Cells were incubated with 5 μM GSK3β Inhibitor VIII (Calbiochem) or equivalent volumes of vehicle (EtOH) 30 min prior to AβO or vehicle treatment.

4.3.3. Live imaging and analysis of KIF1A transport

KIF1A-GFP transport was analyzed using a standard wide-field fluorescence microscope equipped with a cooled charge-coupled device camera and controlled by MetaMorph (Molecular Devices, Sunnyvale, CA) as described previously (Kwinter and Silverman, 2009). All imaging—typically 100 frames—was recorded by the "stream acquisition module" in MetaMorph. Briefly, cells were sealed in a heated imaging chamber, and recordings were acquired from double transfectants at an exposure time of 250 ms for 90 s. This captured dozens of transport events per cell in 50-μm segments of the dendrite or 100-μm segments of the axon. Dendrites and axons were initially identified based on morphology and confirmed retrospectively by immunostaining against MAP2, a dendritic cytoskeletal protein. Soluble BFP detection was necessary to determine the orientation of the cell body relative to the axon and thus to distinguish between anterograde and retrograde transport events. Vesicle flux, velocity, and run lengths were obtained through tracing kymographs in MetaMorph. Vesicle flux was defined as the total distance traveled by vesicles standardized by the length and

duration of each movie (in micron-minutes): $\frac{\sum_{i=1}^{n} d_i}{\ell \times t}$ where d are the individual DCV run lengths, ℓ is the length of axon imaged and t is the duration of the imaging session. A vesicle was defined as undergoing a directed run if it traveled a distance of ≥2 μm. This distance was determined as a safe estimate of the limit of diffusion based on the assumption that root-mean-squared displacement equals $\sqrt{2Dt}$, where D is the diffusion coefficient (D=0.01 $\mu m^2/s$ for DCVs) and t is the duration of the imaging period (t=50 s) (Abney et al., 1999). A run was defined as terminating if the vesicle remained in the same position for at least four consecutive frames. Percentage flux represents the flux in treated neurons normalized to controls (100%).

4.3.4. KIF1A immunoprecipitation and GSK3β immunoblotting

Hippocampal neurons were lysed in ice-cold RIPA buffer containing protease and phosphatase inhibitors. 500 μg of lysate was mixed overnight at 4oC with 12 μg of KIF1A antibody (BD Biosciences). Samples were then combined with 50 μl of Protein A/G-agarose (Santa Cruz Biotechnology) beads and mixed at 4^{o}C for 3 hr. Samples were gently pelleted and rinsed three times with RIPA buffer. The immunoprecipitated proteins (5-10 μg) were resolved on 10% SDS-polyacrylamide gels and transferred to PVDF membranes. Membranes were probed with anti-GSKβ (1:000, Cell Signaling) overnight at 4°C. Immunoreactive bands were visualized using enhanced chemiluminescent substrate (ECL) (Thermo Scientific) for detection of peroxidase activity from HRP-conjugated antibodies. Densitometric scanning and quantitative analysis were carried out using ImageJ.

4.3.5. Tandem mass spectrometry and KIF1A phosphosite analysis

KIF1A was immunoprecipitated from 14-month old Tg2576 AD (APPSwe) mouse brain and age-matched wild type control brain as described previously. Coomassie-stained protein bands were excised from the SDS-PAGE gel, digested with trypsin, and used for tandem mass spectrometry with TiO2 enrichment for phosphopeptides (U. of Victoria Genome BC Proteomics Centre). KIF1A phosphorylation from Tg2576 and wild

type brain were compared using the algorithm PhosphoRS, which calculates the probability of each phosphorylation site within a peptide. GSK3β phosphosites were identified by comparison to existing sequences within the Phosida (phosida.com) and Phosphonet (kinexus.ca) databases.

4.4. Results

4.4.1. GSK3β inhibition prevents AβO-induced KIF1A transport defects independent of tau

Recently, we discovered that AβOs disrupt BDNF transport independent of the microtubule-associated protein, tau, microtubule destabilization, and acute cell death (Ramser et al., 2013). We prevented these defects by inhibiting GSK3β, a downstream kinase that regulates motor-cargo interactions. KIF1A, the primary kinesin motor required for BDNF transport (Lo et al. 2011; Yonekawa et al., 1998; Barkus et al., 2008), is implicated in neurodegeneration (Riviere et al., 2001; Klebe et al., 2012); however, precise phosphorylation-dependent mechanisms that regulate KIF1A are unclear, and their contribution to AD pathogenesis has not been investigated. Previous work in isolated squid axoplasm showed that AβOs induce robust tau hyperphosphorylation, initiate its detachment from microtubules, and expose a phosphatase-activating domain within the N-terminus of tau that activates PP1-GSK3β signaling and impedes KIF5-based anterograde transport (Kanaan et al., 2011). To determine if tau impairs KIF1A motility, $tau^{+/+}$ and $tau^{-/-}$ hippocampal neurons expressing KIF1A-enhanced green fluorescent protein (eGFP) were imaged after treatment with 500 nM AβOs for 18 h (Figure 4.1). Irreversible AβO binding was confirmed retrospectively by immunocytochemistry (Figure 4.1 A) using an oligomer-specific antibody (NU-4; (Lambert et al., 1998). Representative kymographs illustrate differences between KIF1A transport in control (vehicle-treated) and AβO-treated neurons (Figure 4.1 B). Total axonal flux was similarly and markedly reduced by AβOs both in the presence and absence of tau (44% and 46% decrease, respectively; Figure 4.1 B). AβOs also significantly decreased anterograde average velocity and run length by approximately 32% and 45%, respectively, in $tau^{-/-}$ neurons. Notably, pretreatment with 5 µM Inhibitor VIII, a selective, cell-permeant, competitive blocker of GSK3β, prevented KIF1A

transport defects. GSK3β coimmunoprecipitated with KIF1A, indicating that they bind through a direct or indirect mechanism (Figure 4.1 C). Collectively, results show that GSK3β interacts with KIF1A and reduces its motility independent of tau.

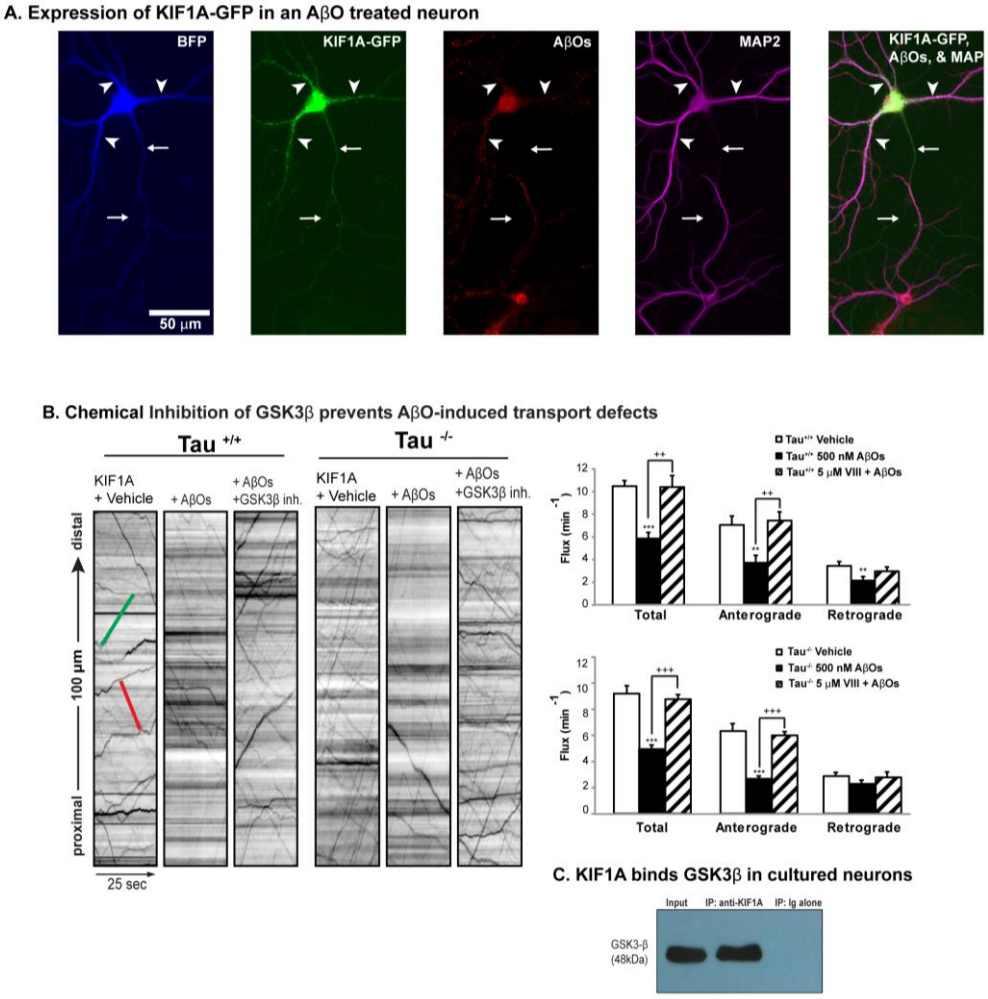

Figure 4.1 GSK3β inhibition prevents AβO-induced KIF1A transport defects independent of tau

A) Expression of soluble BFP and KIF1A-eGFP in an AβO-treated tau$^{+/+}$ neuron (from left to right). Overlay of BFP and AβO images shows binding of AβOs exclusively to dendrites. Immunocytochemistry shows that AβOs remain oligomeric after 18 h in culture. Arrows indicate axon; arrowheads indicate dendrites. B) Effects of AβOs and Inhibitor VIII treatment on KIF1A-GFP flux in tau$^{+/+}$ and tau$^{-/-}$ neurons. Representative kymographs comparing KIF1A-GFP transport in control and treated neurons. Lines with a positive slope represent anterograde transport (green); lines with a negative slope represent retrograde transport (red). C) A monoclonal antibody to KIF1A immunoprecipitated GSK3β from neuronal lysates.

4.4.2. The KIF1A dimerization domain is phosphorylated at a conserved GSK3β consensus site

To test whether KIF1A is indeed a substrate for phosphorylation and determine which residues may be targets for analysis, we performed tandem mass spectrometry on KIF1A isolated from 14-month-old Tg2576 AD (APP_{Swe}) mouse brain (U. of Victoria Genome BC Proteomics Centre). We detected 12 phosphopeptides, six of which conform to sites targeted by kinases that are aberrantly activated in AD, such as MAPK, casein kinase II, and GSK3β (Figure 4.2). We compared KIF1A phosphorylation from Tg2576 to an age-matched, wild type control using the algorithm PhosphoRS, which calculates the probability of each phosphorylation site within a peptide. Phosphorylation within specific KIF1A sequences varied significantly between genotypes; for example, serine 932, within the cargo-binding peptide CPVVGMS*RSGTSQEEL, was hyperphosphorylated (denoted by *) in Tg2576 mice (Figure 4.2 A). We also detected significant phosphorylation on peptide MTMALVGNS*PSSSLSALSSR at Ser 402 (S402), which conforms to a GSK3β consensus site according to the Phosida and Phosphonet databases. Intriguingly, this site is conserved between zebrafish, mouse, rat, and human, suggesting a critical role in KIF1A transport (Figure 4.2 A). S402 is present in the forkhead associated domain of KIF1A and is therefore likely to regulate dimerization and motility (Figure 4.2 B).

4.4.3. The phosphomutant KIF1A-S402A remains motile in AβO-treated neurons

To determine if AβO-induced phosphorylation at S402 impairs KIF1A motility, we generated a non-phosphorylatable form of KIF1A-GFP by inducing a Ser-to-Ala point mutation (S402A) at this site. We expressed this mutant in control and AβO-treated $tau^{+/+}$ and $tau^{-/-}$ neurons. No significant differences in KIF1A-S402A flux, velocity, and run length were observed for either genotype upon AβO treatment, implicating S402 phosphorylation in transport impairment (Figure 4.3). Conversely, we induced a Ser-to-Glu point mutation to create a phosphomimic of S402 (S402E) and imaged transport similarly. Unexpectedly, KIF1A-S402E flux was not diminished in control neurons, and its transport was only weakly perturbed in AβO-treated neurons (data not shown). This could be attributed to the presence of endogenous wild type KIF1A, which may dimerize

with S402E monomers or preferentially bind to cargo, thus masking any effects of the mutation on KIF1A motility. RNAi experiments are underway to characterize KIF1A-S402E transport in the absence of endogenous KIF1A.

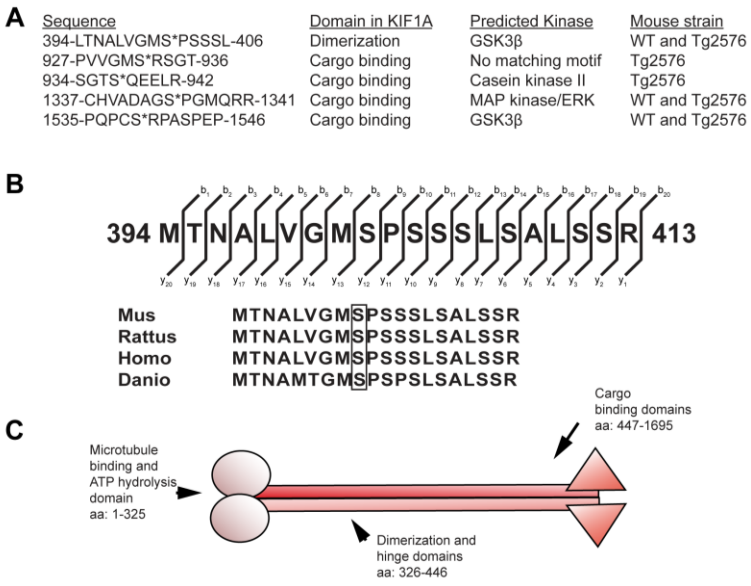

Figure 4.2 The KIF1A dimerization domain is phosphorylated at a conserved GSK3β consensus site

A) Detection of 12 phosphopeptides, six of which conform to sites targeted by kinases that are aberrantly activated in AD, such as MAPK, casein kinase II, and GSK3β. B) Tandem mass spectroscopy on KIF1A isolated from AD model mouse (APPswe) brain identified a phospho-peptide within the dimerization domain (amino acids 394-413). Phospho-serine 402 in this peptide conforms to a GSK3β site according to Phosida (phosida.com) and Phosphonet (kinexus.ca). Sequence alignment shows that Ser 402 is conserved between zebrafish, mouse, rat, and human. C) Basic schematic of KIF1A, a kinesin-3 family member. KIF1A has a similar "body plan" to other characterized kinesins.

Furthermore, our collaborator (K. Verhey, Univ. of Michigan) will employ a FRET-based strategy to confirm that the S402E mutation hinders KIF1A dimerization and cargo binding. Wild type and mutant KIF1A will be tagged with monomeric versions of FRET donor (mCFP) and acceptor (mCitrine) fluorescent proteins either at the N-terminus to measure the proximity of the motor domains or at the C-terminus to measure the proximity of the tail (cargo-binding) domains. The motors will be recruited to early endosomes, which typically exhibit low motility, by placing the PH domain of KIF16B (PX) on the tail of KIF1A. Wild type KIF1A should exhibit high FRET efficiencies, consistent with motor dimerization irrespective of where the FRET pairs are placed.

KIF1A recruitment to early endosomes and subsequent activation should result in cargo transport to the cell periphery. KIF1A-S402A, which is resistant to inhibitory phosphorylation, should behave similarly. In contrast, low levels of FRET may be detected for KIF1A-S402E if it indeed fails to dimerize and bind cargo. Collectively, these experiments would support a critical role for inhibitory phosphorylation of KIF1A in AβO-induced FAT disruption.

4.5. Discussion

FAT disruption is an early pathological manifestation that leads to loss of synapse function and axonal degeneration in AD (Millecamps and Julien, 2013). AβOs are central to AD pathology and impair axonal organelle transport (Morfini et al., 2002; Decker et al., 2012; Ramser and Gan et al., 2013; Vossel et al., 2010; Tang et al., 2012; Wang et al., 2010). KIF1A, the primary kinesin motor required for vesicular BDNF transport, is implicated in neurodegeneration; however, phosphorylation-dependent mechanisms that regulate KIF1A are unclear, and their contribution to AD pathogenesis has not been investigated. Here, through direct assessment of trafficking at high spatial and temporal resolution in living neurons, we demonstrate that AβOs impair KIF1A motility independent of tau in the absence of microtubule stabilization or cell death as in our previous studies. This implies that the microtubule-binding capacity and signaling properties of pathological tau are not required for AβO-induced disruption of KIF1A transport. We combined multiple approaches, including live imaging, coimmunoprecipitation, immunoblotting, and tandem mass spectrometry, to demonstrate that inhibition of GSK3β prevents KIF1A transport defects, and that aberrant phosphorylation at a conserved GSK3β consensus site within the dimerization domain of KIF1A reduces its motility. Our findings implicate GSK3β in phosphorylation-dependent KIF1A dysregulation during early AD pathogenesis.

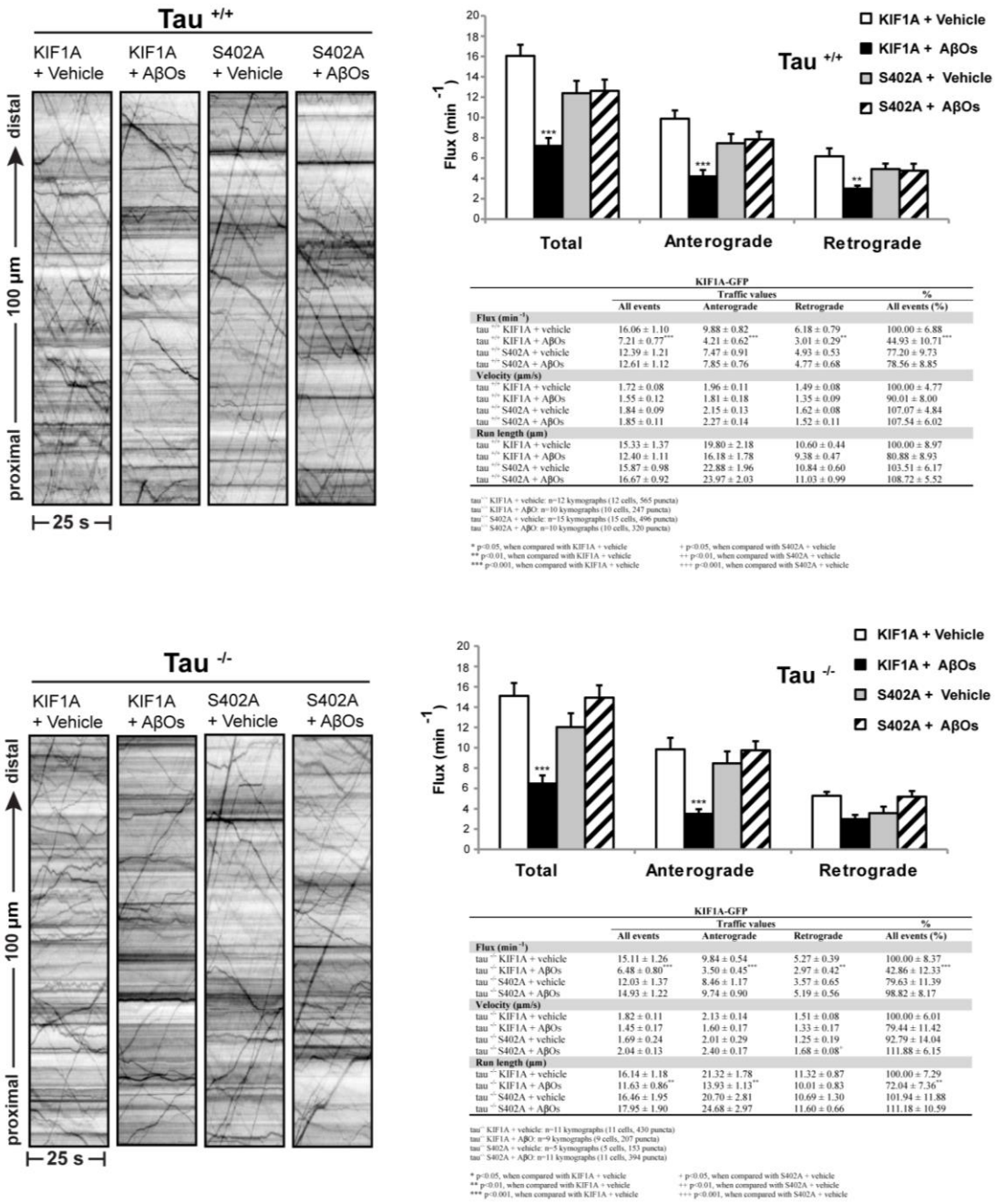

KIF1A-GFP

	Traffic values			%
	All events	Anterograde	Retrograde	All events (%)
Flux (min^{-1})				
tau$^{+/+}$ KIF1A + vehicle	16.06 ± 1.10	9.88 ± 0.82	6.18 ± 0.79	100.00 ± 6.88
tau$^{+/+}$ KIF1A + AβOs	7.21 ± 0.77***	4.21 ± 0.62***	3.01 ± 0.29**	44.93 ± 10.71***
tau$^{+/+}$ S402A + vehicle	12.39 ± 1.21	7.47 ± 0.91	4.93 ± 0.53	77.20 ± 9.73
tau$^{+/+}$ S402A + AβOs	12.61 ± 1.12	7.85 ± 0.76	4.77 ± 0.68	78.56 ± 8.85
Velocity (µm/s)				
tau$^{+/+}$ KIF1A + vehicle	1.72 ± 0.08	1.96 ± 0.11	1.49 ± 0.08	100.00 ± 4.77
tau$^{+/+}$ KIF1A + AβOs	1.55 ± 0.12	1.81 ± 0.18	1.35 ± 0.09	90.01 ± 8.00
tau$^{+/+}$ S402A + vehicle	1.84 ± 0.09	2.15 ± 0.13	1.62 ± 0.08	107.07 ± 4.84
tau$^{+/+}$ S402A + AβOs	1.85 ± 0.11	2.27 ± 0.14	1.52 ± 0.11	107.54 ± 6.02
Run length (µm)				
tau$^{+/+}$ KIF1A + vehicle	15.33 ± 1.37	19.80 ± 2.18	10.60 ± 0.44	100.00 ± 8.97
tau$^{+/+}$ KIF1A + AβOs	12.40 ± 1.11	16.18 ± 1.78	9.38 ± 0.47	80.88 ± 8.93
tau$^{+/+}$ S402A + vehicle	15.87 ± 0.98	22.88 ± 1.96	10.84 ± 0.60	103.51 ± 6.17
tau$^{+/+}$ S402A + AβOs	16.67 ± 0.92	23.97 ± 2.03	11.03 ± 0.99	108.72 ± 5.52

tau$^{+/+}$ KIF1A + vehicle: n=12 kymographs (12 cells, 565 puncta)
tau$^{+/+}$ KIF1A + AβO: n=10 kymographs (10 cells, 247 puncta)
tau$^{+/+}$ S402A + vehicle: n=15 kymographs (15 cells, 496 puncta)
tau$^{+/+}$ S402A + AβO: n=10 kymographs (10 cells, 320 puncta)

* p<0.05, when compared with KIF1A + vehicle
** p<0.01, when compared with KIF1A + vehicle
*** p<0.001, when compared with KIF1A + vehicle
+ p<0.05, when compared with S402A + vehicle
++ p<0.01, when compared with S402A + vehicle
+++ p<0.001, when compared with S402A + vehicle

KIF1A-GFP

	Traffic values			%
	All events	Anterograde	Retrograde	All events (%)
Flux (min^{-1})				
tau$^{-/-}$ KIF1A + vehicle	15.11 ± 1.26	9.84 ± 0.54	5.27 ± 0.39	100.00 ± 8.37
tau$^{-/-}$ KIF1A + AβOs	6.48 ± 0.80***	3.50 ± 0.45***	2.97 ± 0.42**	42.86 ± 12.33***
tau$^{-/-}$ S402A + vehicle	12.03 ± 1.37	8.46 ± 1.17	3.57 ± 0.65	79.63 ± 11.39
tau$^{-/-}$ S402A + AβOs	14.93 ± 1.22	9.74 ± 0.90	5.19 ± 0.56	98.82 ± 8.17
Velocity (µm/s)				
tau$^{-/-}$ KIF1A + vehicle	1.82 ± 0.11	2.13 ± 0.14	1.51 ± 0.08	100.00 ± 6.01
tau$^{-/-}$ KIF1A + AβOs	1.45 ± 0.17	1.60 ± 0.17	1.33 ± 0.17	79.44 ± 11.42
tau$^{-/-}$ S402A + vehicle	1.69 ± 0.24	2.01 ± 0.29	1.25 ± 0.19	92.79 ± 14.04
tau$^{-/-}$ S402A + AβOs	2.04 ± 0.13	2.40 ± 0.17	1.68 ± 0.08+	111.88 ± 6.15
Run length (µm)				
tau$^{-/-}$ KIF1A + vehicle	16.14 ± 1.18	21.32 ± 1.78	11.32 ± 0.87	100.00 ± 7.29
tau$^{-/-}$ KIF1A + AβOs	11.63 ± 0.86**	13.93 ± 1.13**	10.01 ± 0.83	72.04 ± 7.36++
tau$^{-/-}$ S402A + vehicle	16.46 ± 1.95	20.70 ± 2.81	10.69 ± 1.30	101.94 ± 11.88
tau$^{-/-}$ S402A + AβOs	17.95 ± 1.90	24.68 ± 2.97	11.60 ± 0.66	111.18 ± 10.59

tau$^{-/-}$ KIF1A + vehicle: n=11 kymographs (11 cells, 430 puncta)
tau$^{-/-}$ KIF1A + AβO: n=9 kymographs (9 cells, 207 puncta)
tau$^{-/-}$ S402A + vehicle: n=5 kymographs (5 cells, 153 puncta)
tau$^{-/-}$ S402A + AβO: n=11 kymographs (11 cells, 394 puncta)

* p<0.05, when compared with KIF1A + vehicle
** p<0.01, when compared with KIF1A + vehicle
*** p<0.001, when compared with KIF1A + vehicle
+ p<0.05, when compared with S402A + vehicle
++ p<0.01, when compared with S402A + vehicle
+++ p<0.001, when compared with S402A + vehicle

Figure 4.3 The phosphomutant KIF1A-S402A remains motile in AβO-treated neurons

KIF1A-GFP Ser 402 Ala flux is comparable to wild type KIF1A in tau$^{+/+}$ and tau$^{-/-}$ neurons treated with 500 nM AβOs.

According to the “GSK3 hypothesis of AD”, abnormal activation of GSK3β predominantly accounts for many pathological hallmarks of the disease, including increased Aβ production, tau hyperphosphorylation, and impaired learning and memory (Hooper et al., 2008). Traditionally, FAT defects were thought to arise from axonal dystrophy, microtubule dissolution, tau aggregation, and tau-induced kinase activation during later stages of disease progression (Mandelkow et al., 2003; Stokin and Goldstein, 2006; LaPointe et al., 2009; Morfini et al., 2009; Kanaan et al., 2011). However, we and others have shown that transport defects can occur independent of tau, prior to overt morphological decline and cell death (Ramser et al., 2013; Pigino et al., 2003; Lazarov et al., 2007; Stokin et al., 2008; Rodrigues et al., 2012; Goldstein, 2012). These studies support the notion that GSK3β also mediates FAT disruption by earlier, subtler mechanisms that involve inhibitory phosphorylation of motor proteins (see Chapter 2 for an extensive discussion).

We show that AβOs induce phosphorylation of KIF1A at a conserved GSK3β consensus site (S402) within its dimerization domain. This may impair KIF1A motility by two distinct mechanisms. First, aberrant or excessive S402 phosphorylation may prevent KIF1A dimerization and activation. Some models contend that KIF1A is monomeric in the inactive state, and that activation results from concentration-driven dimerization prior to cargo binding or on the cargo surface (Klopfenstein et al., 2002; Tomishige et al., 2002). Other findings show that KIF1A is dimeric in the inactive state and is therefore not activated by cargo-induced dimerization (Hammond et al., 2009); rather, KIF1A motors are autoinhibited, and dimeric KIF1A motors are activated by cargo binding (Soppina et al., 2014). Because only dimeric KIF1A motors undergo ATP-dependent, superprocessive motility (Soppina et al., 2014), failure to dimerize may preclude cargo binding and permit only diffusive movement of KIF1A monomers along the microtubule surface. Second, placement of a negative charge at S402 through phosphorylation could alter the flexibility of the neck coil domain and favor the folded, autoinhibited conformation of KIF1A. Indeed, phosphorylation of S137 within the motor domain of KIF5 stabilizes the ionic interaction between the tail and motor domains, promoting KIF5 autoinhibition and decreasing the applied force required for motor stalling (DeBerg et al., 2013). Moreover, Aurora-B-dependent phosphorylation of S196 diminishes the interaction between the C-terminal domain of kinesin-13 and its neck coil,

opening its conformation. This results in decreased kinesin-13 affinity for microtubules (Ems-McClung et al., 2013). Thus, constitutive phosphorylation of KIF1A at S402 may impair DCV transport by preventing motor dimerization and activation, blocking cargo binding, and reducing motor processivity along microtubules.

Based on our previous findings (Decker et al., 2010; Ramser and Gan et al., 2013) and present data, we propose the following model for BDNF/KIF1A transport dysregulation in Alzheimer's disease (Figure 4.4). AβOs bind to dendrites and axons, dysregulating Ca^{2+} homeostasis and triggering intracellular signaling cascades that converge on GSK3β. Upon activation, GSK3β disrupts BDNF transport by aberrantly phosphorylating KIF1A at S402. This may prevent motor dimerization and activation, block cargo binding, and reduce KIF1A processivity. Additional research is required to determine if transport impairment contributes to synapse loss and axonal degeneration in AD. In the adult brain, BDNF enhances synaptic transmission, facilitates synaptic plasticity, and increases the size and number of dendritic spines. KIF1A dysregulation may deplete the synaptic pool of BDNF available for release; thus, preventing or rescuing FAT defects may aid in synaptic repair. Furthermore, a constant neurotrophin supply is required to maintain dendritic and axonal morphology and function. Transport defects may deprive processes of BDNF and lead to degeneration by inducing cytoskeletal-based retraction, increasing endocytosis, and promoting microtubule destabilization. Finally, impaired FAT of other KIF1A cargoes, such as synaptic vesicle precursors containing synapsin and bassoon required for synaptic maintenance (Waites et al., 2013), may reduce neurotransmission and lead to synaptic loss in AD. Therapeutic interventions designed to restore KIF1A motility may exhibit fewer off-target effects compared to upstream, ubiquitous signaling proteins and be more effective at preventing or reversing cell death.

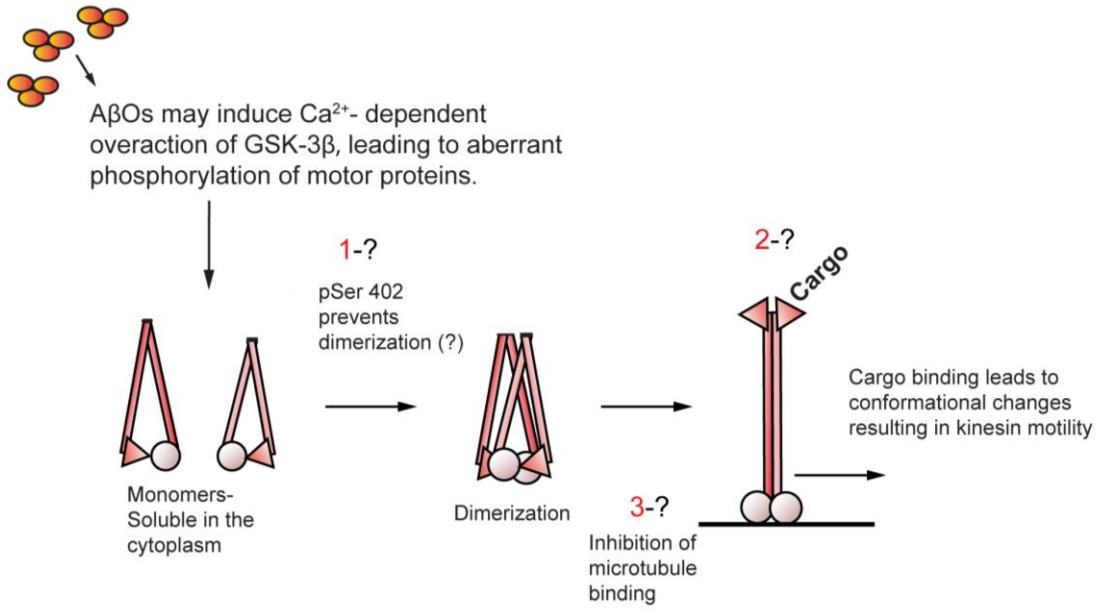

Figure 4.4 Proposed mechanism for KIF1 transport disruption in Alzheimer's disease

At dendrites, AβOs aberrantly activate NMDARs and induce Ca^{2+} influx, elevating cytosolic Ca^{2+}. Activated calcineurin relieves inhibition of PP1, which activates GSK3β. GSK3β may inhibit motor protein activity by disrupting motor dimerization (1), via motor-cargo interactions (2), and/or preventing the motor-cargo complex from binding microtubules (3).

4.6. Acknowledgements

This research was supported by grants from the National Science and Engineering Research Council of Canada (NSERC; 327100-06) and the Canadian Institutes of Health Research (CIHR; 90396) to M.A.S. We are grateful to L. Chen for her expert technical assistance. K.J.G. is funded by a C.D. Nelson Memorial Graduate Scholarship from Simon Fraser University and an NSERC Postgraduate Scholarship. We also thank the Simon Fraser University Animal Care Services staff for their essential assistance in our experiments.

Chapter 5. Conclusions and future directions

5.1. Dysregulation of Ca^{2+} signaling impairs BDNF transport independent of tau

The purpose of this research was to investigate Ca^{2+}-dependent mechanisms of FAT disruption in a cellular model of AD. I discovered that AβOs perturb axonal BDNF transport by non-excitotoxic activation of CaN-GSK3β signaling. Contrary to the dominant paradigm, I found that these defects occur independent of tau, microtubule destabilization, and acute cell death. I correlated the onset, severity, and spatiotemporal progression of dendritic and axonal BDNF transport impairment with Ca^{2+} elevation and CaN activation first in dendrites and subsequently in axons. Importantly, I demonstrated that postsynaptic CaN activation converges with mechanisms of axonal Ca^{2+} dysregulation to disrupt FAT. Specifically, AβOs colocalize with axonal VGCCs, and blocking VGCCs prevents FAT defects. Despite the multitude of extracellular routes for AβO-induced Ca^{2+} influx, normal BDNF transport is maintained by dantrolene, a clinical compound that reduces CICR through RyRs that are present in dendritic and axonal ER membranes. Finally, I showed that AβOs reduce the motility of KIF1A, the primary motor required for BDNF transport. This is accomplished by phosphorylation at S402, a highly conserved GSK3β consensus site within the dimerization domain of KIF1A. Inhibitory phosphorylation by GSK3β may disrupt motor-cargo interactions and/or prevent the motor-cargo complex from binding microtubules. Collectively, this thesis establishes novel roles for Ca^{2+} dysregulation in BDNF transport disruption and tau-independent toxicity during early AD pathogenesis.

5.2. BDNF transport defects may reduce BDNF secretion

Although FAT defects were first observed in neurodegenerative diseases over 35 years ago, it is still unclear how defects in transport mechanisms compromise neuronal

health and survival. A possible physiological consequence of FAT disruption is reduced secretion of neurotransmitters and neuropeptides. In the adult brain, BDNF enhances synaptic transmission, facilitates synaptic plasticity, and increases the size and number of dendritic spines (Rothman and Mattson, 2012; Lu et al., 2013). In AD, KIF1A dysregulation may deplete the synaptic pool of BDNF available for release (Kondo et al., 2012); thus, preventing or rescuing FAT defects may aid in synaptic repair. To determine if BDNF transport defects reduce BDNF secretion from pre- and postsynaptic sites, control and AβO-treated neurons may be cultured in chambers that permit fluidic isolation of dendrites and axons, and enzyme-linked immunosorbent assays (ELISAs) may be conducted on cell culture media collected from either compartment. If BDNF secretion is indeed significantly impaired, the role of FAT in synaptic resupply may be investigated at high resolution by live cell imaging. Although DCVs are readily tracked within postsynaptic sites, they are densely arranged within presynaptic sites, obscuring detection of individual vesicles. Hence, the photoconvertible tag Dendra2 can be used to unequivocally track incoming vesicles and normalize variable BDNF expression between cells. Neurons may be co-transfected with BDNF-Dendra2, which converts from green to red upon exposure to blue light (Baker et al., 2010), and synapsin-BFP to mark presynaptic sites. Following treatment with vehicle and AβOs, unconverted (green) BDNF-Dendra2 may be imaged within synaptic sites and proximal axon segments. The cells may then be depolarized with KCl to rid terminals of DCVs and create new docking sites for incoming DCVs (Wong et al., 2012). BDNF-Dendra2 may be photoconverted within an axonal segment distal to the synapse. A green image may be acquired to verify DCV clearance and represent total BDNF, followed by a red stream to visualize motile DCVs entering the synapse. The ratio of red to green vesicles would represent the normalized, mobile fraction of BDNF that enters the synapse. If BDNF presynaptic transport is impaired in AβO-treated neurons, non-phosphorylatable forms of KIF1A may be expressed to prevent or rescue these defects.

5.3. Non-invasive detection of FAT defects in AD mice and patients by manganese-enhanced MRI (MEMRI)

Compounds that restore Ca^{2+} homeostasis can improve learning and memory in transgenic AD animal models (Demuro et al., 2010; Oules et al., 2012). Amelioration of Ca^{2+}-dependent FAT defects in vivo may underlie improved cognitive function; thus, the transport apparatus may constitute a novel target for the detection and treatment of early-stage AD. I demonstrated that FK506, VGCC inhibitors, and dantrolene can prevent or rescue AβO-induced FAT defects in cultured neurons. To translate these findings to preclinical models, manganese-enhanced magnetic resonance imaging (MEMRI) may be employed to detect FAT defects in live AD mice and determine if intraperitoneal administration of Ca^{2+} channel and CaN inhibitors restores normal transport. MEMRI enables in vivo assessment of axonal transport due to unique properties of Mn^{2+}; as a Ca^{2+} analog, Mn^{2+} enters neurons through VGCCs, flows into the ER, and ultimately leaves in membrane-bound organelles that undergo microtubule-based transport (Inoue et al., 2011). MEMRI has predominantly focused on axonal transport in the fascicles of the olfactory bulbs, and recent work identified a deficit in olfactory bulb axonal transport in aged and AD model mice (Minoshima and Cross, 2008; Kim et al., 2011; Smith et al., 2011). Significantly, FAT defects were observed by MEMRI in APP_{swe}/PS1dE9 mice prior to Aβ plaque formation and extensive p-tau (Minoshima and Cross, 2008). Non-invasive MEMRI studies can be performed repeatedly on live animals and will enable longitudinal measurements of FAT throughout AD progression, unlike traditional approaches using cell tracer dyes (Inoue et al., 2011). Cellular toxicity has prevented the extension of MEMRI into human use; however, the recent development of new Mn^{2+}-based contrast agents and the increased Mn^{2+} detection sensitivity of scanners with lower magnetic fields will lessen the risk of Mn^{2+}-based toxicity. Ultimately, MEMRI may become a powerful in vivo method to diagnose early-stage AD and test clinical compounds that prevent or treat FAT defects.

MEMRI may be performed in combination with optogenetics studies to correlate FAT defects with impaired synaptic transmission in AD brain. Optogenetics uses light to excite or inhibit neurons expressing opsin-based ion channels and pumps. This revolutionary technique permits manipulation of electrical activity in genetically or

functionally defined neurons with high temporal precision (Tye and Deisseroth, 2012). To initiate and optimize these studies in vitro, an optogenetic probe may be expressed and activated by light in AβO-treated neurons that exhibit reduced KIF1A-dependent transport of synaptic vesicle precursors (SVPs). Miniature excitatory postsynaptic responses (mEPSPs) could then be measured by whole cell patch-clamp recording to determine if synaptic transmission is simultaneously impaired in neurons with reduced SVP transport. If these processes are indeed interdependent, pharmacological rescue of transport may also restore neurotransmission. To translate these findings to preclinical models, a promoter-dependent optogenetic probe may be delivered into the hippocampi of wild type and transgenic AD mice by viral injection. Subsequent illumination of the CA3 hippocampal region may fail to activate postsynaptic CA1 neurons in AD mice, which exhibit severe FAT defects as diagnosed by MEMRI studies. Intraperitoneal administration of Ca^{2+} channel and CaN inhibitors may ultimately rescue neurotransmission in vivo.

5.4. Analysis of BDNF transport in human stem cell models of AD

Although vertebrate and invertebrate models have provided important insights into AD, studies are often confounded by overexpression artefacts, and mutations introduced into endogenous genes fail to recapitulate all phenotypes and behaviours associated with human AD pathology (Duff and Suleman, 2004; Young and Goldstein, 2012)). Human pluripotent stem cells (hPSCs) are valuable to disease research because they can differentiate into all cell types, and genes of interest are expressed at endogenous levels. Recent advances in reprogramming technology have enabled the expression of defined factors in somatic cells, such as skin fibroblasts, from an individual patient to induce a pluripotent stem cell state (iPSCs) (Takahashi et al., 2007). These iPSCs can be differentiated into neurons that retain the unique genetic background of the individual. Alternatively, patient fibroblasts can be exposed to forebrain transcription factors that directly convert them to neurons (induced neuronal cells, iNs) (Young and Goldstein, 2012). This strategy bypasses the time-consuming and potentially mutagenic IPSC reprogramming process; however, it cannot generate a self-renewing, stable

progenitor population. IPSC models of neurodegeneration were first created for monogenic disorders or versions of polygenic diseases caused by known mutations, such as Parkinson's disease (Soldner et al., 2009) and amyotrophic lateral sclerosis (Dimos et al., 2008). IPSC and iN models of AD have only recently been developed due to the complex nature of the disease. They are derived from presenilin point mutations (PS1 A246E, PS2 N141) (Yagi et al., 2011) and APP gene duplications (Rovelet-Lecrux et al., 2006) associated with familial forms of AD. Sporadic AD genomes confer similar cellular phenotypes: neurons from a sporadic AD patient exhibit elevated levels of $A\beta_{1-40}$, increased GSK3β activity, and tau hyperphosphorylation compared to neurons from age-matched, normal individuals (Israel et al., 2012).

Several strategies could be designed to characterize and attenuate BDNF transport defects in human stem cell models of AD. First, iPSCs or iNs derived from wild type patients may be transfected with BDNF-mRFP and treated with extracellular AβOs to impair BDNF transport, as described previously. If similar Ca^{2+}-dependent mechanisms regulate BDNF transport in human neurons, treatment with compounds that maintain Ca^{2+} homeostasis and inhibit CaN-GSK3β signaling may prevent and/or rescue BDNF transport defects. Second, BDNF transport could be assessed in iPSCs generated from familial AD patients or well characterized sporadic AD genomes and compared to age-matched, wild type controls. These experiments may define a novel role for presenilin point mutations, APP duplication, and intracellular Aβ overproduction in BDNF transport impairment and further characterize the sporadic AD phenotype.

Third, patient-specific hPSCs may be modified using genome editing techniques, such as Tal effector nucleases (TALENs) and clustered regulatory interspaced short palindromic repeat-based endonucleases (CRISPR/Cas systems), to establish causal roles for motor proteins and their regulators in AD pathogenesis. These techniques are superior to knockdown by RNA interference, which is often incomplete, varies between experiments and laboratories, has unpredictable off-target effects, and provides only temporary inhibition of gene function. Briefly, TALEN and CRISPR/Cas systems induce targeted DNA double-strand breaks that stimulate cellular DNA repair mechanisms to alter the gene of interest. Error-prone non-homologous end joining (NHEJ) yields small insertion or deletion mutations to disrupt the target gene, whereas homology directed

repair (HDR) in the presence of a donor plasmid introduces transgenes to correct or replace existing genes (Gaj et al., 2013). For BDNF trafficking studies in human stem cells, TALEN or CRISPR/Cas systems may be used to knock down tau and GSK3β to determine if they regulate BDNF transport. Furthermore, point mutations may be introduced within GSK3β phosphorylation sites on KIF1A to normalize BDNF transport in an AD mutant background. Recent work suggests that alternative splicing of motor proteins plays a causal role in AD pathogenesis (Morihara et al., 2014). Thus, potential KIF1A splice variants that are overexpressed in the disease state and perturb BDNF transport by compromising cargo binding or preferentially adopting an autoinhibited conformation may also be reduced by genome editing. Because KIF1A is highly enriched in the brain, approaches designed to restore its motility may exhibit minimal off-target effects compared to targeting upstream, ubiquitous Ca^{2+} signaling proteins. Collectively, these functional studies may help to identify mechanisms of transport dysregulation in AD patients and unveil new therapeutic avenues.

5.5. Closing remarks

My thesis establishes novel roles and a translational basis for Ca^{2+} dysregulation in tau-independent FAT disruption. It challenges dogmatic perspectives on mechanisms of Aβ toxicity and their subcellular sites of action. Despite its importance for neuronal survival and synaptic plasticity, learning, and memory, the role of impaired BDNF trafficking in early AD progression has received little attention, and my work contributes substantially to this field. From a clinical perspective, my findings are significant because intracellular Ca^{2+} dysregulation and FAT impairment precede late-stage hallmarks of AD, such as Aβ plaque deposition and neurofibrillary tangle formation. Compounds and genetic interventions targeted to these early disease mechanisms may be more effective at preventing or reversing axonal pathologies, synapse loss, and cell death.

References

Abney JR, Meliza CD, Cutler B, Kingma M, Lochner JE, Scalettar BA (1999) Real-time imaging of the dynamics of secretory granules in growth cones. Biophysical journal 77:2887-2895.

Adalbert R, Coleman MP (2012) Axon pathology in age-related neurodegenerative disorders. Neuropathol Appl Neurobiol.

Adasme T, Haeger P, Paula-Lima AC, Espinoza I, Casas-Alarcon MM, Carrasco MA, Hidalgo C (2011) Involvement of ryanodine receptors in neurotrophin-induced hippocampal synaptic plasticity and spatial memory formation. Proceedings of the National Academy of Sciences of the United States of America 108:3029-3034.

Allan V (2014) Cell biology. One, two, three, cytoplasmic dynein is go! Science 345:271-272.

Ally S, Larson AG, Barlan K, Rice SE, Gelfand VI (2009) Opposite-polarity motors activate one another to trigger cargo transport in live cells. The Journal of cell biology 187:1071-1082.

Almeida S, Domingues A, Rodrigues L, Oliveira CR, Rego AC (2004) FK506 prevents mitochondrial-dependent apoptotic cell death induced by 3-nitropropionic acid in rat primary cortical cultures. Neurobiology of disease 17:435-444.

Anekonda TS, Quinn JF (2011) Calcium channel blocking as a therapeutic strategy for Alzheimer's disease: the case for isradipine. Biochimica et biophysica acta 1812:1584-1590.

Apelt J, Ach K, Schliebs R (2003) Aging-related down-regulation of neprilysin, a putative beta-amyloid-degrading enzyme, in transgenic Tg2576 Alzheimer-like mouse brain is accompanied by an astroglial upregulation in the vicinity of beta-amyloid plaques. Neuroscience letters 339:183-186.

Arispe N, Pollard HB, Rojas E (1993) Giant multilevel cation channels formed by Alzheimer disease amyloid beta-protein [A beta P-(1-40)] in bilayer membranes. Proceedings of the National Academy of Sciences of the United States of America 90:10573-10577.

Avila J, Perez M, Lucas JJ, Gomez-Ramos A, Santa Maria I, Moreno F, Smith M, Perry G, Hernandez F (2004) Assembly in vitro of tau protein and its implications in Alzheimer's disease. Current Alzheimer research 1:97-101.

Avramopoulos D (2009) Genetics of Alzheimer's disease: recent advances. Genome medicine 1:34.

Baker KD, Edwards TM, Rickard NS (2013) The role of intracellular calcium stores in synaptic plasticity and memory consolidation. Neuroscience and biobehavioral reviews 37:1211-1239.

Bandara S, Malmersjo S, Meyer T (2013) Regulators of calcium homeostasis identified by inference of kinetic model parameters from live single cells perturbed by siRNA. Science signaling 6:ra56.

Bardo S, Cavazzini MG, Emptage N (2006) The role of the endoplasmic reticulum Ca2+ store in the plasticity of central neurons. Trends in pharmacological sciences 27:78-84.

Barkus RV, Klyachko O, Horiuchi D, Dickson BJ, Saxton WM (2008) Identification of an Axonal Kinesin-3 Motor for Fast Anterograde Vesicle Transport that Facilitates Retrograde Transport of Neuropeptides. Molecular biology of the cell 19:274-283.

Bateman RJ, Munsell LY, Morris JC, Swarm R, Yarasheski KE, Holtzman DM (2006) Human amyloid-beta synthesis and clearance rates as measured in cerebrospinal fluid in vivo. Nature medicine 12:856-861.

Baughman JM, Perocchi F, Girgis HS, Plovanich M, Belcher-Timme CA, Sancak Y, Bao XR, Strittmatter L, Goldberger O, Bogorad RL, Koteliansky V, Mootha VK (2011) Integrative genomics identifies MCU as an essential component of the mitochondrial calcium uniporter. Nature 476:341-345.

Baumgartel K, Mansuy IM (2012) Neural functions of calcineurin in synaptic plasticity and memory. Learning & memory 19:375-384.

Benilova I, Karran E, De Strooper B (2012) The toxic Abeta oligomer and Alzheimer's disease: an emperor in need of clothes. Nature neuroscience 15:349-357.

Berezuk MA, Schroer TA (2007) Dynactin enhances the processivity of kinesin-2. Traffic 8:124-129.

Berridge MJ (2010a) Calcium hypothesis of Alzheimer's disease. Pflugers Arch 459:441-449.

Berridge MJ (2010b) Calcium signalling and Alzheimer's disease. Neurochem Res 36:1149-1156.

Berridge MJ (2012) Calcium signalling remodelling and disease. Biochemical Society transactions 40:297-309.

Berridge MJ (2013) Dysregulation of neural calcium signaling in Alzheimer disease, bipolar disorder and schizophrenia. Prion 7:2-13.

Berridge MJ, Bootman MD, Lipp P (1998) Calcium--a life and death signal. Nature 395:645-648.

Bezprozvanny I (2013) Presenilins and calcium signaling--systems biology to the rescue. Science signaling 6:pe24.

Bezprozvanny I, Mattson MP (2008) Neuronal calcium mishandling and the pathogenesis of Alzheimer's disease. Trends in neurosciences 31:454-463.

Biernat J, Mandelkow EM (1999) The development of cell processes induced by tau protein requires phosphorylation of serine 262 and 356 in the repeat domain and is inhibited by phosphorylation in the proline-rich domains. Molecular biology of the cell 10:727-740.

Biernat J, Wu YZ, Timm T, Zheng-Fischhofer Q, Mandelkow E, Meijer L, Mandelkow EM (2002) Protein kinase MARK/PAR-1 is required for neurite outgrowth and establishment of neuronal polarity. Molecular biology of the cell 13:4013-4028.

Black MM, Slaughter T, Moshiach S, Obrocka M, Fischer I (1996) Tau is enriched on dynamic microtubules in the distal region of growing axons. J Neurosci 16:3601-3619.

Bliss TV, Collingridge GL (1993) A synaptic model of memory: long-term potentiation in the hippocampus. Nature 361:31-39.

Bloom GS, Wagner MC, Pfister KK, Brady ST (1988) Native structure and physical properties of bovine brain kinesin and identification of the ATP-binding subunit polypeptide. Biochemistry 27:3409-3416.

Bobich JA, Zheng Q, Campbell A (2004) Incubation of nerve endings with a physiological concentration of Abeta1-42 activates CaV2.2(N-Type)-voltage operated calcium channels and acutely increases glutamate and noradrenaline release. Journal of Alzheimer's disease : JAD 6:243-255.

Bomfim TR, Forny-Germano L, Sathler LB, Brito-Moreira J, Houzel JC, Decker H, Silverman MA, Kazi H, Melo HM, McClean PL, Holscher C, Arnold SE, Talbot K, Klein WL, Munoz DP, Ferreira ST, De Felice FG (2012) An anti-diabetes agent protects the mouse brain from defective insulin signaling caused by Alzheimer's disease- associated Abeta oligomers. The Journal of clinical investigation 122:1339-1353.

Borrell-Pages M, Zala D, Humbert S, Saudou F (2006) Huntington's disease: from huntingtin function and dysfunction to therapeutic strategies. Cellular and molecular life sciences : CMLS 63:2642-2660.

Braithwaite SP, Stock JB, Lombroso PJ, Nairn AC (2012) Protein phosphatases and Alzheimer's disease. Prog Mol Biol Transl Sci 106:343-379.

Burgoyne RD (2007) Neuronal calcium sensor proteins: generating diversity in neuronal Ca2+ signalling. Nature reviews Neuroscience 8:182-193.

Cantuti Castelvetri L, Givogri MI, Hebert A, Smith B, Song Y, Kaminska A, Lopez-Rosas A, Morfini G, Pigino G, Sands M, Brady ST, Bongarzone ER (2013) The sphingolipid psychosine inhibits fast axonal transport in Krabbe disease by activation of GSK3beta and deregulation of molecular motors. The Journal of neuroscience : the official journal of the Society for Neuroscience 33:10048-10056.

Castellani RJ, Nunomura A, Lee HG, Perry G, Smith MA (2008) Phosphorylated tau: toxic, protective, or none of the above. Journal of Alzheimer's disease : JAD 14:377-383.

Cataldi M (2013) The changing landscape of voltage-gated calcium channels in neurovascular disorders and in neurodegenerative diseases. Current neuropharmacology 11:276-297.

Chakroborty S, Stutzmann GE (2011) Early calcium dysregulation in Alzheimer's disease: setting the stage for synaptic dysfunction. Science China Life sciences 54:752-762.

Chakroborty S, Stutzmann GE (2014) Calcium channelopathies and Alzheimer's disease: insight into therapeutic success and failures. European journal of pharmacology 739:83-95.

Chakroborty S, Goussakov I, Miller MB, Stutzmann GE (2009) Deviant ryanodine receptor-mediated calcium release resets synaptic homeostasis in presymptomatic 3xTg-AD mice. The Journal of neuroscience : the official journal of the Society for Neuroscience 29:9458-9470.

Chakroborty S, Briggs C, Miller MB, Goussakov I, Schneider C, Kim J, Wicks J, Richardson JC, Conklin V, Cameransi BG, Stutzmann GE (2012) Stabilizing ER Ca2+ channel function as an early preventative strategy for Alzheimer's disease. PloS one 7:e52056.

Cheung KH, Shineman D, Muller M, Cardenas C, Mei L, Yang J, Tomita T, Iwatsubo T, Lee VM, Foskett JK (2008) Mechanism of Ca2+ disruption in Alzheimer's disease by presenilin regulation of InsP3 receptor channel gating. Neuron 58:871-883.

Cho C, Vale RD (2012) The mechanism of dynein motility: insight from crystal structures of the motor domain. Biochimica et biophysica acta 1823:182-191.

Chong SA, Benilova I, Shaban H, De Strooper B, Devijver H, Moechars D, Eberle W, Bartic C, Van Leuven F, Callewaert G (2011) Synaptic dysfunction in hippocampus of transgenic mouse models of Alzheimer's disease: a multi-electrode array study. Neurobiology of disease 44:284-291.

Chua JJ, Butkevich E, Worseck JM, Kittelmann M, Gronborg M, Behrmann E, Stelzl U, Pavlos NJ, Lalowski MM, Eimer S, Wanker EE, Klopfenstein DR, Jahn R (2012) Phosphorylation-regulated axonal dependent transport of syntaxin 1 is mediated by a Kinesin-1 adapter. Proceedings of the National Academy of Sciences of the United States of America 109:5862-5867.

Citron M et al. (1997) Mutant presenilins of Alzheimer's disease increase production of 42-residue amyloid beta-protein in both transfected cells and transgenic mice. Nature medicine 3:67-72.

Cochran JN, Hall AM, Roberson ED (2013) The dendritic hypothesis for Alzheimer's disease pathophysiology. Brain Res Bull.

Coghlan VM, Perrino BA, Howard M, Langeberg LK, Hicks JB, Gallatin WM, Scott JD (1995) Association of protein kinase A and protein phosphatase 2B with a common anchoring protein. Science 267:108-111.

Cohen PT, Klee CB (1988) Calmodulin. Amsterdam: Elsevier.

Copenhaver PF, Anekonda TS, Musashe D, Robinson KM, Ramaker JM, Swanson TL, Wadsworth TL, Kretzschmar D, Woltjer RL, Quinn JF (2011) A translational continuum of model systems for evaluating treatment strategies in Alzheimer's disease: isradipine as a candidate drug. Disease models & mechanisms 4:634-648.

Craig AM, Banker G (1994) Neuronal polarity. Annual review of neuroscience 17:267-310.

Culver-Hanlon TL, Lex SA, Stephens AD, Quintyne NJ, King SJ (2006) A microtubule-binding domain in dynactin increases dynein processivity by skating along microtubules. Nature cell biology 8:264-270.

D'Amelio M, Cavallucci V, Middei S, Marchetti C, Pacioni S, Ferri A, Diamantini A, De Zio D, Carrara P, Battistini L, Moreno S, Bacci A, Ammassari-Teule M, Marie H, Cecconi F (2011) Caspase-3 triggers early synaptic dysfunction in a mouse model of Alzheimer's disease. Nature neuroscience 14:69-76.

Das U, Scott DA, Ganguly A, Koo EH, Tang Y, Roy S (2013) Activity-induced convergence of APP and BACE-1 in acidic microdomains via an endocytosis-dependent pathway. Neuron 79:447-460.

Dawson HN, Ferreira A, Eyster MV, Ghoshal N, Binder LI, Vitek MP (2001) Inhibition of neuronal maturation in primary hippocampal neurons from tau deficient mice. Journal of cell science 114:1179-1187.

de Calignon A, Spires-Jones TL, Pitstick R, Carlson GA, Hyman BT (2009) Tangle-bearing neurons survive despite disruption of membrane integrity in a mouse model of tauopathy. J Neuropathol Exp Neurol 68:757-761.

de Calignon A, Fox LM, Pitstick R, Carlson GA, Bacskai BJ, Spires-Jones TL, Hyman BT (2010) Caspase activation precedes and leads to tangles. Nature 464:1201-1204.

De Felice FG, Velasco PT, Lambert MP, Viola K, Fernandez SJ, Ferreira ST, Klein WL (2007) Abeta oligomers induce neuronal oxidative stress through an N-methyl-D-aspartate receptor-dependent mechanism that is blocked by the Alzheimer drug memantine. The Journal of biological chemistry 282:11590-11601.

De Felice FG, Wu D, Lambert MP, Fernandez SJ, Velasco PT, Lacor PN, Bigio EH, Jerecic J, Acton PJ, Shughrue PJ, Chen-Dodson E, Kinney GG, Klein WL (2008) Alzheimer's disease-type neuronal tau hyperphosphorylation induced by A beta oligomers. Neurobiology of aging 29:1334-1347.

De Stefani D, Raffaello A, Teardo E, Szabo I, Rizzuto R (2011) A forty-kilodalton protein of the inner membrane is the mitochondrial calcium uniporter. Nature 476:336-340.

De Vos KJ, Grierson AJ, Ackerley S, Miller CC (2008) Role of axonal transport in neurodegenerative diseases. Annual review of neuroscience 31:151-173.

Dean C, Liu H, Dunning FM, Chang PY, Jackson MB, Chapman ER (2009) Synaptotagmin-IV modulates synaptic function and long-term potentiation by regulating BDNF release. Nature neuroscience 12:767-776.

DeBerg HA, Blehm BH, Sheung J, Thompson AR, Bookwalter CS, Torabi SF, Schroer TA, Berger CL, Lu Y, Trybus KM, Selvin PR (2013) Motor domain phosphorylation modulates kinesin-1 transport. The Journal of biological chemistry 288:32612-32621.

Decker H, Lo KY, Unger SM, Ferreira ST, Silverman MA (2010a) Amyloid-beta peptide oligomers disrupt axonal transport through an NMDA receptor-dependent mechanism that is mediated by glycogen synthase kinase 3beta in primary cultured hippocampal neurons. The Journal of neuroscience : the official journal of the Society for Neuroscience 30:9166-9171.

Decker H, Jurgensen S, Adrover MF, Brito-Moreira J, Bomfim TR, Klein WL, Epstein AL, De Felice FG, Jerusalinsky D, Ferreira ST (2010b) N-methyl-D-aspartate receptors are required for synaptic targeting of Alzheimer's toxic amyloid-beta peptide oligomers. Journal of neurochemistry 115:1520-1529.

DeFuria J, Shea TB (2007) Arsenic inhibits neurofilament transport and induces perikaryal accumulation of phosphorylated neurofilaments: roles of JNK and GSK-3beta. Brain research 1181:74-82.

Demuro A, Parker I (2013) Cytotoxicity of intracellular abeta42 amyloid oligomers involves Ca2+ release from the endoplasmic reticulum by stimulated production of inositol trisphosphate. The Journal of neuroscience : the official journal of the Society for Neuroscience 33:3824-3833.

Demuro A, Parker I, Stutzmann GE (2010) Calcium signaling and amyloid toxicity in Alzheimer disease. The Journal of biological chemistry 285:12463-12468.

Demuro A, Mina E, Kayed R, Milton SC, Parker I, Glabe CG (2005) Calcium dysregulation and membrane disruption as a ubiquitous neurotoxic mechanism of soluble amyloid oligomers. The Journal of biological chemistry 280:17294-17300.

Deng CY, Lei WL, Xu XH, Ju XC, Liu Y, Luo ZG (2014) JIP1 mediates anterograde transport of Rab10 cargos during neuronal polarization. The Journal of neuroscience : the official journal of the Society for Neuroscience 34:1710-1723.

Di Scala C, Chahinian H, Yahi N, Garmy N, Fantini J (2014) Interaction of Alzheimer's beta-amyloid peptides with cholesterol: mechanistic insights into amyloid pore formation. Biochemistry 53:4489-4502.

Diefenbach RJ, Mackay JP, Armati PJ, Cunningham AL (1998) The C-terminal region of the stalk domain of ubiquitous human kinesin heavy chain contains the binding site for kinesin light chain. Biochemistry 37:16663-16670.

Dietrich KA, Sindelar CV, Brewer PD, Downing KH, Cremo CR, Rice SE (2008) The kinesin-1 motor protein is regulated by a direct interaction of its head and tail. Proceedings of the National Academy of Sciences of the United States of America 105:8938-8943.

Dikeakos JD, Di Lello P, Lacombe MJ, Ghirlando R, Legault P, Reudelhuber TL, Omichinski JG (2009) Functional and structural characterization of a dense core secretory granule sorting domain from the PC1/3 protease. Proceedings of the National Academy of Sciences of the United States of America 106:7408-7413.

Dimos JT, Rodolfa KT, Niakan KK, Weisenthal LM, Mitsumoto H, Chung W, Croft GF, Saphier G, Leibel R, Goland R, Wichterle H, Henderson CE, Eggan K (2008) Induced pluripotent stem cells generated from patients with ALS can be differentiated into motor neurons. Science 321:1218-1221.

Dineley KT, Hogan D, Zhang WR, Taglialatela G (2007) Acute inhibition of calcineurin restores associative learning and memory in Tg2576 APP transgenic mice. Neurobiology of learning and memory 88:217-224.

Dineley KT, Kayed R, Neugebauer V, Fu Y, Zhang W, Reese LC, Taglialatela G (2010) Amyloid-beta oligomers impair fear conditioned memory in a calcineurin-dependent fashion in mice. Journal of neuroscience research 88:2923-2932.

Diniz BS, Teixeira AL (2011) Brain-derived neurotrophic factor and Alzheimer's disease: physiopathology and beyond. Neuromolecular Med 13:217-222.

Dixit R, Ross JL, Goldman YE, Holzbaur EL (2008) Differential regulation of dynein and kinesin motor proteins by tau. Science 319:1086-1089.

Dolev I, Michaelson DM (2004) A nontransgenic mouse model shows inducible amyloid-beta (Abeta) peptide deposition and elucidates the role of apolipoprotein E in the amyloid cascade. Proceedings of the National Academy of Sciences of the United States of America 101:13909-13914.

Dolma K, Iacobucci GJ, Hong Zheng K, Shandilya J, Toska E, White JA, 2nd, Spina E, Gunawardena S (2014) Presenilin influences glycogen synthase kinase-3 beta (GSK-3beta) for kinesin-1 and dynein function during axonal transport. Human molecular genetics 23:1121-1133.

Dolphin AC (2012) Calcium channel auxiliary alpha2delta and beta subunits: trafficking and one step beyond. Nature reviews Neuroscience 13:542-555.

Duff K, Suleman F (2004) Transgenic mouse models of Alzheimer's disease: how useful have they been for therapeutic development? Briefings in functional genomics & proteomics 3:47-59.

Dumanchin C, Camuzat A, Campion D, Verpillat P, Hannequin D, Dubois B, Saugier-Veber P, Martin C, Penet C, Charbonnier F, Agid Y, Frebourg T, Brice A (1998) Segregation of a missense mutation in the microtubule-associated protein tau gene with familial frontotemporal dementia and parkinsonism. Human molecular genetics 7:1825-1829.

Duncan RR, Greaves J, Wiegand UK, Matskevich I, Bodammer G, Apps DK, Shipston MJ, Chow RH (2003) Functional and spatial segregation of secretory vesicle pools according to vesicle age. Nature 422:176-180.

El Ayadi A, Stieren ES, Barral JM, Boehning D (2012) Ubiquilin-1 regulates amyloid precursor protein maturation and degradation by stimulating K63-linked polyubiquitination of lysine 688. Proceedings of the National Academy of Sciences of the United States of America 109:13416-13421.

Emilsson L, Saetre P, Jazin E (2006) Alzheimer's disease: mRNA expression profiles of multiple patients show alterations of genes involved with calcium signaling. Neurobiology of disease 21:618-625.

Ems-McClung SC, Hainline SG, Devare J, Zong H, Cai S, Carnes SK, Shaw SL, Walczak CE (2013) Aurora B inhibits MCAK activity through a phosphoconformational switch that reduces microtubule association. Current biology : CB 23:2491-2499.

Fang C, Decker H, Banker G (2014) Axonal transport plays a crucial role in mediating the axon-protective effects of NmNAT. Neurobiology of disease 68:78-90.

Farrer MJ et al. (2009) DCTN1 mutations in Perry syndrome. Nature genetics 41:163-165.

Ferreira ST, Klein WL (2011) The Abeta oligomer hypothesis for synapse failure and memory loss in Alzheimer's disease. Neurobiology of learning and memory 96:529-543.

Ferreira ST, Vieira MN, De Felice FG (2007) Soluble protein oligomers as emerging toxins in Alzheimer's and other amyloid diseases. IUBMB Life 59:332-345.

Finch EA, Turner TJ, Goldin SM (1991) Calcium as a coagonist of inositol 1,4,5-trisphosphate-induced calcium release. Science 252:443-446.

Fischer D, Mukrasch MD, Biernat J, Bibow S, Blackledge M, Griesinger C, Mandelkow E, Zweckstetter M (2009) Conformational changes specific for pseudophosphorylation at serine 262 selectively impair binding of tau to microtubules. Biochemistry 48:10047-10055.

Fitzjohn SM, Collingridge GL (2002) Calcium stores and synaptic plasticity. Cell calcium 32:405-411.

Foskett JK, White C, Cheung KH, Mak DO (2007) Inositol trisphosphate receptor Ca2+ release channels. Physiological reviews 87:593-658.

Fu MM, Holzbaur EL (2013) JIP1 regulates the directionality of APP axonal transport by coordinating kinesin and dynein motors. The Journal of cell biology 202:495-508.

Fu MM, Holzbaur EL (2014) Integrated regulation of motor-driven organelle transport by scaffolding proteins. Trends in cell biology.

Fukami S, Watanabe K, Iwata N, Haraoka J, Lu B, Gerard NP, Gerard C, Fraser P, Westaway D, St George-Hyslop P, Saido TC (2002) Abeta-degrading endopeptidase, neprilysin, in mouse brain: synaptic and axonal localization inversely correlating with Abeta pathology. Neuroscience research 43:39-56.

Gaj T, Gersbach CA, Barbas CF, 3rd (2013) ZFN, TALEN, and CRISPR/Cas-based methods for genome engineering. Trends in biotechnology 31:397-405.

Gallagher JJ, Zhang X, Ziomek GJ, Jacobs RE, Bearer EL (2012) Deficits in axonal transport in hippocampal-based circuitry and the visual pathway in APP knock-out animals witnessed by manganese enhanced MRI. Neuroimage 60:1856-1866.

Garaschuk O, Schneggenburger R, Schirra C, Tempia F, Konnerth A (1996) Fractional Ca2+ currents through somatic and dendritic glutamate receptor channels of rat hippocampal CA1 pyramidal neurones. The Journal of physiology 491 (Pt 3):757-772.

Gill SR, Schroer TA, Szilak I, Steuer ER, Sheetz MP, Cleveland DW (1991) Dynactin, a conserved, ubiquitously expressed component of an activator of vesicle motility mediated by cytoplasmic dynein. The Journal of cell biology 115:1639-1650.

Gindhart JG, Jr., Desai CJ, Beushausen S, Zinn K, Goldstein LS (1998) Kinesin light chains are essential for axonal transport in Drosophila. The Journal of cell biology 141:443-454.

Goedert M, Spillantini MG, Jakes R, Rutherford D, Crowther RA (1989) Multiple isoforms of human microtubule-associated protein tau: sequences and localization in neurofibrillary tangles of Alzheimer's disease. Neuron 3:519-526.

Goldstein LS (2012) Axonal transport and neurodegenerative disease: Can we see the elephant? Progress in neurobiology.

Gomez-Isla T, Hollister R, West H, Mui S, Growdon JH, Petersen RC, Parisi JE, Hyman BT (1997) Neuronal loss correlates with but exceeds neurofibrillary tangles in Alzheimer's disease. Annals of neurology 41:17-24.

Goussakov I, Miller MB, Stutzmann GE (2010) NMDA-mediated Ca(2+) influx drives aberrant ryanodine receptor activation in dendrites of young Alzheimer's disease mice. The Journal of neuroscience : the official journal of the Society for Neuroscience 30:12128-12137.

Green KN, LaFerla FM (2008) Linking calcium to Abeta and Alzheimer's disease. Neuron 59:190-194.

Groth RD, Dunbar RL, Mermelstein PG (2003) Calcineurin regulation of neuronal plasticity. Biochemical and biophysical research communications 311:1159-1171.

Guillaud L, Wong R, Hirokawa N (2008) Disruption of KIF17-Mint1 interaction by CaMKII-dependent phosphorylation: a molecular model of kinesin-cargo release. Nature cell biology 10:19-29.

Gyoeva FK, Bybikova EM, Minin AA (2000) An isoform of kinesin light chain specific for the Golgi complex. Journal of cell science 113 (Pt 11):2047-2054.

Gyoeva FK, Sarkisov DV, Khodjakov AL, Minin AA (2004) The tetrameric molecule of conventional kinesin contains identical light chains. Biochemistry 43:13525-13531.

Hall DH, Hedgecock EM (1991) Kinesin-related gene unc-104 is required for axonal transport of synaptic vesicles in C. elegans. Cell 65:837-847.

Hamilton SL (2005) Ryanodine receptors. Cell calcium 38:253-260.

Hammond JW, Cai D, Blasius TL, Li Z, Jiang Y, Jih GT, Meyhofer E, Verhey KJ (2009) Mammalian Kinesin-3 motors are dimeric in vivo and move by processive motility upon release of autoinhibition. PLoS Biol 7:e72.

Handley MT, Haynes LP, Burgoyne RD (2007) Differential dynamics of Rab3A and Rab27A on secretory granules. Journal of cell science 120:973-984.

Harada A, Oguchi K, Okabe S, Kuno J, Terada S, Ohshima T, Sato-Yoshitake R, Takei Y, Noda T, Hirokawa N (1994) Altered microtubule organization in small-calibre axons of mice lacking tau protein. Nature 369:488-491.

Hardingham GE (2009) Coupling of the NMDA receptor to neuroprotective and neurodestructive events. Biochemical Society transactions 37:1147-1160.

Hell JW, Westenbroek RE, Warner C, Ahlijanian MK, Prystay W, Gilbert MM, Snutch TP, Catterall WA (1993) Identification and differential subcellular localization of the neuronal class C and class D L-type calcium channel alpha 1 subunits. The Journal of cell biology 123:949-962.

Henriques AG, Vieira SI, da Cruz ESEF, da Cruz ESOA (2010) Abeta promotes Alzheimer's disease-like cytoskeleton abnormalities with consequences to APP processing in neurons. J Neurochem 113:761-771.

Hermann D, Mezler M, Muller MK, Wicke K, Gross G, Draguhn A, Bruehl C, Nimmrich V (2013) Synthetic Abeta oligomers (Abeta(1-42) globulomer) modulate presynaptic calcium currents: prevention of Abeta-induced synaptic deficits by calcium channel blockers. European journal of pharmacology 702:44-55.

Herrup K (2010) Reimagining Alzheimer's disease--an age-based hypothesis. The Journal of neuroscience : the official journal of the Society for Neuroscience 30:16755-16762.

Hinckelmann MV, Zala D, Saudou F (2013) Releasing the brake: restoring fast axonal transport in neurodegenerative disorders. Trends in cell biology 23:634-643.

Hirokawa N, Takemura R (2005) Molecular motors and mechanisms of directional transport in neurons. Nature reviews Neuroscience 6:201-214.

Hirokawa N, Noda Y (2008) Intracellular transport and kinesin superfamily proteins, KIFs: structure, function, and dynamics. Physiological reviews 88:1089-1118.

Hirokawa N, Niwa S, Tanaka Y (2010) Molecular motors in neurons: transport mechanisms and roles in brain function, development, and disease. Neuron 68:610-638.

Hiruma H, Katakura T, Takahashi S, Ichikawa T, Kawakami T (2003) Glutamate and amyloid beta-protein rapidly inhibit fast axonal transport in cultured rat hippocampal neurons by different mechanisms. J Neurosci 23:8967-8977.

Hooper C, Killick R, Lovestone S (2008) The GSK3 hypothesis of Alzheimer's disease. Journal of neurochemistry 104:1433-1439.

Horiuchi D, Collins CA, Bhat P, Barkus RV, Diantonio A, Saxton WM (2007) Control of a kinesin-cargo linkage mechanism by JNK pathway kinases. Current biology : CB 17:1313-1317.

Hsieh H, Boehm J, Sato C, Iwatsubo T, Tomita T, Sisodia S, Malinow R (2006) AMPAR removal underlies Abeta-induced synaptic depression and dendritic spine loss. Neuron 52:831-843.

Hyman BT (2011) Caspase activation without apoptosis: insight into Abeta initiation of neurodegeneration. Nature neuroscience 14:5-6.

Ihara Y, Morishima-Kawashima M, Nixon R (2012) The ubiquitin-proteasome system and the autophagic-lysosomal system in Alzheimer disease. Cold Spring Harbor perspectives in medicine 2.

Inoue S (2008) In situ Abeta pores in AD brain are cylindrical assembly of Abeta protofilaments. Amyloid : the international journal of experimental and clinical investigation : the official journal of the International Society of Amyloidosis 15:223-233.

Inoue T, Majid T, Pautler RG (2011) Manganese enhanced MRI (MEMRI): neurophysiological applications. Rev Neurosci 22:675-694.

Israel MA, Yuan SH, Bardy C, Reyna SM, Mu Y, Herrera C, Hefferan MP, Van Gorp S, Nazor KL, Boscolo FS, Carson CT, Laurent LC, Marsala M, Gage FH, Remes AM, Koo EH, Goldstein LS (2012) Probing sporadic and familial Alzheimer's disease using induced pluripotent stem cells. Nature 482:216-220.

Itkin A, Dupres V, Dufrene YF, Bechinger B, Ruysschaert JM, Raussens V (2011) Calcium ions promote formation of amyloid beta-peptide (1-40) oligomers

causally implicated in neuronal toxicity of Alzheimer's disease. PloS one 6:e18250.

Ittner LM, Gotz J (2011) Amyloid-beta and tau--a toxic pas de deux in Alzheimer's disease. Nature reviews Neuroscience 12:65-72.

Ittner LM, Ke YD, Delerue F, Bi M, Gladbach A, van Eersel J, Wolfing H, Chieng BC, Christie MJ, Napier IA, Eckert A, Staufenbiel M, Hardeman E, Gotz J (2010) Dendritic function of tau mediates amyloid-beta toxicity in Alzheimer's disease mouse models. Cell 142:387-397.

Iwata N, Takaki Y, Fukami S, Tsubuki S, Saido TC (2002) Region-specific reduction of A beta-degrading endopeptidase, neprilysin, in mouse hippocampus upon aging. Journal of neuroscience research 70:493-500.

Iwata N, Mizukami H, Shirotani K, Takaki Y, Muramatsu S, Lu B, Gerard NP, Gerard C, Ozawa K, Saido TC (2004) Presynaptic localization of neprilysin contributes to efficient clearance of amyloid-beta peptide in mouse brain. The Journal of neuroscience : the official journal of the Society for Neuroscience 24:991-998.

Jan A, Gokce O, Luthi-Carter R, Lashuel HA (2008) The ratio of monomeric to aggregated forms of Abeta40 and Abeta42 is an important determinant of amyloid-beta aggregation, fibrillogenesis, and toxicity. The Journal of biological chemistry 283:28176-28189.

Janke C, Kneussel M (2010) Tubulin post-translational modifications: encoding functions on the neuronal microtubule cytoskeleton. Trends Neurosci 33:362-372.

Jho YS, Zhulina EB, Kim MW, Pincus PA (2010) Monte carlo simulations of tau proteins: effect of phosphorylation. Biophysical journal 99:2387-2397.

Jiang S, Li Y, Zhang X, Bu G, Xu H, Zhang YW (2014) Trafficking regulation of proteins in Alzheimer's disease. Mol Neurodegener 9:6.

Jolly AL, Gelfand VI (2011) Bidirectional intracellular transport: utility and mechanism. Biochemical Society transactions 39:1126-1130.

Jovanovic JN, Sihra TS, Nairn AC, Hemmings HC, Jr., Greengard P, Czernik AJ (2001) Opposing changes in phosphorylation of specific sites in synapsin I during Ca2+-dependent glutamate release in isolated nerve terminals. The Journal of neuroscience : the official journal of the Society for Neuroscience 21:7944-7953.

Jurgensen S, Antonio LL, Mussi GE, Brito-Moreira J, Bomfim TR, De Felice FG, Garrido-Sanabria ER, Cavalheiro EA, Ferreira ST Activation of D1/D5 dopamine receptors protects neurons from synapse dysfunction induced by amyloid-beta oligomers. The Journal of biological chemistry 286:3270-3276.

Kaan HY, Hackney DD, Kozielski F (2011) The structure of the kinesin-1 motor-tail complex reveals the mechanism of autoinhibition. Science 333:883-885.

Kaech S, Banker G (2006) Culturing hippocampal neurons. Nature protocols 1:2406-2415.

Kamal A, Stokin GB, Yang Z, Xia CH, Goldstein LS (2000) Axonal transport of amyloid precursor protein is mediated by direct binding to the kinesin light chain subunit of kinesin-I. Neuron 28:449-459.

Kamal A, Almenar-Queralt A, LeBlanc JF, Roberts EA, Goldstein LS (2001) Kinesin-mediated axonal transport of a membrane compartment containing beta-secretase and presenilin-1 requires APP. Nature 414:643-648.

Kanaan NM, Pigino GF, Brady ST, Lazarov O, Binder LI, Morfini GA (2013) Axonal degeneration in Alzheimer's disease: When signaling abnormalities meet the axonal transport system. Exp Neurol 246:44-53.

Kanaan NM, Morfini GA, LaPointe NE, Pigino GF, Patterson KR, Song Y, Andreadis A, Fu Y, Brady ST, Binder LI (2011) Pathogenic forms of tau inhibit kinesin-dependent axonal transport through a mechanism involving activation of axonal phosphotransferases. The Journal of neuroscience : the official journal of the Society for Neuroscience 31:9858-9868.

Kanai Y, Okada Y, Tanaka Y, Harada A, Terada S, Hirokawa N (2000) KIF5C, a novel neuronal kinesin enriched in motor neurons. The Journal of neuroscience : the official journal of the Society for Neuroscience 20:6374-6384.

Kandel ER, Schwartz JH, Jessell TM, Siegelbaum SA, Hudspeth AJ (2013) Principles of Neural Science, 5 Edition. United States of America: McGraw-Hill Companies, Inc.

Kapitein LC, Hoogenraad CC (2011) Which way to go? Cytoskeletal organization and polarized transport in neurons. Molecular and cellular neurosciences 46:9-20.

Kardon JR, Vale RD (2009) Regulators of the cytoplasmic dynein motor. Nat Rev Mol Cell Biol 10:854-865.

Kelliher M, Fastbom J, Cowburn RF, Bonkale W, Ohm TG, Ravid R, Sorrentino V, O'Neill C (1999) Alterations in the ryanodine receptor calcium release channel correlate with Alzheimer's disease neurofibrillary and beta-amyloid pathologies. Neuroscience 92:499-513.

Kelly BL, Ferreira A (2006) beta-Amyloid-induced dynamin 1 degradation is mediated by N-methyl-D-aspartate receptors in hippocampal neurons. The Journal of biological chemistry 281:28079-28089.

Kempf M, Clement A, Faissner A, Lee G, Brandt R (1996) Tau binds to the distal axon early in development of polarity in a microtubule- and microfilament-dependent manner. The Journal of neuroscience : the official journal of the Society for Neuroscience 16:5583-5592.

Kennedy MJ, Ehlers MD (2011) Mechanisms and function of dendritic exocytosis. Neuron 69:856-875.

Kennedy MJ, Davison IG, Robinson CG, Ehlers MD (2010) Syntaxin-4 defines a domain for activity-dependent exocytosis in dendritic spines. Cell 141:524-535.

Kern JV, Zhang YV, Kramer S, Brenman JE, Rasse TM (2013) The kinesin-3, unc-104 regulates dendrite morphogenesis and synaptic development in Drosophila. Genetics 195:59-72.

Khachaturian ZS (1987) Hypothesis on the regulation of cytosol calcium concentration and the aging brain. Neurobiology of aging 8:345-346.

Khachaturian ZS (1989) The role of calcium regulation in brain aging: reexamination of a hypothesis. Aging 1:17-34.

Khodjakov A, Lizunova EM, Minin AA, Koonce MP, Gyoeva FK (1998) A specific light chain of kinesin associates with mitochondria in cultured cells. Molecular biology of the cell 9:333-343.

Kim DH, Yeo SH, Park JM, Choi JY, Lee TH, Park SY, Ock MS, Eo J, Kim HS, Cha HJ (2014) Genetic markers for diagnosis and pathogenesis of Alzheimer's disease. Gene 545:185-193.

Kim J, Choi IY, Michaelis ML, Lee P (2011) Quantitative in vivo measurement of early axonal transport deficits in a triple transgenic mouse model of Alzheimer's disease using manganese-enhanced MRI. Neuroimage 56:1286-1292.

King ME, Kan HM, Baas PW, Erisir A, Glabe CG, Bloom GS (2006) Tau-dependent microtubule disassembly initiated by prefibrillar beta-amyloid. The Journal of cell biology 175:541-546.

Klebe S et al. (2012) KIF1A missense mutations in SPG30, an autosomal recessive spastic paraplegia: distinct phenotypes according to the nature of the mutations. Eur J Hum Genet 20:645-649.

Klee CB, Crouch TH, Krinks MH (1979) Calcineurin: a calcium- and calmodulin-binding protein of the nervous system. Proceedings of the National Academy of Sciences of the United States of America 76:6270-6273.

Klopfenstein DR, Vale RD (2004) The lipid binding pleckstrin homology domain in UNC-104 kinesin is necessary for synaptic vesicle transport in Caenorhabditis elegans. Molecular biology of the cell 15:3729-3739.

Klopfenstein DR, Holleran EA, Vale RD (2002) Kinesin motors and microtubule-based organelle transport in Dictyostelium discoideum. Journal of muscle research and cell motility 23:631-638.

Kokubo H, Kayed R, Glabe CG, Yamaguchi H (2005a) Soluble Abeta oligomers ultrastructurally localize to cell processes and might be related to synaptic dysfunction in Alzheimer's disease brain. Brain research 1031:222-228.

Kokubo H, Saido TC, Iwata N, Helms JB, Shinohara R, Yamaguchi H (2005b) Part of membrane-bound Abeta exists in rafts within senile plaques in Tg2576 mouse brain. Neurobiology of aging 26:409-418.

Kondo M, Takei Y, Hirokawa N (2012) Motor protein KIF1A is essential for hippocampal synaptogenesis and learning enhancement in an enriched environment. Neuron 73:743-757.

Kourtis N, Tavernarakis N (2011) Cellular stress response pathways and ageing: intricate molecular relationships. The EMBO journal 30:2520-2531.

Krafft GA, Klein WL (2010) ADDLs and the signaling web that leads to Alzheimer's disease. Neuropharmacology 59:230-242.

Kuchibhotla KV, Goldman ST, Lattarulo CR, Wu HY, Hyman BT, Bacskai BJ (2008) Abeta plaques lead to aberrant regulation of calcium homeostasis in vivo resulting in structural and functional disruption of neuronal networks. Neuron 59:214-225.

Kuczewski N, Porcher C, Lessmann V, Medina I, Gaiarsa JL (2009) Activity-dependent dendritic release of BDNF and biological consequences. Mol Neurobiol 39:37-49.

Kudo T, Okumura M, Imaizumi K, Araki W, Morihara T, Tanimukai H, Kamagata E, Tabuchi N, Kimura R, Kanayama D, Fukumori A, Tagami S, Okochi M, Kubo M, Tanii H, Tohyama M, Tabira T, Takeda M (2006) Altered localization of amyloid precursor protein under endoplasmic reticulum stress. Biochemical and biophysical research communications 344:525-530.

Kuliawat R, Arvan P (1994) Distinct molecular mechanisms for protein sorting within immature secretory granules of pancreatic beta-cells. The Journal of cell biology 126:77-86.

Kuno T, Mukai H, Ito A, Chang CD, Kishima K, Saito N, Tanaka C (1992) Distinct cellular expression of calcineurin A alpha and A beta in rat brain. Journal of neurochemistry 58:1643-1651.

Kwinter D, Silverman MA (2009) Live imaging of dense-core vesicles in primary cultured hippocampal neurons. J Vis Exp.

Kwinter DM, Lo K, Mafi P, Silverman MA (2009) Dynactin regulates bidirectional transport of dense-core vesicles in the axon and dendrites of cultured hippocampal neurons. Neuroscience 162:1001-1010.

Lacor PN, Buniel MC, Furlow PW, Clemente AS, Velasco PT, Wood M, Viola KL, Klein WL (2007) Abeta oligomer-induced aberrations in synapse composition, shape, and density provide a molecular basis for loss of connectivity in Alzheimer's disease. The Journal of neuroscience : the official journal of the Society for Neuroscience 27:796-807.

LaFerla FM, Green KN, Oddo S (2007) Intracellular amyloid-beta in Alzheimer's disease. Nature reviews Neuroscience 8:499-509.

Lambert MP, Velasco PT, Chang L, Viola KL, Fernandez S, Lacor PN, Khuon D, Gong Y, Bigio EH, Shaw P, De Felice FG, Krafft GA, Klein WL (2007) Monoclonal antibodies that target pathological assemblies of Abeta. Journal of neurochemistry 100:23-35.

Lambert MP, Barlow AK, Chromy BA, Edwards C, Freed R, Liosatos M, Morgan TE, Rozovsky I, Trommer B, Viola KL, Wals P, Zhang C, Finch CE, Krafft GA, Klein WL (1998) Diffusible, nonfibrillar ligands derived from Abeta1-42 are potent central nervous system neurotoxins. Proceedings of the National Academy of Sciences of the United States of America 95:6448-6453.

LaPointe NE, Morfini G, Pigino G, Gaisina IN, Kozikowski AP, Binder LI, Brady ST (2009) The amino terminus of tau inhibits kinesin-dependent axonal transport: implications for filament toxicity. Journal of neuroscience research 87:440-451.

Lawrence CJ et al. (2004) A standardized kinesin nomenclature. The Journal of cell biology 167:19-22.

Lazarov O, Morfini GA, Pigino G, Gadadhar A, Chen X, Robinson J, Ho H, Brady ST, Sisodia SS (2007) Impairments in fast axonal transport and motor neuron deficits in transgenic mice expressing familial Alzheimer's disease-linked mutant presenilin 1. The Journal of neuroscience : the official journal of the Society for Neuroscience 27:7011-7020.

Lazarov O, Morfini GA, Lee EB, Farah MH, Szodorai A, DeBoer SR, Koliatsos VE, Kins S, Lee VM, Wong PC, Price DL, Brady ST, Sisodia SS (2005) Axonal transport, amyloid precursor protein, kinesin-1, and the processing apparatus: revisited. The Journal of neuroscience : the official journal of the Society for Neuroscience 25:2386-2395.

Lee JR, Shin H, Ko J, Choi J, Lee H, Kim E (2003) Characterization of the movement of the kinesin motor KIF1A in living cultured neurons. The Journal of biological chemistry 278:2624-2629.

Lee S, Sunil N, Shea TB (2011) C-terminal neurofilament phosphorylation fosters neurofilament-neurofilament associations that compete with axonal transport. Cytoskeleton (Hoboken) 68:8-17.

Lee YI, Seo M, Kim Y, Kim SY, Kang UG, Kim YS, Juhnn YS (2005) Membrane depolarization induces the undulating phosphorylation/dephosphorylation of glycogen synthase kinase 3beta, and this dephosphorylation involves protein phosphatases 2A and 2B in SH-SY5Y human neuroblastoma cells. J Biol Chem 280:22044-22052.

Leitch B, Szostek A, Lin R, Shevtsova O (2009) Subcellular distribution of L-type calcium channel subtypes in rat hippocampal neurons. Neuroscience 164:641-657.

Li S, Yang L, Selzer ME, Hu Y (2013) Neuronal endoplasmic reticulum stress in axon injury and neurodegeneration. Annals of neurology 74:768-777.

Li S, Hong S, Shepardson NE, Walsh DM, Shankar GM, Selkoe D (2009) Soluble oligomers of amyloid Beta protein facilitate hippocampal long-term depression by disrupting neuronal glutamate uptake. Neuron 62:788-801.

Lieberman DN, Mody I (1994) Regulation of NMDA channel function by endogenous Ca(2+)-dependent phosphatase. Nature 369:235-239.

Lin H, Bhatia R, Lal R (2001) Amyloid beta protein forms ion channels: implications for Alzheimer's disease pathophysiology. FASEB journal : official publication of the Federation of American Societies for Experimental Biology 15:2433-2444.

Lipka J, Kuijpers M, Jaworski J, Hoogenraad CC (2013) Mutations in cytoplasmic dynein and its regulators cause malformations of cortical development and neurodegenerative diseases. Biochemical Society transactions 41:1605-1612.

Liu F, Grundke-Iqbal I, Iqbal K, Oda Y, Tomizawa K, Gong CX (2005) Truncation and activation of calcineurin A by calpain I in Alzheimer disease brain. J Biol Chem 280:37755-37762.

Liu J, Farmer JD, Jr., Lane WS, Friedman J, Weissman I, Schreiber SL (1991) Calcineurin is a common target of cyclophilin-cyclosporin A and FKBP-FK506 complexes. Cell 66:807-815.

Lo KY, Kuzmin A, Unger SM, Petersen JD, Silverman MA (2011) KIF1A is the primary anterograde motor protein required for the axonal transport of dense-core vesicles in cultured hippocampal neurons. Neuroscience letters.

Lopez JR, Lyckman A, Oddo S, Laferla FM, Querfurth HW, Shtifman A (2008) Increased intraneuronal resting [Ca2+] in adult Alzheimer's disease mice. Journal of neurochemistry 105:262-271.

Lu B, Nagappan G, Guan X, Nathan PJ, Wren P (2013) BDNF-based synaptic repair as a disease-modifying strategy for neurodegenerative diseases. Nature reviews Neuroscience 14:401-416.

Luo C, Shaw KT, Raghavan A, Aramburu J, Garcia-Cozar F, Perrino BA, Hogan PG, Rao A (1996) Interaction of calcineurin with a domain of the transcription factor NFAT1 that controls nuclear import. Proceedings of the National Academy of Sciences of the United States of America 93:8907-8912.

MacLennan DH, Duff C, Zorzato F, Fujii J, Phillips M, Korneluk RG, Frodis W, Britt BA, Worton RG (1990) Ryanodine receptor gene is a candidate for predisposition to malignant hyperthermia. Nature 343:559-561.

MacManus A, Ramsden M, Murray M, Henderson Z, Pearson HA, Campbell VA (2000) Enhancement of (45)Ca(2+) influx and voltage-dependent Ca(2+) channel activity by beta-amyloid-(1-40) in rat cortical synaptosomes and cultured cortical neurons. Modulation by the proinflammatory cytokine interleukin-1beta. The Journal of biological chemistry 275:4713-4718.

Maeder CI, San-Miguel A, Wu EY, Lu H, Shen K (2014) In vivo neuron-wide analysis of synaptic vesicle precursor trafficking. Traffic 15:273-291.

Mandelkow EM, Stamer K, Vogel R, Thies E, Mandelkow E (2003) Clogging of axons by tau, inhibition of axonal traffic and starvation of synapses. Neurobiology of aging 24:1079-1085.

Mandelkow EM, Schweers O, Drewes G, Biernat J, Gustke N, Trinczek B, Mandelkow E (1996) Structure, microtubule interactions, and phosphorylation of tau protein. Annals of the New York Academy of Sciences 777:96-106.

Mandell JW, Banker GA (1996) A spatial gradient of tau protein phosphorylation in nascent axons. The Journal of neuroscience : the official journal of the Society for Neuroscience 16:5727-5740.

Mansuy IM (2003) Calcineurin in memory and bidirectional plasticity. Biochemical and biophysical research communications 311:1195-1208.

Marr RA, Spencer BJ (2010) NEP-like endopeptidases and Alzheimer's disease [corrected]. Current Alzheimer research 7:223-229.

Marr RA, Rockenstein E, Mukherjee A, Kindy MS, Hersh LB, Gage FH, Verma IM, Masliah E (2003) Neprilysin gene transfer reduces human amyloid pathology in

transgenic mice. The Journal of neuroscience : the official journal of the Society for Neuroscience 23:1992-1996.

Mawuenyega KG, Sigurdson W, Ovod V, Munsell L, Kasten T, Morris JC, Yarasheski KE, Bateman RJ (2010) Decreased clearance of CNS beta-amyloid in Alzheimer's disease. Science 330:1774.

McCart AE, Mahony D, Rothnagel JA (2003) Alternatively spliced products of the human kinesin light chain 1 (KNS2) gene. Traffic 4:576-580.

McKenney RJ, Huynh W, Tanenbaum ME, Bhabha G, Vale RD (2014) Activation of cytoplasmic dynein motility by dynactin-cargo adapter complexes. Science 345:337-341.

McNally FJ (2013) Mechanisms of spindle positioning. The Journal of cell biology 200:131-140.

Medina M, Avila J (2014) New insights into the role of glycogen synthase kinase-3 in Alzheimer's disease. Expert Opin Ther Targets 18:69-77.

Mezler M, Barghorn S, Schoemaker H, Gross G, Nimmrich V (2012) A beta-amyloid oligomer directly modulates P/Q-type calcium currents in Xenopus oocytes. British journal of pharmacology 165:1572-1583.

Miki H, Okada Y, Hirokawa N (2005) Analysis of the kinesin superfamily: insights into structure and function. Trends in cell biology 15:467-476.

Miki H, Setou M, Kaneshiro K, Hirokawa N (2001) All kinesin superfamily protein, KIF, genes in mouse and human. Proceedings of the National Academy of Sciences of the United States of America 98:7004-7011.

Millecamps S, Julien JP (2013) Axonal transport deficits and neurodegenerative diseases. Nature reviews Neuroscience 14:161-176.

Minoshima S, Cross D (2008) In vivo imaging of axonal transport using MRI: aging and Alzheimer's disease. Eur J Nucl Med Mol Imaging 35 Suppl 1:S89-92.

Miranda CJ, Braun L, Jiang Y, Hester ME, Zhang L, Riolo M, Wang H, Rao M, Altura RA, Kaspar BK (2012) Aging brain microenvironment decreases hippocampal neurogenesis through Wnt-mediated survivin signaling. Aging Cell 11:542-552.

Morel E, Chamoun Z, Lasiecka ZM, Chan RB, Williamson RL, Vetanovetz C, Dall'Armi C, Simoes S, Point Du Jour KS, McCabe BD, Small SA, Di Paolo G (2013) Phosphatidylinositol-3-phosphate regulates sorting and processing of amyloid precursor protein through the endosomal system. Nature communications 4:2250.

Morel M, Heraud C, Nicaise C, Suain V, Brion JP (2012) Levels of kinesin light chain and dynein intermediate chain are reduced in the frontal cortex in Alzheimer's disease: implications for axoplasmic transport. Acta neuropathologica 123:71-84.

Morfini G, Szebenyi G, Elluru R, Ratner N, Brady ST (2002) Glycogen synthase kinase 3 phosphorylates kinesin light chains and negatively regulates kinesin-based motility. The EMBO journal 21:281-293.

Morfini G, Szebenyi G, Brown H, Pant HC, Pigino G, DeBoer S, Beffert U, Brady ST (2004) A novel CDK5-dependent pathway for regulating GSK3 activity and kinesin-driven motility in neurons. The EMBO journal 23:2235-2245.

Morfini GA, Burns M, Binder LI, Kanaan NM, LaPointe N, Bosco DA, Brown RH, Jr., Brown H, Tiwari A, Hayward L, Edgar J, Nave KA, Garberrn J, Atagi Y, Song Y, Pigino G, Brady ST (2009) Axonal transport defects in neurodegenerative diseases. The Journal of neuroscience : the official journal of the Society for Neuroscience 29:12776-12786.

Morihara T et al. (2014) Transcriptome analysis of distinct mouse strains reveals kinesin light chain-1 splicing as an amyloid-beta accumulation modifier. Proceedings of the National Academy of Sciences of the United States of America.

Morris M, Maeda S, Vossel K, Mucke L (2011) The many faces of tau. Neuron 70:410-426.

Moughamian AJ, Holzbaur EL (2012) Synaptic vesicle distribution by conveyor belt. Cell 148:849-851.

Mulkey RM, Endo S, Shenolikar S, Malenka RC (1994) Involvement of a calcineurin/inhibitor-1 phosphatase cascade in hippocampal long-term depression. Nature 369:486-488.

Muresan V, Muresan Z (2009) Is abnormal axonal transport a cause, a contributing factor or a consequence of the neuronal pathology in Alzheimer's disease? Future Neurol 4:761-773.

Nelson O, Tu H, Lei T, Bentahir M, de Strooper B, Bezprozvanny I (2007) Familial Alzheimer disease-linked mutations specifically disrupt Ca2+ leak function of presenilin 1. The Journal of clinical investigation 117:1230-1239.

Niclas J, Navone F, Hom-Booher N, Vale RD (1994) Cloning and localization of a conventional kinesin motor expressed exclusively in neurons. Neuron 12:1059-1072.

Nishitsuji K, Tomiyama T, Ishibashi K, Ito K, Teraoka R, Lambert MP, Klein WL, Mori H (2009) The E693Delta mutation in amyloid precursor protein increases intracellular accumulation of amyloid beta oligomers and causes endoplasmic

reticulum stress-induced apoptosis in cultured cells. The American journal of pathology 174:957-969.

Nixon RA (2007) Autophagy, amyloidogenesis and Alzheimer disease. Journal of cell science 120:4081-4091.

Nixon RA, Wegiel J, Kumar A, Yu WH, Peterhoff C, Cataldo A, Cuervo AM (2005) Extensive involvement of autophagy in Alzheimer disease: an immuno-electron microscopy study. Journal of neuropathology and experimental neurology 64:113-122.

Okada Y, Yamazaki H, Sekine-Aizawa Y, Hirokawa N (1995) The neuron-specific kinesin superfamily protein KIF1A is a unique monomeric motor for anterograde axonal transport of synaptic vesicle precursors. Cell 81:769-780.

Orefice LL, Waterhouse EG, Partridge JG, Lalchandani RR, Vicini S, Xu B (2013) Distinct roles for somatically and dendritically synthesized brain-derived neurotrophic factor in morphogenesis of dendritic spines. The Journal of neuroscience : the official journal of the Society for Neuroscience 33:11618-11632.

Otsuka AJ, Jeyaprakash A, Garcia-Anoveros J, Tang LZ, Fisk G, Hartshorne T, Franco R, Born T (1991) The C. elegans unc-104 gene encodes a putative kinesin heavy chain-like protein. Neuron 6:113-122.

Oules B, Del Prete D, Greco B, Zhang X, Lauritzen I, Sevalle J, Moreno S, Paterlini-Brechot P, Trebak M, Checler F, Benfenati F, Chami M (2012) Ryanodine receptor blockade reduces amyloid-beta load and memory impairments in Tg2576 mouse model of Alzheimer disease. The Journal of neuroscience : the official journal of the Society for Neuroscience 32:11820-11834.

Pacheco-Quinto J, Herdt A, Eckman CB, Eckman EA (2013) Endothelin-converting enzymes and related metalloproteases in Alzheimer's disease. Journal of Alzheimer's disease : JAD 33 Suppl 1:S101-110.

Pagani L, Eckert A (2011) Amyloid-Beta interaction with mitochondria. Int J Alzheimers Dis 2011:925050.

Palmer AE, Tsien RY (2006) Measuring calcium signaling using genetically targetable fluorescent indicators. Nature protocols 1:1057-1065.

Park JJ, Cawley NX, Loh YP (2008) A bi-directional carboxypeptidase E-driven transport mechanism controls BDNF vesicle homeostasis in hippocampal neurons. Molecular and cellular neurosciences 39:63-73.

Park M, Salgado JM, Ostroff L, Helton TD, Robinson CG, Harris KM, Ehlers MD (2006) Plasticity-induced growth of dendritic spines by exocytic trafficking from recycling endosomes. Neuron 52:817-830.

Park SY, Ferreira A (2005) The generation of a 17 kDa neurotoxic fragment: an alternative mechanism by which tau mediates beta-amyloid-induced neurodegeneration. J Neurosci 25:5365-5375.

Paula-Lima AC, Adasme T, SanMartin C, Sebollela A, Hetz C, Carrasco MA, Ferreira ST, Hidalgo C (2011) Amyloid beta-peptide oligomers stimulate RyR-mediated Ca2+ release inducing mitochondrial fragmentation in hippocampal neurons and prevent RyR-mediated dendritic spine remodeling produced by BDNF. Antioxid Redox Signal 14:1209-1223.

Peineau S, Bradley C, Taghibiglou C, Doherty A, Bortolotto ZA, Wang YT, Collingridge GL (2008) The role of GSK-3 in synaptic plasticity. British journal of pharmacology 153 Suppl 1:S428-437.

Peineau S, Taghibiglou C, Bradley C, Wong TP, Liu L, Lu J, Lo E, Wu D, Saule E, Bouschet T, Matthews P, Isaac JT, Bortolotto ZA, Wang YT, Collingridge GL (2007) LTP inhibits LTD in the hippocampus via regulation of GSK3beta. Neuron 53:703-717.

Perez DI, Gil C, Martinez A (2011) Protein kinases CK1 and CK2 as new targets for neurodegenerative diseases. Med Res Rev 31:924-954.

Pernigo S, Lamprecht A, Steiner RA, Dodding MP (2013) Structural basis for kinesin-1:cargo recognition. Science 340:356-359.

Petersen JD, Kaech S, Banker G (2014) Selective microtubule-based transport of dendritic membrane proteins arises in concert with axon specification. The Journal of neuroscience : the official journal of the Society for Neuroscience 34:4135-4147.

Pierrot N, Santos SF, Feyt C, Morel M, Brion JP, Octave JN (2006) Calcium-mediated transient phosphorylation of tau and amyloid precursor protein followed by intraneuronal amyloid-beta accumulation. The Journal of biological chemistry 281:39907-39914.

Pigino G, Morfini G, Pelsman A, Mattson MP, Brady ST, Busciglio J (2003) Alzheimer's presenilin 1 mutations impair kinesin-based axonal transport. The Journal of neuroscience : the official journal of the Society for Neuroscience 23:4499-4508.

Pigino G, Morfini G, Atagi Y, Deshpande A, Yu C, Jungbauer L, LaDu M, Busciglio J, Brady S (2009) Disruption of fast axonal transport is a pathogenic mechanism for intraneuronal amyloid beta. Proceedings of the National Academy of Sciences of the United States of America 106:5907-5912.

Pineda JR, Pardo R, Zala D, Yu H, Humbert S, Saudou F (2009) Genetic and pharmacological inhibition of calcineurin corrects the BDNF transport defect in Huntington's disease. Molecular brain 2:33.

Popugaeva E, Bezprozvanny I (2013) Role of endoplasmic reticulum Ca2+ signaling in the pathogenesis of Alzheimer disease. Frontiers in molecular neuroscience 6:29.

Price SA, Held B, Pearson HA (1998) Amyloid beta protein increases Ca2+ currents in rat cerebellar granule neurones. Neuroreport 9:539-545.

Puthanveettil SV, Monje FJ, Miniaci MC, Choi YB, Karl KA, Khandros E, Gawinowicz MA, Sheetz MP, Kandel ER (2008) A new component in synaptic plasticity: upregulation of kinesin in the neurons of the gill-withdrawal reflex. Cell 135:960-973.

Puzzo D, Privitera L, Leznik E, Fa M, Staniszewski A, Palmeri A, Arancio O (2008) Picomolar amyloid-beta positively modulates synaptic plasticity and memory in hippocampus. The Journal of neuroscience : the official journal of the Society for Neuroscience 28:14537-14545.

Puzzo D, Privitera L, Fa M, Staniszewski A, Hashimoto G, Aziz F, Sakurai M, Ribe EM, Troy CM, Mercken M, Jung SS, Palmeri A, Arancio O (2011) Endogenous amyloid-beta is necessary for hippocampal synaptic plasticity and memory. Annals of neurology 69:819-830.

Querfurth HW, Selkoe DJ (1994) Calcium ionophore increases amyloid beta peptide production by cultured cells. Biochemistry 33:4550-4561.

Querfurth HW, LaFerla FM (2010) Alzheimer's disease. N Engl J Med 362:329-344.

Quist A, Doudevski I, Lin H, Azimova R, Ng D, Frangione B, Kagan B, Ghiso J, Lal R (2005) Amyloid ion channels: a common structural link for protein-misfolding disease. Proceedings of the National Academy of Sciences of the United States of America 102:10427-10432.

Ramsden M, Henderson Z, Pearson HA (2002) Modulation of Ca2+ channel currents in primary cultures of rat cortical neurones by amyloid beta protein (1-40) is dependent on solubility status. Brain research 956:254-261.

Ramser EM, Gan KJ, Decker H, Fan EY, Suzuki MM, Ferreira ST, Silverman MA (2013) Amyloid-beta oligomers induce tau-independent disruption of BDNF axonal transport via calcineurin activation in cultured hippocampal neurons. Molecular biology of the cell 24:2494-2505.

Rapoport M, Dawson HN, Binder LI, Vitek MP, Ferreira A (2002) Tau is essential to beta -amyloid-induced neurotoxicity. Proceedings of the National Academy of Sciences of the United States of America 99:6364-6369.

Reddy PH (2014) Misfolded proteins, mitochondrial dysfunction, and neurodegenerative diseases. Biochimica et biophysica acta 1842:1167.

Reese LC, Taglialatela G (2011) A role for calcineurin in Alzheimer's disease. Current neuropharmacology 9:685-692.

Reifert J, Hartung-Cranston D, Feinstein SC (2011) Amyloid beta-mediated cell death of cultured hippocampal neurons reveals extensive Tau fragmentation without increased full-length tau phosphorylation. The Journal of biological chemistry 286:20797-20811.

Reilly CE (2001) Neprilysin content is reduced in Alzheimer brain areas. Journal of neurology 248:159-160.

Renner M, Lacor PN, Velasco PT, Xu J, Contractor A, Klein WL, Triller A (2010) Deleterious effects of amyloid beta oligomers acting as an extracellular scaffold for mGluR5. Neuron 66:739-754.

Riederer BM, Leuba G, Vernay A, Riederer IM (2011) The role of the ubiquitin proteasome system in Alzheimer's disease. Experimental biology and medicine 236:268-276.

Riviere JB et al. (2011) KIF1A, an axonal transporter of synaptic vesicles, is mutated in hereditary sensory and autonomic neuropathy type 2. Am J Hum Genet 89:219-230.

Roberson ED, Halabisky B, Yoo JW, Yao J, Chin J, Yan F, Wu T, Hamto P, Devidze N, Yu GQ, Palop JJ, Noebels JL, Mucke L (2011) Amyloid-beta/Fyn-induced synaptic, network, and cognitive impairments depend on tau levels in multiple mouse models of Alzheimer's disease. The Journal of neuroscience : the official journal of the Society for Neuroscience 31:700-711.

Rodrigues EM, Weissmiller AM, Goldstein LS (2012) Enhanced beta-secretase processing alters APP axonal transport and leads to axonal defects. Human molecular genetics 21:4587-4601.

Rothman SM, Mattson MP (2012) Activity-dependent, stress-responsive BDNF signaling and the quest for optimal brain health and resilience throughout the lifespan. Neuroscience 239:228-240.

Roussel BD, Kruppa AJ, Miranda E, Crowther DC, Lomas DA, Marciniak SJ (2012) Endoplasmic reticulum dysfunction in neurological disease. Lancet Neurol 12:105-118.

Rovelet-Lecrux A, Hannequin D, Raux G, Le Meur N, Laquerriere A, Vital A, Dumanchin C, Feuillette S, Brice A, Vercelletto M, Dubas F, Frebourg T, Campion D (2006) APP locus duplication causes autosomal dominant early-onset Alzheimer disease with cerebral amyloid angiopathy. Nature genetics 38:24-26.

Roy AK, Oh T, Rivera O, Mubiru J, Song CS, Chatterjee B (2002) Impacts of transcriptional regulation on aging and senescence. Ageing research reviews 1:367-380.

Rui Y, Tiwari P, Xie Z, Zheng JQ (2006) Acute impairment of mitochondrial trafficking by beta-amyloid peptides in hippocampal neurons. J Neurosci 26:10480-10487.

Rusnak F, Mertz P (2000) Calcineurin: form and function. Physiological reviews 80:1483-1521.

Saido T, Leissring MA (2012) Proteolytic degradation of amyloid beta-protein. Cold Spring Harbor perspectives in medicine 2:a006379.

Scharfman HE, Chao MV (2013) The entorhinal cortex and neurotrophin signaling in Alzheimer's disease and other disorders. Cogn Neurosci 4:123-135.

Schlager MA, Hoogenraad CC (2009) Basic mechanisms for recognition and transport of synaptic cargos. Molecular brain 2:25.

Schlager MA, Serra-Marques A, Grigoriev I, Gumy LF, Esteves da Silva M, Wulf PS, Akhmanova A, Hoogenraad CC (2014) Bicaudal D Family Adaptor Proteins Control the Velocity of Dynein-Based Movements. Cell reports.

Schreiber SL, Crabtree GR (1992) The mechanism of action of cyclosporin A and FK506. Immunology today 13:136-142.

Schroer TA (2004) Dynactin. Annu Rev Cell Dev Biol 20:759-779.

Schwaller B (2009) The continuing disappearance of "pure" Ca2+ buffers. Cellular and molecular life sciences : CMLS 66:275-300.

Schwenk BM, Lang CM, Hogl S, Tahirovic S, Orozco D, Rentzsch K, Lichtenthaler SF, Hoogenraad CC, Capell A, Haass C, Edbauer D (2014) The FTLD risk factor TMEM106B and MAP6 control dendritic trafficking of lysosomes. The EMBO journal 33:450-467.

Seitz A, Kojima H, Oiwa K, Mandelkow EM, Song YH, Mandelkow E (2002) Single-molecule investigation of the interference between kinesin, tau and MAP2c. The EMBO journal 21:4896-4905.

Selkoe DJ (2001) Clearing the brain's amyloid cobwebs. Neuron 32:177-180.

Shankar GM, Bloodgood BL, Townsend M, Walsh DM, Selkoe DJ, Sabatini BL (2007) Natural oligomers of the Alzheimer amyloid-beta protein induce reversible synapse loss by modulating an NMDA-type glutamate receptor-dependent signaling pathway. The Journal of neuroscience : the official journal of the Society for Neuroscience 27:2866-2875.

Shankar GM, Li S, Mehta TH, Garcia-Munoz A, Shepardson NE, Smith I, Brett FM, Farrell MA, Rowan MJ, Lemere CA, Regan CM, Walsh DM, Sabatini BL, Selkoe DJ (2008) Amyloid-beta protein dimers isolated directly from Alzheimer's brains impair synaptic plasticity and memory. Nature medicine 14:837-842.

Shaw JL, Chang KT (2013) Nebula/DSCR1 upregulation delays neurodegeneration and protects against APP-induced axonal transport defects by restoring calcineurin and GSK-3beta signaling. PLoS Genet 9:e1003792.

Shen X, Li H, Ou Y, Tao W, Dong A, Kong J, Ji C, Yu S (2008) The secondary structure of calcineurin regulatory region and conformational change induced by calcium/calmodulin binding. The Journal of biological chemistry 283:11407-11413.

Shenolikar S, Nairn AC (1991) Protein phosphatases: recent progress. Advances in second messenger and phosphoprotein research 23:1-121.

Shin H, Wyszynski M, Huh KH, Valtschanoff JG, Lee JR, Ko J, Streuli M, Weinberg RJ, Sheng M, Kim E (2003) Association of the kinesin motor KIF1A with the multimodular protein liprin-alpha. The Journal of biological chemistry 278:11393-11401.

Shipton OA, Leitz JR, Dworzak J, Acton CE, Tunbridge EM, Denk F, Dawson HN, Vitek MP, Wade-Martins R, Paulsen O, Vargas-Caballero M (2011) Tau protein is required for amyloid {beta}-induced impairment of hippocampal long-term potentiation. The Journal of neuroscience : the official journal of the Society for Neuroscience 31:1688-1692.

Silverman MA, Kaech S, Jareb M, Burack MA, Vogt L, Sonderegger P, Banker G (2001) Sorting and directed transport of membrane proteins during development of hippocampal neurons in culture. Proceedings of the National Academy of Sciences of the United States of America 98:7051-7057.

Smith KD, Paylor R, Pautler RG (2011) R-flurbiprofen improves axonal transport in the Tg2576 mouse model of Alzheimer's disease as determined by MEMRI. Magn Reson Med 65:1423-1429.

Snyder EM, Nong Y, Almeida CG, Paul S, Moran T, Choi EY, Nairn AC, Salter MW, Lombroso PJ, Gouras GK, Greengard P (2005) Regulation of NMDA receptor trafficking by amyloid-beta. Nature neuroscience 8:1051-1058.

Soderberg O, Gullberg M, Jarvius M, Ridderstrale K, Leuchowius KJ, Jarvius J, Wester K, Hydbring P, Bahram F, Larsson LG, Landegren U (2006) Direct observation of individual endogenous protein complexes in situ by proximity ligation. Nature methods 3:995-1000.

Sohal RS, Mockett RJ, Orr WC (2002) Mechanisms of aging: an appraisal of the oxidative stress hypothesis. Free radical biology & medicine 33:575-586.

Sola C, Tusell JM, Serratosa J (1999) Comparative study of the distribution of calmodulin kinase II and calcineurin in the mouse brain. Journal of neuroscience research 57:651-662.

Soldner F, Hockemeyer D, Beard C, Gao Q, Bell GW, Cook EG, Hargus G, Blak A, Cooper O, Mitalipova M, Isacson O, Jaenisch R (2009) Parkinson's disease patient-derived induced pluripotent stem cells free of viral reprogramming factors. Cell 136:964-977.

Soppina V, Norris SR, Dizaji AS, Kortus M, Veatch S, Peckham M, Verhey KJ (2014) Dimerization of mammalian kinesin-3 motors results in superprocessive motion. Proceedings of the National Academy of Sciences of the United States of America 111:5562-5567.

Stambolic V, Woodgett JR (1994) Mitogen inactivation of glycogen synthase kinase-3 beta in intact cells via serine 9 phosphorylation. Biochem J 303 (Pt 3):701-704.

Stefan MI, Edelstein SJ, Le Novere N (2008) An allosteric model of calmodulin explains differential activation of PP2B and CaMKII. Proceedings of the National Academy of Sciences of the United States of America 105:10768-10773.

Stenoien DL, Brady ST (1997) Immunochemical analysis of kinesin light chain function. Molecular biology of the cell 8:675-689.

Stokin GB, Goldstein LS (2006) Axonal transport and Alzheimer's disease. Annu Rev Biochem 75:607-627.

Stokin GB, Lillo C, Falzone TL, Brusch RG, Rockenstein E, Mount SL, Raman R, Davies P, Masliah E, Williams DS, Goldstein LS (2005) Axonopathy and transport deficits early in the pathogenesis of Alzheimer's disease. Science 307:1282-1288.

Stokin GB, Almenar-Queralt A, Gunawardena S, Rodrigues EM, Falzone T, Kim J, Lillo C, Mount SL, Roberts EA, McGowan E, Williams DS, Goldstein LS (2008) Amyloid precursor protein-induced axonopathies are independent of amyloid-beta peptides. Human molecular genetics 17:3474-3486.

Stutzmann GE (2007) The pathogenesis of Alzheimers disease is it a lifelong "calciumopathy"? Neuroscientist 13:546-559.

Stutzmann GE, Caccamo A, LaFerla FM, Parker I (2004) Dysregulated IP3 signaling in cortical neurons of knock-in mice expressing an Alzheimer's-linked mutation in presenilin1 results in exaggerated Ca2+ signals and altered membrane excitability. The Journal of neuroscience : the official journal of the Society for Neuroscience 24:508-513.

Stutzmann GE, Smith I, Caccamo A, Oddo S, Laferla FM, Parker I (2006) Enhanced ryanodine receptor recruitment contributes to Ca2+ disruptions in young, adult, and aged Alzheimer's disease mice. The Journal of neuroscience : the official journal of the Society for Neuroscience 26:5180-5189.

Stutzmann GE, Smith I, Caccamo A, Oddo S, Parker I, Laferla F (2007) Enhanced ryanodine-mediated calcium release in mutant PS1-expressing Alzheimer's mouse models. Annals of the New York Academy of Sciences 1097:265-277.

Supnet C, Bezprozvanny I (2010) The dysregulation of intracellular calcium in Alzheimer disease. Cell Calcium 47:183-189.

Szatmari E, Habas A, Yang P, Zheng JJ, Hagg T, Hetman M (2005) A positive feedback loop between glycogen synthase kinase 3beta and protein phosphatase 1 after stimulation of NR2B NMDA receptors in forebrain neurons. J Biol Chem 280:37526-37535.

Takahashi K, Tanabe K, Ohnuki M, Narita M, Ichisaka T, Tomoda K, Yamanaka S (2007) Induction of pluripotent stem cells from adult human fibroblasts by defined factors. Cell 131:861-872.

Tang Y, Scott DA, Das U, Edland SD, Radomski K, Koo EH, Roy S (2012) Early and selective impairments in axonal transport kinetics of synaptic cargoes induced by soluble amyloid beta-protein oligomers. Traffic 13:681-693.

Tanzi RE, Moir RD, Wagner SL (2004) Clearance of Alzheimer's Abeta peptide: the many roads to perdition. Neuron 43:605-608.

Terry RD (1998) The cytoskeleton in Alzheimer disease. J Neural Transm Suppl 53:141-145.

Tomishige M, Klopfenstein DR, Vale RD (2002) Conversion of Unc104/KIF1A kinesin into a processive motor after dimerization. Science 297:2263-2267.

Tomiyama T, Matsuyama S, Iso H, Umeda T, Takuma H, Ohnishi K, Ishibashi K, Teraoka R, Sakama N, Yamashita T, Nishitsuji K, Ito K, Shimada H, Lambert MP, Klein WL, Mori H (2010) A mouse model of amyloid beta oligomers: their contribution to synaptic alteration, abnormal tau phosphorylation, glial activation, and neuronal loss in vivo. The Journal of neuroscience : the official journal of the Society for Neuroscience 30:4845-4856.

Troen BR (2003) The biology of aging. The Mount Sinai journal of medicine, New York 70:3-22.

Tu H, Nelson O, Bezprozvanny A, Wang Z, Lee SF, Hao YH, Serneels L, De Strooper B, Yu G, Bezprozvanny I (2006) Presenilins form ER Ca2+ leak channels, a function disrupted by familial Alzheimer's disease-linked mutations. Cell 126:981-993.

Twelvetrees AE, Yuen EY, Arancibia-Carcamo IL, MacAskill AF, Rostaing P, Lumb MJ, Humbert S, Triller A, Saudou F, Yan Z, Kittler JT (2010) Delivery of GABAARs to synapses is mediated by HAP1-KIF5 and disrupted by mutant huntingtin. Neuron 65:53-65.

Tye KM, Deisseroth K (2012) Optogenetic investigation of neural circuits underlying brain disease in animal models. Nature reviews Neuroscience 13:251-266.

Vagnoni A, Rodriguez L, Manser C, De Vos KJ, Miller CC (2011) Phosphorylation of kinesin light chain 1 at serine 460 modulates binding and trafficking of calsyntenin-1. Journal of cell science 124:1032-1042.

Vallee RB, Seale GE, Tsai JW (2009) Emerging roles for myosin II and cytoplasmic dynein in migrating neurons and growth cones. Trends in cell biology 19:347-355.

Verhey KJ, Kaul N, Soppina V (2011) Kinesin assembly and movement in cells. Annual review of biophysics 40:267-288.

Verhey KJ, Meyer D, Deehan R, Blenis J, Schnapp BJ, Rapoport TA, Margolis B (2001) Cargo of kinesin identified as JIP scaffolding proteins and associated signaling molecules. The Journal of cell biology 152:959-970.

Vossel KA, Zhang K, Brodbeck J, Daub AC, Sharma P, Finkbeiner S, Cui B, Mucke L (2010) Tau reduction prevents Abeta-induced defects in axonal transport. Science 330:198.

Waites CL, Leal-Ortiz SA, Okerlund N, Dalke H, Fejtova A, Altrock WD, Gundelfinger ED, Garner CC (2013) Bassoon and Piccolo maintain synapse integrity by regulating protein ubiquitination and degradation. The EMBO journal 32:954-969.

Wang H, Saunders AJ (2014) The role of ubiquitin-proteasome in the metabolism of amyloid precursor protein (APP): implications for novel therapeutic strategies for Alzheimer's disease. Discovery medicine 18:41-50.

Wang HG, Pathan N, Ethell IM, Krajewski S, Yamaguchi Y, Shibasaki F, McKeon F, Bobo T, Franke TF, Reed JC (1999) Ca2+-induced apoptosis through calcineurin dephosphorylation of BAD. Science 284:339-343.

Wang JZ, Liu F (2008) Microtubule-associated protein tau in development, degeneration and protection of neurons. Progress in neurobiology 85:148-175.

Wang X, Schwarz TL (2009) The mechanism of Ca2+ -dependent regulation of kinesin-mediated mitochondrial motility. Cell 136:163-174.

Wang X, Perry G, Smith MA, Zhu X (2010) Amyloid-beta-derived diffusible ligands cause impaired axonal transport of mitochondria in neurons. Neuro-degenerative diseases 7:56-59.

Watanabe T, Hikichi Y, Willuweit A, Shintani Y, Horiguchi T (2012) FBL2 regulates amyloid precursor protein (APP) metabolism by promoting ubiquitination-dependent APP degradation and inhibition of APP endocytosis. The Journal of neuroscience : the official journal of the Society for Neuroscience 32:3352-3365.

Weaver C, Leidel C, Szpankowski L, Farley NM, Shubeita GT, Goldstein LS (2013) Endogenous GSK-3/shaggy regulates bidirectional axonal transport of the amyloid precursor protein. Traffic 14:295-308.

Weingarten MD, Lockwood AH, Hwo SY, Kirschner MW (1975) A protein factor essential for microtubule assembly. Proceedings of the National Academy of Sciences of the United States of America 72:1858-1862.

Welte MA (2004) Bidirectional transport along microtubules. Current biology : CB 14:R525-537.

Welte MA (2009) Bidirectional transport: matchmaking for motors. Curr Biol 20:R410-413.

Wong MY, Shakiryanova D, Levitan ES (2009) Presynaptic ryanodine receptor-CamKII signaling is required for activity-dependent capture of transiting vesicles. Journal of molecular neuroscience : MN 37:146-150.

Wong MY, Zhou C, Shakiryanova D, Lloyd TE, Deitcher DL, Levitan ES (2012) Neuropeptide delivery to synapses by long-range vesicle circulation and sporadic capture. Cell 148:1029-1038.

Wong YL, Rice SE (2010) Kinesin's light chains inhibit the head- and microtubule-binding activity of its tail. Proceedings of the National Academy of Sciences of the United States of America 107:11781-11786.

Wozniak MJ, Allan VJ (2006) Cargo selection by specific kinesin light chain 1 isoforms. The EMBO journal 25:5457-5468.

Wu B, Yamaguchi H, Lai FA, Shen J (2013) Presenilins regulate calcium homeostasis and presynaptic function via ryanodine receptors in hippocampal neurons.

Proceedings of the National Academy of Sciences of the United States of America.

Wu HY, Hudry E, Hashimoto T, Uemura K, Fan ZY, Berezovska O, Grosskreutz CL, Bacskai BJ, Hyman BT (2012) Distinct dendritic spine and nuclear phases of calcineurin activation after exposure to amyloid-beta revealed by a novel fluorescence resonance energy transfer assay. The Journal of neuroscience : the official journal of the Society for Neuroscience 32:5298-5309.

Wu HY, Hudry E, Hashimoto T, Kuchibhotla K, Rozkalne A, Fan Z, Spires-Jones T, Xie H, Arbel-Ornath M, Grosskreutz CL, Bacskai BJ, Hyman BT (2010) Amyloid beta induces the morphological neurodegenerative triad of spine loss, dendritic simplification, and neuritic dystrophies through calcineurin activation. The Journal of neuroscience : the official journal of the Society for Neuroscience 30:2636-2649.

Yadav S, Linstedt AD (2011) Golgi positioning. Cold Spring Harbor perspectives in biology 3.

Yagi T, Ito D, Okada Y, Akamatsu W, Nihei Y, Yoshizaki T, Yamanaka S, Okano H, Suzuki N (2011) Modeling familial Alzheimer's disease with induced pluripotent stem cells. Human molecular genetics 20:4530-4539.

Yan Y, Wang C (2007) Abeta40 protects non-toxic Abeta42 monomer from aggregation. J Mol Biol 369:909-916.

Yang SA, Klee CB (2000) Low affinity Ca2+-binding sites of calcineurin B mediate conformational changes in calcineurin A. Biochemistry 39:16147-16154.

Ye X, Tai W, Zhang D (2012) The early events of Alzheimer's disease pathology: from mitochondrial dysfunction to BDNF axonal transport deficits. Neurobiology of aging 33:1122 e1121-1110.

Yin X, Takei Y, Kido MA, Hirokawa N (2011) Molecular motor KIF17 is fundamental for memory and learning via differential support of synaptic NR2A/2B levels. Neuron 70:310-325.

Yonekawa Y, Harada A, Okada Y, Funakoshi T, Kanai Y, Takei Y, Terada S, Noda T, Hirokawa N (1998) Defect in synaptic vesicle precursor transport and neuronal cell death in KIF1A motor protein-deficient mice. The Journal of cell biology 141:431-441.

Yoshii A, Zhao JP, Pandian S, van Zundert B, Constantine-Paton M (2013) A Myosin Va mutant mouse with disruptions in glutamate synaptic development and mature plasticity in visual cortex. The Journal of neuroscience : the official journal of the Society for Neuroscience 33:8472-8482.

Young JE, Goldstein LS (2012) Alzheimer's disease in a dish: promises and challenges of human stem cell models. Human molecular genetics 21:R82-89.

Yu WH, Cuervo AM, Kumar A, Peterhoff CM, Schmidt SD, Lee JH, Mohan PS, Mercken M, Farmery MR, Tjernberg LO, Jiang Y, Duff K, Uchiyama Y, Naslund J, Mathews PM, Cataldo AM, Nixon RA (2005) Macroautophagy--a novel Beta-amyloid peptide-generating pathway activated in Alzheimer's disease. The Journal of cell biology 171:87-98.

Yuan A, Kumar A, Peterhoff C, Duff K, Nixon RA (2008) Axonal transport rates in vivo are unaffected by tau deletion or overexpression in mice. The Journal of neuroscience : the official journal of the Society for Neuroscience 28:1682-1687.

Yuan A, Kumar A, Sasaki T, Duff K, Nixon RA (2013) Global axonal transport rates are unaltered in htau mice in vivo. Journal of Alzheimer's disease : JAD 37:579-586.

Zempel H, Thies E, Mandelkow E, Mandelkow EM Abeta oligomers cause localized Ca(2+) elevation, missorting of endogenous Tau into dendrites, Tau phosphorylation, and destruction of microtubules and spines. The Journal of neuroscience : the official journal of the Society for Neuroscience 30:11938-11950.

Zhang C, Browne A, Kim DY, Tanzi RE (2010) Familial Alzheimer's disease mutations in presenilin 1 do not alter levels of the secreted amyloid-beta protein precursor generated by beta-secretase cleavage. Current Alzheimer research 7:21-26.

Zhang C, Wu B, Beglopoulos V, Wines-Samuelson M, Zhang D, Dragatsis I, Sudhof TC, Shen J (2009) Presenilins are essential for regulating neurotransmitter release. Nature 460:632-636.

Zhang F, Phiel CJ, Spece L, Gurvich N, Klein PS (2003) Inhibitory phosphorylation of glycogen synthase kinase-3 (GSK-3) in response to lithium. Evidence for autoregulation of GSK-3. J Biol Chem 278:33067-33077.

Zhang S, Zhang M, Cai F, Song W (2013) Biological function of Presenilin and its role in AD pathogenesis. Transl Neurodegener 2:15.

Zhao C, Deng W, Gage FH (2008) Mechanisms and functional implications of adult neurogenesis. Cell 132:645-660.

Zhao D, Watson JB, Xie CW (2004) Amyloid beta prevents activation of calcium/calmodulin-dependent protein kinase II and AMPA receptor phosphorylation during hippocampal long-term potentiation. Journal of neurophysiology 92:2853-2858.

Zhao WQ, Santini F, Breese R, Ross D, Zhang XD, Stone DJ, Ferrer M, Townsend M, Wolfe AL, Seager MA, Kinney GG, Shughrue PJ, Ray WJ (2010) Inhibition of

calcineurin-mediated endocytosis and alpha-amino-3-hydroxy-5-methyl-4-isoxazolepropionic acid (AMPA) receptors prevents amyloid beta oligomer-induced synaptic disruption. The Journal of biological chemistry 285:7619-7632.

Zou K, Kim D, Kakio A, Byun K, Gong JS, Kim J, Kim M, Sawamura N, Nishimoto S, Matsuzaki K, Lee B, Yanagisawa K, Michikawa M (2003) Amyloid beta-protein (Abeta)1-40 protects neurons from damage induced by Abeta1-42 in culture and in rat brain. Journal of neurochemistry 87:609-619.